Extracellular matrix remodeling and the control of branching morphogenetic programs

by

Tamar Yael Feinberg

A dissertation submitted in partial fulfillment
of the requirements for the degree of
Doctor of Philosophy
(Cellular and Molecular Biology)
in the University of Michigan
2016

Doctoral Committee:

Professor Stephen J. Weiss, Chair
Professor James D. Engel
Professor Eric R. Fearon
Adjunct Professor Jun-Lin Guan
Professor Alan R. Saltiel

DEDICATION

To my late mother, Saundra Katz-Feinberg, for her love, friendship, inspiration, and tireless pursuit of knowledge and understanding.

ACKNOWLEDGEMENTS

Many thanks to my mentor, Stephen J. Weiss, and the members of my thesis committee - James D. Engel, Eric Fearon, Jun-Lin Guan and Alan Saltiel - for their time, consideration, invaluable feedback and support. Many thanks to our collaborators David Ginsburg and Thomas Saunders, as well as Dorothy Sorenson, Craig Johnson and Gertraud Robinson for helpful conversations and technical assistance. Lastly, many thanks to my family and close friends for their love and constant encouragement.

TABLE OF CONTENTS

LIST OF TABLES

LIST OF FIGURES

LIST OF ABBREVIATIONS

BM: Basement membrane

ECM: Extracellular matrix

MMP: Matrix metalloproteinase

MT-MMP: Membrane-tethered matrix metalloproteinase

TIMP: Tissue inhibitor of matrix metalloproteinase

2-D: 2-dimensional

3-D: 3-dimensional

KASH: Klarsicht, ANC-1, Syne homology domain

LINC: linker of cytoskeleton and nucleus complex

ABSTRACT

Epithelial cells and endothelial cells initiate distinct branching morphogenetic programs during their coordinated invasion and proliferation into the interstitial compartment, a tissue comprised of mesenchymal stromal cells and extracellular matrix (ECM). While mammary gland development occurs in a specialized stromal environment dominated by adipocytes and fibroblasts, endothelial cell branching proceeds throughout all tissues in the absence of a specific stromal cell population. Nevertheless, both epithelial cells and endothelial cells engaged in morphogenetic responses have been posited to mobilize proteolytic enzymes to penetrate ECM barriers. However, transgenic mouse models have failed to identify required proteolytic effectors or uncover the mechanisms whereby proteolytic changes in tissue microenvironments regulate cell behavior. Herein, we characterize functional roles performed by the two dominant transmembrane proteinases expressed during epithelial and endothelial cell branching processes, the membrane-anchored matrix metalloproteinases, MT1-MMP and MT2-MMP. Using a series of transgenic mouse models, we identify new and unanticipated roles for MT1-MMP and MT2-MMP in mammary gland morphogenesis as well as angiogenesis. Tissue-specific targeting of MT1-MMP and MT2-MMP demonstrate that early mammary gland branching, which takes place within an immature ECM, proceeds independently of either proteinase. Instead, both proteinases play important, but diametrically opposed, roles in mammary gland adipocytes, where MT1-MMP stimulates adipogenesis and lipid metabolism, while MT2-MMP represses the development of thermogenic beige/brown adipocytes. In marked contrast, during the major phases of postnatal

mammary gland development where a mature ECM is actively deposited, branching requires stromal cell-, rather than epithelial cell-, derived MT1-MMP, where the proteinase regulates branching by remodeling a periductal network of ECM macromolecules dominated by type I collagen. Endothelial cells also rely on MT1-MMP to direct branching, but unexpectedly, the proteinase also controls proliferative responses via a novel regulatory axis wherein pericellular proteolysis of the ECM governs the cytoskeletal-nuclear membrane interactions responsible for regulating transcriptional activity. Together, these data create new paradigms relevant to morphogenesis and tissue remodeling, as well as identify novel roles for membrane-anchored metalloproteinases in governing ECM proteolysis and associated transcriptional programs.

CHAPTER 1: Introduction

Branching morphogenesis as a general developmental paradigm.

Epithelial and endothelial organ development, function and homeostasis require the formation and remodeling of ramified tubular networks, processes known as branching morphogenesis and angiogenesis, respectively (Andrew and Ewald, 2010; Carmeliet and Jain, 2011; Scarpa and Mayor, 2016; Vandekeere et al., 2015). The established tubules control the transport of fluids, gases, nutrients and waste products under physiologic as well as pathophysiologic conditions (Carmeliet and Jain, 2011; Scarpa and Mayor, 2016; Vandekeere et al., 2015). The tissue sculpting that occurs coincident with branching morphogenesis drives the formation of the respiratory, circulatory and secretory organ systems of developing vertebrate as well as invertebrate organisms. Malformation and dysfunction of these branching tubular networks contribute to embryonic lethality and the pathogenesis of many diseases, ranging from inflammatory disorders, pulmonary hypertension, and blinding ocular diseases to cancer (Carmeliet and Jain, 2011). Across organ systems, epithelial and endothelial tubules branch through a combination of either single cell movement or collective patterns of cell migration where groups of cells move together in a coordinated fashion (Ewald et al., 2008; Ewald et al., 2012; Scarpa and Mayor, 2016). Further, both types of branching networks are composed of an inner compartment of adherent cells (i.e. epithelial cells and endothelial cells) that are inter-

connected by junctional complexes, and an outer compartment of mesenchymal stromal cells that regulate proliferation, cell survival and differentiation (Carmeliet and Jain, 2011; Howard and Lu, 2014). However, the relative roles of these two compartments in coordinating branching morphogenesis *in vivo* remains undefined.

Early evidence implicating cell movement and collective cell migrations in branching morphogenesis came from seminal work performed with fruit flies (*Drosophila melanogaster*) and the development of their respiratory tubules (trachea). Similar to vertebrate branching programs, tracheal development begins when ectoderm-derived tracheal epithelial cell clusters form epithelial placodes and invaginate into underlying stromal tissue in response to inductive chemokines secreted from the surrounding mesenchyme (Affolter and Caussinus, 2008; Sutherland et al., 1996). Primary branches form when individual tracheal epithelial cells migrate outward in stereotyped directions and undergo further ramification for maximal oxygen transport (Affolter and Caussinus, 2008; Glasheen et al., 2010; Sutherland et al., 1996). Tracheal cells at the tip of elongating terminal ends exert leader roles, display long cellular protrusions, and are thought to drive collective migration. The trailing adherent "follower" cells, referred to as stalk cells, show fewer cellular protrusions and instead contribute to branch elongation via their intercalation (Affolter and Caussinus, 2008; Carmeliet and Jain, 2011; Lebreton and Casanova, 2014; Scarpa and Mayor, 2016; Vandekeere et al., 2015). Unlike the *Drosophila* trachea and vertebrate vasculature, branching of epithelial organ systems, such as the mammary gland, is thought to largely occur in the absence of leader cell protrusions (Andrew and Ewald, 2010; Ewald et al., 2008; Williams and Daniel, 1983); and the molecular machinery required for single cell migration and coordinated tubule elongation in vertebrate models have not been defined.

Herein, we focus on two different postnatal branching programs in vertebrates using transgenic mouse models and primary cell cultures: (1) the branching morphogenesis of epithelial cells during mouse mammary gland development, and (2) the branching of endothelial cells during angiogenesis. These two systems offer a unique means to evaluate how distinct branching programs coordinate the cell proliferation, differentiation, motility, adhesion and signaling cascades required for functional morphogenesis.

Mammary gland branching morphogenesis.

The outgrowth of branching mammary epithelial tubules depends on complex reciprocal crosstalk between the epithelium and the surrounding mammary mesenchyme - composed of fibroblasts, adipocytes, endothelial cells, and immune cells - for inducing the proliferative responses, signaling cascades, and differentiation programs required for morphogenesis (Ewald et al., 2008; Ewald et al., 2012). However, the relative roles that the epithelial and stromal compartments in this dynamic tissue sculpting process remain unclear. Mouse mammary gland development begins during embryonic development on gestation day 10 (E10), with the formation of two ventral-oriented mammary lines just inside the fore- and hind-limb buds from the neck to the genital region (Inman et al., 2015; Veltmaat et al., 2003). Between E11 and E14, lens-shaped multi-layered ectoderm-derived structures (referred to as mammary placodes or anlagen) appear at five reproducible and symmetric positions along each mammary line and transform into epithelial buds that protrude into the underlying dermis (Inman et al., 2015; Veltmaat et al., 2003) (Fig. 1-1 A). In male embryos, testosterone secreted from the developing testes activates androgen receptor signaling in the mammary gland mesenchyme around E14 and induces apoptosis of the epithelial rudiments, thereby eliminating the mammary epithelial compartment (Brisken and

O'Malley, 2010; Durnberger and Kratochwil, 1980). In female embryos, mammary gland branching resumes on or near E15 when each mammary bud sprouts toward the adjacent mesenchyme and undergoes reiterative branching into the primordial stromal tissue beneath the dermis to form small primitive branching networks by birth (Inman et al., 2015; Robinson, 2007; Watson and Khaled, 2008) (Fig. 1-1 A,B). In female embryos, these initial stages of mammary gland development are largely independent of systemic hormone signaling and rely more on reciprocal cross-talk between branching epithelial cells and the surrounding mesenchyme (Brisken and O'Malley, 2010; Sternlicht, 2006).

Unlike other epithelial organ systems, mammary gland development predominantly occurs after the onset of puberty (at approximately 3 weeks after birth in mice), when the steroid sex hormones, estrogen and progesterone, stimulate the resident mammary epithelial tubules to extend, bifurcate, and branch throughout an adipocyte-populated stroma, termed the mammary "fat pad" (Inman et al., 2015) (Fig. 1-1 C). Mammary epithelial tubules (ducts) are bipolar structures composed of inner-facing luminal epithelial cells and basal-oriented myoepithelial cells (Fig. 1-1 D,E). During puberty, mammary gland branching is thought to largely depend on the hormone-dependent development and dichotomous branching of bulbous epithelial structures at the tips of the elongating ducts, known as terminal end buds (TEBs), which have implied motility based on their proliferative activity and position facing the epithelium-free, unoccupied expanse of the mammary fat pad (Hinck and Silberstein, 2005; Jackson-Fisher et al., 2004; Kurley et al., 2012) (Fig. 1-1 F).

Mammary gland TEBs have a similar bilayered architecture to the ducts with an outer monolayer of undifferentiated/ basal progenitor "cap" cells that give rise to the myoepithelial cells that surround the ducts, and an inner multilayered compartment of luminal progenitor cells referred

to as “body” cells (Hinck and Silberstein, 2005; Jackson-Fisher et al., 2004; Khokha and Werb, 2011) (Fig. 1-1 F). During this mammary duct elongation process, secondary branches sprout laterally from the ductal regions of existing mammary tubules and further ramify in the absence of TEBs (Khokha and Werb, 2011). Structural defects in TEBs correspond with impaired branching morphogenesis and stunted ductal invasion through the mammary fat pad (Jackson-Fisher et al., 2004; Kurley et al., 2012), suggesting a critical role for TEBs in mammary epithelial branching. While TEBs regress once the fat pad is laced with mammary ductal structures, at ~ 9 weeks of age (Lu et al., 2008), the established mammary ductal tree continues to expand and retract with regard to tertiary branch number every 4-to-5 days as a consequence of the epithelial cell proliferation and apoptosis induced by cycling ovarian hormone levels (Fata et al., 2001; Sternlicht, 2006).

Adult mammary glands also undergo extensive remodeling with each round of pregnancy at which time progesterone and pituitary-derived prolactin stimulate the resident mammary epithelium to undergo extensive proliferation as well as differentiation (Hennighausen and Robinson, 2001; Inman et al., 2015). Indeed, in the later stages of pregnancy epithelial cell number increases ~ 100-fold in tandem with the generation of secretory luminal epithelial (alveolar) structures and a commensurate decrease in mammary gland adipocyte numbers (Khokha and Werb, 2011). Changes in circulating hormone levels induce these alveolar epithelial cells to synthesize and secrete milk proteins into the lumen during lactation, which is maintained by the suckling newborns and subsequent milk clearance (Inman et al., 2015; Khokha and Werb, 2011). Weaning and milk stasis induces a mammary gland involution program characterized by rapid regression of the differentiated secretory epithelium and reformation of the epithelial and stromal compartments to resemble the virgin mammary gland (Khokha and Werb, 2011).

Angiogenesis and blood vessel remodeling.

Coincident with epithelial cell branching morphogenesis, endothelial cells and their associated stromal cells, including pericytes and vascular smooth muscle cells, drive sprouting angiogenesis into the surrounding mesenchyme (Betterman et al., 2012; Carmeliet and Jain, 2011). Blood vessels provide developing epithelial organ systems, including the mammary gland, with oxygen and critical instructive signals for their morphogenesis (Pierreux et al., 2010; Ramasamy et al., 2015). Vascular development begins early in embryogenesis when endothelial progenitor cells (angioblasts) assemble a primordial vascular plexus of small capillaries that expands by vessel sprouting and remodeling to form a highly ramified network of endothelial vessels (Fig. 1-2 A,B). Further, this network is ensheathed by pericytes and vascular smooth muscle cells that together with the endothelium regulate blood vessel stability and permeability (Carmeliet and Jain, 2011; Ramasamy et al., 2015) (Fig. 1-2 C).

After birth, sprouting angiogenesis continues to contribute to organ growth and development. By adulthood, however, most blood vessels are largely quiescent unless exposed to (patho)-physiologic stimuli such as inflammation or tissue damage (Carmeliet and Jain, 2011; Ramasamy et al., 2015). Similar to the epithelial-stromal cell cross-talk required for mammary gland branching morphogenesis, blood vessel development and remodeling requires a balance of stimulatory and inhibitory signals from the mesenchyme. New blood vessel sprouts initiate when local concentrations of chemo-attractive angiogenic growth factors (including vascular endothelial growth factor, VEGF-A) stimulate individual endothelial cells to loosen their junctions and send out polarized cellular protrusions (filopodia) into the surrounding mesenchyme (Carmeliet and Jain, 2011) (Fig. 1-2 D). The endothelial cells that express the highest levels of VEGF-A receptor, VEGFR2, often termed, tip cells, guide sprouting and inhibit their neighboring endothelial cells

from adopting a migratory phenotype by activating NOTCH signaling in adjacent endothelial cells, which in turn down-regulates VEGFR2 expression and VEGF-A responsiveness (Carmeliet and Jain, 2011; Vandekeere et al., 2015) (Fig. 1-2 D). The cell shape changes in the protrusive endothelial tip cells are thought to activate the cytoskeleton-dependent contractile responses that trigger proliferation and morphogenesis (Adams and Alitalo, 2007; Tung et al., 2012; Zhou et al., 2008). Mesenchyme-supplied angiogenic growth factors then induce sprout elongation by directing the migration of the endothelial tip cells and stimulating the proliferation of the trailing stalk cells (Tung et al., 2012; Zhou et al., 2008) (Fig. 1-2 D). However, the mechanisms by which attendant cell shape informs cell function during sprouting angiogenesis remain unknown.

Extracellular matrix (ECM) and its relationship with branching tubular structures.

During all branching morphogenesis programs, advancing tubular structures navigate through a complex environment of densely arrayed extracellular networks of collagens, glycoproteins and proteoglycans, collectively known as the extracellular matrix (ECM). A specialized 100-to-300nm-thick sheet-like ECM predominantly composed of intertwined supramolecular networks of polymeric laminin glycoproteins and type IV collagen, referred to as basement membrane (BM), envelopes branching epithelium and separates endothelial cells, smooth muscle cells and adipocytes from the underlying stromal mesenchyme (Rowe and Weiss, 2008; Williams and Daniel, 1983) (Fig. 1-3 A,B). The laminin constituents are heterotrimeric (composed of α, β and ɣ chains) and are thought to assemble a provisional template of enmeshed heterotrimers at the plasma membrane surface, via their binding interactions with cellular surface receptors (Kelleher et al., 2004; Rowe and Weiss, 2008). The laminin template then guides the assembly of supramolecular polygonal networks of type IV collagen polymers that are stabilized

by covalent cross-links, thereby providing the BM with its mechanical integrity (Kelleher et al., 2004; Rowe and Weiss, 2008) (Fig. 1-3 B,C). The resulting pore size of ~ 50 nm only allows the passive diffusion of small molecules, as migrating cells cannot negotiate pores less than 2 μm in size due to the deformation limits of their nuclei, the most rigid component of a cell (Rowe and Weiss, 2008).

Outside the BM, branching epithelial and endothelial structures are further surrounded by a dynamic periductal stroma dominated by a type I collagen-enriched interstitial ECM (Fig. 1-3 D,E). Type I collagen is a triple-helical heterotrimer of two distinct polypeptide chains (α1- and α2- chains) whose synthesis is essential for embryonic development and blood vessel stability (Kelleher et al., 2004; Lohler et al., 1984; Niederreither et al., 1995). Homozygous disruption of the type I collagen α1-chain (*Col1a1*) results in necrosis of mesenchymal cells in the developing embryo and embryonic lethality between E12 and E14 due to rupture of large blood vessels (Lohler et al., 1984), highlighting the importance of type I collagen in the maintenance of the vertebrate circulatory systems. Interstitial fibronectin binds to type I collagen and is also crucial for the organization and integrity of the heart and blood vessels (George et al., 1993). Following targeted homozygous disruption of fibronectin (*Fn1*) in mice, both embryonic and extra-embryonic vasculature fail to develop and severe defects in mesoderm-derived tissues result in embryonic lethality by E11 (George et al., 1993). The tissue defects and embryonic lethality observed in mouse models bearing mutations in these and other ECM genes illustrate the functional importance of ECM architecture in normal tissue development (Bateman et al., 2009).

Both BM and interstitial ECM provide structural scaffolding and mechanical support for tissue architecture as well as functional cues by virtue of their resident repertoire of adhesion receptor ligands for cell surface receptors with roles in regulating migration and homeostasis,

proliferation, apoptosis and differentiation (Bateman et al., 2009; Bonnans et al., 2014; Rowe and Weiss, 2008). Further, ECM serves as a reservoir for sequestered, matrix-bound, growth factors and signaling molecules implicated in branching programs, such as epidermal growth factor (EGF), fibroblast growth factor (FGF), hepatocyte growth factor (HGF), Wnt ligands and transforming growth factor (TGFβ) (Bonnans et al., 2014; Rowe and Weiss, 2008).

Current *in vitro* and *ex vivo* models to dissect cell-ECM interactions.

Various *in vitro* and *ex vivo* model systems have been designed to recapitulate the *in vivo* setting and dissect the requirements of *in vivo* branching programs. Standard two-dimensional (2-D) culture systems (i.e., performed classically with cells grown/ maintained in tissue-culture plastic ware) fall short of recapitulating cellular processes that normally operate within a more complex three-dimensional (3-D) ECM environment *in vivo,* as manifested by differences in cell morphology, cell-cell crosstalk and cell-ECM interactions (Baker and Chen, 2012; Rowe and Weiss, 2008; Yamada and Cukierman, 2007). 3-D *in vitro* models have therefore been developed to bridge the disconnect between conventional 2-D cell culture and the *in vivo* setting wherein single cells or multicellular aggregates are embedded within purified ECM, synthetic hydrogels or tissue extracts (Baker and Chen, 2012; Rowe and Weiss, 2008; Yamada and Cukierman, 2007). In many cases, cells embedded with 3-D ECM have been shown to adopt similar morphologies and cytoskeletal arrangements, as well as engage similar cell-ECM adhesive interactions and differentiation programs to those observed *in vivo* (Chun et al., 2006; Rowe and Weiss, 2008; Tang et al., 2013). For instance, endothelial cells embedded in 3-D hydrogels of the coagulation protein, fibrin, or purified type I collagen can be triggered to undergo angiogenic processes that mimic the behavior of neovessels developing in the interstitial ECM *in vivo* (Zhou et al., 2008).

Alternatively, *ex vivo* culture of intact organ explants allows for the maintenance of native tissue architecture and has been widely used for short-term visualization of embryonic branching programs, including those for the lung, kidney, mammary gland, and submandibular salivary glands (Hens et al., 2009; Oblander et al., 2005; Rebustini et al., 2009; Riggins et al., 2010; Yamada and Cukierman, 2007). For such studies, rudimentary epithelial buds are isolated with their associated mesenchyme from E12-to-E14 embryos and shown to undergo branching *ex vivo* in response to mitogenic stimuli when cultured at the air-liquid interface (Oblander et al., 2005; Rebustini and Hoffman, 2009; Rebustini et al., 2009; Riggins et al., 2010).

The mammary organoid model system.

As postnatal mouse mammary gland branching morphogenesis takes place within an adipocyte-rich stroma that scatters light and limits *ex vivo* imaging, studies aimed at dissecting the molecular machinery required for mammary epithelial branching have largely relied on *in vitro* model systems (Ewald et al., 2012). Current dogma in the literature maintains that mammary gland branching morphogenesis - and epithelial organ development, in general - relies on the epithelium as the functional tissue remodeling unit, while the surrounding stromal cells serve only to supply the necessary growth factors and steroid hormones required for regulated morphogenesis (Bonnans et al., 2014; Haslam et al., 2008; Khokha and Werb, 2011). An *in vitro* model system has been therefore established wherein primary mouse mammary epithelial cells are largely stripped of their surrounding mesenchymal tissue through collagenase-mediated digestion of minced mammary gland tissue, and isolated as intact clusters of luminal and myo-epithelial cells (termed mammary "organoids") for culture in 3-D ECM (Ewald et al., 2012; Haslam et al., 2008; Simian et al., 2001) (Fig. 1-4 A). In keeping with the notion that the mammalian epithelium drives branching

morphogenesis, mammary organoids have been shown to mount a branching program within purified type I collagen or ECM hydrogels in a largely stromal cell-independent fashion when stimulated with mitogenic growth factors, including EGF, basic FGF/ FGF2, and HGF (Ewald et al., 2012; Haslam et al., 2008; Simian et al., 2001) (Fig. 1-4 A). However, the *in vivo* application of observations gleaned from such *in vitro* and *ex vivo* studies remains unclear and the subject of ongoing debate.

Models for angiogenesis.

Angiogenesis involves a range of cell types and organ systems, and several different pro-angiogenic growth factors, including VEGF, FGF2 and HGF (Baker et al., 2012). *In vitro* and *ex vivo* models have therefore been established to interrogate the requirements of blood vessel branching outside the paracrine effects of adjacent tissues and/or stromal cell types (Baker et al., 2012). Since type I collagen is the dominant interstitial ECM barrier surrounding blood vessels *in vivo,* isolated vascular cells (i.e. endothelial cells and smooth muscle cells) and tissue fragments are routinely embedded within 3-D hydrogels of type I collagen (Baker et al., 2012; Yana et al., 2007; Zhou et al., 2008). With regard to inducing neovessel formation *in vitro,* VEGF is known to induce an increase in blood vessel permeability during sprouting angiogenesis *in vivo* that allows circulating fibrinogen to leak out into the surrounding tissues where it forms a network of cross-linked fibrin within the interstitial compartment (Carmeliet and Jain, 2011; Zhou et al., 2008). To recapitulate a similar scenario *in vitro,* vascular cell morphogenesis of endothelial cells is commonly examined in 3-D fibrin or type I collagen matrices. In this setting, isolated endothelial cells stretch, proliferate, and form tubular structures when suspended within 3-D hydrogels of either fibrin or type I collagen in response to angiogenic growth factors VEGF, HGF and FGF2

(Yana et al., 2007; Zhou et al., 2008) (Fig. 1-4 B,C). Murine and rat tissue explants can also be cultured in 3-D ECM *ex vivo* to examine sprouting angiogenesis from native tissue, thereby preserving the intercellular crosstalk that drives branching morphogenesis *in vivo*. Indeed, fragments of intracostal muscle, diaphragm, or aorta can each undergo sprouting angiogenesis, ultimately forming anastomosing networks of endothelial vessels in 3-D type hydrogels (Chun et al., 2004; Yana et al., 2007) (Fig. 1-4 D,E).

Matrix metalloproteinases and developmental tissue sculpting.

Although temporal and spatial changes in ECM biosynthesis take place during tissue morphogenesis, increasing evidence supports a model where branching tubules - of either epithelial or endothelial cell origin - mobilize proteolytic machinery to establish and remodel the mature structures found in adult tissue (Inman et al., 2015; Khokha and Werb, 2011). More than 600 proteinases are encoded within the mammalian genome of the aspartate, cysteine, metallo, serine and threonine subfamilies (Page-McCaw et al., 2007), and hundreds of these proteinases are capable of operating in the extracellular milieu (Rowe and Weiss, 2008). However, an evolutionarily conserved subclass of zinc-dependent endopeptidases from the metalloproteinase gene family, known as the matrix metalloproteinases (MMPs), has been shown to play dominant roles in remodeling ECM components, and comprise some of the key proteolytic enzymes implicated in developmental tissue sculpting (Bonnans et al., 2014; Rowe and Weiss, 2008).

The Matrix Metalloproteinase (MMP) family.

While the discovery of the first MMP was reported in 1962, in a study of the interstitial collagen remodeling that coincides with tadpole tail metamorphosis (Gross and Lapiere, 1962), an

absolute requirement for MMP activity in development was not established until 2003 in Drosophila, a model organism that expresses only two MMP family members (Bond et al., 2011; Guha et al., 2009; Jia et al., 2014; Page-McCaw et al., 2003; Srivastava et al., 2007; Wang et al., 2010). However, efforts to identify roles for MMPs or ECM remodeling in branching morphogenesis in more complex mammalian systems have remained inconclusive due to the continued reliance on *in vitro* or *ex vivo* model systems. Indeed, the relative requirements for mammalian MMPs in controlling branching morphogenesis *in vivo* remain largely undefined. This stand-still is, in part, due to the complexity of the mammalian genome. In contrast with Drosophila, more than 24 proteinases make up the mammalian MMP gene family and belong to two general classes – the secreted MMPs (of > 18 in number), and the membrane-tethered (MT)-MMPs (6 in number) that are anchored to the cell membrane surface either by a single-pass hydrophobic transmembrane domain or a glycosylphosphatidyl inositol (GPI)-anchor (Page-McCaw et al., 2007).

In mammalian systems, both secreted and membrane-associated MMPs are synthesized as latent zymogens with a conserved modular domain structure containing (i) an auto-inhibitory propeptide domain that stabilizes the zymogen in an inactive state, (ii) an N-terminal zinc-dependent catalytic domain, and (iii) a C-terminal hemopexin domain with functional roles in protein-protein interactions and substrate recognition (Li et al., 2008; Page-McCaw et al., 2007; Pei and Weiss, 1995; Pei and Weiss, 1996) (Fig. 1-5 A). Unlike most secreted MMPs, MT-MMP zymogens also contain a short sequence of basic amino acids (RRKR) located between the propeptide and the catalytic domains that functions as a recognition site for the proprotein convertase family member, furin (Pei and Weiss, 1995; Pei and Weiss, 1996; Wu et al., 2007) (Fig. 1-5 B). As a consequence, while most secreted MMPs are activated in the extracellular space, MT-

MMPs undergo intracellular activation through the proteolytic removal of their pro-domains via a proprotein convertase-dependent pathway that results in the display of the active enzyme on the cell surface (Pei and Weiss, 1995; Pei and Weiss, 1996; Wu et al., 2007) (Fig. 1-5 B). Global knockouts have been generated for most of the mammalian MMP family members, and none of the knockouts display marked defects in embryonic development (Page-McCaw et al., 2007), a finding that has thus far been rationalized on the basis of either genetic redundancy or functional compensation between MMP family members.

In vivo assessments of mammalian MMPs are further complicated by their endogenous regulation by proteinaceous tissue inhibitors of MMPs (TIMPs), which harbor N-terminal domains that interact with MMP catalytic domains (Seals and Courtneidge, 2003). The mammalian genome expresses 4 homologous TIMP family members, which differ in the efficacy of their MMP inhibition. For example, while TIMP1 specifically inhibits secreted and GPI-anchored MMPs, TIMP2 and TIMP3 target all secreted and membrane-anchored MMP family members (Arpino et al., 2015; Rowe and Weiss, 2008). Yet, the TIMPs are not entirely specific for the MMP family members as they have also been shown to inhibit a closely related family of zinc-dependent proteinases termed the adamalysins (Arpino et al., 2015). These proteinases display active-site domains that bear considerable homology to those of the MMP family (Seals and Courtneidge, 2003). Further, increasing evidence implicates adamalysins in the proteolytic activation of several cell surface proteins that drive epithelial tissue morphogenesis, including HB-EGF, TGFα and Amphiregulin, as well as receptor tyrosine kinases of the EGFR family (Black et al., 1997; Peschon et al., 1998; Sternlicht et al., 2005). Further, TIMP family members also have metalloproteinase-independent functions; as exemplified by TIMP1 and TIMP3, which regulate angiogenesis by

interacting directly with the β1-integrin receptor and VEGF receptor, respectively (Arpino et al., 2015).

Invertebrate evidence implicating (MT)-MMPs in postnatal tissue sculpting.

The MMP and TIMP families are evolutionarily conserved among multicellular organisms with homologs in vertebrate and invertebrate phyla. Given the limited number of *Drosophila melanogaster* (fruit fly) MMPs (termed dMMPs), that harbor the same conserved MMP domain structure as that present in mammalian MMPs, this model organism provided a simpler model system for interrogating the general roles of MMPs in developmental morphogenesis (Page-McCaw, 2008). Further, the Drosophila genome also only encodes one TIMP protein (dTIMP) that inhibits both dMMPs. Importantly, one Drosophila MMP is secreted (dMMP1) while the other is membrane-tethered via a GPI anchor (dMMP2) (Page-McCaw, 2008), offering an unbiased platform from which the relative roles of secreted and membrane-associated MMPs in tissue morphogenesis might be assessed.

Interestingly, following the targeted deletion of either dMMP1 alone, dMMP2 alone, or both dMMPs in combination, embryonic development proceeds in a normal fashion (Page-McCaw et al., 2003), thereby demonstrating that MMPs are not required during embryogenesis. Instead, Drosophila MMP knockouts display major defects during later stages of larval (early postnatal) maturation and die before reaching adulthood (Page-McCaw et al., 2003), suggesting a previously unsuspected role for the proteinases in postnatal developmental events that potentially extends to mammalian systems. Interestingly, while knockout screens reveal critical, albeit complex, roles for dMMP1 (i.e., the secreted dMMP) in epithelial cell adhesion and apical membrane expansion in larval trachea (Glasheen et al., 2010; Jia et al., 2014; Page-McCaw et al., 2003), growing

evidence supports dominant roles for membrane-associated dMMP2 in both larval tissue sculpting (histolysis) and the ECM remodeling events that drive metamorphosis as flies transition from larval to adult body plans (Bond et al., 2011; Guha et al., 2009; Jia et al., 2014; Page-McCaw et al., 2003). Unlike mutants for *dMmp1*, null mutants for *dMmp2* retain larval tissue, fail to undergo larval histolysis, and display stunted development of the dorsal air sacs associated with the tracheal tubes – all of which correlate with a failure to remodel ECM (Bond et al., 2011; Guha et al., 2009). Importantly, these phenotypes also recapitulate the defects observed following dTIMP overexpression (Guha et al., 2009).

Shifting the focus to mammalian MT1-MMP (and MT2-MMP).

Given the fly phenotypes, one might well posit that more careful analyses of mouse *MMP* knockouts would similarly reveal a host of postnatal defects. To date, however, *MMP* global knockouts display only subtle defects in postnatal development that are either transient, or at best subtle, with the exception of one membrane-tethered MMP family member, MT1-MMP/ MMP14. *Mmp14* global knockout (*Mmp14*$^{-/-}$) mice are born indistinguishable from their wild-type and heterozygous littermates, but mice undergo progressive postnatal wasting characterized by striking skeletal abnormalities, dwarfism and death by 3-to-12 weeks after birth (Holmbeck et al., 1999; Zhou et al., 2000). While MT1-MMP was first discovered based on its ability to directly activate a subset of secreted MMP family members, namely Gelatinase A/ MMP2 (Sato et al., 1994) and MMP13 (Knauper et al., 1996), growing evidence supports direct roles for MT1-MMP in hydrolyzing a wide variety of substrates, ranging from cell surface molecules and growth factors to ECM components, including those associated with the BM and interstitial compartment (Barbolina and Stack, 2008; Itoh, 2015; Rowe and Weiss, 2009). While major defects in postnatal

branching have not been reported to date, MT1-MMP has been posited to control branching events *in vitro* by both proteolytic mechanisms whereby epithelial cells dissolve confronting ECM barriers as well as proteinase-independent mechanisms by acting as a scaffolding hub for signal transduction cascades critical to cell motility and cell sorting (Alcaraz et al., 2011; Brownfield et al., 2013; Mori et al., 2009; Simian et al., 2001; Weaver et al., 2014). However, these data are confined to *in vitro* models and the roles of endogenous MT1-MMP during postnatal development *in vivo* remain unknown.

Interestingly, the closely related membrane-tethered MMP, MT2-MMP/ MMP15, which shares >50% homology with MT1-MMP at the amino acid level (Tanaka et al., 1997), is enriched in the epithelial cell compartment of the developing mammary gland (Szabova et al., 2005), and has also been reported to regulate branching morphogenesis *in vitro* by remodeling the BM and regulating growth factor expression (Rebustini et al., 2009). Nevertheless, conclusions regarding roles for MT2-MMP in branching morphogenesis and tissue sculpting again derive entirely from model systems. In fact, *Mmp15* has remained one of the few untargeted MMPs in the mammalian genome, begging the question of its functional roles during development.

Similar to the postnatal branching of epithelial structures, endothelial and mural cells (i.e., pericytes and vascular smooth muscle cells) have been reported to mobilize MT1-MMP *in vitro* to form capillary-like sprouts in 3-D hydrogels (Chun et al., 2004; Hiraoka et al., 1998; Tung et al., 2012; Zhou et al., 2008). Nevertheless, the *in vivo* roles of MT1-MMP in supporting angiogenic responses have yet to be determined as do the mechanisms by which matrix remodeling impacts cell function. Unlike epithelial cells, which are always subtended by a BM and subsequently separated from the interstitial compartment, endothelial cells break through their underlying BM during the initial phases of new blood vessel development and make direct contact with the

interstitial ECM (Chun et al., 2004). Much of the difficulty in assigning roles to MT1-MMP *in vivo* arises from the fact that the morbid status and shortened lifespan of *Mmp14*-null mice, coupled with organ failure in multiple systems, precludes mechanism-based analyses of specific tissues. To circumvent this issue, the Weiss lab recently generated and characterized the first *Mmp14* conditional knockout mouse model (Tang et al., 2013). Likewise, while *Mmp15* global knockouts might be predicted to display similar phenotypes, *Mmp15* conditional knockout mice had not yet been generated by any group. However, the Weiss lab recently engineered *Mmp15-lacZ* knock-in and *Mmp15-flox* mice to begin assessing its role(s) *in vivo*.

Herein, using recently derived global knockout and conditional knockout mouse lines, we provide the first *in vivo* evidence of a heretofore overlooked mammary gland branching program, which occurs during the first 10 days of early postnatal development through sparsely populated interstitial ECM (Chapter 2). While embryonic and early postnatal mammary gland branching morphogenesis through this more primitive ECM does not depend on either MT1-MMP or MT2-MMP (Chapter 2); a critical requirement for MT1-MMP was uncovered following the onset of puberty, when sex hormones estrogen and progesterone stimulate a more robust branching program through a more mature ECM (Chapter 3). Importantly, postnatal mammary gland branching morphogenesis proceeds independently of epithelial cell-derived MMPs (Chapter 3). Unexpectedly, and contrary to current dogma, mammary gland branching relies on MT1-MMP expression from the periductal mammary stroma to orchestrate the remodeling of stromal ECM; introducing a novel role for stromal cell-derived proteolytic machinery in directing tissue sculpting (Chapter 3). Further, in the process of examining endothelial and vascular smooth muscle cell responses to growth factor stimulation within 3-D ECM microenvironments, an unexpected link was established between MT1-MMP, nuclear architecture, and the regulation of transcriptional

activity in both *in vitro* and *in vivo* settings (Chapter 4). Both the mammary gland and the vasculature therefore rely on MT1-MMP-dependent pericellular remodeling of 3-D interstitial ECM for regulated tissue morphogenesis.

Fig. 1-1.

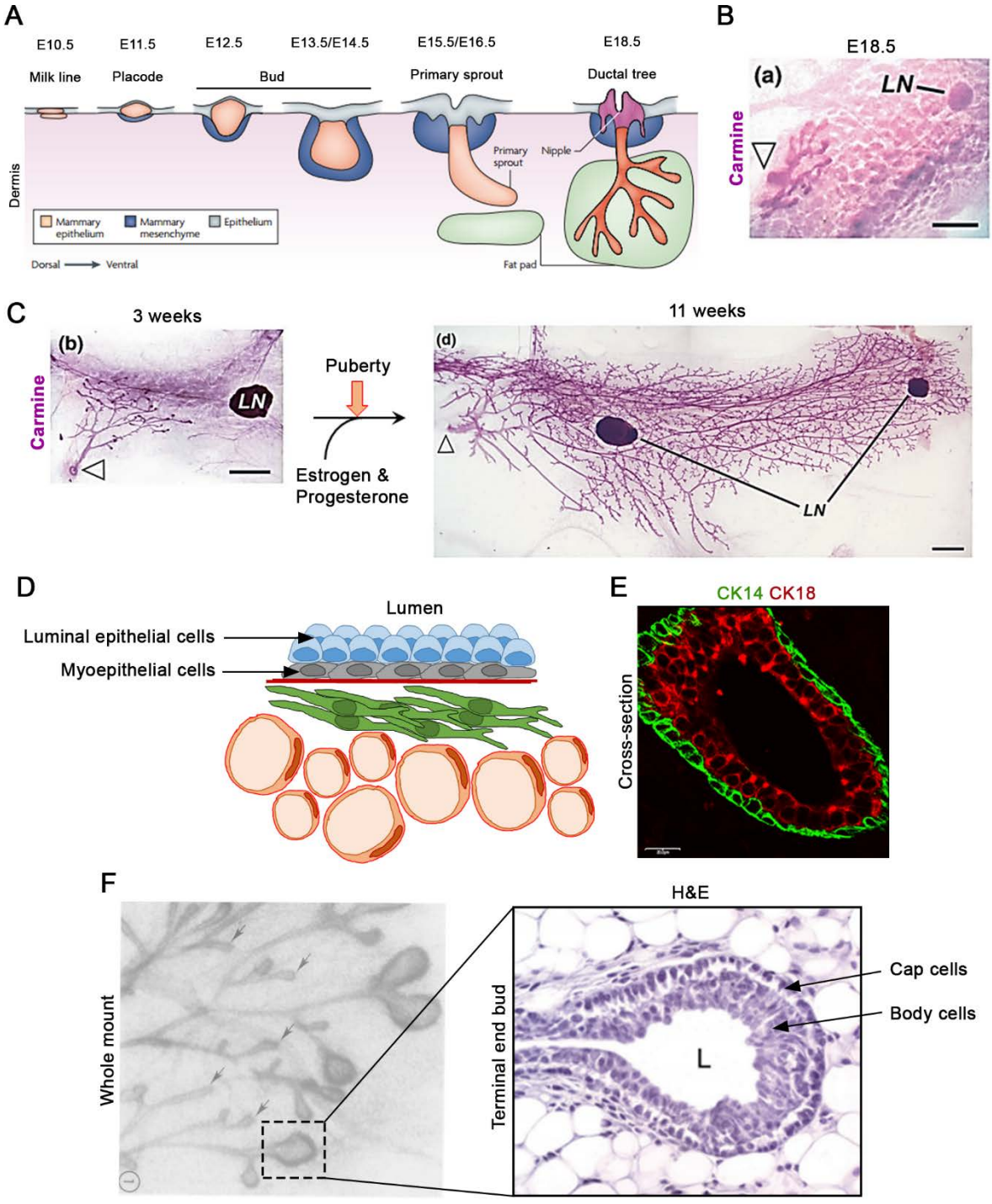

Fig. 1-1. Embryonic and postnatal mammary gland development.
(A) Cartoon schematic of embryonic mammary gland morphogenesis, which occurs between gestation days 10.5 (E10.5) and E18.5, and establishes a primitive ductal tree by E18.5 (Robinson, 2007). (B) Carmine staining of mammary gland whole mount shows the branching network at

E18.5 (scale bar = 0.5 mm) (Sternlicht, 2006). (C) Carmine staining of mammary gland whole mounts at 3 weeks and 11 weeks after birth show the branching structures (ducts) before and after the onset of puberty (scale bar = 1 mm) (Sternlicht, 2006). (B,C) Arrow heads indicate the initial branching site/ nipple region (LN = lymph node). (D) Cartoon of the luminal epithelial and myoepithelial cells which compose mammary epithelial ducts and the surrounding stromal cells dominated by fibroblasts (green) and lipid-laden adipocytes (orange). (E) Immunofluorescence of myoepithelial cell-associated cytokeratin-14 (CK14) and luminal epithelial cell-associated cytokeratin-18 (CK18) in cross-section through mammary gland duct. (F) Ductal network at 5 weeks after birth, which is characterized by bulb-like structures, known as terminal end buds, at the ends of growing ducts (Williams and Daniel, 1983). H&E staining of cross-section through terminal end bud with arrows indicating the lumen (L)-facing body epithelial cells and outer-lying cap epithelial cells (Hinck and Silberstein, 2005).

Fig. 1-2.

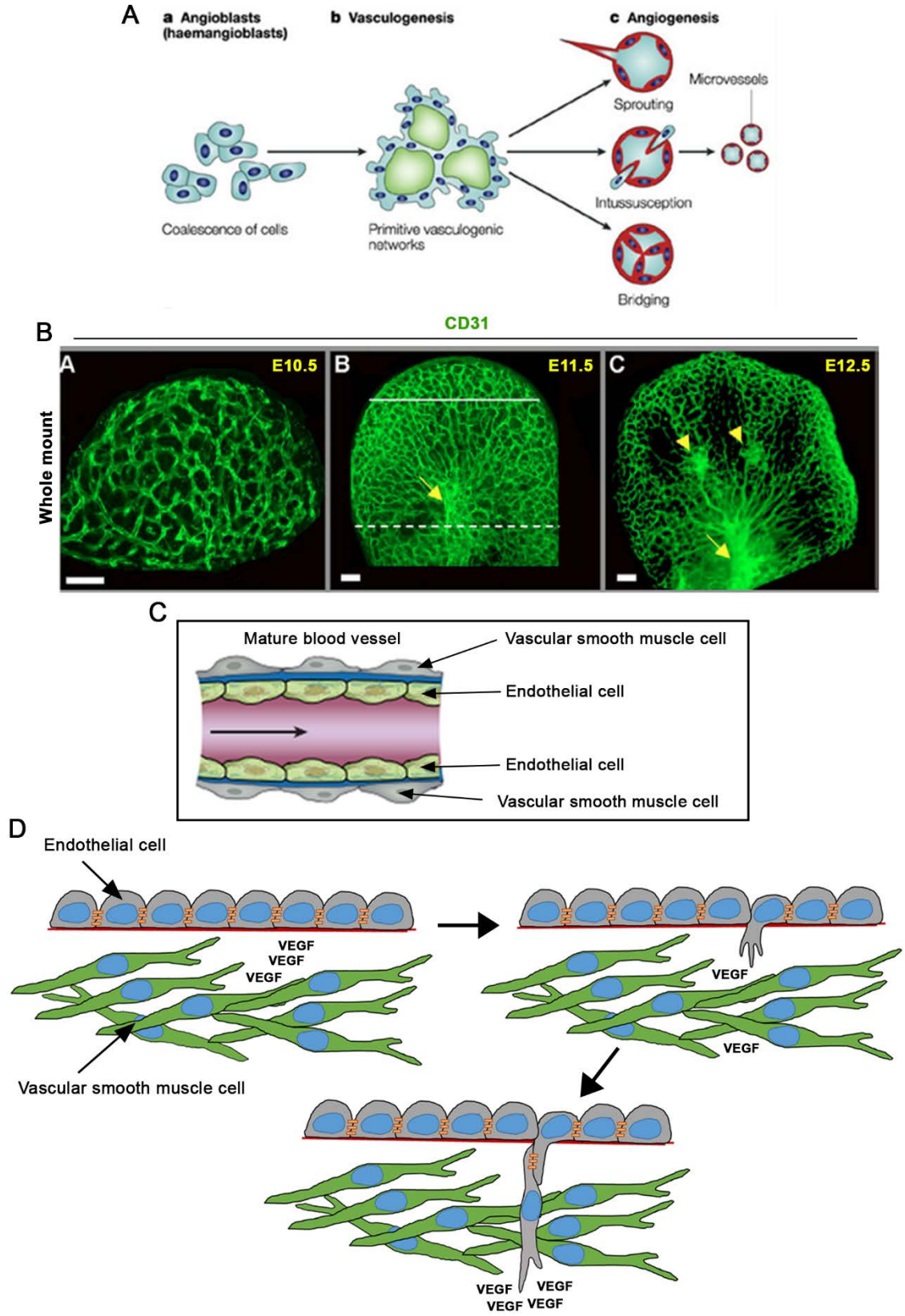
A
a Angioblasts (haemangioblasts)
b Vasculogenesis
c Angiogenesis
Sprouting
Microvessels
Intussusception
Coalescence of cells
Primitive vasculogenic networks
Bridging
B
CD31
Whole mount
A
E10.5
B
E11.5
C
E12.5
C
Mature blood vessel
Vascular smooth muscle cell
Endothelial cell
Endothelial cell
Vascular smooth muscle cell
D
Endothelial cell
VEGF
VEGF
VEGF
Vascular smooth muscle cell
VEGF
VEGF
VEGF
VEGF
VEGF

Fig. 1-2. Embryonic and postnatal blood vessel development.
(A) Cartoon illustrating the formation of primitive vascular networks during embryonic development from the coalescence of precursor cells (angioblasts), which differentiate into the endothelial cells that constitute mature blood vessels (Hendrix et al., 2003). (B) Immuno-fluorescence of endothelial cell-associated CD31 shows the vascular networks in E10.5 (left), E11.5 (middle), and E12.5 (right) whole limbs and the avascular areas of developing digit structures (Eshkar-Oren et al., 2009). (C) Cartoon of a mature blood vessel to show the inner-facing endothelial cells and the outer-lying stromal vascular smooth muscle cells (Carmeliet and Jain, 2011). (D) Schematic illustrating the initiation and development of new blood vessel sprouts from pre-existing blood vessels in response to local concentrations of VEGF.

Fig. 1-3.

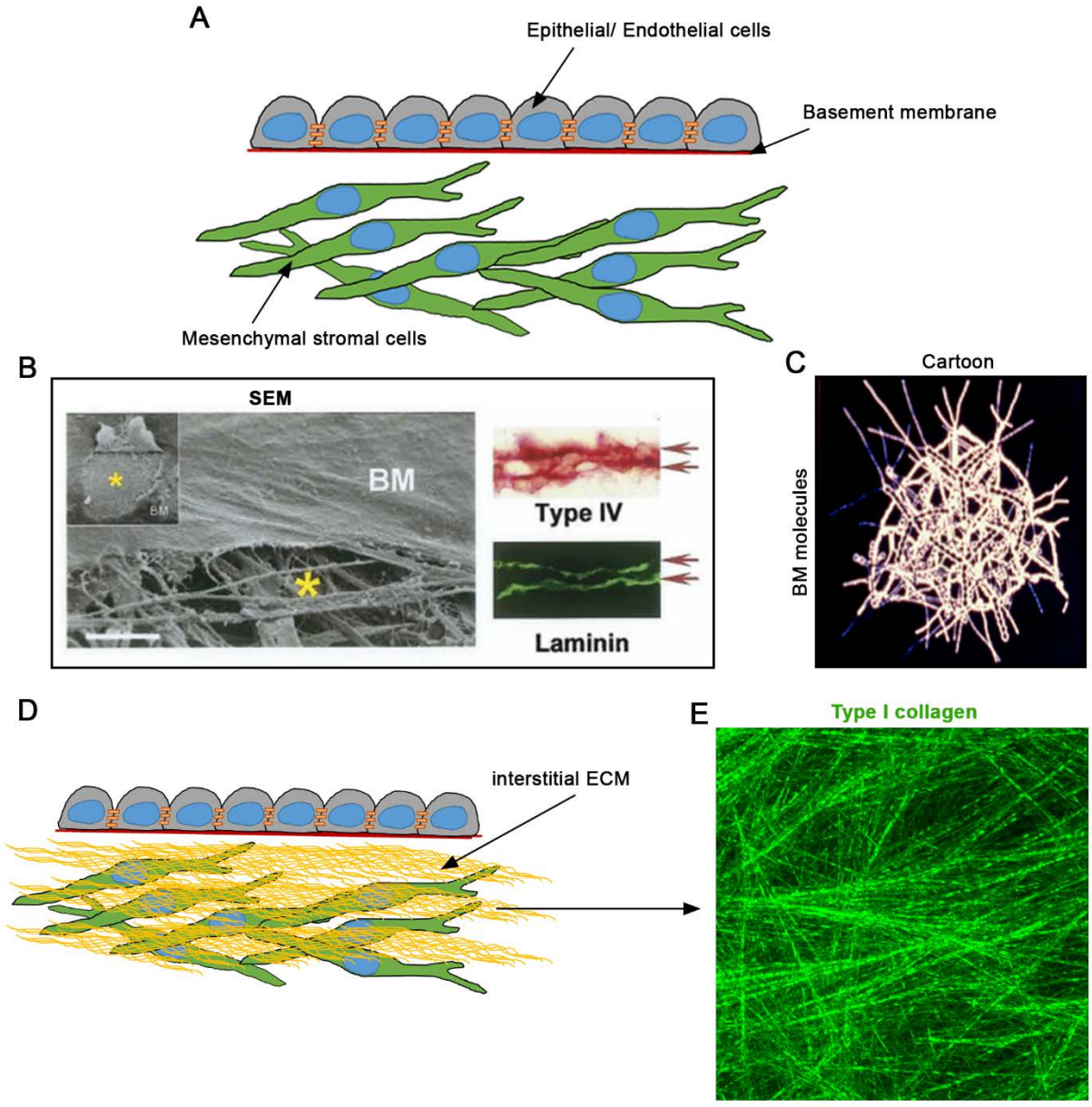

Fig. 1-3. Extracellular matrix (ECM) and its relationship with branching tubular structures. (A) Cartoon representing the epithelium and endothelium of branching structures, and the extracellular basement membrane (BM) that encloses and separates both epithelial and endothelial structures from surrounding mesenchymal stromal cells. (B) Scanning electron micrograph (SEM) highlights the sheet-like structure of BM with an asterisk indicating the fibrillar interstitial matrix lying beneath. Inset shows a lower magnification image (scale bar = 20 μm). Immuno-staining for type IV collagen and laminin in the peritoneal BM. The two layers are the upper and lower surfaces of the peritoneum that are lined by BM (Hotary et al., 2006). (C) Cartoon illustrating the complex meshwork of structural molecules that constitute mature BM. (D) Cartoon of the fibrillar interstitial ECM which surrounds the mesenchymal stromal cells. (E) Confocal reflection

micrograph of a 3-dimensional (3-D) type I collagen matrix shows the fibrillar architecture of interstitial type I collagen.

Fig. 1-4.

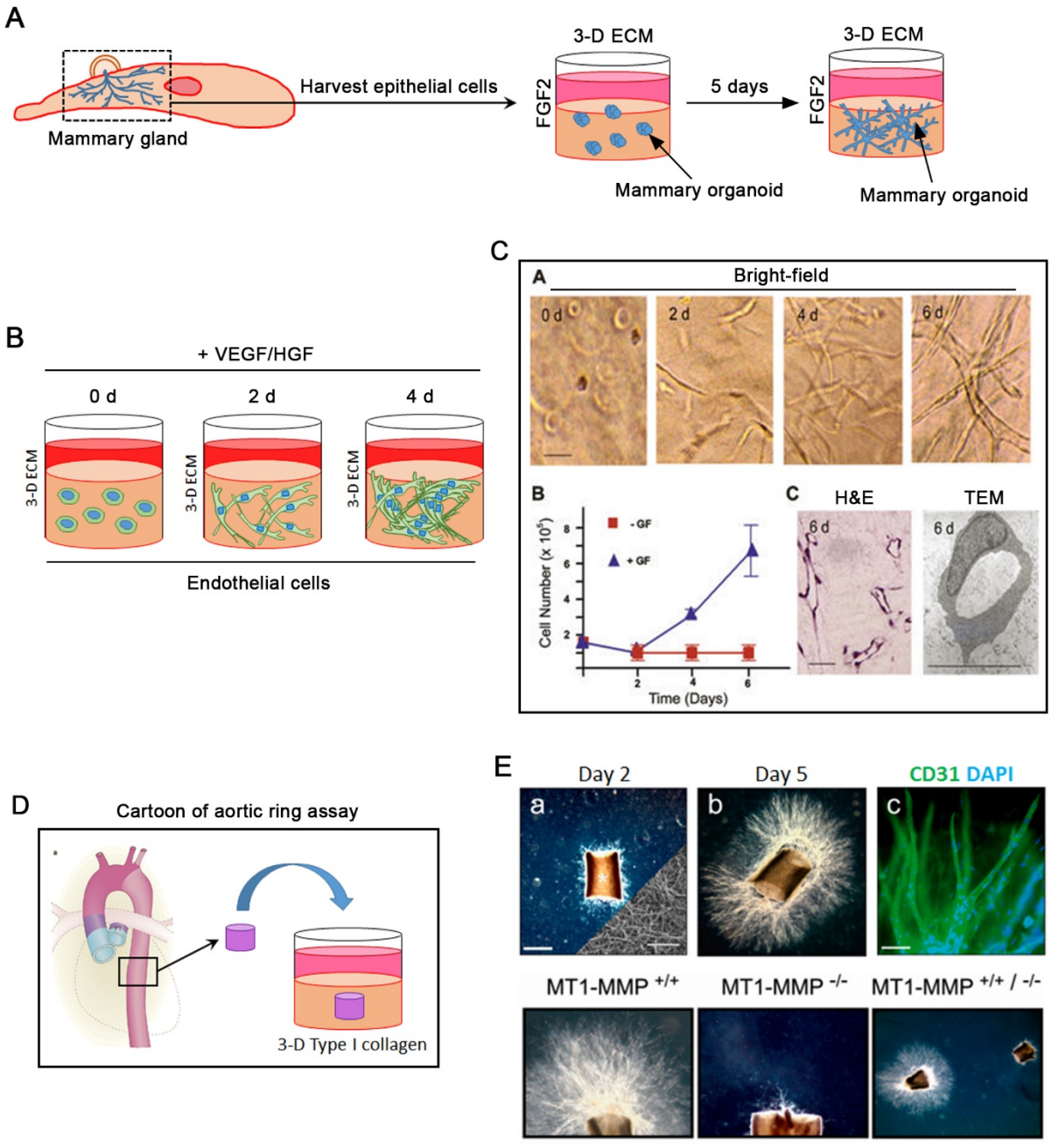

Fig. 1-4. *In vitro* and *ex vivo* models to dissect cell-ECM interactions.
(A) Schematic describing the isolation of mammary epithelial fragments (organoids) from intact mammary glands for culture within 3-D ECM. Mammary organoids undergo morphogenesis *in vitro* in response to mitogenic growth factor, FGF2, to form branching structures by day 5 of culture. (B) Schematic illustrating the *in vitro* morphogenesis of endothelial cells, which stretch and proliferate in 3-D ECM in response to angiogenic growth factors, VEGF and HGF, over a 4-day culture period. (C) Bright-field images of endothelial cells cultured within 3-D fibrin gels with

angiogenic growth factors at 0, 2, 4 and 6 days in culture. Endothelial cell number within 3-D fibrin matrices in the presence or absence of growth factors. Patent endothelial cell tubules form by day 6 of culture, as visualized by H&E staining and a transmission electron micrograph (Zhou et al., 2008). (D) Cartoon of aortic ring assay illustrating the retrieval of an aortic fragment (ring) for embedding in 3-D type I collagen. (E) Bright-field images of the neovessels formed from mouse aortic ring explants following 5 days of culture in 3-D type I collagen with angiogenic growth factors. Immunofluorescence of CD31 with DAPI nuclear counter-staining to visualize the branching endothelial cells. Aortic ring explants from wild-type and *Mt1-mmp*$^{-/-}$ mice in 3-D type I collagen (Chun et al., 2004).

Fig. 1-5.

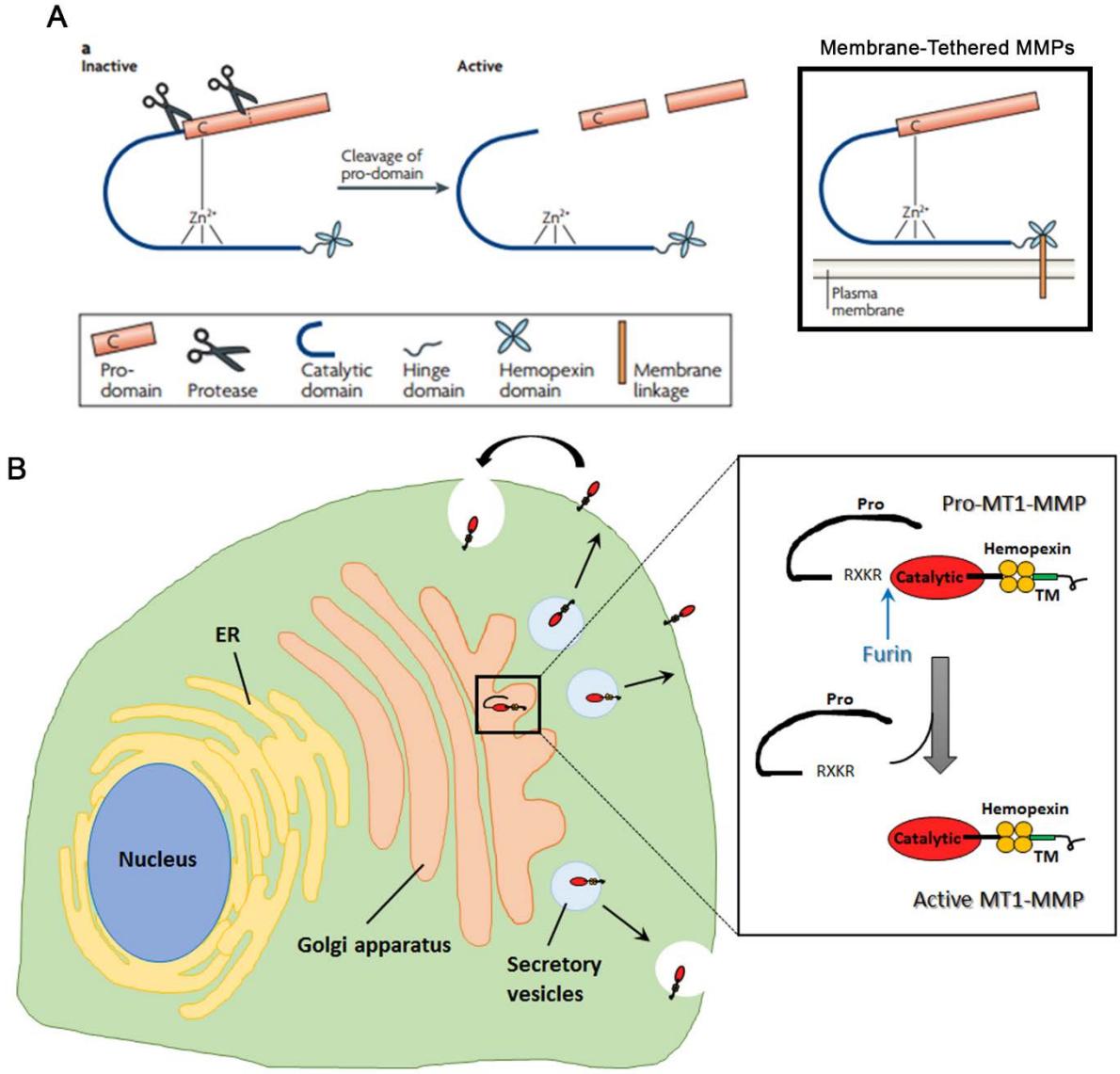

Fig 1-5. The matrix metalloproteinase (MMP) family.
(A) Schematics of secreted and membrane-tethered MMPs. Both secreted and membrane-tethered MMP precursors (Pro-MMPs) undergo post-translational processing for the removal of their auto-inhibitory pro-domains and generation of active enzyme. (B) Cartoon schematic of the processing and trafficking of membrane-tethered MMP14/ MT1-MMP, which undergoes intracellular activation in the trans Golgi network via a proprotein convertase, furin-dependent pathway, where furin recognizes and cleaves a short basic amino acid motif (RXKR) in the prodomain. Processed MT1-MMP is then trafficked to the cell surface in secretory vesicles and displayed on the cell surface as an active protease.

CHAPTER 2: Functional Roles of MT1-MMP and MT2-MMP in Early Postnatal Mammary Gland Development

Abstract.

During embryogenesis, mammary epithelial cells initiate migration programs that drive ductal invasion into the surrounding adipose-rich mesenchyme. Currently, branching morphogenesis is thought to depend on the mobilization of the membrane-anchored matrix metalloproteinases, MT1-MMP/MMP14 and MT2-MMP/MMP15, which drive epithelial cell invasion by remodeling the extracellular matrix and triggering associated signaling cascades. However, the roles that these proteinases play during mammary gland development *in vivo* remain undefined. Herein, we characterize the impact of global *Mt1-mmp* and *Mt2-mmp* targeting on early postnatal mammary gland development. Unexpectedly, both *Mt1-mmp*$^{-/-}$ and *Mt2-mmp*$^{-/-}$ mammary glands retain the ability to generate intact ductal networks. Though neither proteinase is required for branching morphogenesis, transcriptome profiling reveals a key role for MT1-MMP and MT2-MMP in regulating mammary gland adipocyte differentiation. Whereas MT1-MMP promotes the generation of white fat depots critical for energy storage, MT2-MMP differentially controls the formation of thermogenic brown fat. Taken together, these data not only indicate that current paradigms relevant to proteinase-dependent morphogenesis need be revisited, but also identify new roles for the enzymes in regulating adipocyte fate determination in the developing mammary gland.

Introduction.

During postnatal mammary gland development, epithelial ducts circumscribed by a contiguous basement membrane mount cell invasion programs that allow them to penetrate a periductal interstitial matrix populated by fibroblasts and a surrounding adipocyte-rich mesenchyme (Ewald et al., 2008; Ewald et al., 2012; Watson and Khaled, 2008). Similar to other epithelial organ systems, branching morphogenesis begins between gestation days E12 and E15 with the invagination of ectoderm-derived placodes to form primary buds that sprout and undergo reiterative branching into the underlying mesenchyme (Ewald et al., 2008; Ewald et al., 2012; Hogg et al., 1983; Watson and Khaled, 2008). Between E16 and E20, these solid, multi-layered mammary epithelial cords give rise to polarized, bilayered mammary tubules composed of inner-facing luminal epithelial cells and basal-oriented myoepithelial cells (Hogg et al., 1983). In tandem with epithelial development, the adipose-rich tissue that surrounds the developing mammary epithelium, termed the mammary fat pad, likewise undergoes morphogenesis (Hovey and Aimo, 2010; Inman et al., 2015). Beginning during late gestation (i.e., E14 to E18) and continuing through early postnatal development, the fat pad is eventually dominated by committed adipocytes that express adipokines and morphogens that support epithelial morphogenesis and tissue homeostasis (Wang et al., 2015). At birth, the mammary gland rudiment is a small, simply branched structure that is believed to lie dormant until the onset of puberty (~3 weeks of age) (Ewald et al., 2008; Ewald et al., 2012; Hogg et al., 1983; Watson and Khaled, 2008).

Recent studies emphasize critical roles for proteolytic enzymes belonging to the matrix metalloproteinase (MMP) family in the tissue remodeling events that are activated during branching morphogenesis, with specific focus on two closely related membrane-anchored MMPs, termed MT1-MMP and MT2-MMP (Alcaraz et al., 2011; Bonnans et al., 2014; Brownfield et al.,

2013; Mori et al., 2009; Rebustini et al., 2009; Weaver et al., 2014). Consistent with their >50% homology at the amino acid level (Itoh, 2015; Tanaka et al., 1997), both MT1-MMP and MT2-MMP are synthesized as zymogens, and undergo intracellular processing to form mature, catalytically active enzymes with an N-terminal catalytic domain, a more C-terminal hemopexin domain and a single-pass, type I transmembrane domain terminating in a short cytoplasmic tail (Itoh, 2015). Both MT1-MMP and MT2-MMP are capable of hydrolyzing a variety of substrates ranging from cell surface molecules and growth factors to extracellular matrix (ECM) components (Barbolina and Stack, 2008; Itoh, 2015; Rowe and Weiss, 2009). With particular regard to mammary gland morphogenesis, MT1-MMP has been reported to control branching events by both proteolytic mechanisms whereby epithelial cells dissolve confronting ECM barriers as well as proteinase-independent mechanisms by acting as a scaffolding hub for signal transduction cascades that control cell motility and cell sorting (Alcaraz et al., 2011; Brownfield et al., 2013; Mori et al., 2009; Simian et al., 2001; Weaver et al., 2014). Similarly, MT2-MMP has been reported to regulate branching morphogenesis and associated proliferative responses as a consequence of its ability to proteolytically remodel the basement membrane and regulate growth factor expression (Rebustini et al., 2009). Nevertheless, conclusions regarding roles for MT1-MMP and MT2-MMP in branching morphogenesis largely derive from *in vitro* and *ex vivo* models, and the roles that these enzymes play *in vivo* within the developing mammary gland remain undefined.

Herein, we describe a heretofore overlooked mammary gland branching program that occurs during the first 10 days of early postnatal development and gives rise to an organized network of polarized ductal structures that penetrate a mature adipocyte-populated stroma, offering a robust platform in which to characterize the protease-dependent and protease-independent roles

of MT1-MMP and MT2-MMP *in vivo*. Using *Mt1-mmp*$^{-/-}$ mice as well as a newly generated *Mt2-mmp*$^{-/-}$ mouse line, we provide the first full-scale analysis of the differential functions of these MT-MMPs in early postnatal mammary gland development.

Results.

Early postnatal morphogenesis of the developing mouse mammary gland.

At birth (i.e., postnatal day 0; P0), mammary gland rudiments of female mice appear as primitive ductal trees whose ill-defined branches are found adjacent to the nipple (Fig. 2-1 A). In H&E stained cross-sections, the mammary epithelium is organized into cohesive structures containing a mixture of solid cords and hollow ducts (Fig. 2-1 B). Immunohistochemical analyses further reveal that epithelial structures are dominated by cells expressing low levels of the luminal marker, cytokeratin 18 (CK18), in tandem with a heterogeneous distribution of cells expressing the basal marker, cytokeratin 14 (CK14) (Fig. 2-1 C) (Ewald et al., 2008; Ewald et al., 2012; Hogg et al., 1983; Watson and Khaled, 2008). Epithelial cells expressing the myoepithelial marker, α-smooth muscle actin (αSMA) (Ewald et al., 2008; Ewald et al., 2012; Hogg et al., 1983; Watson and Khaled, 2008), are confined to the basal compartment, but in a scattered fashion that outlines the rudiments (Fig. 2-1 C). In marked contrast, between P5 and P10, the mammary gland undergoes a heretofore overlooked morphogenic program wherein an established network of hollow ducts advances through the surrounding mesenchyme (Fig. 2-1 A,B). In the course of this early maturation process, CK18 expression is up-regulated in the luminal compartment while CK14 is confined primarily to basal epithelial cells in association with the continuous circumferential expression of αSMA (Fig. 2-1 C). These changes in epithelial cell and ductal tree organization are complemented by striking changes in the mammary gland fat pad wherein small

lipid-laden adipocyte/adipocyte precursors mature into large, unilocular adipocytes (Fig. 2-1 B). While the P0-P10 mammary ducts are consistently invested by a laminin- and type IV collagen-rich basement membrane (Fig. 2-1 D), a periductal network of organized type I collagen fibrils does not fully develop until P5-P10 (Fig. 2-1 E). Hence, during the early postnatal period, both the mammary epithelia and stroma activate a morphogenetic program that generates an organized network of ducts that predate those more frequently associated with pubertal development (Inman et al., 2015; Watson and Khaled, 2008).

MT1-MMP dependent regulation of branching morphogenesis: In vitro versus in vivo.

Based largely on *in vitro* evidence, MT1-MMP has been proposed to regulate branching morphogenesis by both proteinase- dependent and independent mechanisms (Alcaraz et al., 2011; Brownfield et al., 2013; Mori et al., 2009; Weaver et al., 2014). Using *Mt1-mmp*$^{lacZ/+}$ mice (Yana et al., 2007), β-galactosidase activity is detected in the branching ductal tree as well as the surrounding mesenchyme at birth and P5 (Fig. 2-2 A). By P10, LacZ-expressing cells delineate and circumscribe the entire neonatal mammary gland, from the ducts closest to the nipple to their terminal ends (Fig. 2-2 A) with cross-sections highlighting MT1-MMP expression in luminal epithelial cells and myoepithelial cells as well as the surrounding stroma (Fig. 2-2 B). LacZ expression also correlates with an increase in *Mt1-mmp* levels in the developing gland (Fig. 2-2 C).

To first assess the role of mammary epithelial cell-derived MT1-MMP *in vitro*, *Mt1-mmp*$^{lacZ/+}$ mammary epithelial organoids were embedded in 3-dimensional (3-D) type I collagen hydrogels (Chun et al., 2004; Haslam et al., 2008; Sabeh et al., 2009; Simian et al., 2001). As shown, *Mt1-mmp* is expressed both at time 0 and during the formation of an arborized branching

network generated in the presence of FGF-2 (Fig. 2-2 D) (Haslam et al., 2008; Simian et al., 2001). Consistent with the premise that MMPs are able to drive type I collagen-invasive activity (Alcaraz et al., 2011; Brownfield et al., 2013; Chun et al., 2004; Mori et al., 2009; Sabeh et al., 2009; Simian et al., 2001; Tang et al., 2013; Weaver et al., 2014), branching morphogenesis is inhibited completely when organoids are cultured in the presence of the pan-specific MMP inhibitor, BB-94 (Chun et al., 2004; Sabeh et al., 2009) (Fig. 2-2 E). More importantly, organoids recovered from MT1-MMP-deleted mice display a complete loss of branching activity (Fig. 2-2 E), a result consistent with MT1-MMP's role as the dominant pericellular type I collagenase operative in mammalian cells (Chun et al., 2004; Rowe and Weiss, 2009; Sabeh et al., 2009; Tang et al., 2013). Nevertheless, an MT1-MMP-dependent block in branching morphogenesis through native type I collagen matrices could also result from protease-independent effects on epithelial cell sorting, motility or metabolism (Brownfield et al., 2013; Mori et al., 2009; Sakamoto et al., 2014). As such, *Mt1-mmp*$^{+/+}$ and *Mt1-mmp*$^{-/-}$ mammary epithelial organoids were alternatively embedded in 3-D hydrogels of Matrigel (Ewald et al., 2008; Ewald et al., 2012; Lo et al., 2012), a mixture of basement membrane-associated proteins whose proteolytic remodeling is not required to support cell invasion programs (Rowe and Weiss, 2008). As reported previously (Ewald et al., 2008; Ewald et al., 2012; Lo et al., 2012), wild-type mammary organoids embedded in Matrigel hydrogels form budding lobular structures in response to FGF-2-mediated signaling (Fig. 2-2 F). Inconsistent, however, with the contention that MT1-MMP regulates morphogenesis via proteinase-independent mechanisms (Brownfield et al., 2013; Mori et al., 2009), neither Matrigel-embedded organoids cultured in the presence of BB-94 nor *Mt1-mmp*$^{-/-}$ organoids display defects in branching activity (Fig. 2-2 F). Hence, in the presence of a permissive ECM environment, MMPs are not necessarily required to support morphogenic programs.

While *in vitro* models provide useful tools for dissecting cell function, isolated epithelial cell-based model systems are unlikely to recapitulate the morphogenic programs occurring *in vivo* where the surrounding mesenchyme play active roles in branching (Nelson and Larsen, 2015; Varner and Nelson, 2014). As such, we next sought to directly assess requirements for MT1-MMP during mammary gland morphogenesis *in vivo.* Though the morbid status of *Mt1-mmp*$^{-/-}$ mice and their failure to undergo sexual maturation preclude efforts to analyze late stage mammary gland development (Holmbeck et al., 1999; Zhou et al., 2000), the newly described P0-P10 program provides a unique window of opportunity for such analyses. Interestingly, mammary glands harvested from P0 *Mt1-mmp*$^{-/-}$ mice generate branching ductal networks comparable to those of wild-type and *Mt1-mmp*$^{+/-}$ littermates (Fig. 2-3 A,B). More remarkably, at P5 and P10, *Mt1-mmp* $^{-/-}$ mice mount a mammary gland branching program similar, if not identical, to those observed in *Mt1-mmp*$^{+/+}$ or *Mt1-mmp*$^{+/-}$ littermates (Fig. 2-3 C-F). Further, immunohistologic assessments of *Mt1-mmp*$^{-/-}$ mammary gland sections reveal no differences in the expression or organization of CK18, CK14 or α-SMA from P0 through P10 (Fig. 2-4 A,B). Likewise, epithelial cell organization, as assessed by the apical distribution of the tight junction protein, zonula occludens (ZO)-1, or the adherens junction marker, E-cadherin (Ewald et al., 2008; Ewald et al., 2012; Inman et al., 2015), is indistinguishable between *Mt1-mmp*$^{+/+}$, *Mt1-mmp*$^{+/-}$ or *Mt1-mmp*$^{-/-}$ mice (Fig. 2-4 B). While MT1-MMP has previously been implicated in the proliferation-associated signaling cascades that drive branching morphogenesis (Gutierrez-Fernandez et al., 2015; Riggins et al., 2010), neither Ki67 expression, TUNEL staining nor senescence are affected in *Mt1-mmp*$^{-/-}$ glands (Fig. 2-4 C,D). Finally, deleting MT1-MMP did not discernably alter basement membrane or interstitial matrix assembly, respectively, as reflected in comparable type IV collagen and laminin staining

(Fig. 2-4 E) or levels of type I collagen as assessed by immunofluorescence and Sirius Red staining (Fig. 2-4 F).

Neonatal mammary gland branching morphogenesis also coincides with the increased expression of two secreted members of the MMP gene family that have been previously implicated in mammary gland branching and development, i.e., *Gelatinase A/Mmp2* and *Stromelysin-1/Mmp3* (Correia et al., 2013; Kessenbrock et al., 2013; Lochter et al., 1997; Wiseman et al., 2003; Witty et al., 1995) (Fig. 2-S1 A,C). Further, MT1-MMP can activate MMP2 *in vivo,* a proteinase thought to mediate MT1-MMP function and compensate partially for *Mt1-mmp* deficiency (Itoh, 2015; Oh et al., 2004). Nevertheless, as previously described, $Mmp2^{-/-}$ mammary glands develop comparable branching structures relative to those of littermate controls in pre-pubertal mice (Fig. 2-S1 B) (Wiseman et al., 2003). Further, while recent reports have identified critical protease-dependent as well as protease-independent roles for MMP3 in mammary gland development (Correia et al., 2013; Kessenbrock et al., 2013; Lochter et al., 1997; Wiseman et al., 2003; Witty et al., 1995), $Mmp3^{-/-}$ mammary glands establish branching structures that are comparable in length and complexity to those of $Mmp3^{+/+}$ and $Mmp3^{+/-}$ littermates with normal distribution of luminal epithelial and myoepithelial cell populations (Fig. 2-S1 D,E).

Neonatal mammary gland branching proceeds in the absence of MT2-MMP.

Membrane-anchored MT2-MMP is structurally related to MT1-MMP, enriched in the mammary epithelium (Szabova et al., 2005), and has recently been implicated in branching morphogenesis ex vivo (Rebustini et al., 2009). Using $Mt2\text{-}mmp^{lacZ}$ knock-in mice (Fig. 2-5 A), *Mt2-mmp* expression can be detected throughout the mammary epithelial cell compartment at birth as well as through P10 (Fig. 2-5 B,C), a result further corroborated by up-regulated *Mt2-mmp*

levels (Fig. 2-5 D). *Mt2-mmp*-targeted mice were therefore employed to address the requirement for *Mt2-mmp* in branching morphogenesis wherein exons 4 and 5 of the catalytic domain were flanked by loxP sites (Fig. 2-S2 A), and deleted by breeding *Mt2-mmp*$^{flox/flox}$ mice with EIIA-Cre mice. Crosses between *Mt2-mmp*$^{+/-}$ mice generated *Mt2-mmp*$^{+/+}$, *Mt2-mmp*$^{+/-}$ and *Mt2-mmp*$^{-/-}$ mice in normal Mendelian ratios, yielding a total of 68 *Mt2-mmp*$^{+/+}$, 146 *Mt2-mmp*$^{+/-}$ and 70 *Mt2-mmp* $^{-/-}$ mice in 284 total offspring; and *Mt2-mmp*$^{-/-}$ mice remained similarly viable throughout adulthood. Importantly, germline deletion of *Mt2-mmp* did not affect *Mt1-mmp* expression (Fig. 2-5 E), ruling out any compensatory interactions between these closely related MMP family members.

In vivo assessments of *Mt2-mmp*$^{+/+}$, *Mt2-mmp*$^{+/-}$ and *Mt2-mmp*$^{-/-}$ mammary glands revealed correspondingly similar branching structures as assessed by carmine staining at birth as well as P10 (Fig. 2-5 F-G). Similarly, explanted *Mt2-mmp*$^{-/-}$ and *Mt2-mmp*$^{+/+}$ mammary epithelial cell organoids in 3-D type I collagen or Matrigel mounted comparable branching programs (Fig. 2-5 H,I). Further, *Mt2-mmp*$^{-/-}$ mammary epithelial ducts display an unaltered pattern of CK18, CK14, αSMA and E-cadherin expression (Fig 2-S2 B-D). Though MT2-MMP has been reported to regulate the proliferative and apoptotic responses required for epithelial morphogenesis (Abraham et al., 2005; Rebustini et al., 2009), Ki67 as well as apoptotic levels are unchanged in the absence of *Mt2-mmp* (Fig. 2-S2 E). Similarly, while MT2-MMP can function as a basement membrane remodeling enzyme during branching morphogenesis *ex vivo* (Rebustini et al., 2009) as well as a type I collagenase (Chun et al., 2004; Hotary et al., 2000), neither type IV collagen, laminin nor type I collagen levels are affected in the absence of *Mt2-mmp* (Fig. 2-S2 F).

Differential roles for MT1-MMP and MT2-MMP in mammary gland development.

At this juncture, a preferential focus on the roles of MT1-MMP and MT2-MMP in controlling tissue-invasive activity and branching morphogenesis was predicated on the basis of a number of previously established precedencies – largely performed *in vitro*. In order to probe for unanticipated functional roles of MT1-MMP and MT2-MMP in the early postnatal mammary gland, we analyzed the transcriptome of the ductal networks and associated stroma in wild-type versus null mice. In *Mt1-mmp*$^{-/-}$ mice, gene expression profiling revealed >250 differentially expressed genes relative to *Mt1-mmp*$^{+/+}$ mammary tissue (using a 2-fold enrichment cutoff), with functional annotation clusters bridging 16 different gene ontology (GO) categories, including many associated with the epithelial cell compartment, such as cell adhesion, endocytosis, responses to endogenous stimuli, and G protein-coupled signaling cascades (DAVID Bioinformatics Resource, NIH, p-value/Ease < 0.05; Fig. 2-6 A). Of note, gene expression profiling did not uncover significant changes in the proliferation- or senescence- associated signaling cascades highlighted in earlier work (Gutierrez-Fernandez et al., 2015; Riggins et al., 2010). However, given the number of genes associated with epithelial cell adhesion complexes and cytoskeletal organization [e.g., *Calmin*, *Plakophilin* 2, *Folliculin;* (Arimoto et al., 2014; Khabibullin et al., 2014; Loo et al., 2013)] , we examined mammary ducts recovered from P10 *Mt1-mmp*$^{+/+}$ and *Mt1-mmp*$^{-/-}$ mice by transmission electron microscopy (TEM). Interestingly, *Mt1-mmp*$^{-/-}$ ducts form more intimate cell-cell junctions with a marked increase in the number of apical microvilli (Fig. 2-S3 A,B) – despite mounting a normal branching program. By contrast, the transcriptome of *Mt2-mmp*$^{-/-}$ mammary tissues uncovered only ~30 differentially expressed genes whose classification lacked any major associations with mammary epithelium-related GO categories (Fig. 2-S4 A). Accordingly, TEM analyses of *Mt2-mmp*$^{-/-}$ ducts appear largely normal

(Fig. 2-S4 B,C). Hence, while these data confirm active roles for MT1-MMP and MT2-MMP in early postnatal mammary gland development, the observed transcriptional changes do not significantly impact ductal network organization or the penetration of the surrounding mesenchymal tissues.

Independent of the roles played by MT1-MMP or MT2-MMP in the mammary epithelial compartment, analyses of differentially expressed transcript profiles indicate that both MT-MMPs exert significant effects on the mammary gland stroma. In *Mt1-mmp*$^{-/-}$ mice, the down-regulated GO categories with the highest enrichment scores are tightly linked with the mammary gland fat pad, with decreased expression of multiple transcripts associated with sterol and fatty acid metabolism, lipid biosynthesis and adipocyte maturation (Fig. 2-6 B). In tandem with these changes, mammary gland adipocytes display a marked 2-fold decrease in overall size (mean adipocyte diameter of 43.3 µm ± 1.01 µm in *Mt1-mmp*$^{+/+}$ mammary glands versus 22.8 µm ± 1.60 µm in *Mt1-mmp*$^{-/-}$ mammary glands (n=3 per genotype, p=0.0004)) (Fig. 2-6 C). In an almost diametrically opposed fashion, the metabolic genes repressed in *Mt1-mmp*$^{-/-}$ tissue are either upregulated or unchanged in *Mt2-mmp*-targeted mice as most clearly evidenced by the differential expression of the adipokine, *Leptin* (Fig. 2-6 D) (Wang et al., 2015; Wu et al., 2013). Unexpectedly, transcriptome analysis of *Mt2-mmp*$^{-/-}$ mammary tissue further reveals a marked *increase* in a core suite of positive regulators of brown or induced brown (beige) adipocytes (Fig. 2-S4 A) – thermogenic adipocytes that can be identified based on their restricted expression of uncoupling protein-1 (UCP1) (Wang et al., 2015; Wu et al., 2013). Indeed, whereas adipocyte size is unaffected in many regions of the *Mt2-mmp*$^{-/-}$ mammary glands, large clusters of small, multilocular adipocytes – the hallmark of beige/brown fat – are found throughout the knockout tissues in 4 of 6 animals characterized (Fig. 2-6 E). As confirmed by qPCR, *Mt2-mmp*$^{-/-}$ mammary

tissues display a ~5-fold increase in *Ucp1* transcript levels as well as increased expression of multiple genes required for mitochondrial biogenesis, adipocyte thermogenesis and *Ucp1* induction, including *Dio2*, *Fabp3*, *Prdm16* and *Pgc1α* (Cohen et al., 2014; Marsili et al., 2011; Vergnes et al., 2011; Wu et al., 2013) (Fig. 2-6 F). Cross-sections of *Mt2-mmp*$^{-/-}$ mammary glands further document increased UCP1 protein levels (Fig. 2-6 G). Finally, corroborating the divergent roles of MT1-MMP and MT2-MMP in mammary fat pad development, brown/beige-associated transcripts or protein levels remain unchanged in *Mt1-mmp*$^{-/-}$ glands (Fig. 2-6 G,H). Hence, while MT1-MMP promotes white fat-associated adipogenesis in the developing mammary gland, MT2-MMP alternatively serves as an endogenous suppressor of beige/brown fat production.

Discussion.

MT1-MMP and MT2-MMP have been reported to play roles in a range of morphogenesis-associated processes, including cell adhesion and motility, invasion, proliferation, energy metabolism, senescence, the proteolytic processing of growth factors, cytokines and chemokines as well ECM remodeling (Ager et al., 2015; Alcaraz et al., 2011; Barbolina and Stack, 2008; Bonnans et al., 2014; Brownfield et al., 2013; Chun et al., 2004; Fahlman et al., 2014; Fu et al., 2013; Itoh, 2015; Kajita et al., 2001; Koshikawa et al., 2000; Koziol et al., 2012; Mori et al., 2009; Rebustini et al., 2009; Rowe and Weiss, 2009; Sabeh et al., 2009; Sakamoto et al., 2014; Shimizu-Hirota et al., 2012; Simian et al., 2001; Tang et al., 2013; Taylor et al., 2015; Weaver et al., 2014; Yana et al., 2007). Consistent, in part, with previous reports linking MT-MMPs with epithelial cell tissue-invasive and branching programs (Alcaraz et al., 2011; Bonnans et al., 2014; Brownfield et al., 2013; Mori et al., 2009; Rebustini et al., 2009; Weaver et al., 2014), we find that MT1-MMP, but not MT2-MMP, is required for mammary epithelial organoid branching through 3-D type I

collagen barriers *in vitro*. However, in contrast to earlier findings (Mori et al., 2009), we find that MT1-MMP-expressing mammary epithelial cells in 3D culture lack a competitive sorting advantage relative to MT1-MMP-null epithelial cells. Further, when *Mt1-mmp*$^{-/-}$ or *Mt2-mmp*$^{-/-}$ epithelial organoids are embedded in Matrigel, a hydrogel that recapitulates the assembly of basement membrane-like structures (Ewald et al., 2008; Ewald et al., 2012; Lo et al., 2012), morphogenesis proceeds in an unperturbed fashion – even in the presence of a pan-specific MMP inhibitor. Given these divergent outcomes, and the fact that model systems do not fully recapitulate mammary gland architecture or stromal cell interactions (Nelson and Larsen, 2015), we turned to the *in vivo* setting.

Unlike *in vitro* culture conditions, the primordial mammary ducts of newborn female mice are encased in a coat of type IV collagen and laminin that is surrounded by low levels of type I collagen. Nevertheless, given the broad substrate repertoire of MT1-MMP and the multiple biological activities that have been assigned to its functions (Ager et al., 2015; Alcaraz et al., 2011; Barbolina and Stack, 2008; Bonnans et al., 2014; Brownfield et al., 2013; Chun et al., 2004; Fahlman et al., 2014; Fu et al., 2013; Itoh, 2015; Kajita et al., 2001; Koshikawa et al., 2000; Koziol et al., 2012; Mori et al., 2009; Rebustini et al., 2009; Rowe and Weiss, 2009; Sabeh et al., 2009; Sakamoto et al., 2014; Shimizu-Hirota et al., 2012; Simian et al., 2001; Tang et al., 2013; Taylor et al., 2015; Weaver et al., 2014; Yana et al., 2007), we were surprised to find that deleting the proteinase *in vivo* exerted little, if any, effect on morphogenesis or ductal invasion through the mesenchyme. Likewise, despite the *ex vivo* requirement for MT2-MMP in submandibular gland proliferation, matrix remodeling and branching (Rebustini et al., 2009), mammary glands from *Mt2-mmp*-targeted mice and littermate controls displayed similar ductal networks at birth as well as P10. While our measurements may lack sufficient sensitivity to detect transient differences in

epithelial cell sorting or organization during branching, the overall similarities of the ductal networks generated in *Mt1-mmp*$^{-/-}$ or *Mt2-mmp*$^{-/-}$ mice suggest that any *in vivo* defects related to branching or tissue-invasive activity are, at best, subtle. Of note, a subset of the *Mt1-mmp*$^{-/-}$ mice (i.e., 3 of 15 total) displayed an unusually reduced body size relative to littermate controls with partial mammary gland defects noted at P10 (i.e., mammary ducts branched comparably, but appeared more primitive in their architecture). However, given the reduced size and feeding of this cohort and the known influence of nutrient deprivation on tissue morphogenesis (Londhe et al., 2013), we did not include these animals in our analyses.

Despite the retention of mammary gland branching programs in *Mt1-mmp*$^{-/-}$ or *Mt2-mmp*$^{-/-}$ mice, we did not directly rule out a potential compensatory role for MT1-MMP and MT2-MMP in postnatal morphogenesis. As *Mt1-mmp*/*Mt2-mmp* double-null mice die during embryogenesis (Szabova et al., 2010), we have alternatively targeted both proteinases selectively in the mammary epithelial compartment, but preliminary studies demonstrate that branching morphogenesis nevertheless proceeds in a normal fashion from birth through adulthood (Chapter 3). While MT1-MMP and MT2-MMP have previously been shown to endow neoplastic cells with the ability to degrade and transmigrate BM barriers (Ota et al., 2009), it should be stressed that there is no evidence that mammary epithelial cells dissolve their underlying BM during morphogenesis *in vivo.* Indeed, during postnatal development, mammary epithelial cells remain separated from the periductal type I collagen meshwork by a patent BM while time-lapse analyses of ductal invasion programs fail to detect membrane- based protrusions extending into the ECM at the advancing front (Ewald et al., 2008; Ewald et al., 2012; Williams and Daniel, 1983). More recently, Yamada and colleagues concluded that basement membranes undergo proteolytic remodeling during branching morphogenesis *ex vivo* (Harunaga et al., 2014), but efforts to implicate MMPs in this

process were confined to the use of BB-94, an inhibitor that not only targets all MMP family members, but also ADAM/ADAM-TS family members that play critical roles in proteoglycan turnover as well as the shedding of growth factors critical to morphogenesis (Rowe and Weiss, 2009). Indeed, in their studies, TIMP-2, a potent MMP inhibitor (Chun et al., 2004; Sabeh et al., 2009), did not affect branching (Harunaga et al., 2014). Finally, we note that the early postnatal branching programs tracked in our studies were not mediated by other MMP family members implicated in branching organ development, including MMP2 or MMP3 (Correia et al., 2013; Kessenbrock et al., 2013; Wiseman et al., 2003).

Given the paucity of obvious structural defects in ductal morphogenesis found in *Mt1-mmp* $^{-/-}$ or *Mt2-mmp*$^{-/-}$ mice, we interrogated the mammary gland transcriptomes of the knockout tissues. Though MT1-MMP and MT2-MMP share considerable sequence and structural homology (Itoh, 2015; Tanaka et al., 1997), effects on mammary gland gene expression were notably distinct. For example, *Mt1-mmp*$^{-/-}$, but not *Mt2-mmp*$^{-/-}$, mammary glands increased expression of a number of cell adhesion/cytoskeleton-associated transcripts with *Mt1-mmp*$^{-/-}$ ducts displaying subtle changes in epithelial cell-cell junctions and apical microvilli. While further work will be needed to define the functional consequences of these changes or provide mechanistic insights into their origins, the observed structural alterations highlight the fact that MT1-MMP does, in fact, affect mammary gland development, but not in a fashion that impacts branching-associated invasion programs per se. In contrast with the epithelial cell-associated changes observed in *Mt1-mmp*$^{-/-}$ mammary glands, the effects of deleting *Mt2-mmp* were far more subtle with only a small subset of genes affected. We are, however, unable to assess catalytic activity of MT2-MMP per se as specific antibodies capable of distinguishing between the pro- and active forms of the enzyme have not been generated. Nevertheless, it is intriguing that the breast cancer-associated transcripts, γ-

synuclein (Ahmad et al., 2007) and *Peroxiredoxin 2* (Stresing et al., 2013), are among the most significantly affected (i.e., ~5-fold increase and ~7-fold decrease, respectively).

In the mammary gland, the adipocyte-rich stroma plays important roles in regulating morphogenetic responses (Hovey and Aimo, 2010; Inman et al., 2015). Intriguingly, early in postnatal life, the mammary gland-associated pool of adipocytes contains both white and brown fat (Gouon-Evans and Pollard, 2002; Master et al., 2002), but the factors that control their differential expression have not been defined previously. Independent of the effects of MT1-MMP and MT2-MMP on mammary epithelial cells, their more global and differential effects on mammary fat pad development were unanticipated. *Mt1-mmp* targeting alone triggers a widespread down-regulation of transcripts associated with adipogenesis (Wang et al., 2015). By contrast, an Mt2-mmp-null status exerts little effect on white fat development, but instead strongly enhances the formation of brown and/or beige fat as evidenced by the increased expression of a cohort of thermogenic genes (Wu et al., 2013). Our lab has previously established roles for MT1-MMP in coordinating adipocyte maturation *in vivo*, as evidenced by the aborted white adipose tissue development in the dermal and inguinal adipose tissue depots of male *Mt1-mmp*$^{-/-}$ mice (Chun et al., 2006), but the role of MT1-MMP in the mammary gland stromal fat pad has not been previously appreciated. Indeed, we have recently reported that *Mt1-mmp*$^{-/-}$ mesenchymal stem cells preferentially commit to the adipocyte lineage with resultant increases in bone marrow adiposity (Tang et al., 2013). At this juncture, we posit that the incongruous functional consequences of *Mt1-mmp* deletion in bone marrow versus subcutaneous and mammary gland adipocytes likely derives from reported differences in progenitor cell populations and local tissue environments (Gupta et al., 2012; Tran et al., 2012)

The discovery of a heretofore unrecognized early postnatal mammary gland branching program has provided us with a new platform to dissect the roles of a select group of MMPs in morphogenesis. Recent studies have emphasized the ability of secreted as well as membrane-anchored MMPs to cleave hundreds of intracellular, cell surface-associated or extracellular substrates (Barbolina and Stack, 2008; Fahlman et al., 2014; Fu et al., 2013; Itoh, 2015; Koziol et al., 2012; Rowe and Weiss, 2009). Given these results, it is surprising, if not perplexing, that global targeting of *Mt1-mmp* or *Mt2-mmp* – as well as *Mmp2* and *Mmp3* – did not derail ductal invasion programs or morphogenesis to a more striking degree. Indeed, while MT1-MMP has been implicated – to varying degrees – in early lung, kidney and submandibular gland development, these findings do not extend to mammary gland development (Atkinson et al., 2005; Oblander et al., 2005; Riggins et al., 2010). While results such as ours are often countered by the argument that the mouse genome encodes more than 20 *Mmp* family members, virtually all of these genes have now been targeted, and with the exception of *Mt1-mmp*, each knockout gives rise to viable mice with normal lifespans (Bonnans et al., 2014; Holmbeck et al., 1999; Itoh, 2015; Rowe and Weiss, 2009; Zhou et al., 2000). Further, though redundant and compensatory pathways may exist, no direct experimental evidence has been forwarded to support this contention (Rowe and Weiss, 2009). The fact that only *Mt1-mmp* targeting causes a dramatic increase in the morbidity and mortality of knockout mice (Holmbeck et al., 1999; Zhou et al., 2000), and that dual targeting of *Mt1-mmp* and *Mt2-mmp* results in an embryonic lethal phenotype (Szabova et al., 2010), has, predictably, catalyzed increased efforts to identify the key functions of these proteinases. Recent reports emphasize roles for MT1-MMP and MT2-MMP in events ranging from type I collagen deposition and cellular senescence to TGFβ activation (Ager et al., 2015; Gutierrez-Fernandez et al., 2015; Taylor et al., 2015) – any one of which might have been posited to perturb

branching morphogenesis. As evidenced here, predicted effects fall short of experimental outcomes. Clearly, MT1-MMP and MT2-MMP *do* exert complex effects on mammary gland development, but the observed changes in function are, for the most part, novel and unanticipated from the perspective of current paradigms.

Experimental procedures.

Mouse strains.

Mt1-mmp$^{lacZ/+}$ mice (Yana et al., 2007) were bred onto a C57BL/6J background (Jackson Laboratory, 000664). To generate *Mt2-mmp*$^{lacZ/+}$ mice, C57BL/6J *Mt2-mmp*$^{lacZ/+}$ ES cells clones from the UC Davis KOMP Repository (KOMP) [MGI allele: *Mmp15tm1a* (KOMP) wtsi, clone: EPD0097_3_B09] were introduced into albino C57BL/6J host blastocysts. Chimeras were mated with C57BL/6J mice to test for germline transmission. *Mt2-mmp*$^{lacZ/+}$ mice were bred and maintained on a C57BL/6J background. The *Mt1-mmp*$^{+/-}$ mice (Swiss Black background; (Holmbeck et al., 1999) were maintained on an outbred Swiss Black background (Charles River, NIHBL(S). *Mmp3*$^{-/-}$ mice (C57BL/6J background) and *Mmp2*$^{-/-}$ mice (Swiss Black background) were genotyped as described (Itoh et al., 1997). To generate *Mt2-mmp/Mmp15* global knockout (*Mt2-mmp*$^{-/-}$) mice, 129/SVJ ES cells were electroporated with a targeting vector for *Mmp15* containing a neomycin selection cassette flanked by FRT sites wherein exons 4 and 5 of the catalytic domain were floxed by loxP sites (Fig. 2-S2 A). Following neomycin selection, ES cell recombinants were injected into gestation day E3.5 C57BL/6J blastocysts and subsequently injected into the uteri of pseudo-pregnant FVB mice. Male chimeras were mated to C57BL/6J females, and heterozygous agouti offspring carrying the *Mmp15*^{flox} allele were mated to C57BL/6J FlpE mice to remove the neomycin selection cassette. The resultant *Mmp15*$^{fl/fl}$ mice were crossed

to C57BL/6J EIIA-Cre mice for germline deletion of *Mmp15*, with *Mmp15*$^{+/-}$ mice backcrossed into C57BL/6J mice (n>10 generations). All mouse work was performed with IACUC approval at the University of Michigan.

Mammary organoid isolation and culture.

Organoids were prepared from inguinal mammary glands of P10 mice as described (Fata et al., 2007). Mammary epithelial organoids were then embedded in 2.2 mg/ml acid-extracted rat-tail type I collagen (Sabeh et al., 2009) for 3-D culture in 24-well plates with DMEM/F12 media containing 0.1 mM nonessential amino acids (GIBCO), 0.3 mg/ml L-glutamine, 1X ITS (Sigma, 13146), 10 µg/ml insulin (GIBCO, 12585-014), penicillin and streptomycin, with 50 ng/ml FGF-2 (Simian et al., 2001). Media was changed every 2-3 d over 5-8 d culture periods.

Mammary gland whole mount preparation, imaging and morphometric analysis.

Inguinal mammary glands were harvested, mounted on glass slides, stained with Carmine Alum, and processed (Lu et al., 2008). Whole mounts were imaged (Leica MZFLIII dissecting microscope) with Adobe Photoshop and ImageJ used for image processing (Lu et al., 2008).

RNA extraction from intact mammary gland tissue and gene expression analysis.

Inguinal mammary gland tissue was flash frozen in liquid nitrogen, and homogenized in 1 mL TRIzol (Ambion, Life Technologies). Total RNA was extracted and purified using QIAGEN RNeasy Mini-kit columns (QIAGEN, 74104). RNA quality was confirmed using an Agilent 2100 Bioanalyzer and samples profiled on Affymetrix Mouse MG–430 PM expression array strips. Expression values for each probe set were calculated using a robust multi-array average (RMA)

(Irizarry et al., 2003) and filtered for genes with a greater than 2-fold change. The Affymetrix microarray data are deposited in the NCBI Gene Expression Omnibus (GEO) database (Edgar et al., 2002) and available through GEO Series accession number GSE77679 (http://www.ncbi.nlm.nih.gov/geo/query/acc.cgi?acc=GSE77679). Complementary cDNA was prepared with the Invitrogen SuperScript II First-Strand Synthesis System (11904-018). Quantitative reverse-transcription PCR was performed with SYBR Green (Applied Biosystems) using *Arbp*/*Rplp0* for reference gene expression. Data reported as the mean expression levels with error bars representing the standard error (SEM). p values were calculated with an unpaired t-test with two tails.

Primers.

QPCR primers are provided in Table 2-1. Genotyping primers are provided in Table 2-2.

LacZ staining.

Inguinal *Mt1-mmp*^{lacZ} mammary glands were fixed at 4^{o}C in PBS containing 2% paraformaldehyde and 0.2% glutaraldehyde. *Mt2-mmp*^{lacZ} glands were alternatively fixed in 4% paraformaldehyde. Tissues were either transferred to 30% sucrose/PBS (w/v) for frozen sections, or incubated for 18-24 h in PBS containing 4 mM potassium hexacyanoferrate (III), 4 mM potassium hexacyanoferrate (II) trihydrate, 2 mM $MgCl_2$, 0.2% NP-40, 0.1% sodium deoxycholic acid and 1 mg/ml Xgal. Stained tissues and whole mounts were post-fixed with 10% formalin-phosphate.

Immunofluorescence, immunohistochemistry and morphometric analysis.

Mammary gland tissue was fixed in 10% formalin-phosphate at 4º C overnight and either dehydrated in an ethanol/paraffin series for paraffin embedding or transferred to 30% (w/v) sucrose/PBS for OCT embedding. Sections were permeabilized with 0.5% Triton X-100/PBS, and blocked for 2 h prior to primary antibody addition. Samples were incubated overnight at 4ºC with antibodies directed against [ZO-1 (Invitrogen, 617300, 2.5 µg/ml), E-cadherin (BD Transduction Laboratories, 610181, 1/400), Cytokeratin-14 (Covance, PRB-155P, Clone AF64, 1/400), Cytokeratin-18 (Abcam, ab668, 1/150), α-smooth muscle actin (Abcam, ab5694, 1/400), or UCP1 (Alpha Diagnostic International, UCP11-A, 200 ng/ml)]. For ECM staining, frozen sections were incubated in blocking buffer (10% FBS/1% BSA/PBS) and incubated with primary antibodies directed against type IV collagen (Millipore, AB-769, 1/40) (Nguyen-Ngoc et al., 2012), laminin (Sigma-Aldrich, L9393, 1/250), or type I collagen (Abcam, ab34710, 1/250) overnight at 4ºC. Following primary antibody, sections were incubated with Alexa-488 or Alexa-594-conjugated secondary antibodies (Invitrogen Molecular Probes). Nuclear counter-staining was carried out with either Toto3 (1/200, Invitrogen Molecular Probes) or 2 µg/ml 4, 6-diamidino-2-phenylindole (DAPI). All fluorescence images were acquired with an Olympus FluoView FV500 laser scanning confocal microscope and analyzed with Adobe Photoshop and ImageJ software. For immunohistochemistry, endogenous peroxidase activity was blocked with H_2O_2 and tissues sections developed with the Vectastain ABC (Vector Laboratories, PK-6100) and DAB kits (Vector Laboratories, SK-4100). ImageJ was used to measure the diameter of n>20 adipocytes per 40X field in H&E-stained paraffin cross-sections.

Tissue preparation for TEM.

Samples were fixed (1% glutaraldehyde/1% tannic acid/0.1 M Sorensen's buffer, pH 7.2) and post-fixed with 1% osmium tetroxide as described (Abrahamson and Perry, 1986) prior to embedding in EMbed 812 epoxy resin (Electron Microscopy Sciences). Thin sections (70 nm) were post-stained with uranyl acetate and Reynolds Lead Citrate, and imaged with a JE0L JEM-1400 Plus electron microscope. Images were recorded digitally using a Hamamatsu ORCA-HR digital camera system, operated using AMT software (Advanced Microscopy Techniques Corp., Danvers, MA). ImageJ was used to quantify average number of microvilli per μm from $n > 5$ fields per sample and $n = 3$ per genotype. Results are expressed as mean ± SEM.

Table 2-1.

Gene	**Forward Primer**	**Reverse Primer**
Gapdh	5’-TGAAGCAGGCATCTGAGGG-3’	5’-CGAAGGTGGAAGAGTGGGAG-3’
Arbp	5’-CACTGGTCTAGGACCCGAGAA-3’	5’-AGGGGGAGATGTTCAGCATGT-3’
Mmp2	5’-TCTGGAGCGAGGATACCCCAA-3’	5’-TTCCAGGAGTCTGCGATGAGC-3’
Mmp3	5’-GTT CCT GAT GTT GGT GGC TT-3’	5’-AGC CTC TCC TTC AGA GAT CC-3’
Mmp15	5’-ACATGTCCACCATGCGCTCT-3’	5’-TACCATGATGTCAGCCTCC-3’
Mmp14	5’-CTGCCATTGCCGCCATGCAAAA-3’	5’-TGGCGTGGCACTCTCCCATACT-3’
Ucp1	5’-AGGCTTCCAGTACCATTAGGT-3’	5’-CTGAGTGAGGCAAAGCTGATTT-3’
Dio2	5’-AATTATGCCTCGGAGAAGACCG-3’	5’-GGCAGTTGCCTAGTGAAAGGT-3’
Fabp3	5’-ACCTGGAAGCTAGTGGACAG-3’	5’-TGATGGTAGTAGGCTTGGTCAT-3’
Prdm16	5’-CCACCAGACTTCGAGCTACG-3’	5’-ACACCTCTGTATCCGTCAGCA-3’
Pgc1a	5’-CCACTTCAATCCACCCAGAAAG-3’	5’-TATGGAGTGACATAGAGTGTGCT-3’
Leptin	5’-GAGACCCCTGTGTCGGTTC-3’	5’-CTGCGTGTGTGAAATGTCATTG-3’

Table 2-1. qPCR Primers.

Table 2-2.

Gene	**Forward Primer(s)**	**Reverse Primer(s)**	**PCR Product Size**
Mmp14^{WT}	5'-TAGGCCTGGAACATTCTAACGATC-3'	5'-CTTTGTGGGTGACCCTGACTTGC-3'	900bp
Mmp14^{KO}	5'-TGCGAGGCCAGAGGCCACTTGTGT-3'	5'-CTTTGTGGGTGACCCTGACTTGC-3'	950bp
Mmp14^{lacZ} (+)	5'-ACCTGCGTGCAATCCATCTTG-3'	5'-ATGATGGCGGAGGGATCGTTAG-3'	350bp
Mmp14^{lacZ} (-)	5'-TGAGGTGGAAAACACGACCAG-3'	5'-ATGATGGCGGAGGGATCGTTAG-3'	180bp
Mmp15^{WT}	5'-CCGCCACCAAGCCTCACTGTCT-3'	5'-AAAGCCACCCACGCCATCAAAC-3'	400bp
Mmp15^{KO}	5'-CGCCACCAAGCCTCACTGTCT-3'	5'-AATTGCTGGGGATGGAGGAAGGTA-3'	470bp
Mmp15^{lacZ}	5'-GAGATGGCGCAACGCAATTAATG-3'	5'-TGCACGTCCCATTCTCATGC-3'	292bp
Mmp2^{WT}	5'-GTGCTACTGCAGGATAAACTGATG-3'	5'-CCGGGACAGGAACGTACTGGGTTC-3'	794bp
Mmp2^{KO}	5'-GCGCCTACCGGTGGATGTGGAATGTGT GCG-3'	5'-CCGGGACAGGAACGTACTGGGTTC-3'	310bp
Mmp3^{WT}	5'-ACCGGATTTGCCAAGACAGAGTG-3'	5'-GCATCTCCATTAATCCCTGGTCC-3'	325bp
Mmp3^{KO}	5'-AGGATCTCCTGTCATCTCACCTTGCTC CTG-3'	5'-AAGAACTCGTCAAGAAGGCGATAGAA GGCG-3'	492bp

Table 2-2. Genotyping Primers.

Fig. 2-1.

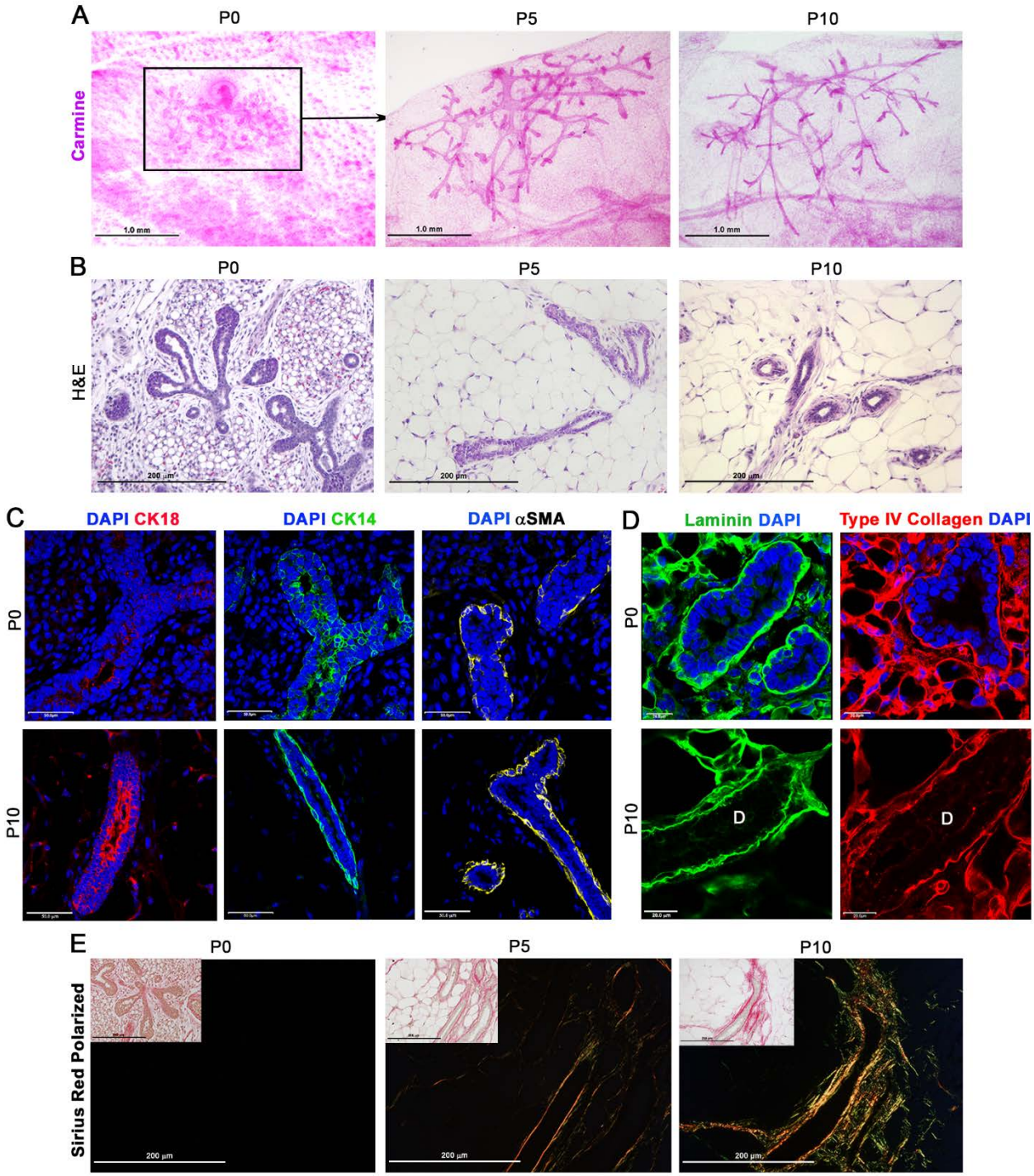

Fig. 2-1. Early postnatal mammary gland morphogenesis program.
(A) Carmine-stained whole mounts of mammary glands isolated from female mice at P0, P5 and P10 (scale bars = 1.0 mm). (B) H&E staining of cross-sections of mammary glands at P0, P5 and P10 (scale bar = 200 μm). (C) Immunofluorescence of cytokeratin-18 (CK18), cytokeratin-14

(CK14), and α-smooth muscle actin (α-SMA) in P0 versus P10 mammary glands with DAPI-mediated nuclear counter-staining (scale bars = 50.0 μm). (D) Immunofluorescence of laminin and type IV collagen in P0 and P10 mammary glands with DAPI counter-staining (scale bars = 50.0 μm). (E) Polarized light images of Sirius Red staining of P0, P5 and P10 mammary gland cross-sections. Insets show the corresponding bright-field images (scale bars = 200 μm). All images are representative of 3 replicates.

Fig. 2-2.

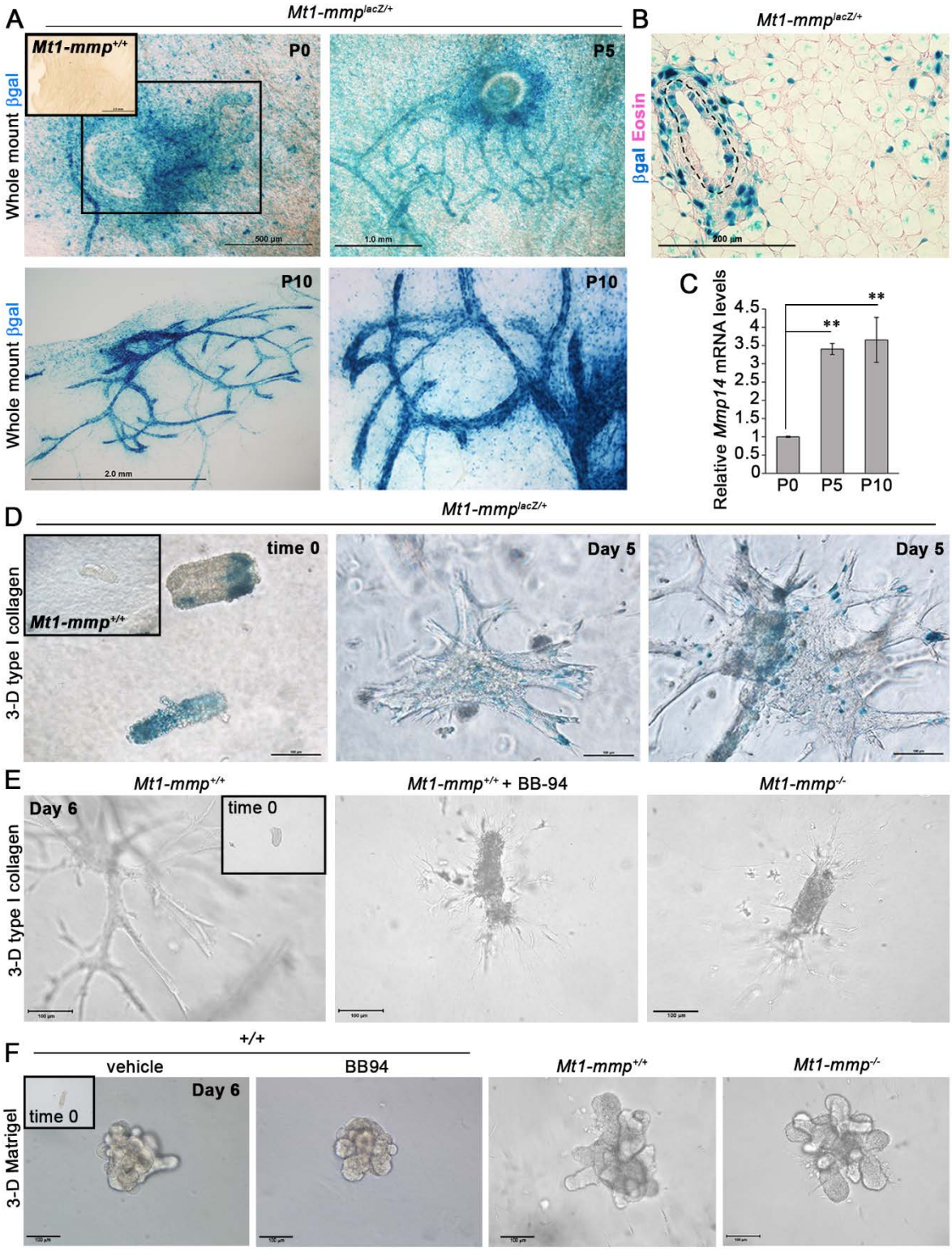
A
Mt1-mmp lacZ/+
Mt1-mmp +/+
P0
P5
Whole mount βgal
500 μm
1.0 mm
P10
P10
Whole mount βgal
2.0 mm
B
Mt1-mmp lacZ/+
βgal Eosin
200 μm
C
Relative Mmp14 mRNA levels
4.5
4
3.5
3
2.5
2
1.5
1
0.5
0
**
**
P0
P5
P10
D
Mt1-mmp lacZ/+
3-D type I collagen
Mt1-mmp +/+
time 0
Day 5
Day 5
E
Mt1-mmp +/+
Mt1-mmp +/+ + BB-94
Mt1-mmp -/-
3-D type I collagen
Day 6
time 0
F
+/+
vehicle
BB94
Mt1-mmp +/+
Mt1-mmp -/-
3-D Matrigel
time 0
Day 6

Fig. 2-2. *In vitro* mammary epithelial branching requires MT1-MMP.
(A) LacZ staining of mammary gland whole mounts isolated from *Mt1-mmp*$^{lacZ/+}$ mice at P0, P5, and P10 (scale bars = 500 µm, 1.0 mm, and 2.0 mm, respectively). The inset shows LacZ staining of the wild-type littermate. (B) Paraffin cross-section through P10 *Mt1-mmp*$^{lacZ/+}$ mammary gland with Eosin counterstaining. Images shown in A, B are representative of 3 replicates. (C) qPCR of *Mt1-mmp* at P0, P5 and P10. Results are expressed as mean expression levels ± SEM of P0 (n=4), P5 (n=3) and P10 (n=4) relative to *Arbp*. **p<0.005, as calculated with an unpaired t-test. (D) LacZ staining of *Mt1-mmp*$^{lacZ/+}$ mammary epithelial organoids cultured in 3-D type I collagen with serum-free media containing 50 ng/ml FGF-2 at time 0 and day 5 (scale bar = 100 µm). The inset shows LacZ staining of wild-type littermate organoids. (E,F) Phase contrast images of *Mt1-mmp*$^{+/+}$ and *Mt1-mmp*$^{-/-}$ mammary epithelial organoids isolated from mice at P10 and embedded within 3-D type I collagen or 3-D Matrigel for 6 days with 50 ng/ml FGF-2 alone, or with FGF-2 in the presence of 5 µm BB-94 (scale bar = 100 µm) . The insets show the mammary epithelial organoids at time 0. Results are representative of 5 experiments performed.

Fig. 2-3.

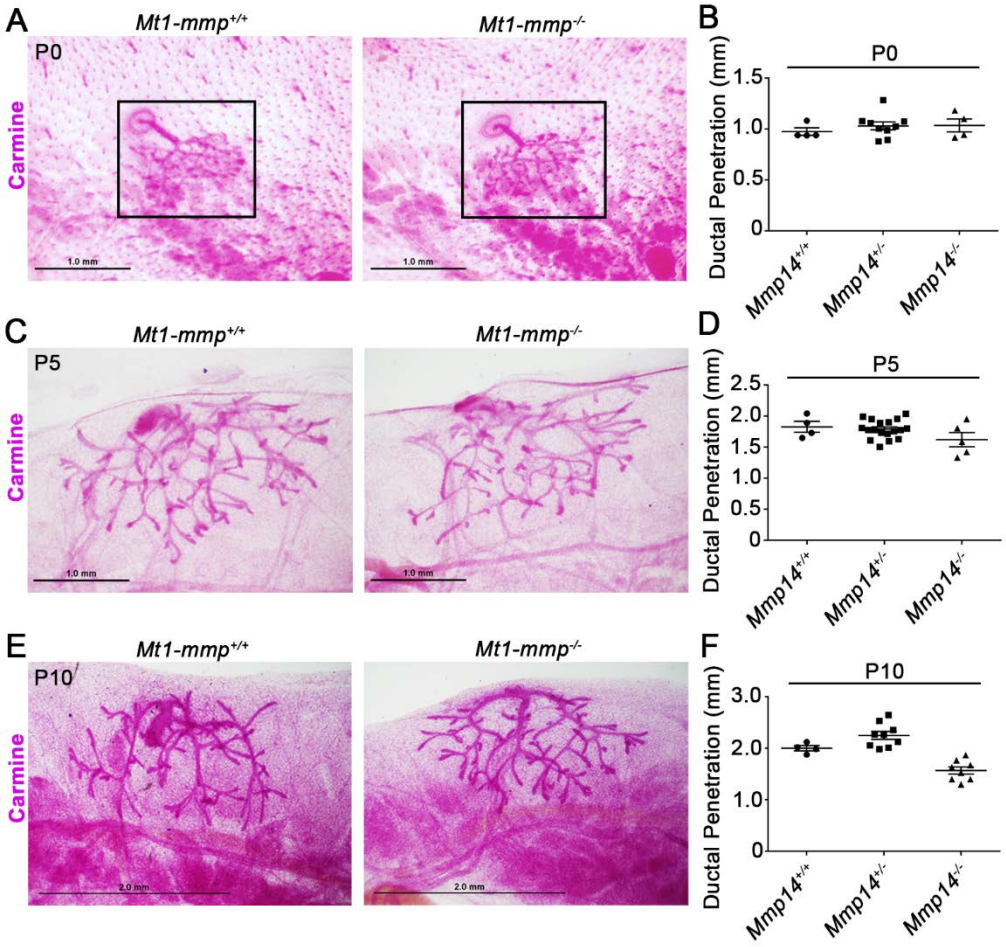

Fig. 2-3. Early mammary gland branching proceeds independently of MT1-MMP.
(A,C,E) Carmine-stained whole mounts of mammary glands isolated from representative P0, P5, and P10 *Mt1-mmp*$^{+/+}$ vs. *Mt1-mmp*$^{-/-}$ female mice. (B,D,F). Ductal length quantifications (mm) of *Mt1-mmp*$^{+/+}$, *Mt1-mmp*$^{+/-}$ and *Mt1-mmp*$^{-/-}$ mice at P0, P5, and P10. Results are plotted with mean ± SEM in *Mt1-mmp*$^{+/+}$ (n=4 per time-point), *Mt1-mmp*$^{+/-}$ mice at P0 (n=9), P5 (n=18) and P10 (n=9), and *Mt1-mmp*$^{-/-}$ mice at P0 (n=4), P5 (n=5) and P10 (n=8). Scale bars represent 500 µm, 1.0 mm, and 2.0 mm, respectively.

Fig. 2-4.

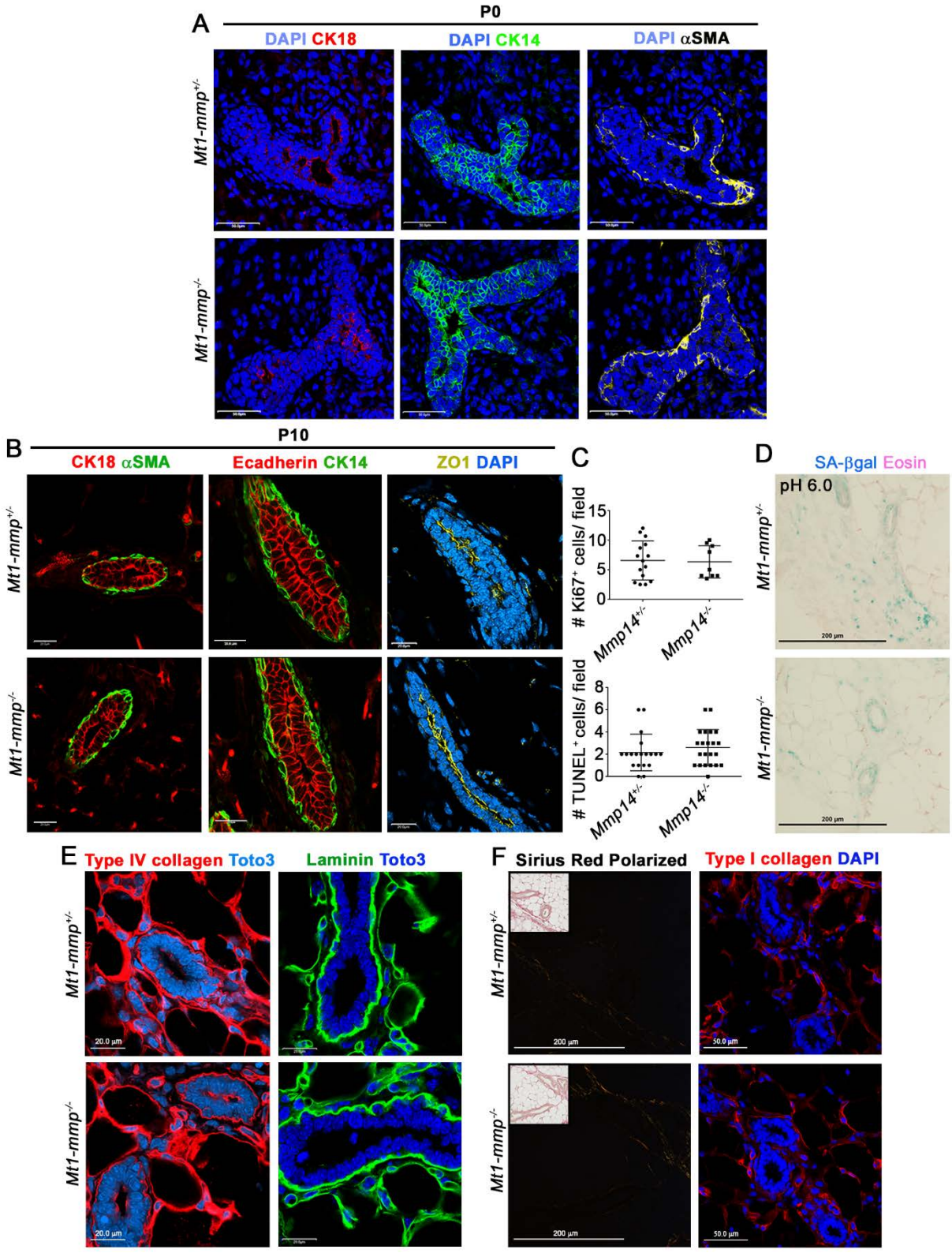
A
P0
DAPI CK18
DAPI CK14
DAPI αSMA
Mt1-mmp+/-
Mt1-mmp-/-
B
P10
CK18 αSMA
Ecadherin CK14
ZO1 DAPI
C
Ki67+ cells/ field
TUNEL+ cells/ field
Mmp14+/-
Mmp14-/-
D
SA-βgal Eosin
pH 6.0
200 μm
E
Type IV collagen Toto3
Laminin Toto3
20.0 μm
F
Sirius Red Polarized
Type I collagen DAPI
200 μm
50.0 μm

Fig. 2-4. MT1-MMP-independent epithelial cell sorting, proliferation, senescence and ECM organization.

(A) Immunofluorescence of cytokeratin-18 (CK18), cytokeratin-14 (CK14) and α-smooth muscle actin (αSMA) in P0 *Mt1-mmp*$^{+/+}$ vs. *Mt1-mmp*$^{-/-}$ mammary glands with DAPI counter-staining (scale bars = 50 μm). (B) Immunofluorescence of CK18 and αSMA (left), E-cadherin and CK14 (middle), and Zonula occludens (ZO)-1 with DAPI counter-staining (right) in P10 *Mt1-mmp*$^{+/+}$ vs. *Mt1-mmp*$^{-/-}$ mammary glands (scale bars = 50 μm). (C) Quantifications of average number of Ki67-positive cells per field and TUNEL-positive cells per field from immunofluorescence of P5 mammary glands at 60X magnification (n=2 per genotype). Results are plotted with mean values of n>10 fields ± 1 SD. (D) Senescence-associated β-galactosidase (SA-βgal) staining of P5 *Mt1-mmp*$^{+/+}$ vs. *Mt1-mmp*$^{-/-}$ mammary glands under pH 6.0 conditions (n=2 per genotype, scale bar = 200 μm). (E) Immunofluorescence of type IV collagen and laminin in P5 *Mt1-mmp*$^{+/+}$ vs. *Mt1-mmp*$^{-/-}$ mammary glands with Toto3-mediated nuclear counter-staining (scale bar = 50 μm). (F) Polarized light images of Sirius Red staining of P5 *Mt1-mmp*$^{+/+}$ vs. *Mt1-mmp*$^{-/-}$ mammary gland cross-sections. Insets show the corresponding bright-field images (scale bar = 200 μm). Type I collagen immunofluorescence in P5 wild-type versus knockout mammary glands with DAPI counter-staining (scale bar = 50.0 μm). All images are representative of 3 replicates.

Fig. 2-5.

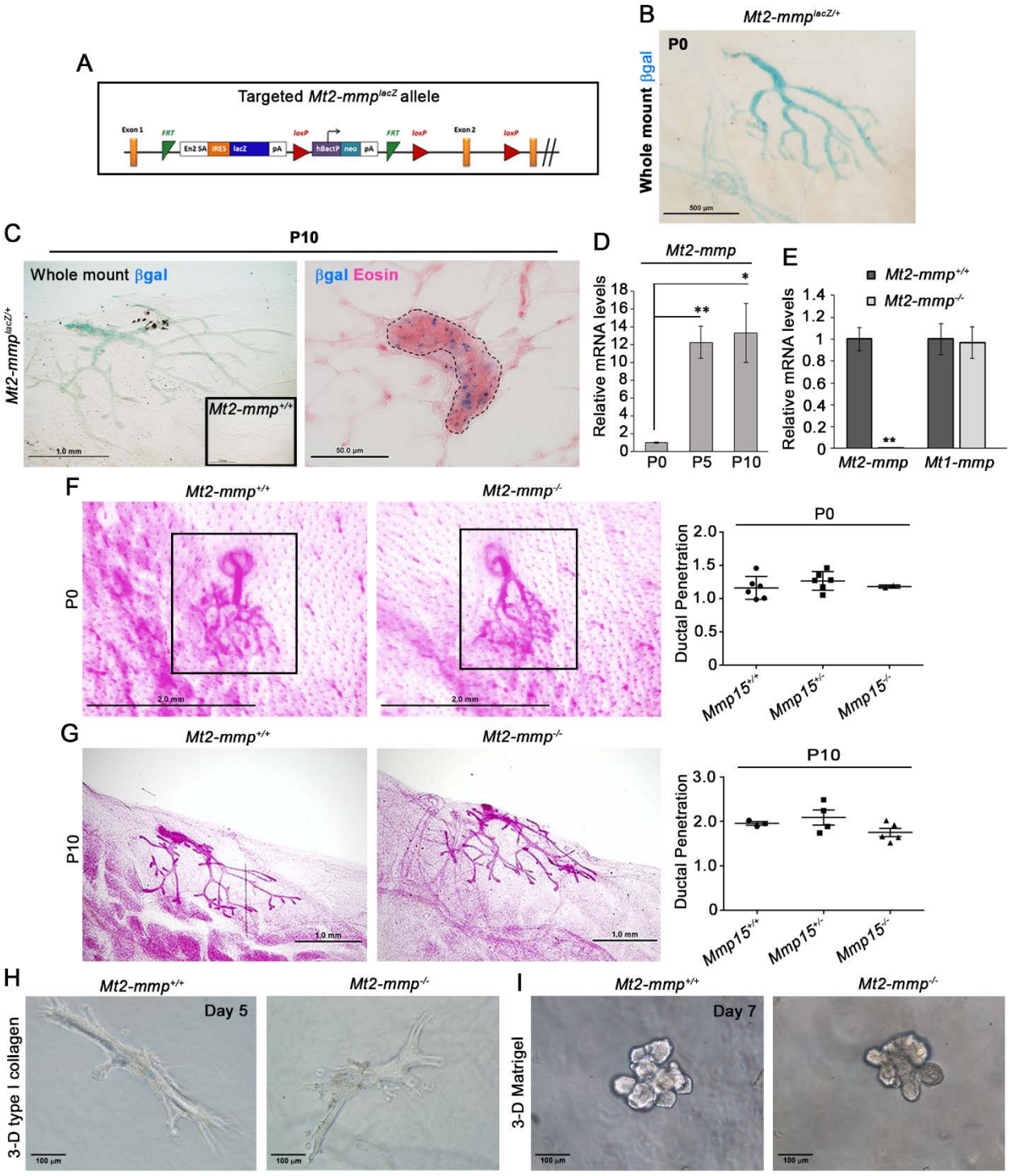
A
Targeted Mt2-mmp^lacZ allele
Exon 1
FRT
En2 SA
IRES
lacZ
pA
loxP
hBactP
neo
pA
FRT
loxP
Exon 2
loxP
B
Mt2-mmp^lacZ/+
P0
Whole mount βgal
500 μm
C
P10
Mt2-mmp^lacZ/+
Whole mount βgal
Mt2-mmp^+/+
1.0 mm
βgal Eosin
50.0 μm
D
Mt2-mmp
Relative mRNA levels
P0
P5
P10
E
Mt2-mmp^+/+
Mt2-mmp^-/-
Relative mRNA levels
Mt2-mmp
Mt1-mmp
F
Mt2-mmp^+/+
Mt2-mmp^-/-
P0
2.0 mm
P0
Ductal Penetration
Mmp15^+/+
Mmp15^+/-
Mmp15^-/-
G
Mt2-mmp^+/+
Mt2-mmp^-/-
P10
1.0 mm
P10
Ductal Penetration
Mmp15^+/+
Mmp15^+/-
Mmp15^-/-
H
Mt2-mmp^+/+
Mt2-mmp^-/-
3-D type I collagen
Day 5
100 μm
I
Mt2-mmp^+/+
Mt2-mmp^-/-
3-D Matrigel
Day 7
100 μm

Fig. 2-5. Early mammary epithelial branching is MT2-MMP-independent.
(A) Schematic of targeted *Mt2-mmp*^{lacZ} allele. (B) LacZ staining of P0 *Mt2-mmp*$^{lacZ/+}$ mammary gland whole mount. (C) LacZ staining of P10 *Mt2-mmp*$^{lacZ/+}$ whole mount (left panel). Inset shows LacZ staining of wild-type mammary tissue. In the right panel, a P10 *Mt2-mmp*$^{lacZ/+}$ gland was sectioned and Eosin-stained to highlight luminal epithelial/myoepithelial-positive cells (scale bars = 500 µm, 1.0 mm, and 50 µm, respectively). (D) qPCR of *Mt2-mmp* at P0, P5 and P10. Results are expressed as mean ± SEM expression levels at P0 (n=4), P5 (n=3) and P10 (n=4) relative to *Arbp*. **$p<0.001$, *$p\leq0.01$. (E) qPCR of *Mt1-mmp* and *Mt2-mmp* levels in P10 wildtype and *Mt2-mmp*$^{-/-}$ mammary glands. Results are expressed as mean expression levels ± SEM of 3 replicates relative to *Arbp*. **$p<0.001$. (F) Carmine-stained mammary gland whole mounts isolated from P0 *Mt2-mmp*$^{+/+}$ and *Mt2-mmp*$^{-/-}$ mice. Ductal lengths for P0 *Mt2-mmp*$^{+/+}$ (n=6), *Mt2-mmp*$^{+/-}$ (n=6) and *Mt2-mmp*$^{-/-}$ (n=2) glands are plotted with the mean ± 1 SD. (G) Carmine-stained whole mounts of mammary glands recovered from representative *Mt2-mmp*$^{+/+}$ and *Mt2-mmp*$^{-/-}$ mice at P10. Ductal lengths for P10 *Mt2-mmp*$^{+/+}$ (n=3), *Mt2-mmp*$^{+/-}$ (n=4) and *Mt2-mmp*$^{-/-}$ (n=5) glands are plotted with mean ± SEM. (H) Phase contrast images of mammary epithelial organoids isolated from mice at P10 and embedded within 3-D type I collagen or 3-D Matrigel in the presence of 50 ng/ml FGF-2 (scale bars = 100 µm). p values were calculated with unpaired t-tests. Results are representative of 2 experiments performed.

Fig. 2-6.

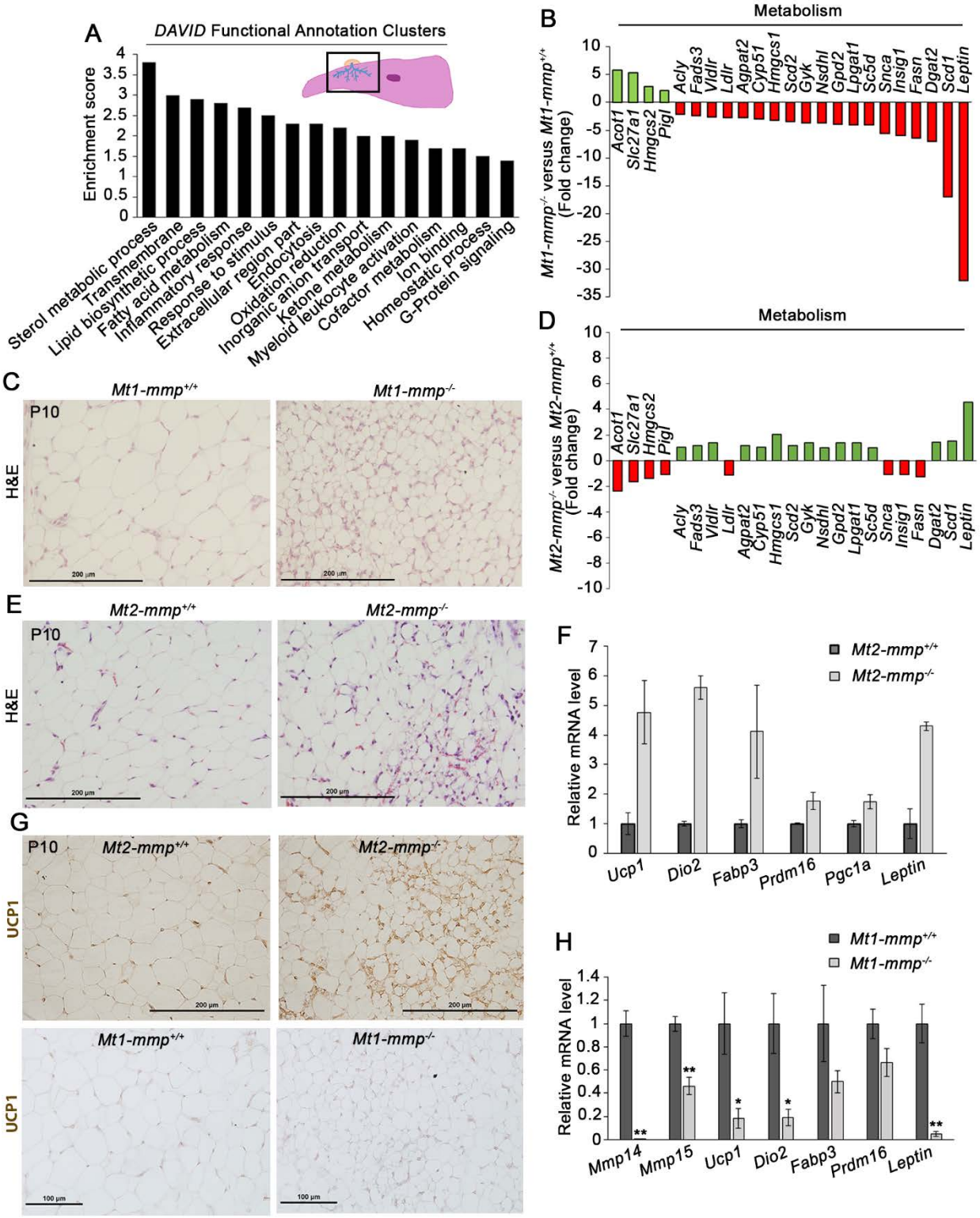
A
DAVID Functional Annotation Clusters
Enrichment score
Sterol metabolic process
Transmembrane
Lipid biosynthetic process
Fatty acid metabolism
Inflammatory response
Response to stimulus
Extracellular region part
Endocytosis
Oxidation reduction
Inorganic anion transport
Ketone metabolism
Myeloid leukocyte activation
Cofactor metabolism
Ion binding
Homeostatic process
G-Protein signaling
B
Metabolism
Mt1-mmp-/- versus Mt1-mmp+/+ (Fold change)
Acot1 Slc27a1 Hmgcs2 Pigl Acly Fads3 Vldlr Ldlr Agpat2 Cyp51 Hmgcs1 Scd2 Gyk Nsdhl Gpd2 Lpgat1 Sc5d Snca Insig1 Fasn Dgat2 Scd1 Leptin
C
Mt1-mmp+/+
Mt1-mmp-/-
P10
H&E
200 μm
D
Metabolism
Mt2-mmp-/- versus Mt2-mmp+/+ (Fold change)
Acot1 Slc27a1 Hmgcs2 Pigl Acly Fads3 Vldlr Ldlr Agpat2 Cyp51 Hmgcs1 Scd2 Gyk Nsdhl Gpd2 Lpgat1 Sc5d Snca Insig1 Fasn Dgat2 Scd1 Leptin
E
Mt2-mmp+/+
Mt2-mmp-/-
P10
H&E
200 μm
F
Mt2-mmp+/+
Mt2-mmp-/-
Relative mRNA level
Ucp1 Dio2 Fabp3 Prdm16 Pgc1a Leptin
G
P10
Mt2-mmp+/+
Mt2-mmp-/-
UCP1
Mt1-mmp+/+
Mt1-mmp-/-
UCP1
200 μm
100 μm
H
Mt1-mmp+/+
Mt1-mmp-/-
Relative mRNA level
Mmp14 Mmp15 Ucp1 Dio2 Fabp3 Prdm16 Leptin

Fig. 2-6. MT1-MMP and MT2-MMP differentially regulate mammary fat pad development. (A) Graphical representation of the enriched DAVID Functional Annotation Clusters in P10 *Mt1-mmp*$^{-/-}$ mammary gland tissue relative to *Mt1-mmp*$^{+/+}$ littermates, with a cartoon illustrating the mammary gland region collected for gene expression profiling. (B) Chart of differentially expressed genes related to cellular metabolism in the *Mt1-mmp*$^{-/-}$ gene expression profile, relative to *Mt1-mmp*$^{+/+}$ littermates, plotted by fold change values (n=2 per genotype). (C) H&E staining of fat pad cross-sections from P10 *Mt1-mmp*$^{+/+}$ and *Mt1-mmp*$^{-/-}$ mammary glands. (D) Chart illustrating the fold-changes in the metabolism genes depicted in panel B in the P10 *Mt2-mmp*$^{-/-}$ gene expression profile relative to *Mt2-mmp*$^{+/+}$ littermates (n=2 per genotype). (E) H&E staining of cross-sections from P10 *Mt2-mmp*$^{+/+}$ and *Mt2-mmp*$^{-/-}$ mammary glands. (F) qPCR of thermogenic and metabolic genes up-regulated in *Mt2-mmp*$^{-/-}$ mammary gland stroma relative to *Mt2-mmp*$^{+/+}$ littermates as normalized to *Arbp*. Results are expressed as mean values ± 1 SD of n=2 mice per genotype. (G) Immunohistochemistry for UCP1 in P10 *Mt2-mmp*$^{-/-}$ and *Mt1-mmp*$^{-/-}$ mammary gland cross-sections with wild-type littermates (scale bars = 200 μm). Results are representative of 3 replicates. (H) qPCR of the genes monitored in panel F in P10 *Mt1-mmp*$^{-/-}$ mammary gland tissue relative to *Mt1-mmp*$^{+/+}$ littermates in *Mt1-mmp*$^{+/+}$ (n=7) and *Mt1-mmp*$^{-/-}$ (n=5). Results are expressed as mean expression levels ± SEM as normalized to *Arbp*. **$p<0.001$, *$p<0.05$. p values were calculated with unpaired t-tests.

Fig. 2-S1.

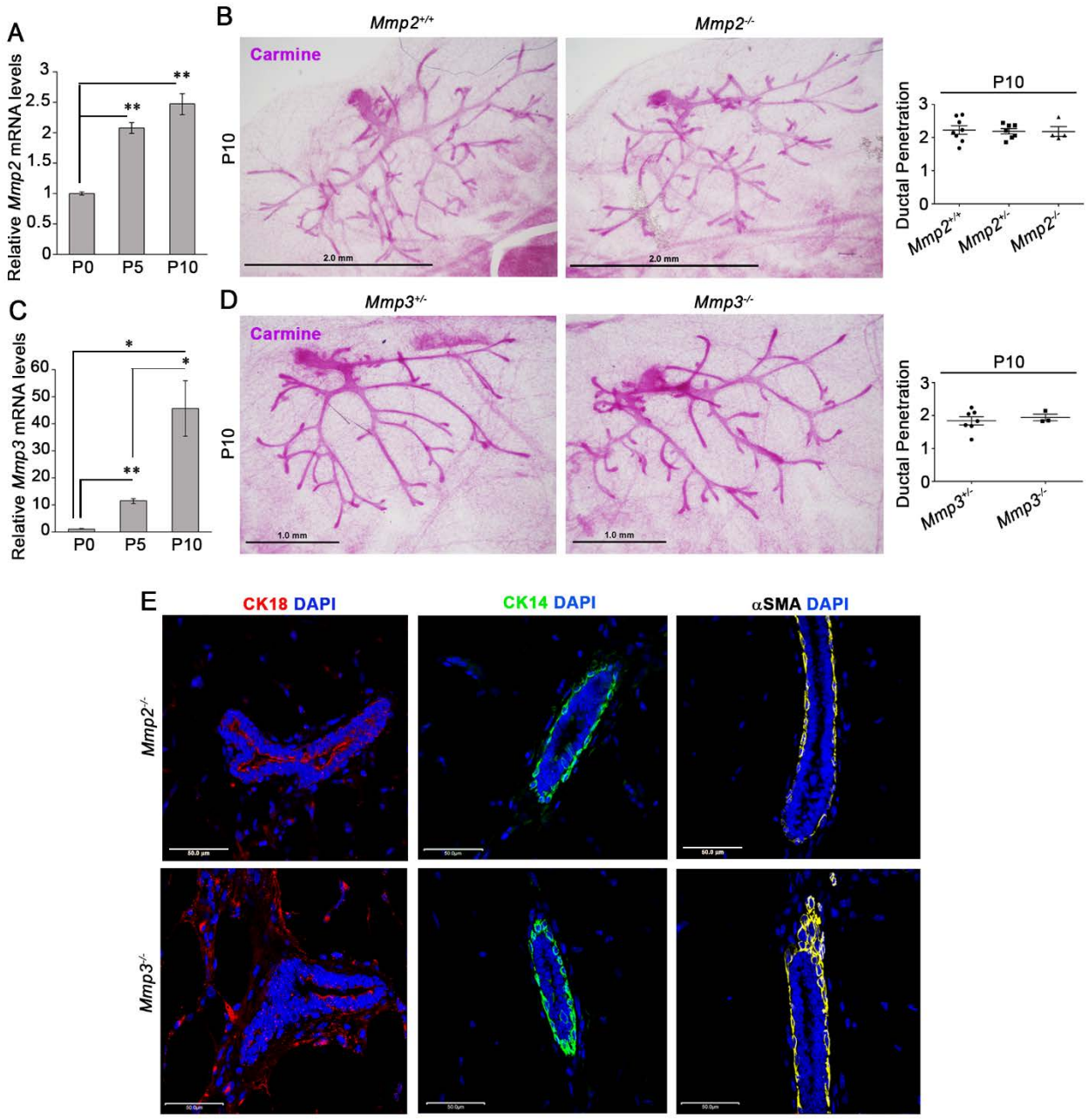

Fig. 2-S1. *Mmp2* and *Mmp3* global knockouts establish early postnatal mammary glands. (A) qPCR of *Mmp2* at P0, P5 and P10 in wild-type mammary glands. Results are expressed as mean expression levels ± SEM at P0 (n=4), P5 (n=3) and P10 (n=4) relative to *Arbp*. **p<0.001, *p<0.05. (B) Carmine-stained whole mounts of mammary glands isolated from P10 $Mmp2^{+/+}$ vs. $Mmp2^{-/-}$ mice (scale bar = 2.0 mm) with quantifications of duct elongation (mm). Results are plotted with mean ± SEM for $Mmp2^{+/+}$ (n=8), $Mmp2^{+/-}$ (n=7) and $Mmp2^{-/-}$ (n=4) mice. (C) qPCR of *Mmp3* at P0, P5 and P10 in wild-type mammary glands. Results are expressed as mean ± SEM for P0 (n=3), P5 (n=3) and P10 (n=4) relative to *Arbp*. **p<0.001, *p<0.05. (D) Carmine-stained whole mounts of P10 mammary glands (scale bars = 1.0 mm) from $Mmp3^{+/-}$ mice (n=7) and

Mmp3$^{-/-}$ mice (n=3) with quantification of duct elongation (mm). Results are plotted with mean ± SEM. (E) Immunofluorescence of CK18, CK14, and αSMA in P10 *Mmp2*$^{-/-}$ and *Mmp3*$^{-/-}$ mammary glands with DAPI counter-staining (scale bars = 50 μm). p values were calculated with unpaired t-tests. Images shown are representative of 2 replicates.

Fig. 2-S2.

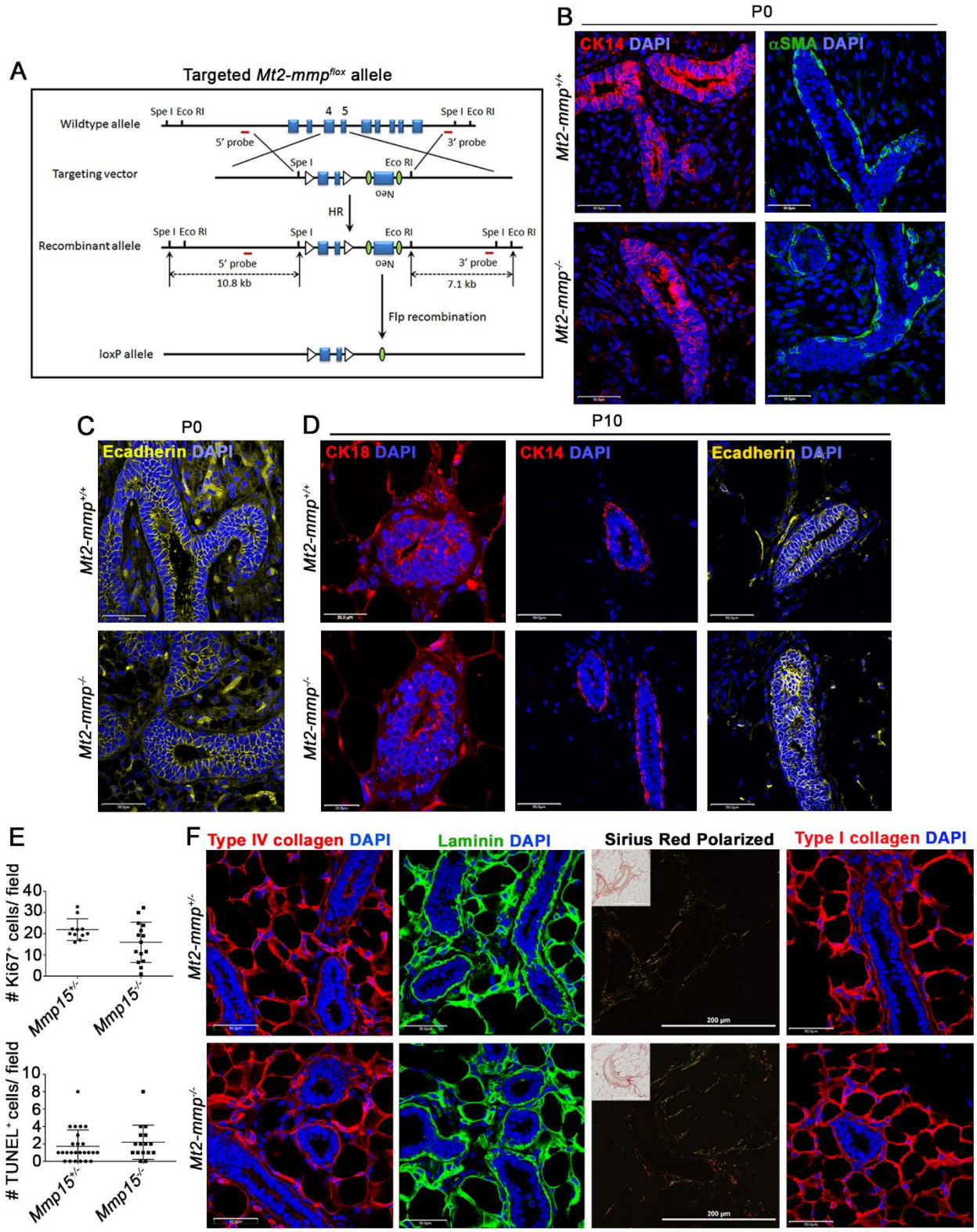
A
Targeted Mt2-mmp^flox allele
Wildtype allele
Spe I Eco RI
4 5
5′ probe
3′ probe
Targeting vector
Spe I
Eco RI
Neo
HR
Recombinant allele
10.8 kb
7.1 kb
Flp recombination
loxP allele
B
P0
CK14 DAPI
αSMA DAPI
Mt2-mmp+/+
Mt2-mmp-/-
C
P0
Ecadherin DAPI
D
P10
CK18 DAPI
CK14 DAPI
Ecadherin DAPI
E
Ki67+ cells/ field
TUNEL+ cells/ field
Mmp15+/-
Mmp15-/-
F
Type IV collagen DAPI
Laminin DAPI
Sirius Red Polarized
Type I collagen DAPI
200 µm

Fig. 2-S2. MT2-MMP-independent orchestration of mammary epithelial cell organization, mammary cell proliferation and ECM.
(A) Schematic of *Mt2-mmp* global knockout targeting strategy and the *Mt2-mmp*^{flox} allele. (B-C) Immunofluorescence of CK14, αSMA and E-cadherin in P0 *Mt2-mmp*$^{+/+}$ and *Mt2-mmp*$^{-/-}$ mammary glands with DAPI nuclear counter-staining (scale bars = 50 μm). (D) Immunofluorescence of CK18, CK14, and E-cadherin in P10 *Mt2-mmp*$^{+/+}$ and *Mt2-mmp*$^{-/-}$ mammary glands with DAPI counter-staining. (E) Quantification of average number of Ki67-positive cells per field and TUNEL-positive cells per field from immunofluorescence of P5 mammary glands (60X magnification). Results are plotted with mean values of n>10 fields per genotype. (F) Immunofluorescence of type IV collagen, laminin, and type I collagen with DAPI counter-staining in P5 *Mt2-mmp*$^{+/+}$ and *Mt2-mmp*$^{-/-}$ mammary glands (scale bars = 50 μm). Polarized light images of Sirius Red staining of P5 mammary gland cross-sections are also shown. Insets show the corresponding bright-field images (scale bar = 200 μm). All images are representative of n≥2 replicates.

Fig. 2-S3.

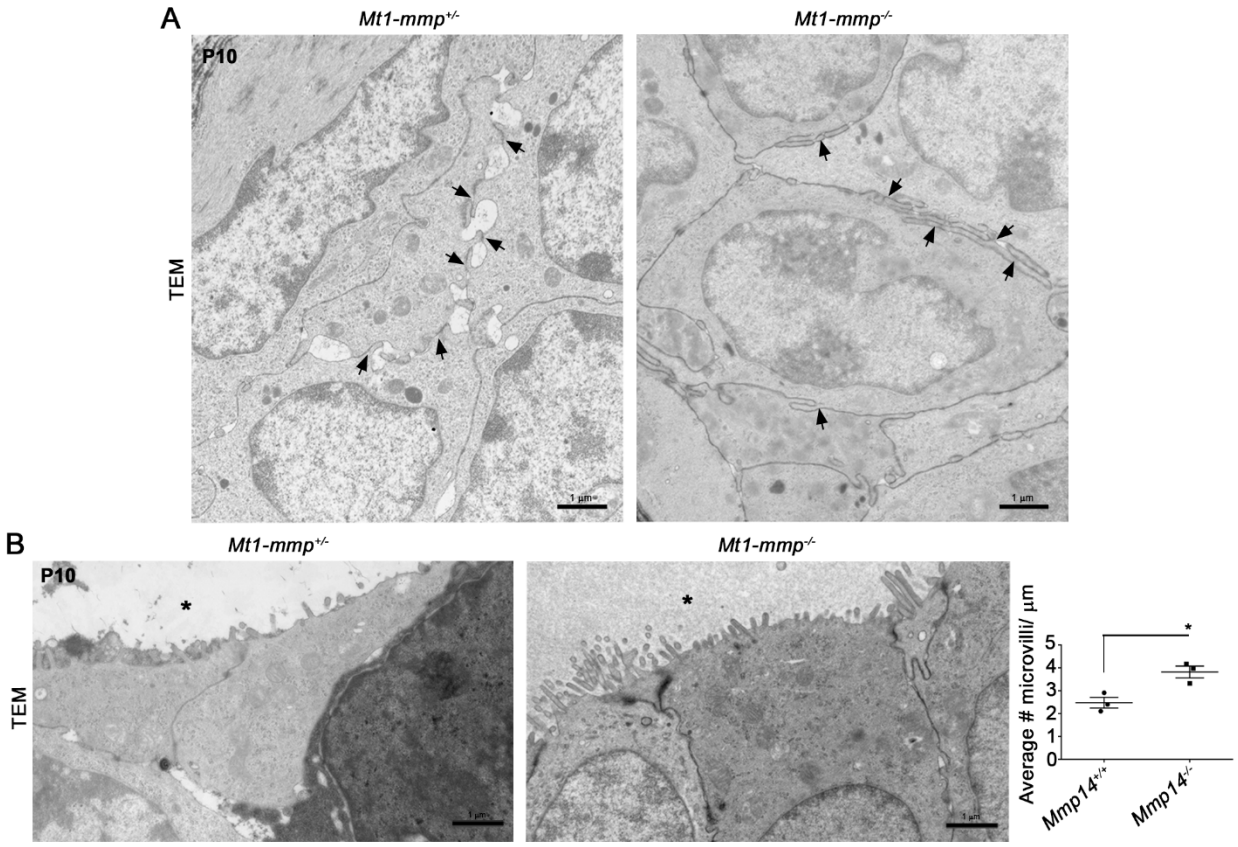

Fig. 2-S3. MT1-MMP-dependent regulation of epithelial cell junctions and microvilli *in vivo*. (A) Transmission electron micrographs (TEM) of representative P10 *Mt1-mmp*$^{+/-}$ and *Mt1-mmp*$^{-/-}$ mammary ducts (15000X) (n=3 per genotype). Arrows denote cell-cell junctions and adjacent spaces in *Mt1-mmp*$^{+/+}$ ducts with corresponding regions in *Mt1-mmp*$^{-/-}$ ducts (scale bars = 1 µm). (B) TEM of P10 mammary duct microvilli (15000X) with quantification of average number of microvilli per µm plotted with mean ± SEM (n=3 per genotype). *p<0.02. Asterisks mark the mammary duct lumen (scale bar = 1 µm). p value was calculated with an unpaired t-test.

Fig. 2-S4.

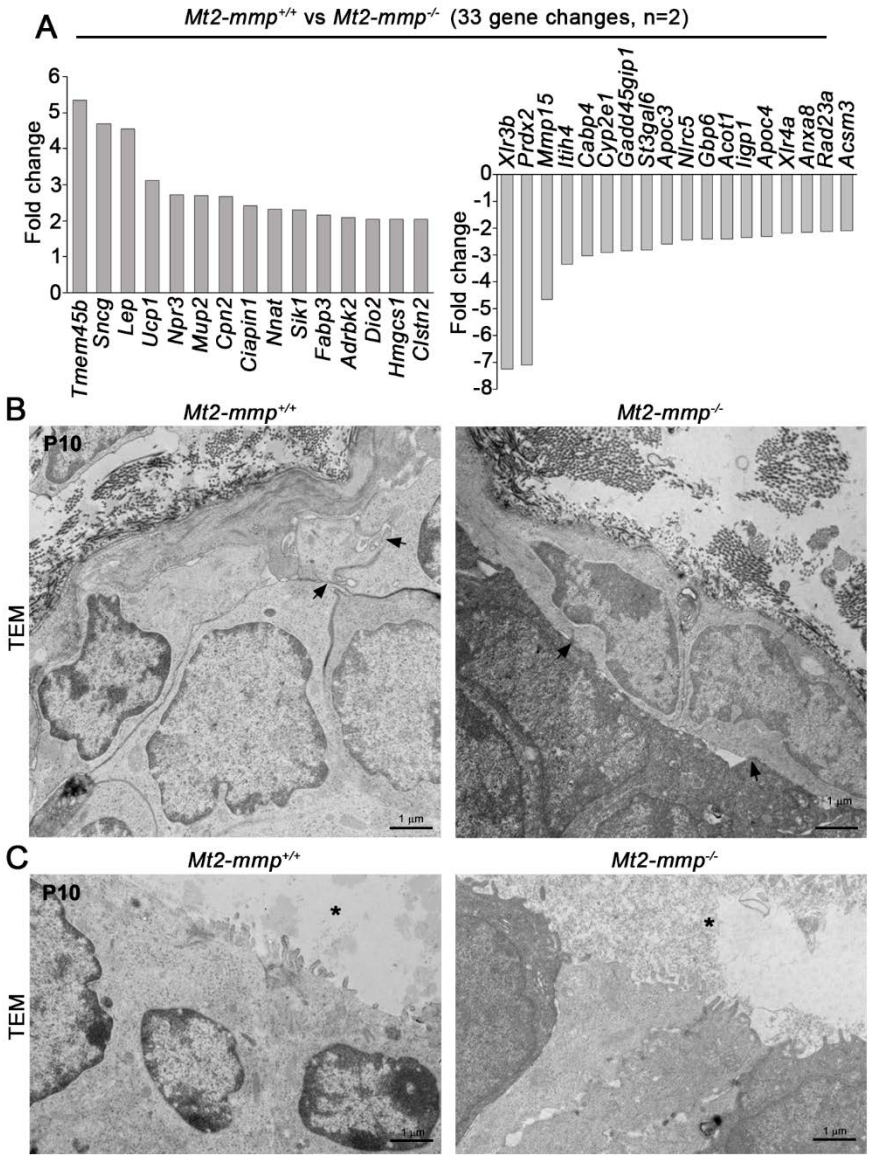

Fig. 2-S4. *Mt2-mmp* knockout mammary glands maintain global gene expression profile and epithelial ultrastructure.
(A) Charts of the up-regulated and down-regulated genes in P10 *Mt2-mmp*$^{-/-}$ mammary glands relative to *Mt2-mmp*$^{+/+}$ mammary glands (n=2 per genotype). (B) TEM of representative *Mt2-mmp*$^{+/+}$ and *Mt2-mmp*$^{-/-}$ mammary ducts (15000X) (scale bar = 1 µm). Arrows mark corresponding cell junctions (n=2 per genotype). (C) TEM of representative P10 mammary duct microvilli (15000X) (n=2 per genotype; scale bars = 1 µm). Asterisks mark the mammary duct lumen.

Note.

* This chapter was submitted as a manuscript, entitled: “Functional Roles of MT1-MMP and MT2-MMP in Early Postnatal Mammary Gland Development,” by Tamar Y. Feinberg, R. Grant Rowe, Thomas L. Saunders and Stephen J. Weiss.

CHAPTER 3: Periductal Remodeling of the Interstitial Matrix Regulates Mammary Gland Morphogenesis

Abstract.

During puberty, the mouse mammary gland initiates a morphogenetic program wherein primordial networks of epithelial tubes elongate and branch into the surrounding mesenchyme. Mechanisms underlying this controlled invasion program remain uncharacterized, but mammary epithelial cells have been posited to mobilize proteolytic enzymes in order to penetrate extracellular matrix barriers *in vivo*. Nevertheless, transgenic models have failed to identify required proteolytic effectors, raising the possibility of redundant systems, compensatory networks or a requirement for heretofore undefined proteinases. Herein, we demonstrate that the membrane-anchored matrix metalloproteinase, MT1-MMP/MMP14, serves as the dominant effector of mammary gland branching morphogenesis *in vivo*. Unexpectedly, epithelial cell-specific targeting of *Mmp14* fails to impair branching, while deleting *Mmp14* expression in the periductal stroma ablates morphogenesis coincident with striking defects in type I collagen remodeling. The effects of conditional knockout of stromal cell-derived *Mmp14* are recapitulated by the *in vivo* knock-in of MMP14-resistant type I collagen, thereby identifying a stromal MMP14-type I collagen axis as the key regulator of morphogenesis.

Introduction.

Epithelial tube formation and branching defines tissue development, function, and homeostasis in a variety of organ systems (Affolter et al., 2009; Khokha and Werb, 2011; Varner and Nelson, 2014). The outgrowth of branching epithelial tubules depends on complex reciprocal crosstalk between the epithelium and the surrounding mesenchyme for inducing the proliferation, signaling and differentiation programs required for tissue morphogenesis (Ochoa-Espinosa and Affolter, 2012; Robinson, 2007), yet the relative functions of the epithelial and stromal compartments in this dynamic process remain unclear. Similar to other epithelial organs, mammary glands initiate branching programs during late embryogenesis when ectoderm-derived epithelial buds mount a coordinated cell invasion program that supports sprout formation into the surrounding mesenchyme (Huebner and Ewald, 2014; Robinson, 2007). Unlike most other epithelial organs, however, mammary gland branching largely occurs postnatally in concert with the onset of puberty where the bi-layered mammary tubules, composed of inner-facing luminal epithelial cells and basal-oriented myoepithelial cells, navigate through an interstitial extracellular matrix (ECM) dominated by type I collagen-enmeshed fibroblasts and a surrounding adipocyte-rich mesenchyme (Affolter et al., 2009; Huebner and Ewald, 2014; Khokha and Werb, 2011; Robinson, 2007; Varner and Nelson, 2014).

Evidence culled from *in vitro* models supports a model where epithelial tubules deploy proteolytic enzymes from the matrix metalloproteinase (MMP) family of zinc-dependent endopeptidases to remodel interstitial ECM barriers so as to create the microenvironmental changes that are permissive for the cellular rearrangements and signaling cascades required for branching morphogenesis (Correia et al., 2013; Mori et al., 2009; Mori et al., 2013; Rebustini et al., 2009; Weaver et al., 2014). However, extensive analyses of transgenic mouse models have

thus far failed to identify any proteolytic enzyme that plays a dominant role in branching, its tissue of origin or mechanism of action (Affolter et al., 2009; Huebner and Ewald, 2014; Khokha and Werb, 2011; Ochoa-Espinosa and Affolter, 2012; Robinson, 2007; Varner and Nelson, 2014).

Results.

MMP14 regulates postnatal mammary gland branching morphogenesis *in vivo.*

Following the onset of puberty in ~3 week-old female mice, increasing levels of estrogen and progesterone stimulate the elongation and bifurcation of a primordial network of branching ducts into the surrounding adipocyte-rich mammary stroma (i.e., fat pad) (Huebner and Ewald, 2014; Khokha and Werb, 2011). By 4 weeks of age, the ductal network increases 2-to-3 fold in size and complexity as marked by the progression of the advancing ducts toward the inguinal lymph node (Fig. 3-S1 A). By 8-to-10 weeks of age, the mammary epithelium effectively branches to the edges of the mammary fat pad to form a complex, arborized tree-like network (Fig. 3-S1 A).

Coincident with the onset of branching morphogenesis, the postnatal mammary gland is known to express several proteolytic enzymes belonging to the matrix metalloproteinase gene family, including *Mmp2/Gelatinase A*, *Mmp3/Stromelysin-1* and *Mmp13/Collagenase 3*, as well as two closely related membrane-anchored MMPs, *Mt1-mmp/Mmp14* and *Mt2-mmp/Mmp15* (Nielsen et al., 2008; Szabova et al., 2005; Wiseman et al., 2003). However, the relative requirements for these proteases in branching morphogenesis *in vivo*, a process demanding coordinated patterns of cell invasion and proliferation, remain undefined. Having confirmed that each of these MMPs is expressed in postnatal mammary glands in both 2 week and 4 week -old mice (data not shown), we characterized branching morphogenesis in each of the respective global knockout mice. Though MMP2 has been implicated in mammary duct elongation and lateral

branching (Wiseman et al., 2003), *Mmp2*$^{+/+}$ and *Mmp2*$^{-/-}$ mammary glands display comparable branching structures at the postnatal 4 week time-point (Fig. 3-S1 B). Similarly, whereas recent reports have identified protease-dependent as well as protease-independent roles for secreted MMP3 in mammary gland development (Correia et al., 2013; Wiseman et al., 2003), *Mmp3*$^{-/-}$ mammary glands establish branching ductal networks indistinguishable from those of *Mmp3*$^{+/+}$ and *Mmp3*$^{+/-}$ littermates (Fig. 3-S1 C). Likewise, targeting *Mmp13* did not affect morphogenic responses in 4 week-old mice (Fig. 3-S1 D).

Recent studies have identified protease-dependent and protease-independent roles for membrane-anchored MMP14 in several developmental processes *in vivo*, including mesenchymal stem cell differentiation (Tang et al., 2013), lung alveolar septal development (Atkinson et al., 2005; Oblander et al., 2005) and adipocyte differentiation (Chun et al., 2006). Yet, efforts to ascertain roles for MMP14 in postnatal mammary gland or epithelial cell branching have relied largely on *in vitro* assay systems (Mori et al., 2009; Mori et al., 2013; Weaver et al., 2014). Using 2 week or 4 week -old *Mmp14-lacZ* knock-in mice (Tang et al., 2013), MMP14 can be detected throughout the mammary gland compartment in luminal epithelial cells, myoepithelial cells and surrounding stromal cells (Fig. 3-1 A,B). The closely related membrane-anchored matrix metalloproteinase, *Mt2-mmp/Mmp15*, is also enriched in the mammary epithelial compartment as visualized in mammary glands isolated from *Mmp15-lacZ* knock-in mice (Fig. 3-1 C,D; Fig. 3-S2 A). To begin to address requirements for MMP14 or MMP15 in postnatal mammary gland development, glands were next harvested from *Mmp14* global knockout mice (Holmbeck et al., 1999; Zhou et al., 2000). In contrast to the *Mmp2*, *Mmp3* and *Mmp13* knockouts, while *Mmp14*$^{+/+}$ and *Mmp14*$^{+/-}$ mammary ducts effectively branch through the mammary fat pad toward the inguinal lymph node, both 2 week and 4 week -old *Mmp14*$^{-/-}$ mice fail to mount branching

programs and harbor 2-fold and ~7-fold smaller branching networks at 2 weeks and 4 weeks, respectively (Fig. 3-1 E; Fig. 3-S2 B,C).

To characterize the role of MMP15 in mammary gland development, global knockout mice were generated wherein exons 4 and 5 of the catalytic domain were flanked by loxP sites using homologous recombination and deleted by breeding homozygous *Mmp15*$^{flox/flox}$ mice with germline-specific *EIIA-Cre* mice (Fig. 3-S2 D). *Mmp15*$^{-/-}$ mice were born in normal Mendelian ratios and remain viable throughout adulthood. However, unlike *Mmp14* global knockouts, mammary glands isolated from 4 week-old *Mmp15*$^{-/-}$ mice mount a branching program indistinguishable from littermate controls (Fig. 3-1 F). Hence, only *Mmp14*$^{-/-}$ mammary glands display marked defects in branching morphogenesis. However, the impaired sexual development of *Mmp14*$^{-/-}$ mice (Holmbeck et al., 1999; Zhou et al., 2000) precludes attempts to assign definitive mammary gland-autonomous roles for the proteinase in branching morphogenesis.

Mammary gland branching proceeds independently of epithelial cell-derived MMP14 *in vivo.*

Current paradigms hold that epithelial cell-derived proteolytic machinery directs mammary gland branching morphogenesis (Inman et al., 2015; Khokha and Werb, 2011; Mori et al., 2009; Mori et al., 2013; Varner and Nelson, 2014; Weaver et al., 2014). As such, *Mmp14-floxed* mice were crossed with a transgenic line wherein Cre recombinase expression is largely restricted to the postnatal mammary epithelium, i.e., *MMTV-Cre* (line A) (Wagner et al., 2001), with epithelial cell-specific targeting confirmed by breeding *MMTV-Cre* expressing mice into a *Rosa26R* reporter background (Soriano, 1999) (Fig. 3-2 A). Unexpectedly, however, despite achieving >90% excision of mammary epithelial cell-derived *Mmp14* (Fig. 3-2 B), *MMTV-Cre*$^{+/-}$*Mmp14*$^{fl/fl}$ mice

mount a mammary gland branching program that is comparable in complexity, duct elongation and branch points to *Mmp14*$^{fl/fl}$ controls as assessed in either 4 week or 8 week –old mice (Fig. 3-2 C,D; Fig. 3-S3 A,B). Furthermore, using *MMTV-Cre*$^{+/-}$*Mmp14*$^{fl/fl}$*Rosa26R*$^{+/loxP}$ mice to differentially track Cre-targeted (i.e., *Mmp14*$^{+/-}$ and *Mmp14*$^{-/-}$) versus non-targeted epithelial (i.e., *Mmp14*$^{+/+}$) cells, we fail to observe a competitive advantage for *Mmp14*-expressing cells in duct formation (Fig. 3-S3 C). Nevertheless, it remains possible that a small sub-population of non-Cre-targeted cells serve as leader-like tip cells that rescue the branching program (Weavers and Skaer, 2014). As such, to unequivocally rule out a required role for epithelial cell-derived MMP14 in branching, ductal fragments were harvested from *Gfp*$^{+/-}$*Mmp14*$^{+/-}$ or *Gfp*$^{+/-}$*Mmp14*$^{-/-}$ donor mice and transplanted into the cleared mammary fat pads of wild-type recipients (Fig. 3-2 E). Despite the marked impact of global *Mmp14* deletion on mammary gland branching morphogenesis, *Gfp*$^{+/-}$*Mmp14*$^{+/-}$ and *Gfp*$^{+/-}$*Mmp14*$^{-/-}$ ductal fragments form comparable branching networks at 6-8 weeks post-transplantation (Fig. 3-2 F). Further, the established ducts display normal epithelial cell organization as marked by myoepithelial cell-associated cytokeratin-5 (CK5) and luminal epithelial cell-associated cytokeratin-18 (CK18) (Fig. 3-2 G) as well as comparable levels of the luminal epithelial cell adherens junction protein, E-cadherin (Fig. 3-2 G), and the tight junction protein, zonula occludens (ZO)-1 (Fig. 3-2 G) (Huebner and Ewald, 2014). Hence, contrary to current dogma, epithelial cell-derived MMP14 is *not* required for mammary gland branching morphogenesis *in vivo*. A compensatory role for MMP15 was also ruled out by demonstrating normal branching in *MMTV-Cre*$^{+/-}$*Mmp14*$^{fl/fl}$*Mmp15*$^{fl/fl}$ mice (Fig. 3-S3 D,E).

Stromal cell-derived MMP14 regulates branching morphogenesis *in vivo.*

The inability of *Mmp14* global knockouts to mount a mammary gland branching program, coupled with the fact that *Mmp14* expression is not restricted to the epithelial compartment, but also extends into the periductal stroma (Fig. 3-S4 A), raises the possibility that the postnatal branching phenotype might result from defects outside the ducts themselves. *Mmp14* was therefore targeted alternatively in the mammary stroma by crossing *Mmp14*$^{fl/fl}$ mice with a *Dermo1/Twist2-Cre* expressing knock-in line, wherein Cre expression is largely confined to mesenchymal cell populations (Tang et al., 2013). As expected, *Dermo1-Cre*-expressing mice crossed onto a *Rosa*^{mTmG} background confirm widespread Cre expression in the mammary stromal cell compartment [with green fluorescence highlighting the periductal fibroblasts and surrounding mammary adipocytes, and red fluorescence chiefly restricted to the mammary epithelium (Fig. 3-3 A). Stromal targeting in *Dermo1-Cre*$^{+/-}$*Mmp14*$^{fl/fl}$ epithelium-free mammary gland tissue resulted in > 90% excision of the *Mmp14* locus at the mRNA level (Fig. 3-3 B) with near complete excision of MMP14 protein expression (Fig. 3-3 C). Remarkably, as these mice age, *Dermo1-Cre*$^{+/-}$*Mmp14*$^{fl/fl}$ mammary glands fail to undergo postnatal branching by either 4 or 8 weeks of age (Fig. 3-3 D; Fig. 3-S4 B,C). Mammary gland cross-sections of the *Dermo1-Cre*$^{+/-}$*Mmp14*$^{fl/fl}$ mammary glands reveal an expansion of periductal fibroblast-like cells surrounding the truncated mammary epithelial ducts (Fig. 3-S4 D,E), and a coincident decrease in adipocyte cell size (Fig. 3-S4 D). While the mammary gland fat pad can, under specific circumstances, regulate branching morphogenesis (e.g., via PPARϒ-dependent pathways or leptin secretion) (Hu et al., 2002; Wang et al., 2013), neither *Pparg, Cebpa, Cebpb,* nor *Leptin* expression are affected in *Dermo1-Cre*$^{+/-}$ *Mmp14*$^{fl/fl}$ mice. Likewise, specific targeting of adipocyte *Mmp14* expression using *Adipoq-Cre* mice (Wang et al., 2013) – though decreasing adipocyte size to a degree similar to that observed

in *Dermo1-Cre*$^{+/-}$*Mmp14*$^{fl/fl}$ mice (Fig. 3-S4 F) – does not impact mammary gland morphogenesis (Fig. 3-S4 G). Interestingly, *Dermo1-Cre*$^{+/-}$*Mmp14*$^{fl/fl}$ ducts display unaltered luminal epithelial cell and myoepithelial cell organization, as defined by CK18 and CK5 expression, respectively, and comparable E-cadherin localization and abundance (Fig. 3-3 E), suggesting the preservation of wild-type epithelial cell organization and structure. Nevertheless, *Dermo1Cre*$^{+/-}$*Mmp14*$^{fl/fl}$ mammary glands display widespread decreases in proliferation (determined by Ki67 immunohistochemistry) in both the epithelial and stromal cell compartments (Fig. 3-3 F). Finally, to rule out possible confounding effects on branching arising as a consequence of *Dermo1-Cre*-mediated *Mmp14* deletion in stromal cell populations residing in other organ systems, intact mammary glands recovered from *Dermo1-Cre*$^{+/-}$*Mmp14*$^{fl/fl}$, *Dermo1-Cre*$^{+/-}$*Mmp14*$^{+/+}$, and *Mmp14*$^{fl/fl}$ donors were transplanted into syngeneic, adult wild-type recipients, and mammary gland branching monitored (Fig. 3-S5 A). By 5 weeks post-transplantation, control *Dermo1-Cre*$^{+/-}$ *Mmp14*$^{+/+}$ or *Mmp14*$^{fl/fl}$ mammary glands branch effectively towards the edges of the transplanted glands (Fig. 3-S5 B). By contrast, the *Dermo1-Cre*$^{+/-}$*Mmp14*$^{fl/fl}$ transplants remain unable to undergo branching (Fig. 3-S5 B), confirming an organ-autonomous role for stromal cell-derived MMP14.

The combination of underdeveloped mammary stroma, widespread proliferation defects, and a concomitant block in postnatal mammary duct advancement in *Mmp14*-targeted mice could potentially be explained as a consequence of defects in the expression of stromal cell-derived growth factors or signaling components critical for postnatal mammary gland branching (Robinson, 2007). Gene expression profiling of tissues isolated from mammary glands of *Dermo1Cre*$^{+/-}$*Mmp14*$^{fl/fl}$ and *Mmp14*$^{+/+}$ mice were therefore carried out, revealing >1000 transcript changes (using a 2-fold enrichment cutoff; $p<0.05$; n=3 per genotype) with 757 genes down-

regulated and 257 genes up-regulated in the targeted mice. Functional annotation clustering and enrichment analysis of these data (DAVID Bioinformatics Resource) indicate wide-ranging effects on Gene Ontology (GO) categories, including those associated with cell adhesion, plasma membranes and chemotaxis, gland morphogenesis and epithelial cell development (Fig. 3-3 G). In terms of stromal cell gene expression, however, growth factors and signaling molecules that have been previously implicated in mammary gland branching (Robinson, 2007), including cytokines (e.g., *Hgf, Igf1, Fgf2, Fgf7, Fgf10, Egf, Tgfa* and *Tgfb*), *Wnt* family members, and growth factor/signaling receptors (e,g, *Esr1*, *Pgr*, *Vdr*, *Met*, *Ghr*, *Fgfr2*, *Egfr*, *Erbb2*, *Erbb3* and *Src*) (Robinson, 2007) are not altered significantly (Fig. 3-S6 A,B). Further, despite recent reports that MMP14 regulates cellular proliferation and tissue development by engaging a cellular senescence-associated gene program (Gutierrez-Fernandez et al., 2015), senescence-associated β-gal (SA-βgal) expression levels are globally reduced, rather than increased, in the mammary epithelium and surrounding stroma of *Dermo1-Cre*$^{+/-}$*Mmp14*$^{fl/fl}$ mammary tissue relative to wild-type littermates (Fig. 3-S6 C). While other stromal cell types have been shown to play critical roles in postnatal mammary gland branching, including macrophages, vascular endothelial cells and lymphatic endothelial cells (Inman et al., 2015; Khokha and Werb, 2011; Varner and Nelson, 2014), macrophage distribution is unaffected in *Dermo1-Cre*$^{-/-}$ *Mmp14*$^{fl/fl}$ glands in tandem with normal, if not increased, numbers of blood vessels and lymphatics (Fig. 3-S7 A,B). Further, specific targeting of macrophage *Mmp14* or endothelial *Mmp14/Mmp15*, using *Csf1r-Cre* or *Tie2-Cre* crosses (Deng et al., 2010; Landskroner-Eiger et al., 2015), respectively, has no effect on mammary gland branching (Fig. 3-S8 A,B).

Stromal cell-derived MMP14 regulates mammary gland extracellular matrix remodeling *in vivo.*

In normal mammary glands, ductal networks are surrounded by a sleeve of type I collagen fibrils (Fig. 3-4 A) (Huebner and Ewald, 2014; Khokha and Werb, 2011). Remarkably, when *Mmp14* is targeted in the stromal cell compartment, periductal type I collagen protein levels as assessed by Sirius Red/polarized light analysis are increased more than 10-fold (Fig. 3-4 A). Further, the basement membrane, a specialized form of ECM that subtends the ductal epithelial cells (Huebner and Ewald, 2014; Khokha and Werb, 2011; Varner and Nelson, 2014), display a ~2-fold increase in type IV collagen levels (Fig. 3-4 B). When assessed by transmission electron microscopy, massive increases in type I collagen fibrils are readily confirmed in tandem with a distinctively thickened basement membrane (Fig. 3-4 C). As analyses of differentially expressed gene products demonstrate that *Mmp14* targeting down-regulates, rather than upregulates, interstitial and basement membrane-associated transcripts (Fig. 3-4 D), we sought to determine whether the mammary gland ECM undergoes active proteolytic remodeling during branching morphogenesis. Interestingly, despite the fact that MMP14 is a potent pericellular collagenase (Chun et al., 2006; Tang et al., 2013), mammary gland ductal morphogenesis has not previously been linked to collagenolytic remodeling in the *in vivo* setting. To this end, type I collagen proteolysis was assessed *in situ* with triple-helical, fluorescently conjugated, collagen mimic peptides (CF-CMPs) (Li et al., 2012). Following heat-mediated denaturation into their single-strand form, CF-CMPs stably hybridize to proteolyzed collagen to reform triple helices that facilitate fluorescent labeling of degraded collagen *in vivo* (Fig. 3-4 E) (Li et al., 2012). Application of CF-CMPs to mammary gland tissues recovered from control $Mmp14^{fl/fl}$ mice reveals dense fields of extracellular degraded collagen fibrils along developing mammary epithelial ducts (Fig.

3-4 F), thereby confirming that ductal morphogenesis engages a matrix remodeling program. In marked contrast, almost no collagen degradation products surround ductal networks in *Dermo1Cre*$^{+/-}$ *Mmp14*$^{fl/fl}$ glands (Fig. 3-4 F). Taken together, these data support a previously undescribed role for MMP14 in remodeling the periductal ECM of branching mammary glands.

An Mmp14-type I collagen axis controls mammary gland branching morphogenesis.

The increased collagen content of *Mmp14*-targeted glands establishes a correlation between MMP14-dependent collagenolysis and branching, but falls short of establishing a causal relationship. Nevertheless, accumulating evidence indicates that type I collagen organization, structure and density can each impact mammary gland branching (Brownfield et al., 2013; Guo et al., 2012; Nguyen-Ngoc et al., 2012). As type I collagen is the most markedly elevated ECM protein in stromal cell *Mmp14*-targeted mice, we sought to establish a direct requirement for type I collagen remodeling in branching morphogenesis by using a mouse knock-in model wherein the collagenase cleavage site in type I collagen is mutated, rendering the molecule collagenase-resistant (Hotary et al., 2003; Liu et al., 1995). Though *Col1a1*$^{r/r}$, *Col1a1*$^{r/+}$ and *Col1a1*$^{+/+}$ mammary glands express comparable protein levels of MMP14 (Fig. 3-5 A), interstitial collagen levels surrounding *Col1a1*$^{r/r}$ mammary ducts are increased dramatically relative to *Col1a1*$^{+/+}$ or *Col1a1*$^{r/+}$ mammary tissues (Fig. 3-5 B). Likewise, as assessed by transmission electron microscopy, while *Col1a1*$^{+/+}$ mammary ducts are surrounded by bundles of sparse or loosely-packed interstitial fibrils (Fig. 3-5 C), *Col1a1*$^{r/r}$ ducts are ensheathed by an almost 100-fold increase in collagen bundles (Fig. 3-5 C) similar to that observed in *Dermo1-Cre*$^{+/-}$ *Mmp14*$^{fl/fl}$ mice (Fig. 3-4 C). Interestingly, *Col1a1*$^{r/r}$ mammary ducts are also ensheathed by a ~5-fold thicker basement membrane despite unchanged type IV collagen and laminin protein levels (Fig. 3-5 C,D).

Most importantly, coincident with these changes in the periductal ECM, *Col1a1*$^{r/r}$ mice display profound defects in ductal branching relative to wild-type littermates with attendant decreases in mammary epithelial cell and stromal cell proliferation and without changes in cellular senescence, in a manner similar, if not identical, to that observed in *Mmp14*-targeted mice (Fig. 3-5 E-G; Fig. 3-S9 A,B). Hence, by rendering type I collagen alone resistant to MMP14-dependent hydrolysis, we recapitulate the key phenotypic features observed in *Mmp14*-deficient mammary gland stroma, thereby identifying the MMP14-type I collagen axis as a dominant regulator of the branching morphogenetic program that characterizes postnatal mammary gland development.

Discussion.

Early studies demonstrated that periductal fibroblasts play critical roles in depositing ECM in the postnatal mammary gland (Keely et al., 1995), yet the notion that mammary stromal cells control ECM remodeling to create conditions permissive for branching morphogenesis has not been considered previously. Largely, this is due to the prevailing notion that epithelial tubules themselves remodel the surrounding stromal environment while the mammary stromal cells more passively supply the necessary instructive signals for morphogenesis (Correia et al., 2013; Inman et al., 2015; Khokha and Werb, 2011; Mori et al., 2009; Mori et al., 2013; Rebustini et al., 2009; Weaver et al., 2014; Wiseman et al., 2003). Using *in vivo* models, we alternatively demonstrate that MMP14 arising from the periductal stromal compartment regulates postnatal mammary gland branching through a requisite process involving remodeling of the periductal type I collagen matrix. Though MMP14 can also serve as an upstream activator of MMP2 and MMP13 zymogens (Rowe and Weiss, 2009), neither of these secreted proteinases play an accessory role here. At first glance, the widespread defects in mammary gland proliferative responses and terminal end bud

formation, coupled with global changes in gene expression in *Mmp14* conditional knockouts, suggest that the proteinase likely regulates events that extend beyond type I collagenolysis per se. Nevertheless, it is remarkable that the *Col1a1*$^{r/r}$ mammary glands, despite expressing wild-type MMP14 levels, display defects in branching and proliferation similar to that observed in stromal *Mmp14*-targeted glands. Taken together, these data demonstrate that inhibiting interstitial type I collagen turnover alone exerts far reaching effects on both primary and lateral branching programs, a finding consistent with the fact that type I collagen density, rigidity and fibril alignment all impact cell function (Brownfield et al., 2013; Guo et al., 2012; Nguyen-Ngoc et al., 2012; Riching et al., 2014).

Early studies with *Mmp14* global knockout mice uncovered more subtle roles for MMP14 in the morphogenic responses of other epithelial organ systems, namely the kidney, salivary glands and lung (Atkinson et al., 2005; Oblander et al., 2005; Riggins et al., 2010). Yet, we find that deletion of stromal cell-derived *Mmp14* does not significantly impact kidney morphogenesis (Fig. 3-S10 A), nor does the absence of stromal *Mmp14* impact the overall branching architecture of the sublingual salivary gland (Fig. 3-S10 B). Interestingly, with regard to each of these morphogenetic programs, the bulk of their respective branching programs occur *in utero* at a time when type I collagen levels are maintained at low levels (Carver et al., 1993; Mays et al., 1988; Van Exan and Hardy, 1984). As such, we posit that there is little requirement for the MMP14/type I collagen remodeling axis during the early development of most branching networks. Importantly, the embryonic and early postnatal mammary gland branching programs that occur in mesenchymal tissues characterized by sparsely populated networks of type I collagen, proceed independently of MMP14 as well (Chapter 2). Interestingly, the lung also undergoes a distinct phase of postnatal morphogenesis marked for alveolar development (Atkinson et al., 2005) wherein we find that

Dermo1-Cre$^{+/-}$*Mmp14*$^{fl/fl}$ lungs display decreases in alveologenesis (Fig. 3-S10 C). However, as this morphologic defect fails to coincide with an increase in interstitial ECM (Fig. 3-S10 D), it appears that stromal cell-derived MMP14 regulates postnatal lung morphogenesis through a distinct, but as yet, uncharacterized mechanism.

Taken together, we demonstrate that elongating mammary ducts are completely dependent upon the surrounding stromal cells to remodel the periductal type I collagen network. In the absence of the type I collagenolysis, the basement membrane thickens in a process that cannot be reversed by epithelial cell-derived MMP14 or MMP15, despite their known ability to remodel type IV collagen as well as laminin during tissue-invasive processes (Hotary et al., 2006; Ota et al., 2009). Interestingly, cancer cell invasion has been linked to fibroblast-mediated remodeling of the interstitial matrix (Albrengues et al., 2014; Gaggioli et al., 2007), but in preliminary studies, we find that mammary carcinoma cells themselves mobilize MMP14 and MMP15 to mediate invasion and metastasis, a finding in keeping with the ability of cancer cells to establish direct contacts with type I collagen after perforating basement membrane barriers (Rowe and Weiss, 2009). In this regard, developmental and neoplastic "solutions" for traversing tissue barriers in the postnatal state – though commonly viewed as conserved – appear distinct, with controlled mammary morphogenetic programs remaining completely reliant on MMP14-mediated, stromal cell-dependent remodeling.

Experimental procedures.

Mouse strains.

Mmp14$^{lacZ/+}$ mice (Tang et al., 2013) were bred onto a C57BL/6J background (Jackson Laboratory, 000664). To generate *Mmp15*$^{lacZ/+}$ mice, C57BL/6J *Mmp15*$^{lacZ/+}$ ES cell clones from the UC Davis KOMP Repository (KOMP) [MGI allele: *Mmp15tm1a* (KOMP) wtsi, clone: EPD0097_3_B09] were introduced into albino C57BL/6J host blastocysts. Chimeras were mated with C57BL/6J mice to test for germline transmission. *Mmp15*$^{lacZ/+}$ mice were bred and maintained on a C57BL/6J background. *Mmp14*$^{+/-}$ mice (Holmbeck et al., 1999) were mated n>5 generations onto a FVB background or bred with a transgenic mouse line expressing enhanced GFP under the control of a chicken beta-actin promoter (FVB background, Jackson Laboratories, 003291). *Mmp3*$^{-/-}$ mice (C57BL/6J background), *Mmp13*$^{-/-}$ (C57BL/6J background), and *Mmp2*$^{-/-}$ mice (129/SvEv background, Taconic) were genotyped as described (Nielsen et al., 2008; Wiseman et al., 2003) . To generate *Mmp15* global knockout (*Mmp15*$^{-/-}$) mice, 129/SVJ ES cells were electroporated with a targeting vector for *Mmp15* containing a neomycin selection cassette flanked by FRT sites wherein exons 4 and 5 of the catalytic domain were floxed by loxP sites (Fig. 3-S2 D). Following neomycin selection, ES cell recombinants were injected into gestation day E3.5 C57BL/6J blastocysts and subsequently injected into the uteri of pseudo-pregnant FVB mice. Male chimeras were mated to C57BL/6J females, and heterozygous agouti offspring carrying the *Mmp15*^{flox} allele were mated to C57BL/6J *FlpE* mice to remove the neomycin selection cassette. The resultant *Mmp15*$^{fl/fl}$ mice were crossed to C57BL/6J *EIIA-Cre* mice for germline deletion of *Mmp15,* with *Mmp15*$^{+/-}$ mice backcrossed into C57BL/6J mice (n>10 generations). *Mmp14*^{flox} mice were generated as described previously (Tang et al., 2013) and maintained on either a C57BL/6J or FVB background (n>10 generations). *MMTV-Cre* transgenic mice (line A)(Wagner et al., 2001)

(Jackson Laboratory, 003551) on a congenic FVB background (n>10 generations) were mated with *Mmp14*$^{fl/fl}$ mice (FVB background) or *Mmp14*$^{fl/fl}$*Mmp15*$^{fl/fl}$ mice (FVB background, n>5 generations). *Dermo1/Twist2-Cre* mice (Tang et al., 2013) (Jackson Laboratory, 008712) were bred with *Mmp14*$^{fl/fl}$ mice (C57BL/6J background) and maintained on a congenic C57BL/6J background or crossed onto a mixed C57BL/6J:FVB background. *Col1a1*$^{r/r}$ mice (Liu et al., 1995) were maintained on a 129/SvEv background. *Tie2-Cre* transgenic mice (Jackson Laboratory, 004128) and *Csflr-Cre* transgenic mice (Jackson Laboratory, 021024) were maintained on mixed C57BL/6J:FVB and congenic FVB backgrounds, respectively. All mouse work was performed with IACUC approval at the University of Michigan.

Genotyping Primers.

Genotyping was performed on purified chromosomal DNA prepared from tail tips. Genotyping primers include the following. For *Mt1-mmp/Mmp14* global knockout litters: *Mmp14*^{WT}-F: 5'-CTA GGC CTG GAA CAT TCT AAC GAT C-3' and *Mmp14*-R: 5'-CTT TGT GGG TGA CCC TGA CTT GC-3'; *Mmp14*^{KO}-F*:* 5'-GTG CGA GGC CAG AGG CCA CTT GTG T-3' and *Mmp14*-R: 5'-CTT TGT GGG TGA CCC TGA CTT GC-3'. For *Mmp14*^{lacZ} litters: *Mmp14*^{lacZ} *(+)*-F: 5'-ACCTGCGTGCAATCCATCTTG-3' and *Mmp14*^{lacZ} *(+)*-R: 5'-ATGATGGCGGAGGGATCGTTAG-3'; *Mmp14*^{lacZ} *(-)*-F: 5'-TGAGGTGGAAAACACGACCAG-3' and *Mmp14*^{lacZ} *(-)*-R: 5'-ATGATGGCGGAGGGATCGTTAG-3'. For *Mmp15*-^{targeted} litters: *Mmp15*^{loxA} -F: 5'-CCG CCA CCA AGC CTC ACT GTC T-3' and *Mmp15*^{loxB}*-R*: 5'-AAA GCC ACC CAC GCC ATC AAA C-3'; *Mmp15*^{KO}*-F:* 5'-CGC CAC CAA GCC TCA CTG TCT-3' and *Mmp15*^{KO}*-R*: 5'-AAT TGC TGG GGA TGG AGG AAG GTA-3'. For *Mmp15*^{lacZ} litters: *Mmp15*^{lacZ}-F: 5'-GAG ATG GCG

CAA CGC AAT TAA TG-3' and *Mmp15*^{lacZ}-R: 5'-TGC ACG TCC CAT TCT CAT GC-3'. For *Mmp2* global knockout litters: *Mmp2*^{WT}*- F:* 5'-GTGCTACTGCAGGATAAACTGATG-3' and *Mmp2*^{WT}*- R:* 5'-CCGGGACAGGAACGTACTGGGTTC-3'; *Mmp2*^{KO}*-F:* 5'-GCGCCTACCGGTGGATGTGGAATGTGT GCG-3' and *Mmp2*^{KO}*-R:* 5'-CCGGGACAGGAACGTACTGGGTTC-3'. For *Mmp3* global knockout litters: *Mmp3*^{WT}*-F*: 5'-ACC GGA TTT GCC AAG ACA GAG TG-3' and *Mmp3*^{WT}*-R*: 5'-GCA TCT CCA TTA ATC CCT GGT CC-3'; *Neo-F*: 5'-AGGATCTCCTGTCATCTCACCTTGCTC CTG-3' and *Neo-R*: 5'-AAGAACTCGTCAAGAAGGCGATAGAA GGCG-3'. *Mmp13* genotyping was carried out as described (Nielsen et al, 2008). For *Mmp14*^{flox} litters: *Mmp14*^{flox}-F: 5'- GTT GAG GCA GGA GGA TTG TGA GTT-3' and *Mmp14*^{flox}-R: 5'- CCT GGA AAA GTG GGC GAG AAG-3'; CreU: 5'-AGG TGT AGA GAA GGC ACT TAG C-3' and CreD: 5'-CTA ATC GCC ATC TTC CAG GAG G -3'; iCre-F: 5'-CCG TTT GCC GGT CGT GGG-3' and iCre-R: 5'-CGA ATA TCC TGG CAG CGA TC-3'.

Mammary gland whole mount preparation, imaging and morphometric analysis.

Inguinal mammary glands were harvested, mounted on glass slides, stained with Carmine Alum, and processed as described previously (Wiseman et al., 2003). Whole mounts were imaged with a Leica MZFLIII dissecting microscope. Adobe Photoshop and ImageJ were used to process images.

RNA extraction and gene expression analysis.

Inguinal mammary gland tissue was flash frozen in liquid nitrogen, and homogenized in TRIzol (Ambion, Life Technologies). Mammary epithelial cells were isolated from inguinal

mammary glands as described (Mori et al., 2013), washed with PBS and directly lysed in TRIzol. Total RNA was extracted and purified using QIAGEN RNeasy Mini-kit columns (QIAGEN, 74104). RNA quality was confirmed using an Agilent 2100 Bioanalyzer and samples profiled on Affymetrix Mouse MG–430 PM expression array strips. Expression values for each probe set were calculated using a robust multi-array average (RMA) (Irizarry et al., 2003) and filtered for genes with a greater than 2-fold change.

Quantitative real-time PCR.

Complementary cDNA was prepared from total RNA with the Invitrogen SuperScript II First-Strand Synthesis System (11904-018). Quantitative reverse-transcription PCR was performed with SYBR Green (Applied Biosystems) using *Gapdh* or *Arbp*/*Rplp0* for reference gene expression. Quantitative PCR primers include the following: *Gapdh*-Forward: 5'-TGAAGCAGGCATCTGAGGG-3' and *Gapdh*-Reverse: 5'-CGAAGGTGGAAGAGTGGGAG-3'; *Arbp*-Forward: 5'-CACTGGTCTAGGACCCGAGAA-3' and *Arbp*-Reverse: 5'-AGGGGGAGATGTTCAGCATGT-3'; *Mmp14*-Forward: 5'-CTGCCATTGCCGCCATGCAAAA-3' and *Mmp14*-Reverse: 5'-TGGCGTGGCACTCTCCCATACT-3'; *Mmp15*-Forward: 5'-ACATGTCCACCATGCGCTCT-3' and *Mmp15*-Reverse: 5'-TACCATGATGTCAGCCTCC-3'; *Mmp2*-Forward: 5'-TCTGGAGCGAGGATACCCCAA-3' and *Mmp2*-Reverse: 5'-TTCCAGGAGTCTGCGATGAGC-3'; *Mmp3*-Forward: 5'-GTT CCT GAT GTT GGT GGC TT-3' and *Mmp3*-Reverse: 5'-AGC CTC TCC TTC AGA GAT CC-3'; *Mmp13*-Forward: CTT TTC CTC CTG GAC CAA ACT and *Mmp13*-Reverse: TCA TGG GCA GCA ACA ATA AA. Data

reported as the mean expression levels with error bars representing the standard error (SEM). p values were calculated with an unpaired t-test with two tails.

Western Blotting.

Inguinal mammary gland tissue was flash frozen in liquid nitrogen and homogenized in lysis buffer. Protein concentrations were determined with the Pierce BCA Protein Assay Kit (Thermo Scientific), and extracts (40-to-50 µg) were analyzed by standard techniques with horseradish peroxidase–conjugated secondary antibodies (Santa Cruz Biotechnology).

LacZ and cellular senescence staining.

Inguinal *Mmp14*$^{lacZ/+}$ mammary glands were fixed at 4^{o}C in PBS containing 2% paraformaldehyde and 0.2% glutaraldehyde. *Mmp15*$^{lacZ/+}$ glands were alternatively fixed in 4% paraformaldehyde. Tissues were either transferred to 30% sucrose/PBS (w/v) for frozen sections, or incubated for 18-24 h in PBS containing 4 mM potassium hexacyanoferrate (III), 4 mM potassium hexacyanoferrate (II) trihydrate, 2 mM $MgCl_2$, 0.2% NP-40, 0.1% sodium deoxycholic acid and 1 mg/ml Xgal. Stained tissues and whole mounts were post-fixed with 10% formalin-phosphate. Senescence-associated β-gal staining was carried out on mammary gland cryo-sections as described for the Senescence β-galactosidase Staining Kit (Cell Signaling, 9860). Sections were stained overnight (12-to-15 h) in a non-humidified 37^{o}C incubator, counter-stained with Eosin, and dehydrated with a graded ethanol/xylene series before mounting with Permount Toluene Solution (Fisher Scientific, SP15-100).

Immunofluorescence, immunohistochemistry and morphometric analysis.

Mammary gland tissue was fixed in 10% formalin-phosphate at 4º C overnight and either dehydrated in an ethanol/paraffin series for paraffin embedding or transferred to 30% (w/v) sucrose/PBS for OCT embedding. Following rehydration with a xylene/ethanol series and microwave-mediated antigen retrieval, paraffin sections were permeabilized with 0.3% Triton X-100/PBS, and blocked for 2 hours prior to primary antibody addition. Samples were incubated overnight at 4ºC with antibodies directed against [ZO-1 (Invitrogen, 617300), E-cadherin (BD Transduction Laboratories, 610181), Cytokeratin-5 (Covance, PRB-160p), Cytokeratin-14 (Covance, PRB-155P, Clone AF64), Cytokeratin-18 (Abcam, ab668), Ki67 (Abcam, ab15580), GFP (Abcam, ab290), α-smooth muscle actin (Abcam, ab5694), and vimentin (Abcam, ab20346)]. Frozen sections were used for immunostaining of basement membrane (BM), macrophages (F4/80, ab6640, Abcam), blood vessels (CD31, 553370, BD Biosciences) and lymphatics (Lyve-1, ab14917, Abcam). For BM staining, frozen sections were permeabilized with 0.5% Triton X-100/ PBS, incubated in blocking buffer (10% FBS/1% BSA/PBS) for 2 hours, and incubated with primary antibodies directed against type IV collagen (Millipore, AB-769) or laminin (Sigma-Aldrich, L9393) overnight at 4ºC. Following primary antibody incubations, sections were incubated with Alexa-488 or Alexa-594-conjugated secondary antibodies (Invitrogen Molecular Probes). Nuclear counter-staining was carried out with either Toto3 (Invitrogen Molecular Probes) or 4, 6-diamidino-2-phenylindole (DAPI). All fluorescence images were acquired with an Olympus FluoView FV500 laser scanning confocal microscope and analyzed with Adobe Photoshop and ImageJ software. For immunohistochemistry, endogenous peroxidase activity was blocked with H_2O_2 and tissues sections developed with the Vectastain ABC (Vector Laboratories, PK-6100) and DAB kits (Vector Laboratories, SK-4100).

Mammary tissue and whole gland transplants.

Mammary tissue fragment transplants were carried out as described previously (Robinson et al., 2000). In brief, inguinal mammary glands of recipient mice (postnatal day 21, 10-to-11 grams body weight) were "cleared" of their endogenous epithelium by surgical removal of the mammary gland tissue between the cauterized femoral artery and the inguinal lymph node. The isolated epithelium-containing mammary tissue was mounted on glass slides for whole mount Carmine staining to confirm clearing. Single 1-to-2 mm fragments of donor mammary epithelium-containing tissue from 2-week-old mice were transplanted into the remaining epithelium-free recipient mammary gland for *in vivo* growth. Transplants were allowed to branch *in vivo* for 6-to-8 weeks prior to whole mount and histological assessments. For transplant of whole mammary glands, the inguinal mammary glands from 6-to-8 week-old recipient mice were excised in entirety following cauterization of the femoral artery, in order to remove the host epithelium, and the isolated tissue was mounted on glass slides for whole mount Carmine staining to confirm clearing. Intact whole mammary glands from 5-to-10 day-old donor mice were sutured onto the gland-free subcutaneous surface. The transplants were allowed to branch *in vivo* for 4-to-5 weeks prior to whole mount assessments. Athymic nude mice (Harlan) were used as recipients for the transplant of $Gfp^{+/-}Mmp14^{+/-}$ and $Gfp^{+/-}Mmp14^{-/-}$ ductal fragments. Syngeneic C57BL/6J mice (Jackson Laboratory) were used as recipients for the transplant of $Mmp14^{fl/fl}$ and $Dermo1Cre^{+/-}Mmp14^{fl/fl}$ mammary glands.

CMP peptide assay.

Mammary gland cryosections (10-to-30 μM thickness) were washed in 1X PBS and blocked in 1% BSA/ 3% goat serum/ PBS at room temperature for 1 hour. During blocking, heat-

activated fluorescently labeled CMP stock solution (CF-CMP [CF-G-$(GPO)_9$]) and sequence-scrambled control peptide stock solution (Li et al., 2012) were diluted to 10-to-30 µM in PBS and incubated at 70°C for 10 minutes, followed by a brief (10-to-30 second) incubation on ice before immediate application to blocked tissue for overnight incubation at 4°C while protected from light. Following washes with PBS, nuclei were counterstained with DAPI and sections were mounted with Prolong Gold anti-fade reagent.

Tissue preparation for TEM.

Samples were fixed (1% glutaraldehyde/1% tannic acid/0.1 M Sorensen's buffer, pH 7.2) and post-fixed with 1% osmium tetroxide prior to embedding in EMbed 812 epoxy resin (Electron Microscopy Sciences). Thin sections (70 nm) were post-stained with uranyl acetate and Reynolds Lead Citrate, and imaged with a JE0L JEM-1400 Plus electron microscope. Images were recorded digitally using a Hamamatsu ORCA-HR digital camera system, operated using AMT software (Advanced Microscopy Techniques Corp., Danvers, MA).

Fig. 3-1.

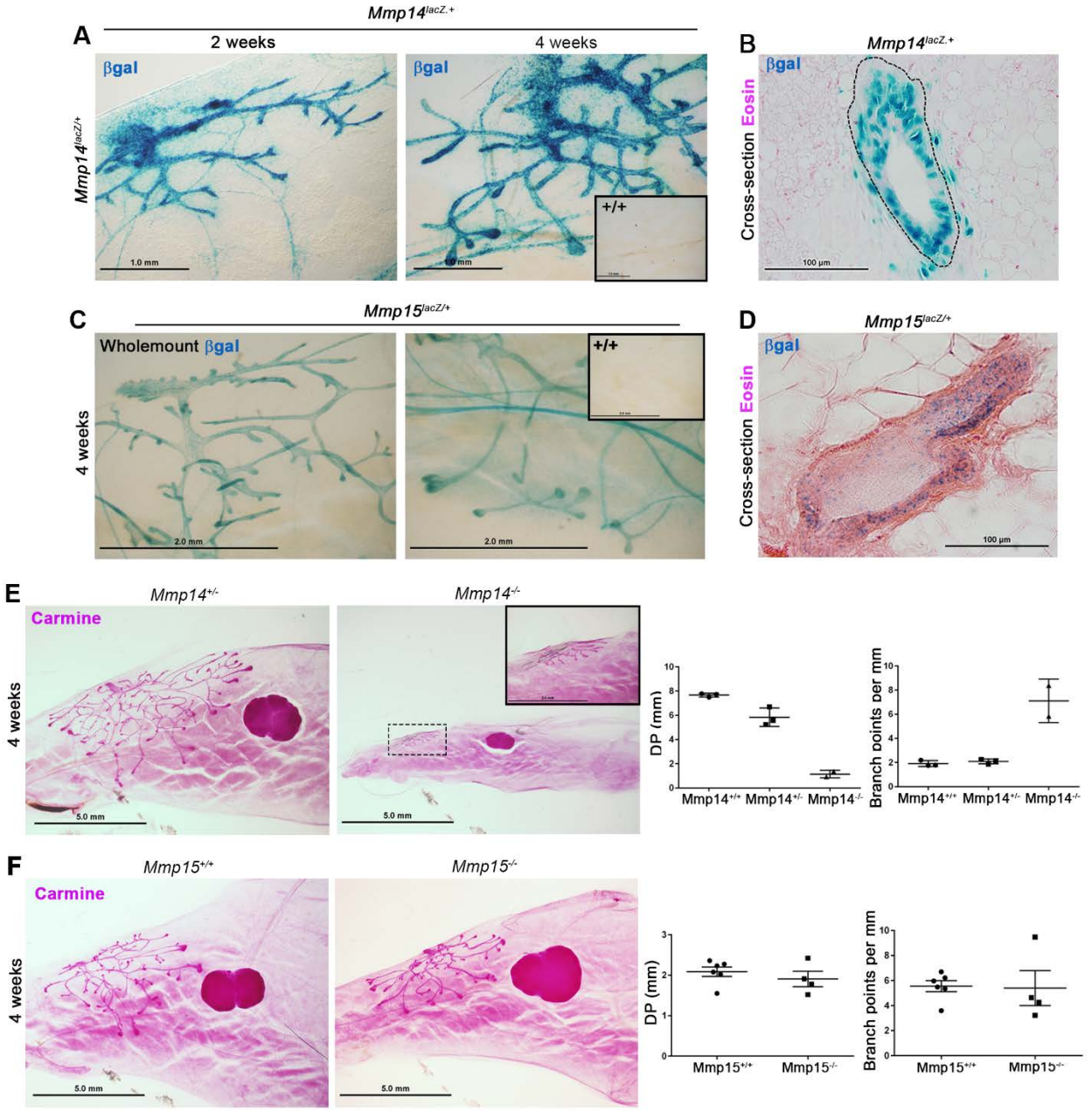

Fig. 3-1. Postnatal mammary gland branching is MMP14-dependent.
(A) LacZ staining of whole mount from *Mmp14*$^{lacZ/+}$ mice at 2 and 4 weeks (bars=1.0 mm) (B) Cross-section of 4 week-old *Mmp14*$^{lacZ/+}$ mammary gland (bar=100 µm). (C) LacZ staining of 4 week-old *Mmp15*$^{lacZ/+}$ gland (bar=2.0 mm). Insets (a,c) show LacZ of littermate controls. (D) Cross-section of 4 week-old *Mmp15*$^{lacZ/+}$ gland (bar=100 µm). (E) Whole mounts from 4 week-old *Mmp14*$^{+/+}$ and *Mmp14*$^{-/-}$ mice. Ductal penetration (DP) (mm) and branch points/mm duct for *Mmp14*$^{+/+}$ (n=3), *Mmp14*$^{+/-}$ (n=3), and *Mmp14*$^{-/-}$ (n=2) glands (mean±s.d.). (F) Whole mounts

from 4 week-old *Mmp15*$^{+/+}$ and *Mmp15*$^{-/-}$ mice. DP and branch points/mm for *Mmp15*$^{+/+}$ (n=6) and *Mmp15*$^{-/-}$ (n=4) (mean±s.e.m.). (E,F) (bar=5.0 mm).

Fig. 3-2.

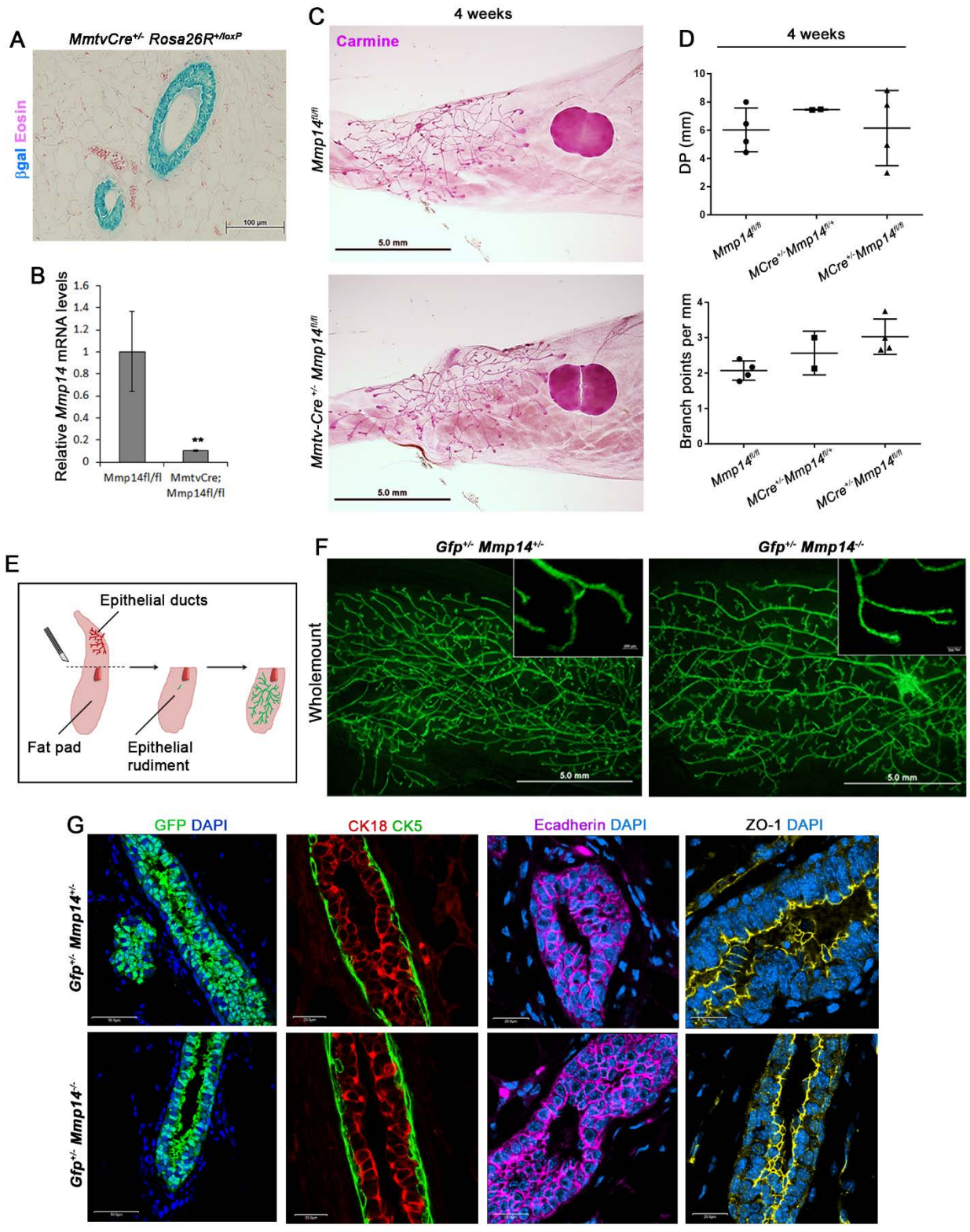
A
MmtvCre+/- Rosa26R+/loxP
βgal Eosin
100 μm
B
Relative Mmp14 mRNA levels
1.6
1.4
1.2
1
0.8
0.6
0.4
0.2
0
**
Mmp14fl/fl
MmtvCre; Mmp14fl/fl
C
4 weeks
Carmine
Mmp14fl/fl
5.0 mm
Mmtv-Cre+/- Mmp14fl/fl
5.0 mm
D
4 weeks
DP (mm)
10
8
6
4
2
0
Mmp14fl/fl
MCre+/-Mmp14fl/+
MCre+/-Mmp14fl/fl
Branch points per mm
4
3
2
1
0
Mmp14fl/fl
MCre+/-Mmp14fl/+
MCre+/-Mmp14fl/fl
E
Epithelial ducts
Fat pad
Epithelial rudiment
F
Gfp+/- Mmp14+/-
Gfp+/- Mmp14-/-
Wholemount
5.0 mm
5.0 mm
G
GFP DAPI
CK18 CK5
Ecadherin DAPI
ZO-1 DAPI
Gfp+/- Mmp14+/-
Gfp+/- Mmp14-/-

Fig. 3-2. Mammary gland branching is independent of epithelial cell-derived MMP14.
(A) LacZ staining of cross-sections from 4 week-old *MmtvCre*$^{+/-}$*Rosa26R*$^{loxP/+}$ mouse (bar=100 µm). (B) *Mmp14* qPCR in epithelial cells harvested from 4 week-old mice (n=3, ** p<0.001). (C) Whole mounts from 4 week-old *Mmp14*$^{fl/fl}$ (n=4) and *MmtvCre*$^{+/-}$*Mmp14*$^{fl/fl}$ (n=4) mice (bar=5.0 mm). (D) DP and branch points/mm (mean±s.d.). (E) Cartoon of mammary duct transplantation. (F) Whole mounts of mammary tissue at 8 weeks post-transplantation of *Gfp*$^{+/-}$*Mmp14*$^{+/-}$ and *Gfp*$^{+/-}$*Mmp14*$^{-/-}$ ducts (n=10 per genotype of 3 replicates) (bar=5.0 mm). (G) Immunofluorescence of GFP with DAPI counter-staining (bar=50.0 µm), Cytokeratin-18 (CK18), Cytokeratin 5 (CK5), E-cadherin and Zonula occludens (ZO)-1 (bar=20.0 µm) at 8 weeks post-transplantation (n=4).

Fig. 3-3.

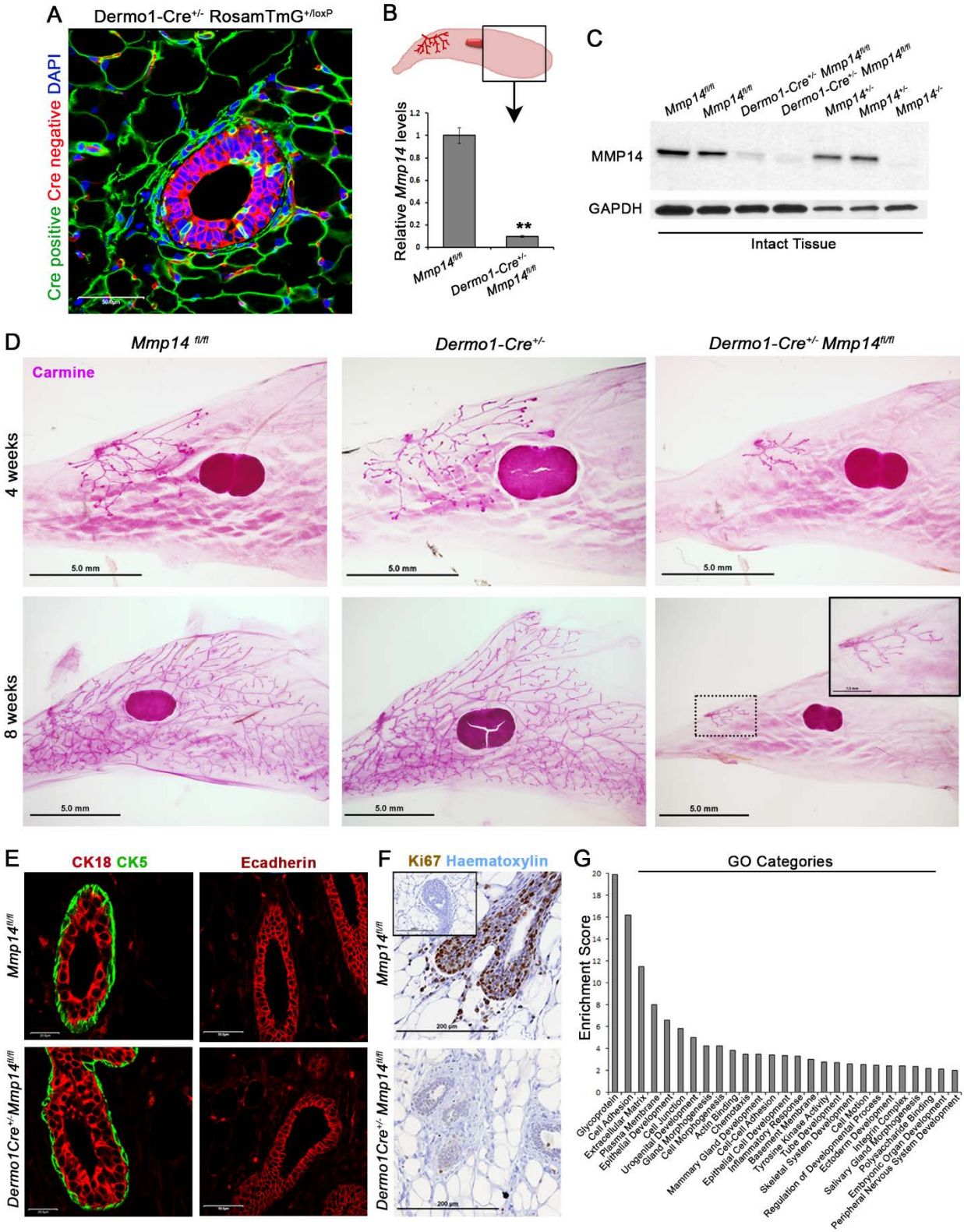
A
Dermo1-Cre+/- RosamTmG+/loxP
Cre positive Cre negative DAPI
B
Relative Mmp14 levels
**
Mmp14fl/fl
Dermo1-Cre+/- Mmp14fl/fl
C
Mmp14fl/fl
Mmp14fl/fl
Dermo1-Cre+/- Mmp14fl/fl
Dermo1-Cre+/- Mmp14fl/fl
Mmp14+/-
Mmp14+/-
Mmp14-/-
MMP14
GAPDH
Intact Tissue
D
Mmp14 fl/fl
Dermo1-Cre+/-
Dermo1-Cre+/- Mmp14fl/fl
Carmine
4 weeks
8 weeks
5.0 mm
E
CK18 CK5
Ecadherin
Mmp14fl/fl
Dermo1Cre+/-Mmp14fl/fl
F
Ki67 Haematoxylin
Mmp14fl/fl
Dermo1Cre+/- Mmp14fl/fl
200 μm
G
GO Categories
Enrichment Score
Glycoprotein
Cell Adhesion
Extracellular Matrix
Plasma Membrane
Epithelial Development
Cell Junction
Urogenital Development
Gland Morphogenesis
Cell Morphogenesis
Actin Binding
Chemotaxis
Mammary Gland Development
Cell-Cell Adhesion
Epithelial Cell Development
Inflammatory Response
Basement Membrane
Tyrosine Kinase Activity
Tube Development
Skeletal System Development
Cell Motion
Regulation of Developmental Process
Ectoderm Development
Integrin Complex
Salivary Gland Morphogenesis
Polysaccharide Binding
Embryonic Organ Development
Peripheral Nervous System Development

Fig. 3-3. Stromal cell-derived MMP14 controls mammary gland branching.
(A) Cross-section of gland isolated from 4 week-old *Dermo1Cre*$^{+/-}$*Rosamtmg*$^{loxP/+}$ mouse with DAPI counter-staining (bar=50 µm). (B,C) *Mmp14* excision at the mRNA and protein level as normalized to *Gapdh* (n=3 replicates, ** $p<0.001$). (D) Carmine-stained whole mounts isolated from *Mmp14*$^{fl/fl}$, *Dermo1Cre*$^{+/-}$, and *Dermo1Cre*$^{+/-}$*Mmp14*$^{fl/fl}$ mice at 4 weeks and 8 weeks ($n\geq4$ per genotype) (bar=5.0 mm). (E) CK18, CK5 and E-cadherin immunofluorescence (bar=50.0 µm), and (F) Ki67 staining with haematoxylin counterstaining (bar=200 µm) in 4 week-old *Mmp14*$^{fl/fl}$ and *Dermo1Cre*$^{+/-}$*Mmp14*$^{fl/fl}$ glands (n=3) (G) Gene ontology (GO) categories differentially expressed in 4 week-old *Dermo1Cre*$^{+/-}$*Mmp14*$^{fl/fl}$ and wildtype mammary tissue (n=3 per genotype).

Fig. 3-4.

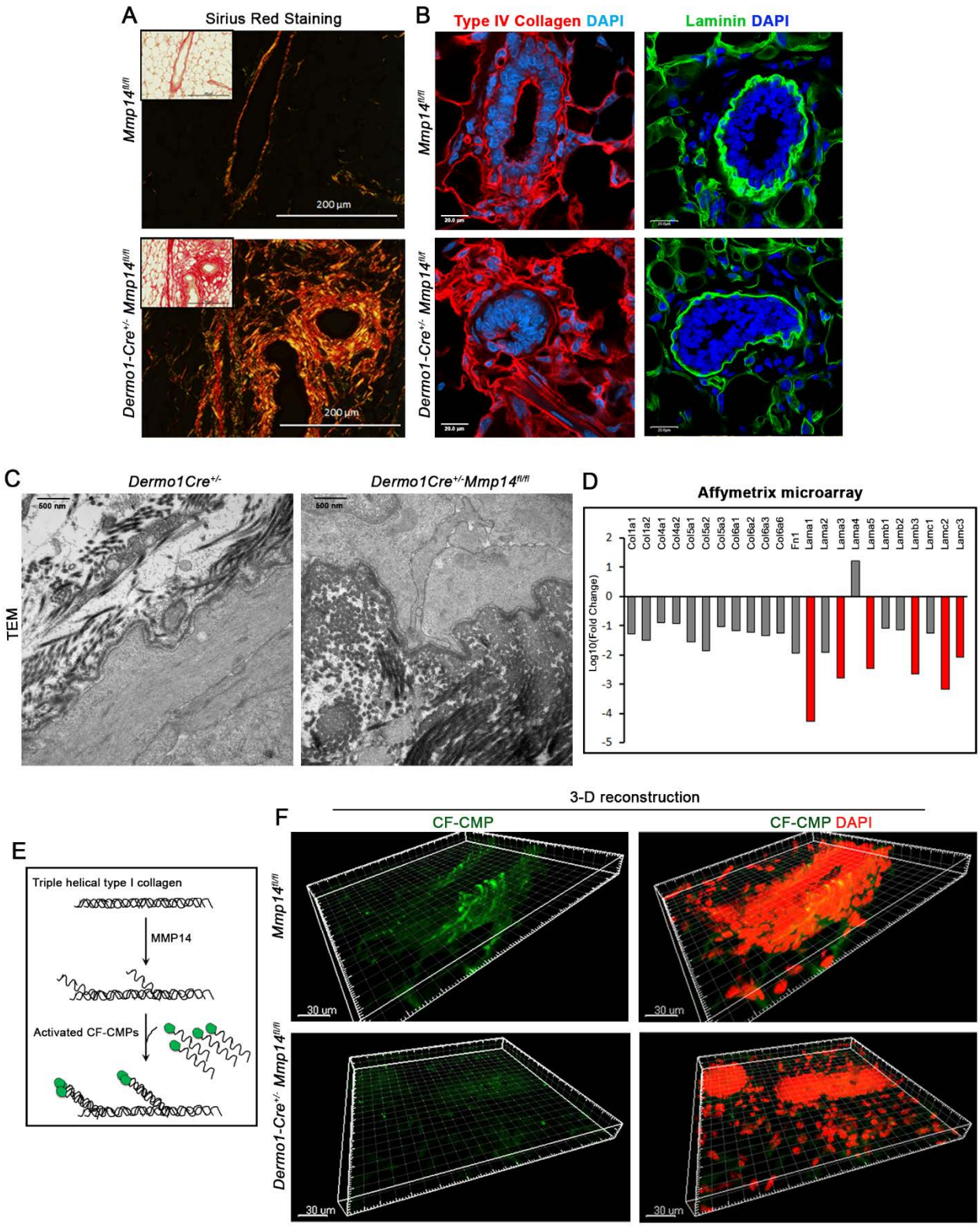
A
Sirius Red Staining
Mmp14fl/fl
Dermo1-Cre+/- Mmp14fl/fl
200 μm
B
Type IV Collagen DAPI
Laminin DAPI
C
Dermo1Cre+/-
Dermo1Cre+/-Mmp14fl/fl
TEM
500 nm
D
Affymetrix microarray
Log10(Fold Change)
Col1a1
Col1a2
Col4a1
Col4a2
Col5a1
Col5a2
Col5a3
Col6a1
Col6a2
Col6a3
Col6a6
Fn1
Lama1
Lama2
Lama3
Lama4
Lama5
Lamb1
Lamb2
Lamb3
Lamc1
Lamc2
Lamc3
E
Triple helical type I collagen
MMP14
Activated CF-CMPs
F
3-D reconstruction
CF-CMP
CF-CMP DAPI
30 μm

Fig. 3-4. Stromal cell-derived MMP14 regulates extracellular matrix remodeling *in vivo.*
(A) Polarized images of Sirius red staining in 4 week-old *Mmp14*$^{fl/fl}$ and *Dermo1Cre*$^{+/-}$*Mmp14*$^{fl/fl}$ glands (bar=200μm). Insets show bright-field images. (B) Type IV collagen and laminin immunofluorescence in *Mmp14*$^{fl/fl}$ and *Dermo1Cre*$^{+/-}$*Mmp14*$^{fl/fl}$ sections with DAPI counter-staining (bar=20μm). (C) TEM of mammary glands isolated from 4 week-old *Dermo1Cre*$^{+/-}$ and *Dermo1Cre*$^{+/-}$*Mmp14*$^{fl/fl}$ mice (bar=500nm). (D) Changes in ECM transcriptomes from 4 week-old *Dermo1Cre*$^{+/-}$*Mmp14*$^{fl/fl}$ and wild-type glands (n=3 per genotype). (E) Schematic of *in situ* labeling of degraded type I collagen with CF-CMPs. (F) 3-D reconstructions of CF-CMP immunofluorescence in mammary glands harvested from 4 week-old *Mmp14*$^{fl/fl}$ and *Dermo1Cre*$^{+/-}$ *Mmp14*$^{fl/fl}$ mice with DAPI counterstaining (bars=30μm; n=3).

Fig. 3-5.

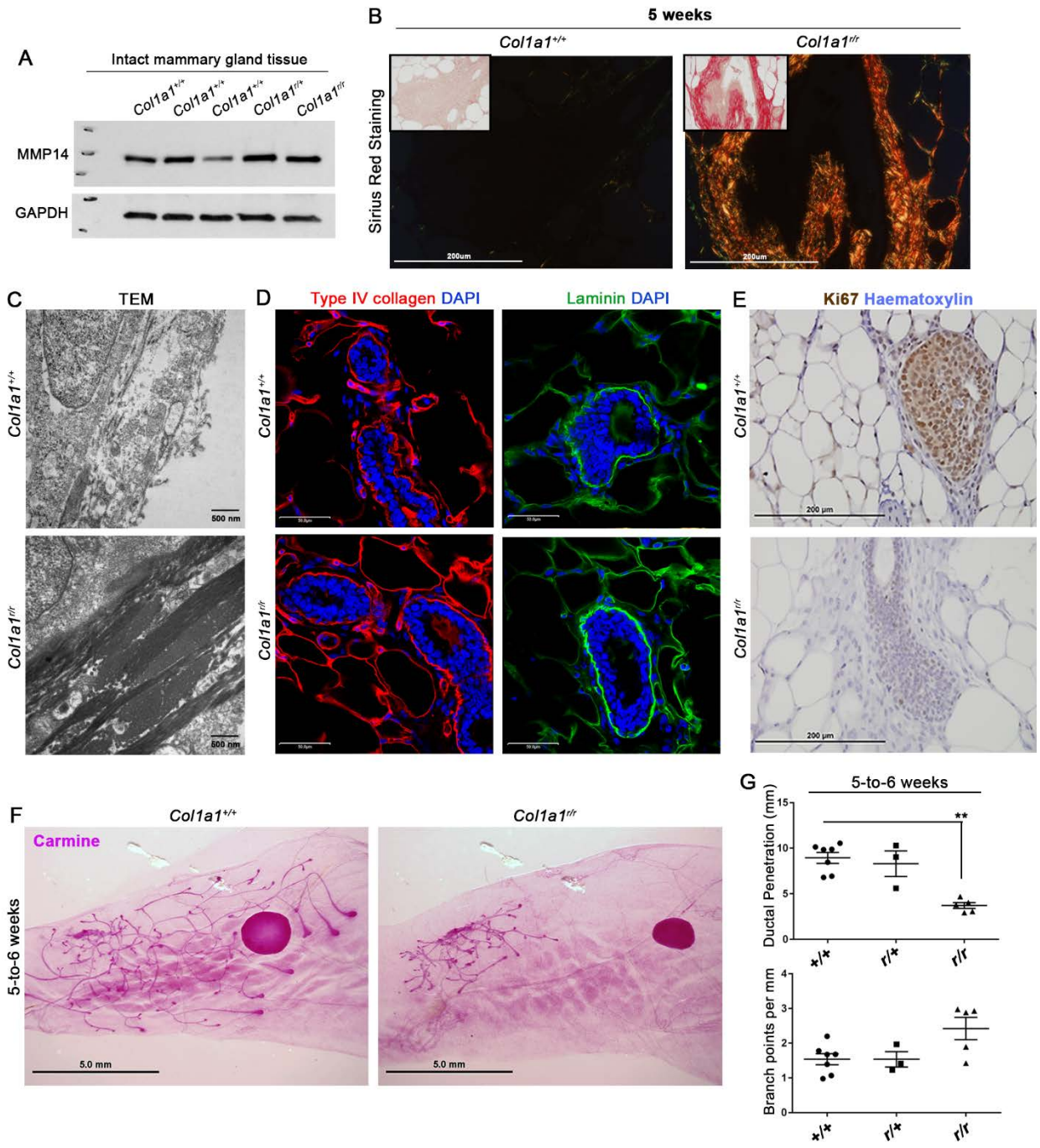

Fig. 3-5. Postnatal mammary gland branching requires type I collagen remodeling.
(A) Western blot of MMP14 in glands harvested from 5 week-old *Col1a1*$^{+/+}$, *Col1a1*$^{r/+}$ and *Col1a1*$^{r/r}$ mice. (B) Polarized images of Sirius red staining in 5 week-old *Col1a1*$^{+/+}$ and *Col1a1*$^{r/r}$ glands. Insets show bright-field images (bar=200 μm). (C) TEM of 5 week-old *Col1a1*$^{+/+}$ and *Col1a1*$^{r/r}$ glands (bar=500 nm). (D) Type IV collagen and laminin Immunofluorescence in 5-6 week-old *Col1a1*$^{+/+}$ and *Col1a1*$^{r/r}$ glands (bar=50μm). (E) Ki67 staining in 5-6 week-old

Col1a1$^{+/+}$ and *Col1a1*$^{r/r}$ glands (bar=200µm; n=3). (F,G) Carmine staining of 5-6 week-old *Col1a1*$^{+/+}$ and *Col1a1*$^{r/r}$ glands (bar=5.0 mm) with DP and branch points/mm in *Col1a1*$^{+/+}$ (n=6), *Col1a1*$^{r/+}$ (n=3), and *Col1a1*$^{r/r}$ (n=5) littermates. **p<0.0001.

Fig. 3-S1.

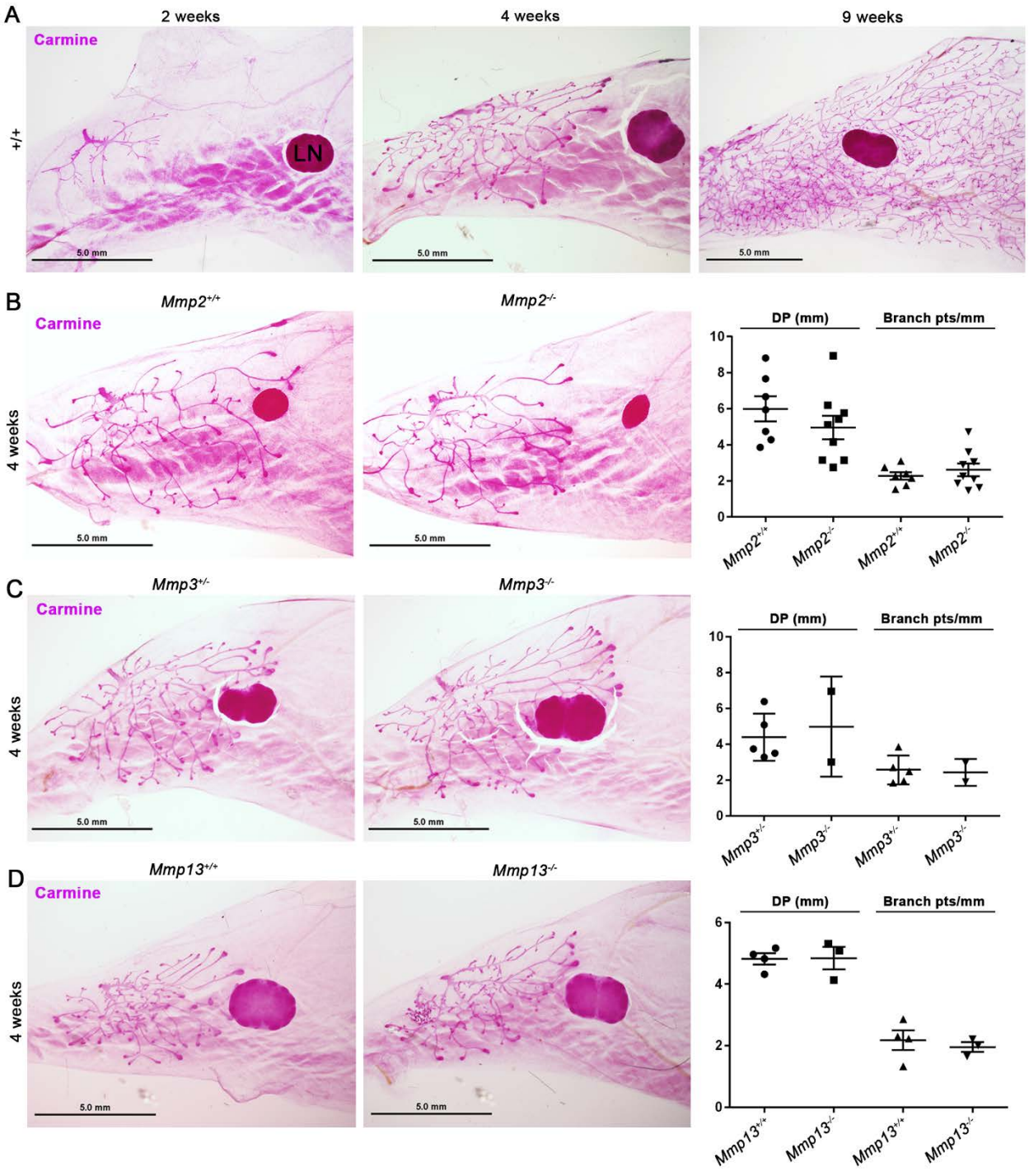

Fig. 3-S1. Postnatal mammary gland branching independent of MMP2, MMP3 and MMP13. (A) Carmine staining of mammary gland whole mounts isolated from wildtype female mice at 2, 4 and 9 weeks postnatal ("LN" marks the inguinal lymph node). (B) Carmine-stained mammary

gland whole mounts from 4 week-old *Mmp2*$^{+/+}$ and *Mmp2*$^{-/-}$ mice with quantification of ductal penetration (DP) (mm) and branch points/mm duct in n≥7 mice per genotype. Results expressed as mean ± s.e.m. (C) Carmine-stained mammary gland whole mounts from 4 week-old *Mmp3*$^{+/-}$ (n=5) and *Mmp3*$^{-/-}$ (n=2) mice with quantification of DP (mm) and branch points/mm. Results expressed as mean ± s.d. (D) Carmine-stained mammary gland whole mounts from 4 week-old *Mmp13*$^{+/+}$ (n=4) and *Mmp13*$^{-/-}$ (n=3) mice with quantifications of DP (mm) and branch points/mm. Results expressed as mean ± s.e.m. (A-D) scale bar=5.0 mm.

Fig. 3-S2.

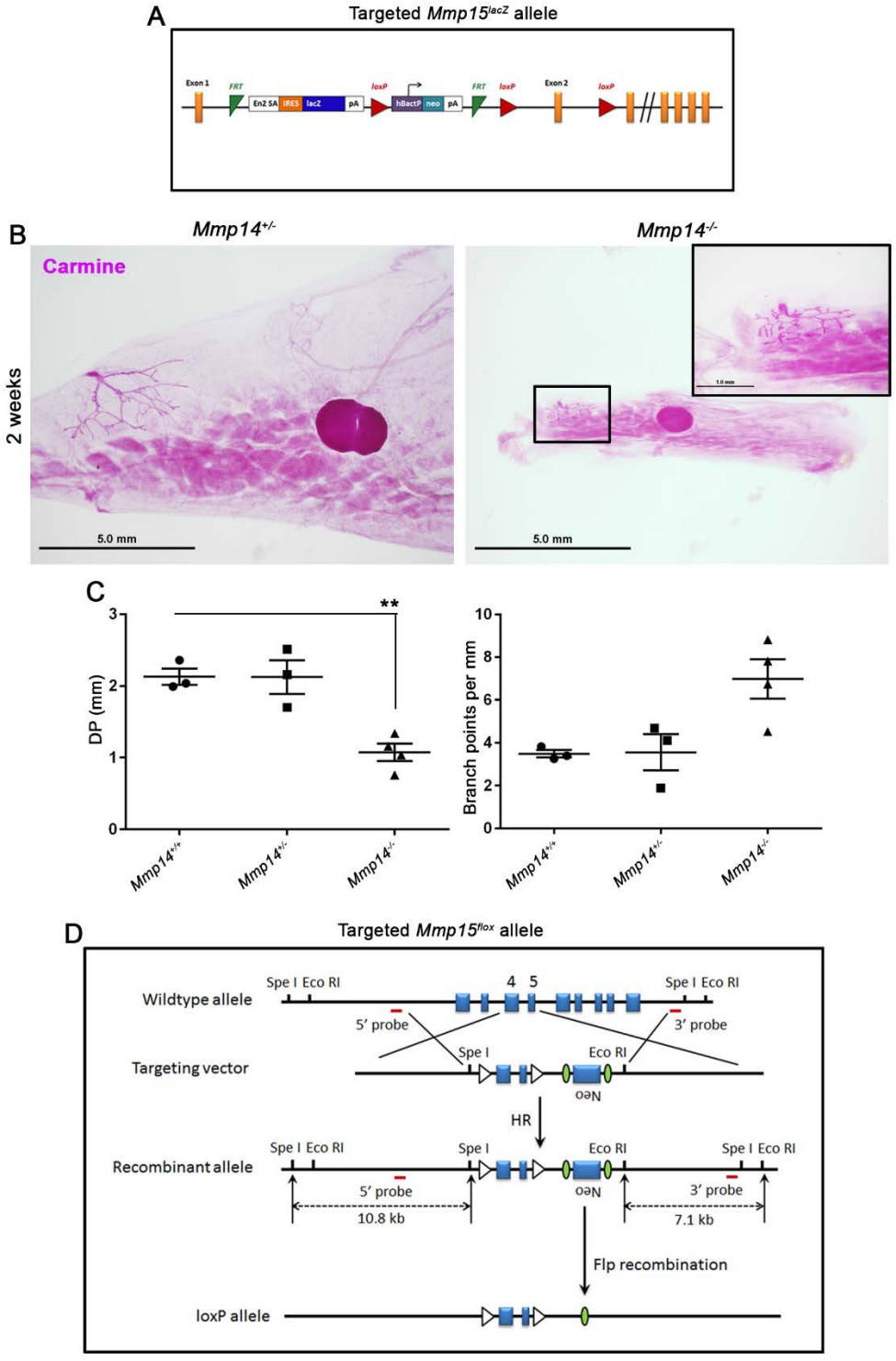
A
Targeted Mmp15lacZ allele
Exon 1
FRT
En2 SA
IRES
lacZ
pA
loxP
hBactP
neo
pA
FRT
loxP
Exon 2
loxP
B
Mmp14+/-
Mmp14-/-
Carmine
2 weeks
5.0 mm
5.0 mm
C
DP (mm)
**
Branch points per mm
Mmp14+/+
Mmp14+/-
Mmp14-/-
D
Targeted Mmp15flox allele
Wildtype allele
Spe I Eco RI
4 5
Spe I Eco RI
5' probe
3' probe
Targeting vector
Spe I
Eco RI
Neo
HR
Recombinant allele
Spe I Eco RI
Spe I
Eco RI
Spe I Eco RI
5' probe
10.8 kb
Neo
3' probe
7.1 kb
Flp recombination
loxP allele

Fig. 3-S2. Postnatal mammary gland branching requires MMP14.
(A) Schematic of *Mmp15*^{lacZ} allele. (B) Carmine staining of mammary gland whole mounts isolated from 2 week-old *Mmp14*$^{+/-}$ or *Mmp14*$^{-/-}$ mice (scale bar=5.0 mm). (C) Quantification of DP (mm) and branch points/mm in *Mmp14*$^{+/+}$ (n=3), *Mmp14*$^{+/-}$ (n=3), and *Mmp14*$^{-/-}$ (n=4) mice. **p<0.002. (D) Schematic of the *Mmp15* targeting strategy and the *Mmp15*^{flox} conditional allele.

Fig. 3-S3.

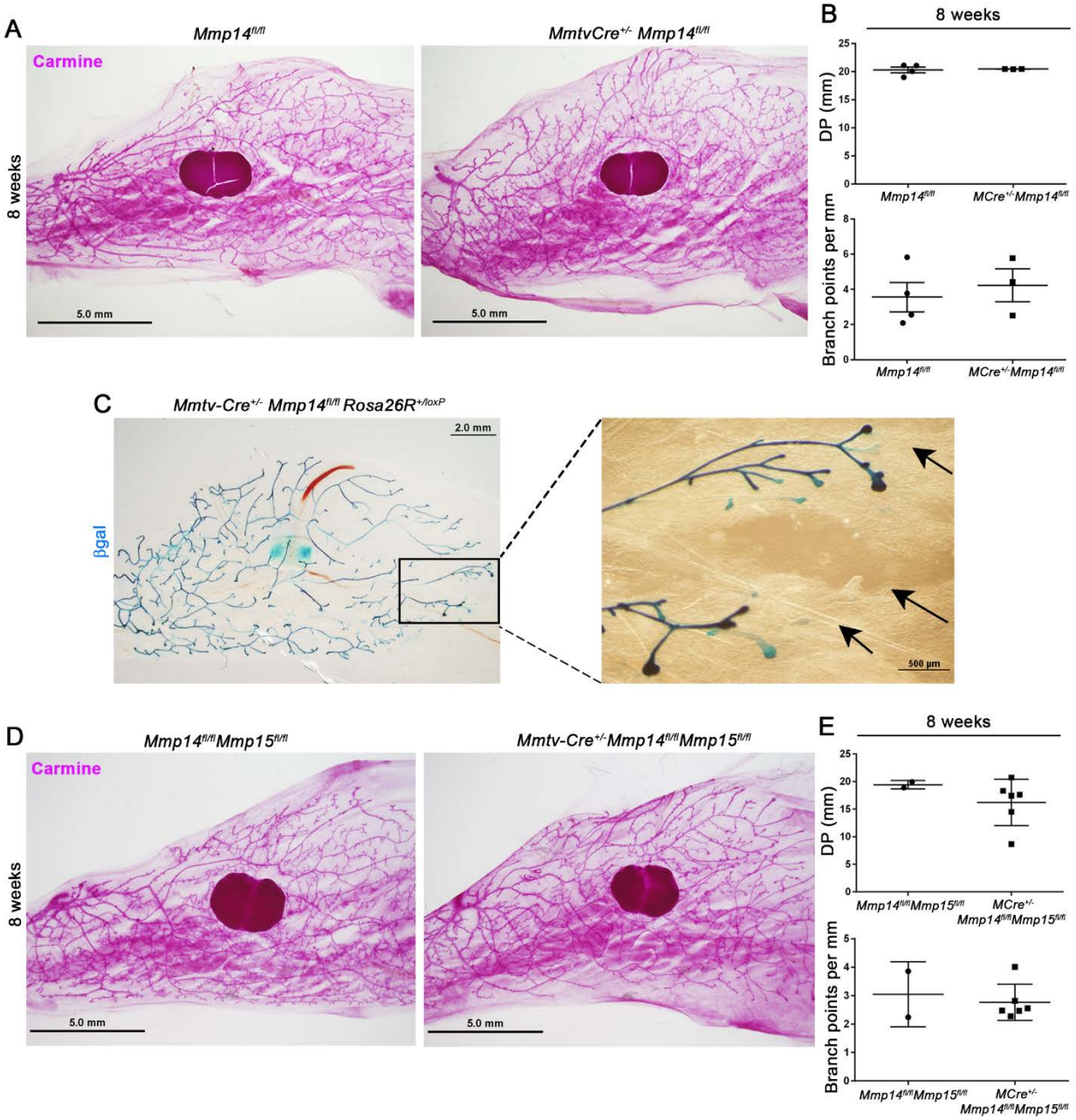

Fig. 3-S3. Mammary gland branching is independent of epithelial cell-derived MMP14 and MMP15.

(A) Carmine-staining of mammary gland whole mounts isolated from 8 week-old *Mmp14*$^{fl/fl}$ or *MmtvCre*$^{+/-}$*Mmp14*$^{fl/fl}$ mice (scale bar=5.0 mm) (B) Quantification of DP (mm) and branch points/mm from n≥3 mice per genotype. (C) LacZ staining of *Mmtv-cre*$^{+/-}$*Mmp14*$^{fl/fl}$*Rosa26R*$^{+/loxP}$ mammary gland whole mount at 7 week-old mice (scale bar=2.0 mm). A box circumscribes the region at higher magnification (scale bar=500 μm). Arrows indicate the wild-type (Cre-negative)

ducts. Image is representative of 3 replicates. (D) Carmine-stained mammary gland whole mounts isolated from 8 week-old *Mmp14*$^{fl/fl}$*Mmp15*$^{fl/fl}$ and *MmtvCre*$^{+/-}$*Mmp14*$^{fl/fl}$*Mmp15*$^{fl/fl}$ mice (scale bar=5.0 mm). (E) Quantification of DP (mm) and branch points/mm in *Mmp14*$^{fl/fl}$*Mmp15*$^{fl/fl}$ (n=2) and *MmtvCre*$^{+/-}$*Mmp14*$^{fl/fl}$*Mmp15*$^{fl/fl}$ (n=6) mice.

Fig. 3-S4.

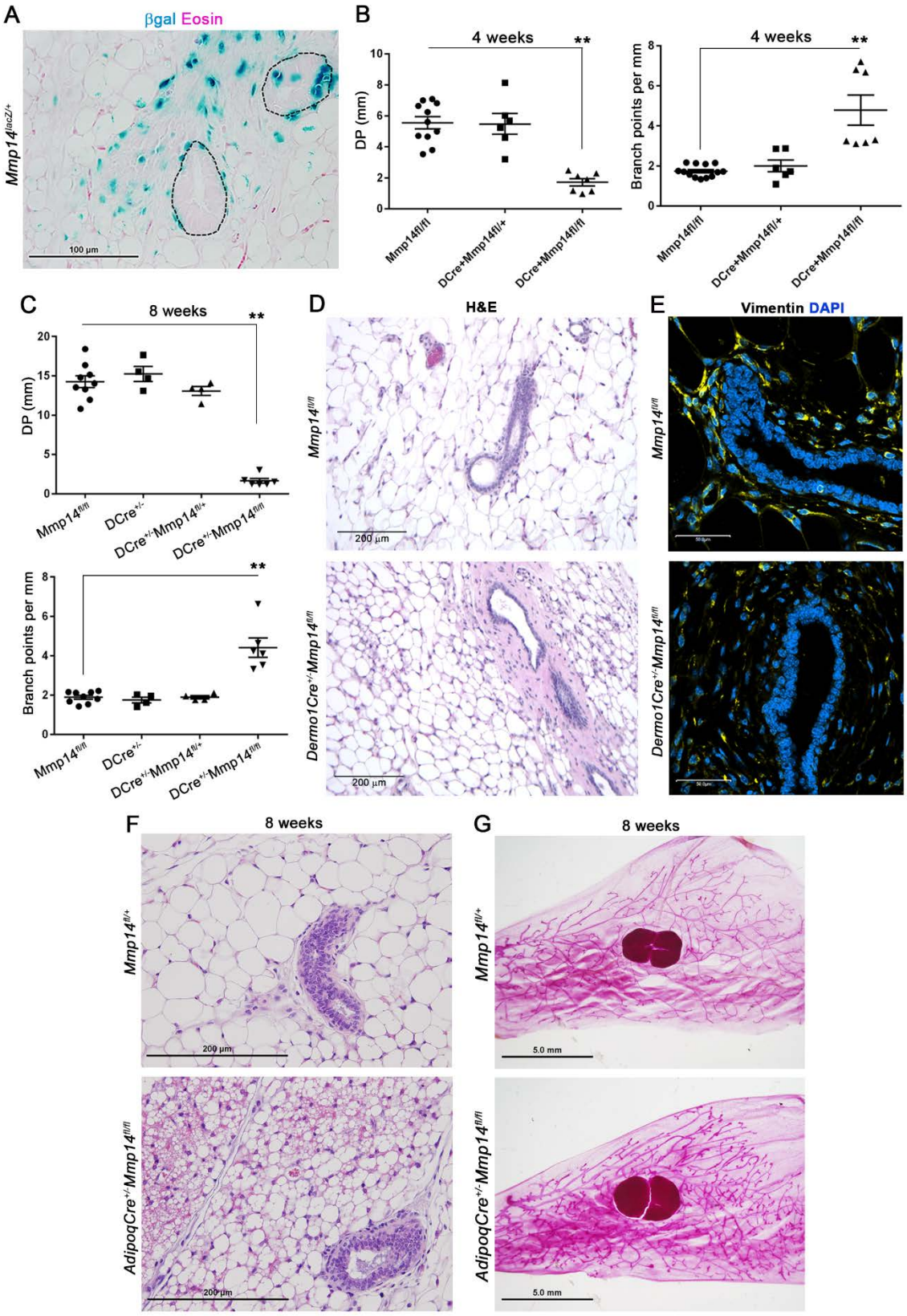
A
βgal Eosin
Mmp14lacZ/+
100 μm
B
4 weeks
**
DP (mm)
Branch points per mm
Mmp14fl/fl
DCre+Mmp14fl/+
DCre+Mmp14fl/fl
C
8 weeks
**
DP (mm)
Branch points per mm
Mmp14fl/fl
DCre+/-
DCre+/-Mmp14fl/+
DCre+/-Mmp14fl/fl
D
H&E
Mmp14fl/fl
Dermo1Cre+/-Mmp14fl/fl
200 μm
E
Vimentin DAPI
Mmp14fl/fl
Dermo1Cre+/-Mmp14fl/fl
F
8 weeks
Mmp14fl/+
AdipoqCre+/-Mmp14fl/fl
200 μm
G
8 weeks
Mmp14fl/+
AdipoqCre+/-Mmp14fl/fl
5.0 mm

Fig. 3-S4. Stromal cell-derived MMP14 regulates mammary gland branching and postnatal mammary gland development.
(A) Cross-sections of 4 week-old *Mmp14*$^{lacZ/+}$ mammary gland recovered from 4 week-old mice with Eosin counter-stain (scale bar=100 μm). Dotted lines circumscribe the mammary ducts. Image is representative of 3 replicates. (B) Quantification of DP (mm) and branch points/mm in 4 week *Mmp14*$^{fl/fl}$ (n=11), *Dermo1Cre*$^{+/-}$*Mmp14*$^{fl/+}$ (n=6), and *Dermo1Cre*$^{+/-}$*Mmp14*$^{fl/fl}$ (n=7) mice. **p<0.0001. (C) Quantification of DP (mm) and branch points/mm in mammary glands from 8 week-old *Mmp14*$^{fl/fl}$ (n=9), *Dermo1Cre*$^{+/-}$ (n=4), *Dermo1Cre*$^{+/-}$*Mmp14*$^{fl/+}$ (n=4), and *Dermo1Cre*$^{+/-}$*Mmp14*$^{fl/fl}$ (n=6) mice. **p<0.0001. (D) H&E staining in mammary gland cross-sections from 4 week-old *Mmp14*$^{fl/fl}$ and *Dermo1Cre*$^{+/-}$*Mmp14*$^{fl/fl}$ mice (scale bar=200 μm). (E) Vimentin immunofluorescence with DAPI nuclear counter-staining in cross-sections of mammary glands isolated from 4 week-old *Mmp14*$^{fl/fl}$ and *Dermo1Cre*$^{+/-}$*Mmp14*$^{fl/fl}$ mice (scale bar=50.0 μm). Images are representative of 3 replicates. (F) H&E staining of representative mammary gland cross-sections from 8 week-old *Mmp14*$^{fl/fl}$ and *Adipoq-Cre*$^{+/-}$ *Mmp14*$^{fl/fl}$ mice (scale bar=200 μm). (G) Carmine staining of mammary gland whole mounts isolated from 8 week-old *Mmp14*$^{fl/fl}$ and *Adipoq-Cre*$^{+/-}$*Mmp14*$^{fl/fl}$ mice (n=2) (scale bar=5.0 mm).

Fig. 3-S5.

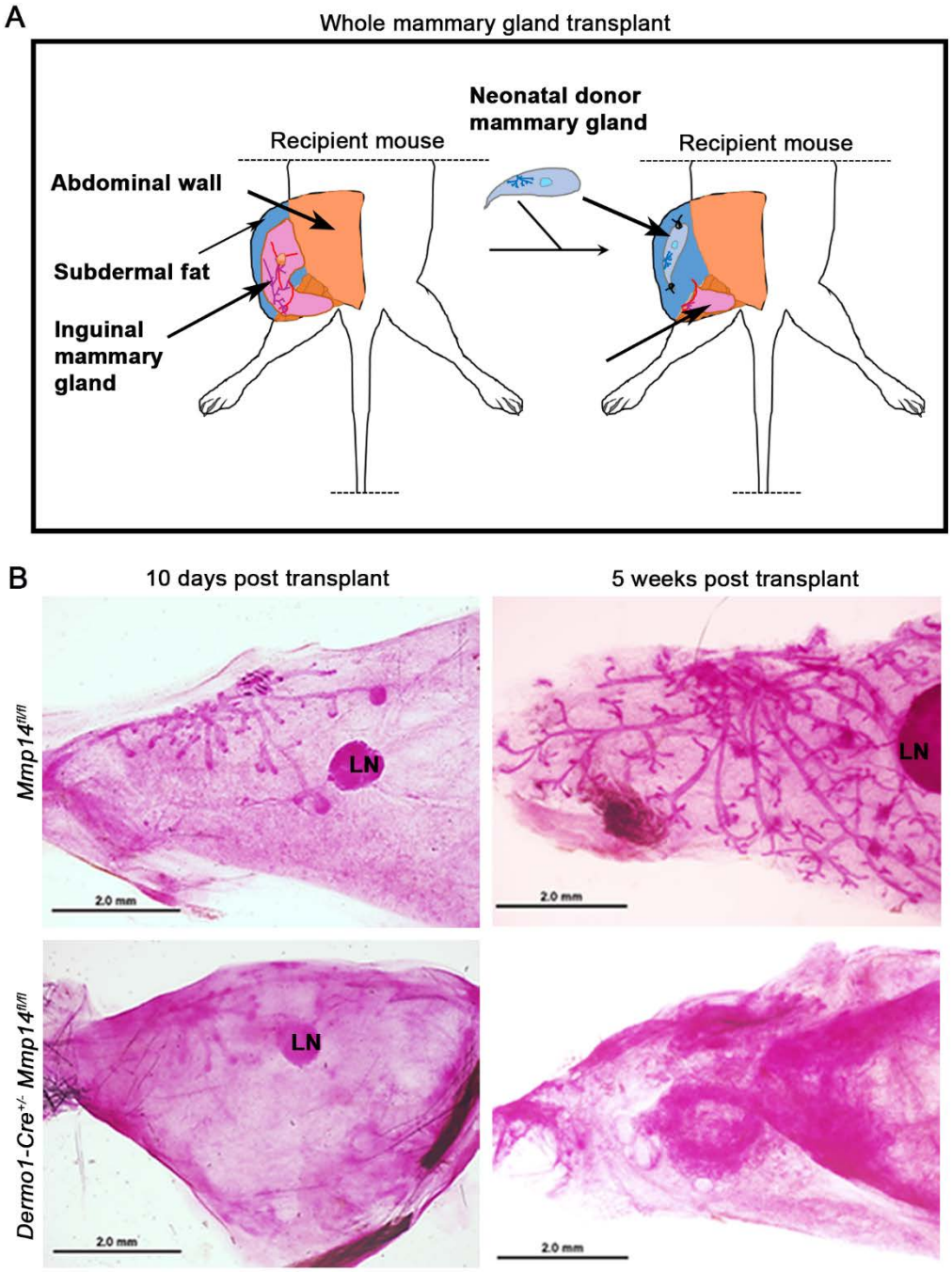

Fig. 3-S5. Stromal cell-derived MMP14 regulates branching in an organ-autonomous manner.

(A) Schematic of whole mammary gland transplant procedure. (B) Carmine-stained whole mounts of transplanted donor mammary glands from *Mmp14*$^{fl/fl}$ or *Dermo1Cre*$^{+/-}$*Mmp14*$^{fl/fl}$ mice at 10 d and 5 weeks post-transplantation (scale bar=2.0 mm). "LN" indicates donor inguinal lymph node. Images are representative of 3 replicates.

Fig. 3-S6.

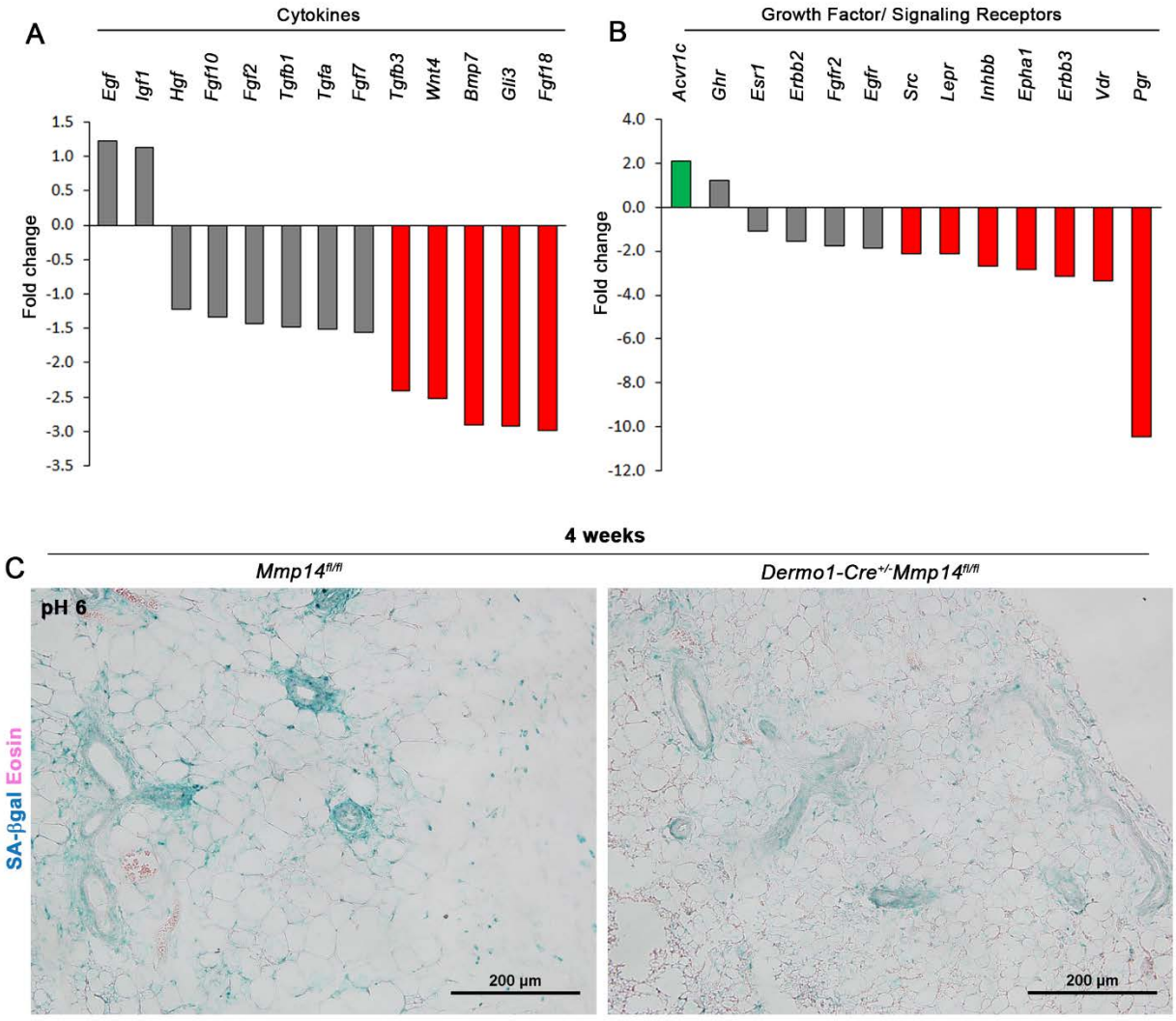

Fig. 3-S6. MMP14-independent regulation of stromal cell growth factors, growth factor/signaling receptors and cellular senescence.
(A) Fold-changes of stromal cell-derived cytokines in *Dermo1Cre*$^{+/-}$*Mmp14*$^{fl/fl}$ mammary glands isolated from 4 week-old mice relative to wild-type littermates (n=3 per genotype). (B) Fold-changes of stromal cell-associated growth factor/signaling receptors in 4 week *Dermo1Cre*$^{+/-}$ *Mmp14*$^{fl/fl}$ mammary glands isolated from 4 week-old mice relative to wild-type littermates (n=3 per genotype). (C) Senescence-associated β-galactosidase (SA-βgal) staining (pH 6.0) of mammary gland cross-sections from 4 week-old *Mmp14*$^{fl/fl}$ and *Dermo1Cre*$^{+/-}$*Mmp14*$^{fl/fl}$ mice with eosin counterstaining (scale bar=200 μm). Images are representative of 2 replicates.

Fig. 3-S7.

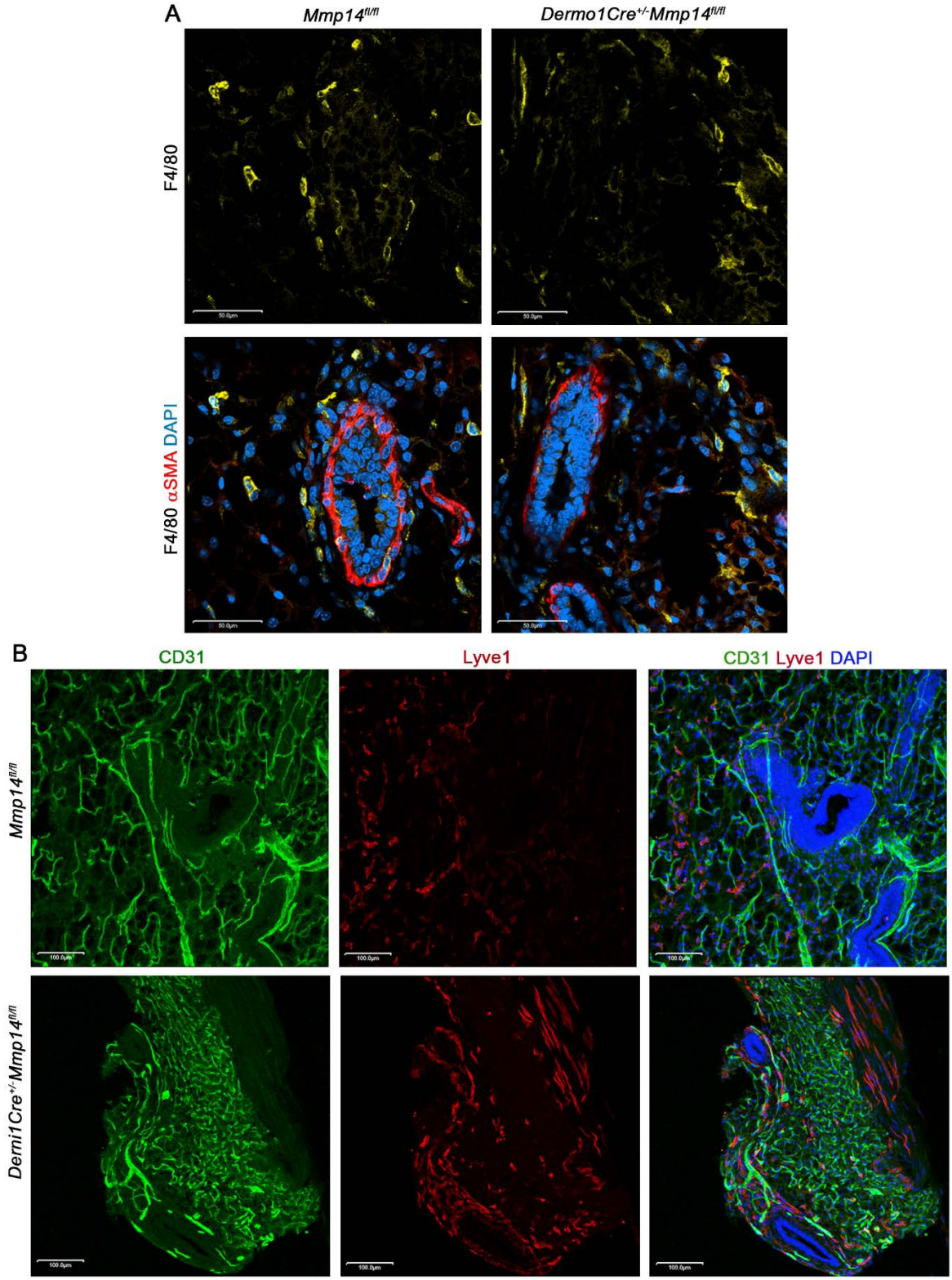
A
Mmp14fl/fl
Dermo1Cre+/-Mmp14fl/fl
F4/80
F4/80 αSMA DAPI
B
CD31
Lyve1
CD31 Lyve1 DAPI
Mmp14fl/fl
Dermi1Cre+/-Mmp14fl/fl

Fig. 3-S7. Stromal cell-targeted mammary glands retain normal distributions of macrophages, blood vessels and lymphatics.
(A) Immunofluorescence for macrophage-associated F4/80 protein with α-smooth muscle actin (αSMA) to delineate the myoepithelial cell compartment and DAPI counter-staining (scale bar=50 μm) in *Mmp14*$^{fl/fl}$ and *Dermo1Cre*$^{+/-}$*Mmp14*$^{fl/fl}$ mammary gland cross-sections. (B) Immunofluorescence for CD31 (vascular endothelial cells) and Lyve1 (lymphatic endothelial cells) with DAPI counter-staining in *Mmp14*$^{fl/fl}$ and *Dermo1Cre*$^{+/-}$*Mmp14*$^{fl/fl}$ mammary gland cross-sections (scale bar=100μm). Images are representative of 2 replicates.

Fig. 3-S8.

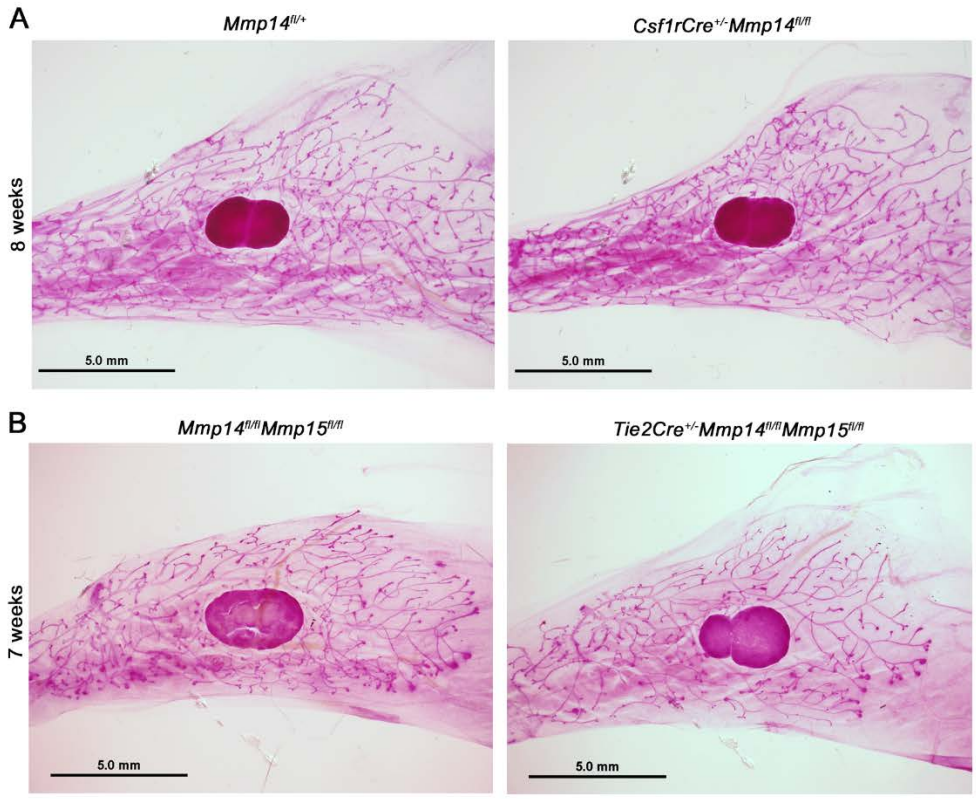

Fig. 3-S8. Postnatal mammary bland branching does not require macrophage-derived *Mmp14* or endothelial cells-derived *Mmp14/Mmp15*.
(A) Carmine staining of mammary gland whole mounts isolated from 8 week-old *Mmp14*$^{fl/fl}$ and *Csflr-Cre*$^{+/-}$*Mmp14*$^{fl/fl}$ littermates (scale bar=5.0 mm), (B) Carmine staining of mammary gland whole mounts isolated from 7 week-old *Mmp14*$^{fl/fl}$*Mmp15*$^{fl/fl}$ and *Tie2-Cre*$^{+/-}$*Mmp14*$^{fl/fl}$*Mmp15*$^{fl/fl}$ littermates (n=2) (scale bar=5.0 mm).

Fig. 3-S9.

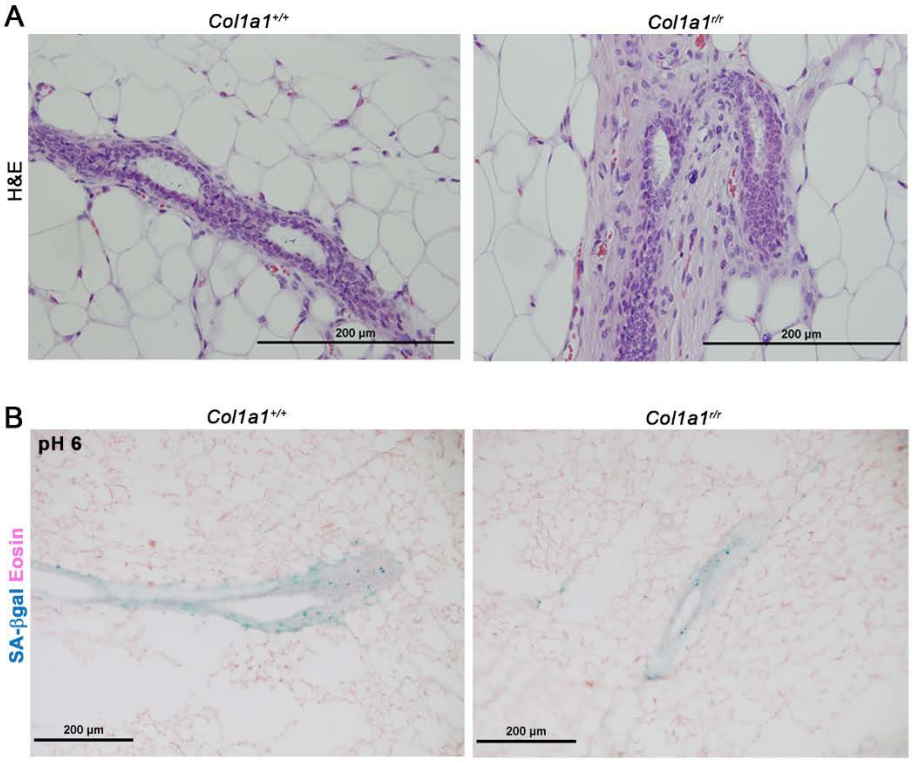

Fig. 3-S9. Type I collagen remodeling regulates the periductal stroma independent of cellular senescence.
(A) H&E staining of cross-sections of *Col1a1*$^{r/r}$ and *Col1a1*$^{+/+}$ littermate mammary glands isolated from 5 week-old mice (scale bar=200 µm). (B) Senescence-associated β-galactosidase (SA-βgal) staining (pH 6.0) of *Col1a1*$^{r/r}$ and *Col1a1*$^{+/+}$ littermate mammary glands isolated from 5 week-old mice. Cross-sections with Eosin counter-staining are shown (scale bar=200 µm). Images are representative of 2 replicates.

Fig. 3-S10.

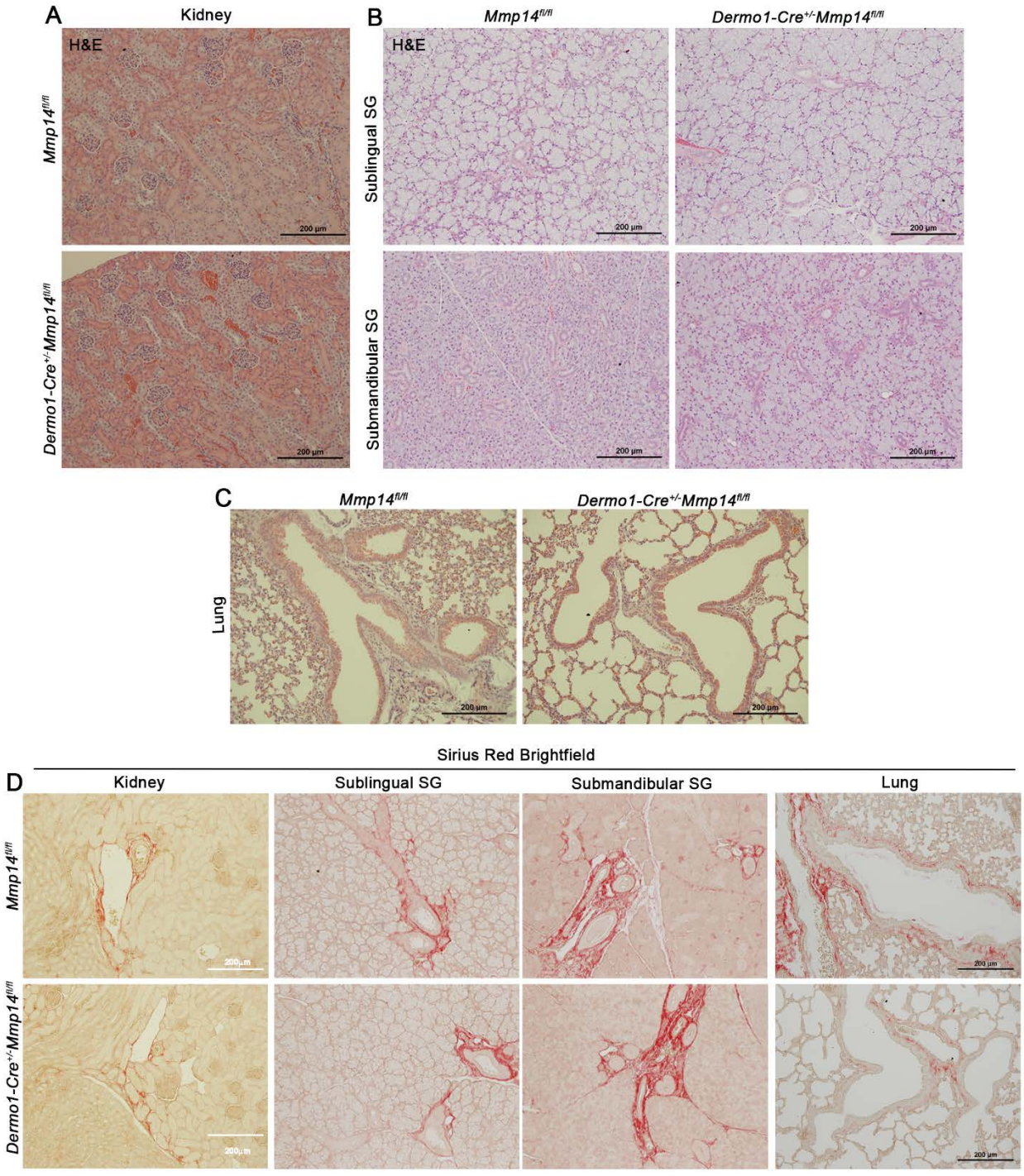
A
Kidney
H&E
Mmp14fl/fl
Dermo1-Cre+/-Mmp14fl/fl
200 µm
B
Mmp14fl/fl
Dermo1-Cre+/-Mmp14fl/fl
H&E
Sublingual SG
Submandibular SG
200 µm
C
Mmp14fl/fl
Dermo1-Cre+/-Mmp14fl/fl
Lung
200 µm
Sirius Red Brightfield
D
Kidney
Sublingual SG
Submandibular SG
Lung
Mmp14fl/fl
Dermo1-Cre+/-Mmp14fl/fl
200µm
200 µm

Fig. 3-S10. Stromal *Mmp14* deletion does not increase interstitial ECM deposition in other epithelial organ systems.
(A) H&E staining of kidney cross-sections isolated from 4 week-old *Mmp14*$^{fl/fl}$ and *Dermo1Cre*$^{+/-}$ *Mmp14*$^{fl/fl}$ mice (scale bar=200 μm). (B) H&E staining of sublingual and submandibular salivary gland cross-sections isolated from 4 week-old *Mmp14*$^{fl/fl}$ and *Dermo1Cre*$^{+/-}$*Mmp14*$^{fl/fl}$ mice (scale bar=200μm). (C) H&E staining of lung tissues recovered from 4 week-old *Mmp14*$^{fl/fl}$ and *Dermo1Cre*$^{+/-}$*Mmp14*$^{fl/fl}$ mice (scale bar=200 μm). (D) Bright-field images of Sirius red staining of kidney, sublingual salivary gland, submandibular salivary gland, and lung cross-sections from 4 week *Mmp14*$^{fl/fl}$ and *Dermo1Cre*$^{+/-}$*Mmp14*$^{fl/fl}$ mice (scale bar=200 μm). Images are representative of 2 replicates.

Note.

* This chapter was submitted as a manuscript, entitled: “Periductal Remodeling of the Interstitial Matrix Regulates Mammary Gland Morphogenesis,” by Tamar Y. Feinberg, Rui Liu, Gertraud W. Robinson and Stephen J. Weiss.

CHAPTER 4: MT1-MMP-Mediated Pericellular Proteolysis controls the KASH·SUN-Dependent Regulation of Vascular Cell Nuclear Architecture and Function

Abstract.

During blood vessel development, endothelial cells and investing mural cells respond to exogenous stimuli that trigger the proteolytic remodeling of the surrounding 3-dimensional (3-D) extracellular matrix (ECM). Changes in the structural properties of the tissue microenvironment result in the transmission of transcriptional cues to the vessel wall that guide morphogenetic programs, but the underlying mechanisms remain undefined. Here, we characterize a novel regulatory axis wherein the coordinated proteolysis of the pericellular ECM by the membrane-anchored matrix metalloprotease, MT1-MMP, and the deposition of a fibronectin network unexpectedly govern nuclear architecture and function. The MT1-MMP/fibronectin fibrillogenesis/nuclear axis is operative specifically within the 3-D – but not 2-dimensional (2-D) – ECM environment *in vitro* as well as *in vivo* wherein mechanical cues are transduced via the cell cytoskeleton to the nucleus via Klarsicht, ANC-1, Syne homology domain (KASH)-containing nuclear envelope bridges. These studies define a proteinase-regulated mechanotransduction program wherein endothelial and mural cells sculpt chromatin organization and transcriptional activity by relaying signals received from the 3-D ECM directly to the nuclear compartment.

Introduction.

In response to wounding, inflammation or neoplasia, endothelial cells and associated mural cells (i.e., pericytes and vascular smooth muscle cells) engage morphogenetic programs to drive neovessel formation within the confines of a surrounding, three-dimensional (3-D) extracellular matrix (ECM) (Adams and Alitalo, 2007; Carmeliet and Jain, 2011). However, the ECM is not a static scaffold; dynamic endothelial and mural cell-mediated remodeling of the pericellular 3-D ECM is required during vasculogenesis as well as angiogenesis. Current evidence indicates that cells engaged in morphogenetic programs within a 3-D ECM display a unique dependence on ECM remodeling relative to cells operating atop a planar, 2-D ECM (Engler et al., 2006; Huang et al., 1998; McBeath et al., 2004; Wang et al., 2009; Yamada and Cukierman, 2007). Indeed, in a 3-D-specific fashion, remodeling of the local ECM microenvironment *via* pericellular proteolysis and fibronectin matrix assembly impact programs that govern cell proliferation, motility and differentiation (Chun et al., 2006; Hotary et al., 2003; Zhou et al., 2008). However, the means by which matrix remodeling regulates cell function in a 3-D ECM-specific fashion remain undefined.

While examining endothelial cell growth responses and neovessel formation within 3-D ECM environments, we uncovered an unexpected link between the membrane-anchored metalloproteinase, MT1-MMP, fibronectin fibrillogenesis, and the regulation of transcriptional activity. In the absence of MT1-MMP activity or fibronectin matrix assembly, chromatin organization and structure fail to reorganize, while the transcriptional profile of 3-D-embedded cells is “frozen” in a resting state. In tandem with these events, nuclear architecture in endothelial cells as well as vascular smooth muscle cells is dramatically altered *in vitro* and *in vivo*, with cells displaying markedly distorted nuclear shapes that closely mimic those commonly observed in the laminopathies (Burke and Stewart, 2006; Dechat et al., 2008; Starr, 2009). Further studies reveal

that both MT1-MMP activity and fibronectin fibrillogenesis impact nuclear structure and function by controlling the relay of mechanical cues from the ECM to a network of cytoskeleton proteins that interact with a family of Klarsicht, ANC-1, Syne homology domain (KASH)–containing proteins that serve as physical bridges to the nuclear envelope. These findings support a new model wherein the remodeling of the 3-D ECM directs cell function by coordinately regulating nuclear architecture and function.

Results.

ECM remodeling regulates endothelial cell shape and nuclear envelope architecture.

Endothelial cells embedded within 3-D hydrogels comprised of cross-linked fibrin or type I collagen (the dominant matrix proteins found at most sites of neovessel formation) (Baker et al., 2012; Yana et al., 2007; Zhou et al., 2008) and stimulated with a pro-angiogenic cocktail containing vascular endothelial growth factor (VEGF) and hepatocyte growth factor (HGF) (Zhou et al., 2008), rapidly alter their cell shape over a 48 h culture period and adopt a distinct elongated, bipolar morphology (Fig. 4-1 A). Cells incorporated within 3-D ECMs require two major types of extracellular matrix remodeling to execute the cell shape changes necessary for motility, proliferation and morphogenesis - both MT1-MMP-dependent proteolysis and the deposition of a neomatrix of fibronectin fibrils (Chun et al., 2006; Chun et al., 2004; Hiraoka et al., 1998; Sabeh et al., 2009; Tang et al., 2013; Zhou et al., 2008). Indeed, when endothelial cells are cultured in 3-D with the pan-specific MMP inhibitor, BB-94, cell shape changes are blocked and the cells assume a distinct spherical shape while adopting a “dormant” status (i.e., immotile and non-proliferative) (Fig. 4-1 A; Fig. 4-S1 A). Consistent with a dominant role for the membrane-anchored MMP, MT1-MMP, in mediating pericellular proteolysis, shRNAs directed against the

protease likewise abrogate VEGF/HGF-initiated cell shape changes in fibrin or type I collagen hydrogels (Fig. 4-1 A). As expected, endothelial cell shape changes are similarly blocked when hydrogels are supplemented with the fibronectin fibrillogenesis inhibitor, FUD, a 49-amino acid-long peptide known to block fibronectin matrix assembly (Zhou et al., 2008) (Fig. 4-1 A). Importantly, treatment of endothelial cells with BB-94 or FUD, or knockdown of MT1-MMP with shRNAs does not affect cell shape, cell survival, or VEGF/HGF-induced proliferation under 2-D culture conditions (Fig. 4-S1 B-C; Fig. 4-S2 A; data not shown); nor do these manipulations induce apoptosis in 3-D culture conditions (Fig. 4-S2 B; data not shown).

While examining changes in endothelial cell morphology, 3-D imaging of the DAPI signal from ECM-embedded cells revealed marked changes in nuclear shape (Fig. 4-1 B). In contrast to the elliptical-shaped nuclei observed in VEGF/HGF-stimulated endothelial cells in 3-D hydrogels, endothelial cells cultured with BB-94 or FUD, or expressing shRNAs targeting MT1-MMP, harbor multi-lobed, dysmorphic nuclei in 3-D hydrogels (Fig. 4-1 B). Nuclear shape and the distribution of the nuclear pore complexes is largely determined by a scaffolding of nucleus-associated filaments, termed the lamins (Davidson and Lammerding, 2014; Swift et al., 2013). To first determine the structural status of the lamin shell, endothelial cells were engineered to express a GFP-tagged form of lamin A. Further, nuclear pore complexes were also immunostained for the nuclear pore component, NUP153 (Glynn and Glover, 2005; Goldman et al., 2004; Hawryluk-Gara et al., 2005). VEGF/HGF-stimulated endothelial cells harboring oval-shaped nuclei in 3-D display a uniform distribution of lamin A and NUP153-containing complexes (Fig. 4-1 C). Under conditions where MT1-MMP activity or fibronectin fibrillogenesis are inhibited, the distorted nuclei show distinct infoldings of the lamin A matrix as well as nuclear pore complex aggregates

within zones of nuclear membrane invaginations (Fig. 4-1 C). Cells cultured under these conditions do not differ in their nuclear architecture in 2-D (Fig. 4-1 C).

ECM remodeling regulates transcriptional activity and chromatin structure in endothelial cells cultured under 3-D culture conditions.

Similar distortions in nuclear matrix architecture have also been observed in the laminopathies, a pleiotropic series of genetic disorders wherein mutations in the genes encoding lamins or associated nuclear envelope proteins give rise to complex phenotypes, which include muscular dystrophies, lipodystrophy and progeria/premature aging (Dechat et al., 2008; Gruenbaum and Foisner, 2015; Starr, 2009). Given the evidence that laminopathy cell nuclei have altered transcriptional activity (Shumaker et al., 2006; Starr, 2009; Stewart et al., 2007), nascent RNA synthesis was directly assessed in endothelial cells cultured under either 3-D or 2-D conditions (Paulsen et al., 2014; Paulsen et al., 2013). Pulse labeling of VEGF/HGF-stimulated endothelial cells within 3-D ECM at 48 h with the bromouridine (BrU) metabolite reveals a marked induction of mRNA transcription, as shown by diffuse nucleoplasmic labeling of BrU-RNA [Fig. 4-2 A; (Paulsen et al., 2013)]. However, this activation process is attenuated significantly when either pericellular proteolysis or fibronectin fibrillogenesis are inhibited in 3-D, but not 2-D, culture conditions (Fig. 4-2 A-D). Importantly, while treatment of endothelial cells with high doses of actinomycin D to block transcription from RNA polymerase I, II and III (5 µg/ml, (Pellizzoni et al., 2001)) abrogates BrU incorporation and the detection of nascent transcripts, actinomycin D treatment does not affect nuclear shape (Fig. 4-S3 A), indicating that the nuclear shape changes observed under conditions with abrogated ECM remodeling are not a consequence of the attenuated transcriptional activity. More accurate assessments of the levels of polyadenylated-

RNA, as an indicator of mRNA adundance, in VEGF/HGF-stimulated 3-D cultures at 48 h revealed a 50% decrease in mRNA levels in endothelial cells cultured under VEGF/HGF-stimulated conditions in the presence of BB-94 or FUD peptide, relative to the mRNA levels of cells cultured under VEGF/HGF-stimulation with vehicle controls (n=3, in triplicate). The distribution of chromatin in endothelial cell nuclei was therefore assessed by monitoring the localization of GFP-tagged histone H2B (Tang et al., 2008). While the nuclei of growth factor-stimulated endothelial cells contain uniformly-distributed histone H2B, blockade of ECM remodeling in 3-D, but not 2-D, triggers chromatin condensation at discrete peripheral nuclear locations, generating significant increases in chromatin-free areas in the nucleus - consistent with an accumulation of inactive heterochromatin (Fig. 4-2 E). Further, using the acetylation status of histone H3 at lysine 9 (Acetyl-H3K9) as a marker of euchromatin - chromatin accessible to transcriptional machinery (Finlan et al., 2008; Haberland et al., 2009), inhibition of MMP activity or fibronectin fibrillogenesis markedly decreases Acetyl-H3K9 levels in a 3-D-specific fashion (Fig. 4-2 F). Importantly, endothelial cells cultured in the absence or presence of these inhibitors showed equivalent levels of an independent histone modification, heterochromatin-associated trimethylated lysine 27 of histone H3 (H3K27Me3), in both 2-D and 3-D conditions (Fig. 4-2 G).

In order to evaluate RNA synthesis on a genome-wide scale and uncover the transcriptionally active regions in the genome of endothelial cells confined in 3-D hydrogels without ECM remodeling activities, the newly generated BrU-RNA was sequenced by BrU-Seq (Paulsen et al., 2014; Paulsen et al., 2013). Interestingly, ~ 200 genes were differentially expressed using a >2-fold change cutoff and the majority of these genes were down-regulated following inhibition of pericellular proteolysis, with enriched Gene Ontology (GO) categories related to cell cycle progression, proliferation and DNA packaging (Fig. 4-2 H). To evaluate whether inhibition

of proliferation induces a similar change in nuclear architecture, DNA polymerase A was inhibited with aphidicolin (Ewald et al., 2008). However, addition of aphidicolin (10 μM) for 48 h failed to induce marked changes in either cell shape or nuclear morphology in 3-D ECM (Fig. 4-S3 B), suggesting that the ECM remodeling-dependent changes in nuclear shape are not an indirect result of reduced proliferative activity.

A cytoskeleton-LINC complex axis couples cell and nuclear shapes.

Recent studies have identified an axis wherein physical interactions between the cytoskeleton and the nuclear envelope are mediated by a family of Klarsicht, ANC-1, Syne homology (KASH) domain-containing proteins, which span the outer nuclear membrane and intermembrane space where they interact with members of the SUN protein family and form the linker of cytoskeleton and nucleus (LINC) complex (Crisp et al., 2006; Dechat et al., 2008; Starr, 2009; Stewart et al., 2007; Wilhelmsen et al., 2006). SUN proteins then span the inner nuclear membrane to establish binding interactions with a scaffold of lamin family members and nuclear pore complexes (Dechat et al., 2008; Starr, 2009; Stewart et al., 2007). Endothelial cells express the KASH domain-containing proteins, nesprins-1 and 2 (also termed Syne-1 and -2), which bind F-actin and microtubules, as well as nesprin-3, which indirectly interacts with intermediate filaments via binding to plectin. These KASH domain-containing nesprin proteins all localize to the nuclear envelope and are diffusely present in the cytoplasm due to their localization in the endoplasmic reticulum [Fig. 4-3 A; (Starr, 2009; Stewart et al., 2007)]. While endothelial cells cultured in 3-D under VEGF/HGF-stimulation display a uniform distribution of nesprins in the nuclear envelope (Fig. 4-3 A), inhibition of MMP activity or fibronectin fibrillogenesis induces the aggregation of nesprin complexes at nuclear membrane invagination sites (Fig. 4-3 A).

As endothelial cell shape changes in 3-D ECM in response to VEGF/HGF-stimulation are accompanied by a reorganization of the actin cytoskeleton and cytosolic microtubule network, the nesprin proteins likely regulate nuclear structure via their simultaneous interactions with plasma membrane-associated cytoskeletal fibers and the nuclear envelope. Indeed, blockade of pericellular proteolysis or fibronectin fibrillogenesis inhibits assembly of F-actin, β-tubulin and vimentin into longitudinal fibers, resulting in an amorphous cortical collection of molecules (Fig. 4-3 B) - effects that are not observed under 2-D culture conditions (Fig. 4-S4 A). Blockade of ECM remodeling in 3-D ECM abrogates the contractile force that VEGF/HGF-stimulated endothelial cells exert on 3-D ECM by more than 60% (Fig. 4-3 C, $*p<0.05$), and impairs the ability of endothelial cells to generate the cytoskeletal tension necessary to transduce forces from the cell surface to the nuclear compartment, as reflected in the 2-fold decrease in pericellular matrix rigidity detected by atomic force micro-indentation (Liu and Tschumperlin, 2011) (Fig. 4-3 D). To address the functional role of the cytoskeleton in directly regulating nuclear structure, VEGF/HGF-stimulated endothelial cells were treated with either blebbistatin, which inhibits myosin ATPase-mediated isometric tension, or nocodazole, which interferes with microtubule assembly (Salpingidou et al., 2007; Zhou et al., 2008). Endothelial cells cultured in the presence of blebbistatin or nocodazole display (i) multi-lobed nuclei with perturbations in nuclear pore distribution, (ii) chromatin condensations at the nuclear periphery with increased interchromatin space, (iii) abrogated nascent transcript production, and iv) attenuated acetylation of histone H3 in response to VEGF/HGF (Fig. 4-3 E-I; Fig. 4-S5 A-D).

Finally, to perturb cytoskeleton/nesprin interactions directly, endothelial cells were transduced with dominant-negative GFP-KASH, which acts as a truncated nesprin protein that still binds the SUN proteins, but lacks the domains required for interacting with cytoskeletal elements

- resulting in the functional uncoupling of the nucleus and cytoplasm (Brosig et al., 2010; Crisp et al., 2006). In contrast to VEGF/HGF-stimulated endothelial cells expressing the empty retroviral vector, endothelial cells expressing GFP-KASH retrovirus in 3-D ECM adopt the multi-lobed, highly concave nuclear architecture characteristic of cells with inhibited ECM remodeling activities (Fig. 4-4 A-B). Importantly, uncoupling of the cytoskeletal and nuclear compartments *via* GFP-KASH expression induces peripheral chromatin condensation, impairs transcriptional activity of endothelial cells in 3-D and attenuates acetylation of histone H3, independently of directly targeted pericellular ECM remodeling (Fig. 4-4 C-D). Similarly, RNAi-mediated knockdown of Nesprin-2 alone, which directly tethers the nuclear envelope to both the actin cytoskeleton and microtubule filaments (Chang et al., 2015), recapitulates the effects of GFP-KASH expression on nuclear architecture, nascent transcript production and chromatin structure (Fig. 4-4 E-G).

Direct coupling of cell geometry with nuclear and chromatin structure.

Taken together, ECM-dependent changes in 3-D cell geometry appear to regulate nuclear architecture. As such, directly modulating endothelial cell shape without inhibiting ECM remodeling activities or cytoskeleton-nuclear membrane interactions would be predicted to impact nuclear organization, chromatin structure and transcriptional activity. As such, endothelial cells were cultured within 3-D, biomimetic poly(ethylene glycol) (PEG) hydrogels containing RGD peptides incorporated pendantly within a transglutaminase-crosslinked structure that is engineered to be either susceptible, or resistant, to MMP-mediated hydrolysis [Fig. 4-5 A; (Ehrbar et al., 2007; Raeber et al., 2007)]. In this framework, endothelial cell shapes are affected as a function of the susceptibility of the 3-D hydrogel to MMP-dependent proteolysis. Within MMP-sensitive gels,

endothelial cells stretch in response to VEGF/HGF and display elliptical nuclei (Fig. 4-5 B-C), but predictably fail to stretch in the presence of BB-94 and exhibit multi-lobed, highly concave nuclei (Fig. 4-5 B). In contrast, in MMP-resistant gels, endothelial cells remain locked in a spherical shape and harbor multi-lobed nuclei in the absence of MMP inhibition (Fig. 4-5 B-C). Further, cells cultured within MMP-degradable hydrogels displayed ~ 4-fold reduced transcriptional activity (*$p<0.01$) and near complete repression of histone H3 acetylation (i.e. 0.0004 ± 0.0003 AU versus 1.0 ± 0.16 AU, $P < 0.0001$), relative to cells cultured within MMP-sensitive hydrogels (Fig. 4-5 D).

Alternatively, endothelial shape can be modulated independently of proteolysis under 2-D conditions by culturing cells atop micropatterned fibronectin islands printed onto polymethylsiloxane substrates to generate ECM-adhesive patches surrounded by regions blocked with a non-adhesive surface coating (Chen et al., 1997; McBeath et al., 2004). In contrast to the freely spreading cells present on homogeneously-coated fibronectin substratum, cells cultured atop 35 x 35 μm fibronectin 'islands' with constrained cell spreading display (i) concave nuclear shape, (ii) condensation of chromatin, and (iii) decreased histone acetylation (Fig. 4-S6 A-C). Hence, ECM-directed control of cell geometry directly determines nuclear shape and architecture as well as chromatin structure.

Nuclear architecture directly regulates transcriptional activity.

This work shows that the cell shape changes associated with pericellular proteolysis and fibronectin fibrillogenesis directly regulate nuclear architecture through the LINC complex, and that morphological changes in both cell and nuclear shape correlate with transcriptional activity. To examine whether the link between nuclear architecture and transcriptional activity is direct or

indirect, we isolated nuclei and performed nuclear run-on transcription assays. Endothelial cell nuclei were extracted in polyethylene glycol (PEG) at 12% w/v in order to mimic the "crowding" forces exerted by insoluble cytoplasmic proteins on the nuclear envelope that dictate nuclear size and the organization of intranuclear compartments in intact cells (Fulton, 1982; Hancock, 2004a; Minton, 2001; Rosania and Swanson, 1995; Zimmerman and Minton, 1993). Endothelial cell nuclei were extracted in the presence of digitonin detergent in order to selectively permeabilize the plasma membrane, conserve the bulk of the nuclear envelope structure, and thereby model the nuclei present under physiologic conditions (Adam et al., 1992; Hancock, 2004b; Hancock and Hadj-Sahraoui, 2009).

Incubation of intact isolated endothelial cell nuclei under the "physiologic," 12% w/v PEG condition, yields a range of nuclear shapes, as visualized in their 3-D reconstructions (Fig. 4-6 A). Relative nuclear concavity measurements show that 20% of the nuclei in 12% w/v PEG exhibit an oval shape (Fig. 4-6 A). Despite the heterogeneity in nuclear shape, only the oval-shaped nuclei under the 12% w/v PEG condition are transcriptionally active. The more concave nuclei under 12% w/v PEG exhibit a 3-fold drop in transcriptional activity (*$p<0.0001$), as demonstrated by incorporation of Br-UTP (Fig. 4-6 A). When the PEG concentration was elevated to 25% w/v, isolated nuclei uniformly adopted a folded state with abrogated transcriptional activity (*$p< 0.0001$, Fig. 4-6 B-E), with a BrU-RNA comparable to that of isolated nuclei pre-treated with a high dose of actinomycin D (Fig. 4-6 E). Transfer of isolated nuclei from 25% w/v PEG to the physiologic 12% w/v PEG condition reversibly rescues both nuclear shape and transcriptional activity (Fig. 4-6 B-E). Lastly, while the oval-shaped isolated nuclei under 12% w/v PEG are enriched for euchromatin-associated Acetyl-H3K9 marks, the crumpled nuclei present under 25%

PEG lack Acetyl-H3K9 staining (Fig. 4-6 F). Taken together, these data identify a cell shape-independent role for nuclear architecture in determining transcriptional competence.

Control of nuclear structure and chromatin activity by ECM remodeling pathways in vascular cells *in vivo.*

While the endothelial cells of patent, fully formed blood vessels exist in 2-D, the vascular smooth muscle cells (VSMCs) that surround the endothelium are enmeshed in 3-D ECM. To determine whether the requirement for pericellular ECM remodeling is confined to the vascular endothelium, aortic VSMCs isolated from *Mt1-mmp*$^{flox/flox}$ mice (Tang et al., 2013) were incubated with adenoviral β-gal or Cre-expression vectors, and embedded in 3-D type I collagen – the predominant ECM component surrounding aortic VSMCs *in vivo* (Filippov et al., 2005; Yana et al., 2007). Just like endothelial cells, VSMCs show major changes in cell and nuclear morphology when MT1-MMP is targeted. While wild-type VSMCs assume an elongated, bipolar cell shape in 3-D hydrogels in the presence of angiogenic growth factors and display elliptical nuclei; *Mt1-mmp*-silenced VSMCs assume a distinct dendritic morphology and retain multi-lobed nuclei (Fig. 4-7 A). Similar to endothelial cells, transcriptional activity and euchromatin-associated Acetyl-H3K9 levels are significantly reduced following MT1-MMP inhibition (Fig. 4-S7 A,B).

To determine whether MT1-MMP serves as a regulator of genomic activity in VSMCs within 3-D ECM *in vivo*, aortae were isolated from *Mt1-mmp*$^{-/-}$ global knockout mice (Holmbeck et al., 1999) or wild-type (*Mt1-mmp*$^{+/+}$) littermates. Aortae exhibit grossly indistinguishable morphologies across genotypes with respect to the VSMC compartment (Fig. 4-7 B). Yet whereas wild-type VSMCs show stress fiber-like α-smooth muscle actin (α-SMA) staining and contain elongated, elliptical nuclei, *Mt1-mmp*$^{-/-}$ VSMCs display a more cortical α-SMA arrangement in

association with distinctly spherical nuclei (Fig. 4-7 B). 3-D reconstructions of wild-type and *Mt1-mmp*$^{-/-}$ VSMC nuclear shapes show that the *Mt1-mmp*$^{-/-}$ VSMCs harbor significantly more folded and multi-lobular nuclei *in vivo* (43.8% folded nuclei, n=4 fields) than wild-type smooth muscle cells (2.6% folded nuclei, n=4 fields) (Fig. 4-7 C). Further, when transcriptional activity was monitored *in vivo* 5' fluorouracil (5'FU) to label nascent transcripts (Spencer et al., 2011), wild-type VSMC nuclei show high levels of F-RNA, and *Mt1-mmp*$^{-/-}$ VSMC nuclei display significantly abrogated transcriptional activity (Fig. 4-7 D). In agreement with these data, aortae from *Mt1-mmp*$^{-/-}$ mice also show markedly reduced levels of Acetyl-H3K9 in the VSMC compartment ($X^2 = 28.9$, $P < 0.0001$; n = 3; Fig. 4-7 E); thereby identifying MT1-MMP as a central regulator of nuclear morphology and transcriptional activity in 3-D ECM in both *in vitro* and *in vivo* milieu.

Discussion.

Growth Factor-Triggered, ECM-Dependent Regulation of Nuclear Architecture.

Recent analyses of cells recovered from patients bearing mutations in the genes encoding lamin A/C, emerin or nesprins have demonstrated that perturbation of normal nuclear architecture impacts tissue morphogenesis and global organism homeostasis – resulting in a family of genetic diseases termed the laminopathies (Cohen et al., 2007; Dechat et al., 2008; Holaska, 2008; Zhang et al., 2007). However, the idea that nuclear structure may be purposefully remodeled during normal development to govern differentiation and morphogenesis has not been investigated. Given the recently described characterization of mechanical linkages between the cell surface and the nuclear envelope (Dahl et al., 2008; Starr, 2009; Stewart et al., 2007), we considered the possibility that growth factor-triggered cell shape changes control tissue morphogenesis by directly impacting nuclear architecture and function. Indeed, using the distribution of the nuclear proteins lamin A and emerin as markers of nuclear envelope architecture (Dahl et al., 2008; Dechat et al.,

2008; Goldman et al., 2004; Holaska, 2008), we find that 3-D-embedded, unstimulated endothelial cells display convoluted nuclei with multiple lobulations and surface invaginations containing nuclear pore complex aggregates. To our knowledge, the appearance of such lobulated, laminopathy-like nuclear shapes has never been described in any normal cell population – likely due to the paucity of analyses performed in 3-D culture. Nevertheless, following stimulation with VEGF/HGF, endothelial cells resculpt nuclear architecture to generate elliptical nuclei marked by a uniformly distributed array of nuclear pore complexes. Surprisingly, under standard, 2-D culture conditions atop mechanically rigid, adhesive substrata, cell shape changes – and consequent nuclear shape changes – are not regulated by vasculogenic signals; this observation compelled us to consider the means by which nuclear structure is controlled by growth factor signals under 3-D-specific conditions.

An ECM-Cytoskeleton-LINC Complex Interaction Continuum Dictates 3-D Nuclear Dynamics.

Pericellular ECM degradation and neomatrix deposition are central modulators of diverse cellular functions ranging from proliferation and differentiation to morphogenesis in a largely 3-D specific manner (Chun et al., 2006; Chun et al., 2004; Hiraoka et al., 1998; Hotary et al., 2003; Saunders et al., 2006; Zhou et al., 2008). Evidence to date indicates that both the mechanical and structural properties of the ECM regulate cellular responses to exogenous soluble signals; however, the mechanism by which ECM-derived cues are interpreted into cellular responses has remained elusive (Ben-Ze'ev et al., 1980; Chen et al., 1997; Chun et al., 2006; Chun et al., 2004; Discher et al., 2005; Engler et al., 2006; Hotary et al., 2003; McBeath et al., 2004; Paszek et al., 2005; Zajac and Discher, 2008; Zhou et al., 2008). Hence, we asked if the growth factor-

dependent, 3-D-specific cell and nuclear shape remolding we observed during vasculogenesis required local ECM proteolysis and deposition, thus providing a possible pathway by which the cell-mediated shifts in the biomechanics of the ECM regulate cell activity. We found that inhibition of either MT-MMP-mediated local proteolysis or fibronectin fibril deposition completely abrogated growth factor triggered endothelial cell and nuclear shape changes in 3-D. In contrast, under 2-D culture conditions where cell shape changes are not constrained by surrounding ECM fibrils, ECM remodeling plays no role in control of nuclear structure.

How might biophysical cues from the ECM be transmitted to the nuclear envelope? The cytoskeleton serves as a central mechanotransducer on the basis of its ability to 'sense' and respond to extracellular rigidity as well as changes in cell shape, though the means by which rigidity sensing is interpreted into regulation of cell function is not well understood (Engler et al., 2006; McBeath et al., 2004; Wang et al., 2009; Wozniak and Chen, 2009; Zajac and Discher, 2008). Recently, a multi-protein complex spanning the nuclear envelope, termed the LINC complex, has been shown to physically connect the cytoskeleton to the nuclear envelope (Crisp and Burke, 2008; Starr, 2009; Stewart et al., 2007), suggesting that ECM-derived cues are mechanically transmitted directly to the nucleus via a continuous network of protein:protein associations. In accordance with their proposed roles in mediating cytoskeletal-nuclear envelope crosstalk, disruption of 3-D endothelial cell cytoskeletal assembly, actomyosin-mediated tension, or physical cytoskeleton-nucleus interactions with the dominant-negative LINC complex protein, GFP-KASH, reproduced the lobulated nuclear structure characteristic of cells unable to recruit pericellular ECM remodeling pathways in response to vasculogenic signals. These data led us to speculate that pericellular ECM remodeling provides a mechanism by which cells actively fine-tune their local 3-D niche to

regulate cell and nuclear geometry via cytoskeleton-LINC complex interactions for appropriate responses to soluble cues.

Nuclear Structure Governs Genome Activity: Clues from Human Disease.

In considering the functional ramifications of ECM remodeling-dependent changes in nuclear shape, we noted that the multi-lobed nuclei and distorted nuclear pore distribution observed in our studies bore striking resemblance to the nuclear shapes observed in cells recovered from human laminopathy patients (Crisp and Burke, 2008; Dechat et al., 2008; Goldman et al., 2004; Holaska, 2008). Study of such cells or mouse models of human laminopathy, as well as cells engineered to silence lamin expression, has demonstrated that disrupted nuclear matrix architecture induces spatial and functional reorganization of the genome, resulting in global alterations in transcription and consequent effects on cell function (Columbaro et al., 2005; Csoka et al., 2004; Dechat et al., 2008; Malhas et al., 2007; Meaburn et al., 2007; Shimi et al., 2008; Shumaker et al., 2006; Tang et al., 2008). While the functional impact of mutations in nuclear envelope proteins on cell function have not been considered to be of necessary relevance to *normal* cell behavior, the structural changes we observed in endothelial cell nuclei in 3-D culture led us to hypothesize that chromatin re-organization might purposefully accompany the nuclear envelope restructuring that occurs during capillary morphogenesis. Consistent with the proposition that chromatin organization is a critical regulator of endothelial cell function (Haberland et al., 2009), VEGF/HGF stimulation induces the translocation of endothelial cell chromatin from a condensed peripheral location to a dispersed, uniform distribution with coincident induction of histone acetylation, a process completely reliant upon fibronectin matrix- or MMP- dependent cell shape changes, cytoskeletal dynamics, and an intact LINC complex.

Inside:Outside Modulation of the Nuclear Compartment.

Our findings suggest a new model wherein pericellular remodeling of the ECM represents a required step in allowing cells to remodel their nuclei in order to activate the transcriptional machinery responsible for controlling growth and differentiation. While our studies have focused on endothelial cell behavior, these findings may apply to all cell populations that reside within a 3-D ECM. By linking ECM remodeling to the ordered transmission of mechanical signals to the nuclear envelope, subtle changes in pericellular ECM remodeling activity – such as proteolysis - would be predicted to profoundly impact phenotype. Indeed, we are intrigued by the fact that the phenotype of *Mt1-mmp*-null mice – characterized by a markedly shortened lifespan with a profound reduction in growth that is associated with the onset of severe bone, muscle, vascular and adipose tissue-related defects shortly after birth - bear considerable similarity to mouse models of laminopathy (Chun et al., 2006; Chun et al., 2004; Holmbeck et al., 1999; Mounkes et al., 2003; Ohtake et al., 2006; Sullivan et al., 1999; Zhou et al., 2000). The overlapping phenotypes raise the possibility that modulating nuclear shape by interfering with ECM remodeling may impact cell function to a degree similar to that observed by directly targeting the nuclear envelope. We conclude that the complex changes in gene expression and cell function known to accompany ECM remodeling are interconnected with matrix-derived cues transmitted to the nuclear envelope, chromatin and transcriptional machinery by a network of protein: protein interactions that span from the cell-ECM interface to the nuclear interior.

Experimental procedures.

Antibodies.

The following commercial antibodies against proteins, histone modifications, and modified nucleotides were used for immunohistochemistry: Acetyl Histone H3 (Lys9) and β-tubulin (Cell Signaling Technologies), Tri-methyl Histone H3 (Lys27) (07-449, Millipore), Vimentin (ab20346, Clone [VI-10] from Abcam), Anti-BrdU (Clone 3D4 from BD Biosciences for immune-labeling BrU-RNA *in vitro*; and ab6326, Clone BU1/75 (ICR1) from Abcam for immunostaining F-RNA *in vivo*), Ki67 (Abcam), and α-smooth muscle actin (ab5694, Abcam). Nesprin-1 and Nesprin-2 antibodies were generously provided by Dr. Angelika A. Noegel (University of Cologne, Germany). To generate the nesprin-3 antibody, full-length human nesprin-3 from FLJ16564 cDNA was cloned into pGEX-2T and expressed in *E.coli* strain BL21 codon-plus and purified according to the manufacturer's protocol. Rabbits were injected with the nesprin-3: GST purified fusion proteins at the laboratory of Comparative Pathology at the School of Veterinary Medicine at UC Davis.

Transgene expression in primary endothelial cells.

To express GFP-KASH (provided by B. Burke, University of Florida) or GFP-lamin (provided by T. Glover, University of Michigan) at high efficiency, endothelial cells were transduced with amphotropic retroviruses in the presence of 50 ng/ml VEGF and 6 μg/ml polybrene (Sigma) and embedded in 3-D fibrin 48 hours later. A GFP-encoding lentivirus was purchased from the University of Michigan Vector Core. The shRNA lentiviral constructs used to target human *MT1-MMP* were (target sequence lower case; hairpin in upper case): Sh-1: 5'

ggccaatgttcgaaggaagtgCTTCCTGTCAcgcttccttcgaacattggcc 3' and Sh-2: 5' ggcacacaaacgaggaatgagCTTCCTGTCActcattcctcgtttgtgtgcc 3'.

Ectopic gene expression in primary endothelial cells.

For expression of GFP-histone H2B or DsRed-Histone H2B, cells were transfected via Lipofectamine 2000 (Invitrogen) according to the manufacturer's protocol. For knockdown of Nesprin-2 with siRNA, Stealth RNAi siRNA were ordered from Invitrogen of the following sequences: Nesprin-2 (siRNA 1) – (RNA) - ucugucaacgugagcagcaaggaau, and (RNA) – auuccuugcugcucacguugacaga; Nesprin-2 (siRNA 2) – (RNA) – cagcagucaggugccuucgacagau, and (RNA) – aucugucgaaggcaccugacugcug. The medium G/C content negative universal control (46-2001, Invitrogen) was used as the scrambled siRNA control. For exogenous expression of scrambled and nesprin 2-targeting siRNA, PepMute siRNA transfection reagent was used according to the manufacturer's protocol (SignaGen Laboratories).

Cell culture.

Human umbilical vein endothelial cells were isolated from umbilical cords by perfusion of the umbilical vein with type 3 collagenase (Worthington Biochemical Corporation) and cultured in Medium-199 (Invitrogen) with 20% human serum and 50 μg/ml endothelial cell growth supplement (ECGS; BD Biosciences). Human vascular smooth muscle cells were purchased from the ATCC (Manassas, VA). Murine *Mt1-mmp* conditional knock-out aortic vascular smooth muscle cells were isolated from mice bearing homozygous *Mt1-mmp*$^{flox/flox}$ alleles, and transduced with either Adenovirus expressing β-galactosidase or Adenovirus expressing Cre recombinase (University of Michigan Vector Core).

3-D cell culture conditions.

For 3-D culture within fibrin, endothelial cells were suspended in a solution of thrombin and aprotinin (Sigma) and mixed 1:1 with a solution of 6 mg/ml fibrinogen (Calbiochem). For 3-D culture within type I collagen, endothelial cells were embedded in a neutralized solution of acid-extracted rat-tail type I collagen at 2.2mg/ml final concentration, as described previously (Sabeh et al., 2009). Vasculogenesis was triggered in endothelial cells by treatment with 100ng/ml VEGF, and 50ng/ml HGF (Genentech). Aortic vascular smooth muscle cells were cultured within neutralized type I collagen (Sabeh et al., 2009) in DMEM with 10% FBS, in the presence of PDGF-BB and FGF-2 (10ng/ml each, Sigma) (Filippov et al., 2005). Fibronectin fibrillogenesis by endothelial cells was inhibited by treatment with FUD peptide (Zhou et al., 2008) and MMPs were inhibited in both endothelial cells and vascular smooth muscle cells with broad-range MMP inhibitor BB-94 (Tocris). Endothelial cells and vascular smooth muscle cells were similarly cultured atop 3-D fibrin or type I collagen for parallel assessments under 2-D planar conditions. Actomyosin contractility and microtubule assembly were inhibited with blebbistatin and nocodazole, respectively (25 μ*M* and 5 μ*M*, respectively; Calbiochem).

3-D synthetic hydrogels.

MMP-resistant or MMP-degradable PEG hydrogels were formed by FXIIIa catalyzed reaction as described (Ehrbar et al., 2007). Briefly, 8-arm PEG-Gln and PEG-Lys were blended to generate stoichiometrically balanced ([Gln]/[Lys]) PEG precursor solutions. The PEG-Lys component was either chosen to contain a linker peptide that is susceptible (GPQG/IWGQ, with / indicating the cleavage site) or resistant (GDQGIAGF) to MMP-mediated degradation. The PEG precursor solutions (1.5, 2.0 and 2% w/v) were cross-linked upon addition of 10 U/mL FXIIIa in

presence of 50mM TrisHCl pH 7.6, 50mM $CaCl_2$, 50μM Lys-RGD (Ac-FKGGRGDSPG-NH_2, NeoMPS Strasbourg, France) and cells suspended in medium 12% (v/v) of the total volume. To form hydrogel discs, 20μL drops of the still liquid reaction mixture were sandwiched between sterile, hydrophobic glass microscopy slides that were separated by 1 mm spacers and clamped with binder clips. Polymerization was then allowed to take place for 30min. at 37°C in a humidified incubator. To visualize the matrix, 25μM Lys-FITC (Ac-FKGGGK-FITC-NH_2, NeoMPS) was added prior to reaction, leading to a homogenous covalent tethering of FITC to the matrix.

Cell culture atop micropatterned substrata.

Micro-contact printing techniques were used to fabricate substrates patterned with regions that were coated with fibronectin and regions that resisted such adsorption, as previously described (Singhvi et al., 1994). 1225 μm^2 islands (35 μm x 35 μm) were used to constrain cell spreading, while continuous surfaces of fibronectin allowed for full spreading. Briefly, PDMS stamps bearing the relevant pattern of islands were washed with ethanol, dried, immersed for 1 hour in an aqueous solution of 25 mg/ml fibronectin, rinsed thoroughly in water, dried, and placed in conformal contact against the culture substrate, blocked with 0.2% Pluronic F127 (BASF), and used under standard culture conditions.

Isolation of nuclei *in situ*.

Endothelial cell nuclei were extracted *in situ* using the following method. Endothelial cells were seeded at 1.5 X 10^5 cells per ml on 4-well Gelatin-coated chamber glass slides, prepared as described previously (Yana and Weiss, 2000), and incubated at 37ºC in 5% CO_2 for 20-24 hours. Endothelial cells were then washed twice with Dulbecco's PBS, and treated with a hypotonic

reducing solution containing 5mM $MgCl_2$, 6mM KCl, 50mM Tris-HCl (pH 7.4), 75mM $(NH_4)_2SO_4$, 25% w/v glycerol and 1mM dithiothreitol to partially extract the cell monolayer and reduce the sedimentation of extracellular and cytoplasmic material. After 3 minutes of incubation at room temperature, this reducing solution was removed, and the partially extracted cell monolayer was washed twice with 12% w/v polyethylene glycol (PEG) (Average MW 8kDa, Promega) solution, containing 100µM K-Hepes (Sigma) buffer at pH 7.4, in order to mimic the macromolecular crowding present in intact cells and maintain the physiologic nuclear shape (Hancock and Hadj-Sahraoui, 2009). The adherent, partially extracted cells were then further extracted and permeabilized *in situ* with 12% w/v PEG solution containing 50µg/ml digitonin for 30 minutes at room temperature on a gentle rotating platform (Hancock and Hadj-Sahraoui, 2009). Isolated nuclei were then washed three times with 12% w/v PEG solution to remove the detergent and incubated in 12% or 25% w/v PEG polymer solutions containing 100µM K-Hepes (pH 7.4), at room temperature for 30 minutes in a humidified chamber. For reversibility studies, control wells were left in 12% or 25% w/v PEG solution for another 30 minutes, and test wells were washed gently twice with 12% w/v PEG solution, and transferred to 12% w/v PEG solution for another 30 minutes of room temperature incubation. For assessments of chromatin structure in isolated nuclei, cell monolayers were pre-treated with 50ng/ml trichostatin A (TSA) for 1 hour at 37^{o}C prior to their extraction to counteract the elevation in histone deacetylase activity following nuclear extraction (Mulholland et al., 2003; Pivot-Pajot et al., 2003).

Nuclear run-on transcription assays.

For assessments of transcriptional activity in intact cells, 2-D and 3-D cultures were incubated with 2mM Bromouridine (BrU) (Sigma) for 1 hour at 37^{o}C (Pellizzoni et al., 2001)

following their 48 hour culture period, and processed as described below. For the actinomycin D-treated negative control, cultures were pre-incubated with actinomycin D at 5µg/ml (Sigma) for 3 hours before the addition of BrU (Pellizzoni et al., 2001). For assessments of transcriptional activity in isolated nuclei, the *in situ* isolated nuclei were equilibrated to 37^{o}C for 10 minutes, the PEG solutions were gently pipetted off and exchanged for 500ul of the same PEG solutions containing 1mM KCl, 100µM ATP, 100µM CTP, 100µM GTP, 100µM Br-UTP and 100units/mL rRNAsin (Promega) for another 30 minutes of incubation at 37ºC [modified from (Hancock and Hadj-Sahraoui, 2009)]. For the actinomycin D treatment condition, isolated nuclei were pre-incubated at 37^{o}C for 10 minutes in the presence of 5µg/ml actinomycin D (Pellizzoni et al., 2001), and the above transcription mix was added in the presence of 5µg/ml actinomycin D. Nuclei were then fixed by overlaying them for 1 hour with the same PEG solution containing 2% PFA, and processed as detailed below for immunofluorescence. For BrU-Seq, approaches were employed as described previously (Paulsen et al., 2013) with the following modifications. Endothelial cells were embedded at 150,000 cells per hydrogel of 3-D type I collagen at 10^6 cells per condition (n=2). Following a 1h incubation with 2 mM BrU, wells with washed twice with ice-cold PBS and homogenized in TRIzol (Ambion, Life Technologies). Total RNA was extracted and purified using QIAGEN RNeasy Mini-kit columns (QIAGEN, 74104). BrU-containing RNA was isolated with anti-BrdU antibodies, processed and sequenced as described (Paulsen et al., 2013).

Isolation of and quantification of poly (A) RNA fractions from 3-D cultures.

Following isopropanol precipitation of RNA from Trizol extracts and overnight incubation in 75% ethanol, the poly(A) fraction was isolated with Oligo$(dT)_{25}$ cellulose beads

(S1408, New England BioLabs) according to the manufacturer's protocol and quantified with the Quant-iT RiboGreen RNA Assay Kit (Invitrogen) using a 96-well plate reader.

Immunofluorescence, proliferation and apoptosis assays.

For immunofluorescent labeling of protein in intact endothelial cells cultured within or atop 3-D hydrogels, or in isolated nuclei, cultures were fixed with 4% paraformaldehyde – unless otherwise noted, washed with PBS, and permeabilized with 0.1% Triton X-100. Cultures were blocked with 3% normal goat serum, and incubated with primary antibodies for 12-to-15 hours. For immunostaining of nascent transcripts labeled with bromouridine, cultures were fixed in 4% paraformaldehyde containing 2% sucrose, permeabilized in 0.1% Triton X-100, and blocked in 1% normal goat serum containing 5% fetal calf serum. After washing with PBS, cultures were incubated with secondary antibodies (Alexa- 488 or 594 -labeled goat anti-mouse or anti-rabbit antibodies; Invitrogen), Alexa- 488 or 594 -labeled phalloidin, or propidium iodide for 1-2 hours, washed with PBS, incubated for 10 minutes with DAPI counterstain (Invitrogen), and washed overnight in PBS. Apoptosis was assessed by TUNEL assay (In situ cell death detection kit, Fluorescein, Roche).

Image acquisition and analysis.

All images were captured using an Olympus FV500 confocal microscope with Fluoview software, and a 60X water immersion objective (1.2 numerical aperture; Olympus). 3-D reconstructions were generated using Volocity (Perkin-Elmer) and Imaris (Bitplane) software. Analysis of chromatin distribution within 2-D and 3-D nuclei was performed using Metamorph software (Molecular Devices). The integrated density and mean fluorescence signal of Acetyl-

H3K9, H3K27Me3 and BrU levels within intact cells (*in vitro* and *in vivo*) were quantified from confocal Z-slices using Image J software (National Institutes of Health). For quantification of the fluorescence signal within isolated nuclei, Imaris imaging software was used to map the surface of the DAPI-stained nuclei and determine the total masked fluorescence signal (BrU or Acetyl-H3K9) within the 3-D reconstructed nuclear surface.

Atomic force microscopy (AFM) micro-indentation.

Fibrin gels were washed briefly with PBS after removing culture medium. Samples were mechanically characterized using an Asylum MFP-3D atomic force microscope (Asylum Research) by performing micro-indentation using a sphere-tipped probe (Novascan) with a sphere diameter of 5 μm and a nominal spring constant of ~60 pN/nm. The cantilever spring constant was confirmed by thermal fluctuation method (Thundat et al., 1994). The AFM system was calibrated by following the manufacturer's recommended standard procedure before each indentation measurement. AFM micro-indentation was performed in PBS solution at room temperature. Individual force-indentation profile was acquired at an indentation rate of 2 μm/s using deflection trigger mode with a trigger value of 200 nm. The AFM tip was positioned either adjacent to or away from a cell. Shear modulus at each position was calculated from fitting force-indentation data using a Hertz sphere model (Richert et al., 2004).

Mice and *in vivo* studies.

Constitutive *Mt1-mmp*$^{-/-}$ mice have been described previously (Holmbeck et al., 1999). To examine nuclear structure within intact aortae, mice were anesthetized with ketamine/xylazine and perfused through the left ventricle with 4% paraformaldehyde to fix aortic mural cells *in situ*. Mice

were then euthanized, and aortae were harvested and frozen in optimal cutting temperature (OCT) medium (Tissue-Tek) for processing by standard techniques. For detection of de novo transcripts in the mouse aorta, a 0.1M solution of 5'Fluorouracil (Sigma) prepared in sterile Dulbecco's PBS (DPBS) was injected into the peritoneal cavity at a dose of 2 µmol/g mouse into 17-21 day old MT1 knockout mice and corresponding wild-type littermate controls, and allowed to incorporate for 2 hours. The mice were then euthanized, and their aortas were excised, flash frozen in OCT medium, sectioned at a thickness of 30µm, and immunostained with an antibody against BrdU, as described previously (Spencer et al., 2011).

Fig. 4-1.

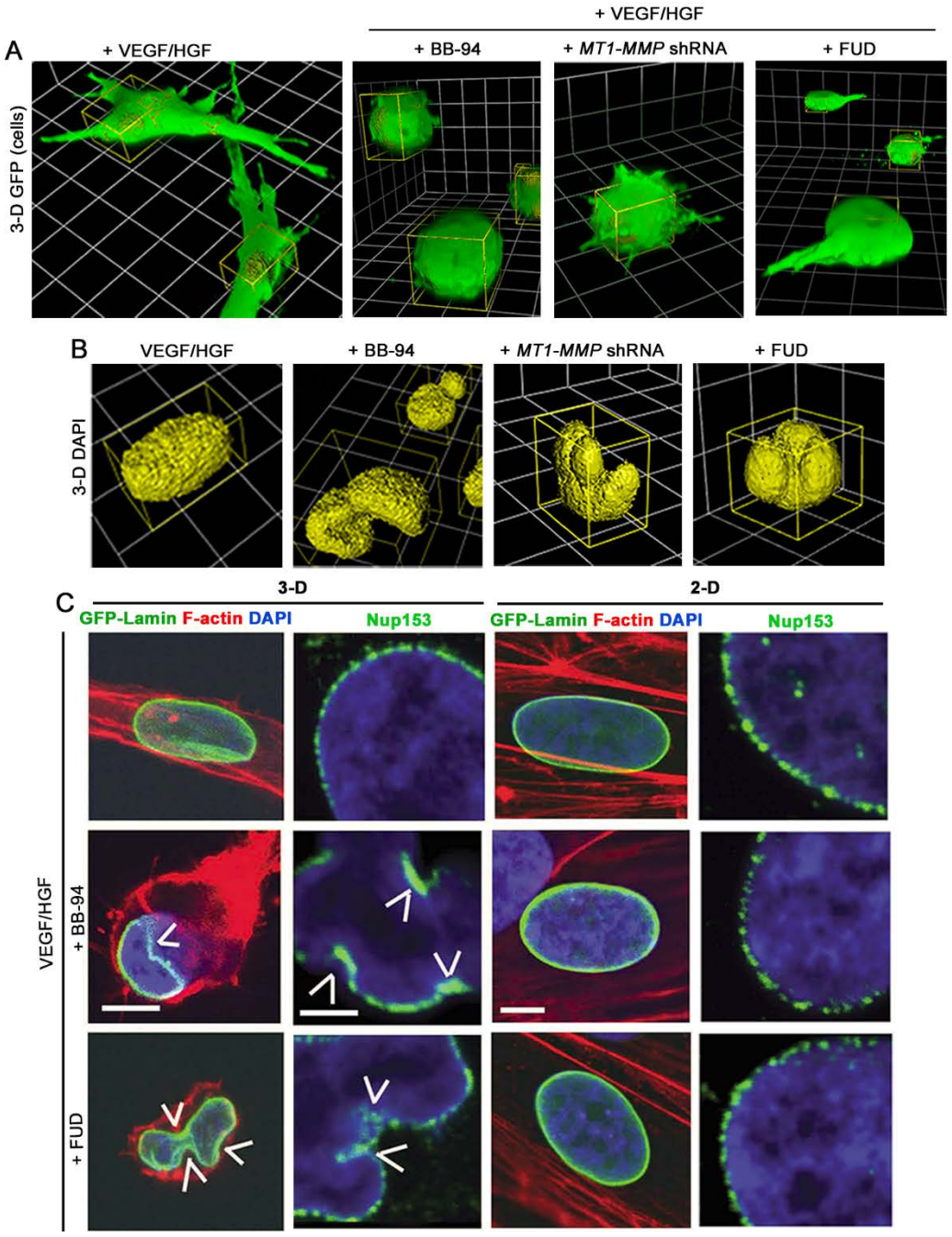

Fig. 4-1. Control of nuclear architecture through fibronectin matrix assembly and MT1-MMP-dependent pericellular proteolysis.
(A) Endothelial cells transduced with GFP lentivirus, with lentivirus expressing GFP-tagged scrambled shRNA, or with shRNA targeting MT1-MMP, and embedded within 3-D fibrin gels for culture with VEGF (100 ng/ml) and HGF (50 ng/ml) (VEGF/HGF) alone or in the presence of BB-

94 (5 μM) or FUD (250 nM) for 48 h. Cell morphology was assessed from 3-D reconstructions of the GFP signal (1 unit = 21.3 μm). (B) 3-D reconstructions of DAPI nuclear staining in VEGF/HGF-stimulated endothelial cells cultured in 3-D fibrin alone or in the presence of BB-94 or FUD; and 3-D reconstruction of the DAPI staining in endothelial cells transduced with MT1-MMP shRNA and cultured in 3-D fibrin under VEGF/HGF stimulation (1 unit = 21.3 μm). (C) Endothelial cells expressing GFP-tagged lamin A within (3-D) fibrin gels or atop (2-D) fibrin gels in the presence or absence of BB-94 or FUD with DAPI nuclear staining. Phalloidin staining highlights the filamentous (F)-actin arrangements in the control and targeted conditions (scale bar = 20 μm). Immunofluorescence for the nuclear pore complex component NUP153 in VEGF/HGF-stimulated endothelial cells cultured under 2-D or 3-D conditions alone, or in the presence of BB-94 or FUD. Nuclei were stained with DAPI (scale bar = 2 μm). Arrowheads indicate nuclear membrane invagination sites.

Fig. 4-2.

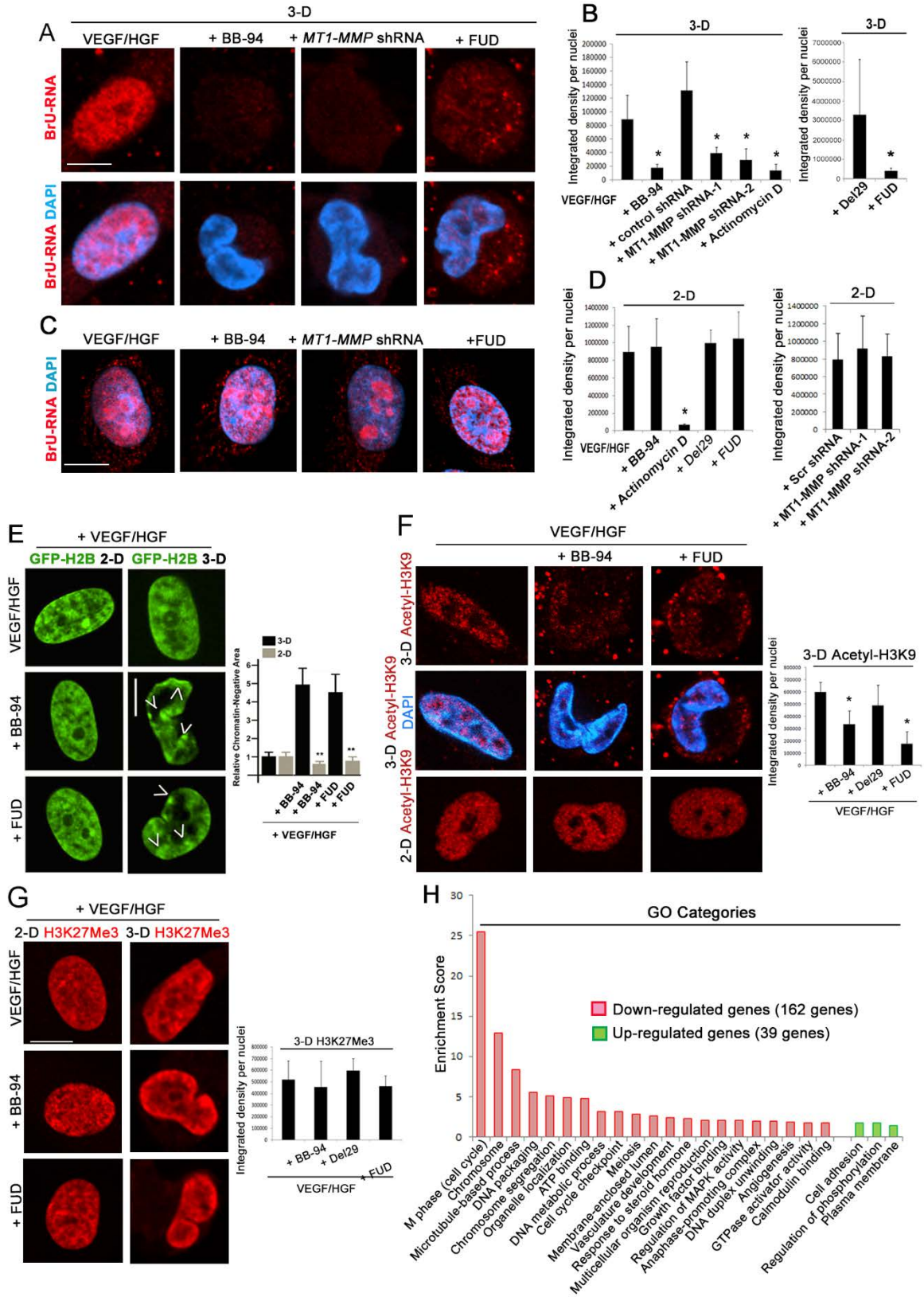
A
3-D
VEGF/HGF
+ BB-94
+ MT1-MMP shRNA
+ FUD
BrU-RNA
BrU-RNA DAPI
B
3-D
Integrated density per nuclei
VEGF/HGF
+ BB-94
+ control shRNA
+ MT1-MMP shRNA-1
+ MT1-MMP shRNA-2
+ Actinomycin D
+ Del29
+ FUD
C
VEGF/HGF
+ BB-94
+ MT1-MMP shRNA
+FUD
BrU-RNA DAPI
D
2-D
Integrated density per nuclei
VEGF/HGF
+ BB-94
+ Actinomycin D
+ Del29
+ FUD
+ Scr shRNA
+ MT1-MMP shRNA-1
+ MT1-MMP shRNA-2
E
+ VEGF/HGF
GFP-H2B 2-D
GFP-H2B 3-D
VEGF/HGF
+ BB-94
+ FUD
Relative Chromatin-Negative Area
3-D
2-D
+ VEGF/HGF
F
VEGF/HGF
+ BB-94
+ FUD
3-D Acetyl-H3K9
3-D Acetyl-H3K9 DAPI
2-D Acetyl-H3K9
Integrated density per nuclei
VEGF/HGF
G
+ VEGF/HGF
2-D H3K27Me3
3-D H3K27Me3
VEGF/HGF
+ BB-94
+ FUD
3-D H3K27Me3
Integrated density per nuclei
VEGF/HGF
H
GO Categories
Enrichment Score
Down-regulated genes (162 genes)
Up-regulated genes (39 genes)
M phase (cell cycle)
Chromosome
Microtubule-based process
DNA packaging
Chromosome segregation
Organelle localization
ATP binding
DNA metabolic process
Cell cycle checkpoint
Meiosis
Membrane-enclosed lumen
Vasculature development
Response to steroid hormone
Multicellular organism reproduction
Growth factor binding
Regulation of MAPK activity
Anaphase-promoting complex
DNA duplex unwinding
Angiogenesis
GTPase activator activity
Calmodulin binding
Cell adhesion
Regulation of phosphorylation
Plasma membrane

Fig. 4-2. Regulation of chromatin structure and transcriptional activity through fibronectin matrix assembly and MT1-MMP-dependent pericellular proteolysis.
(A) *In situ* transcriptional activity in endothelial cells cultured within 3-D fibrin hydrogels for 48 h with VEGF/HGF alone, or in the presence of BB-94 or FUD, or in endothelial cells cultured in 3-D following their transduction with MT1-MMP-targeting shRNA. Following a 1 hour incubation with bromouridine (BrU), labeled RNA (BrU-RNA) was detected by indirect immunofluorescence (scale bar = 5 μm). (B) Quantifications represent the integrated density of the fluorescence signal within individual endothelial cell nuclei from n>10 fields per condition. For a negative control, 3-D cultures were incubated with Actinomycin D (5 μg/ml) prior to the 1 hour incubation with BrU (*p<0.001). (C) Immunofluorescence for BrU-RNA in endothelial cells cultured atop 2-D fibrin gels for 48 h with VEGF/HGF alone or together with BB-94 or FUD, or endothelial cells transduced with MT1-MMP-targeting shRNA and cultured on 2-D fibrin gels for 48 h with VEGF/HGF (scale bar = 5 μm). (D) Quantifications represent the integrated density of the fluorescence signal within individual endothelial cell nuclei from n>10 fields per condition. For a negative control, 3-D cultures were incubated with Actinomycin D (5 μg/ml) prior to the 1 hour incubation with BrU (*p<0.001). (E) Endothelial cells expressing a construct encoding GFP-labeled histone H2B under 2-D or 3-D conditions with VEGF/HGF-stimulation alone or in the presence or absence of BB-94 or FUD. Arrowheads indicate chromatin condensed at the nuclear periphery (scale bar = 5 μm). Quantification of the relative chromatin-negative area in endothelial cell nuclei under 2-D and 3-D conditions (**p<0.05). (F) Immunofluorescence of Acetyl-H3K9 in VEGF/HGF-stimulated endothelial cells cultured alone or in the presence of BB-94 or FUD under 2-D and 3-D condition with DAPI counter-staining, with quantification of the fluorescence density per nuclei from n>10 fields per condition (n=3 experiments). **p<0.001. (G) Immunofluorescence of H3K27Me3 in VEGF/HGF-stimulated endothelial cells cultured alone or in the presence of BB-94 or FUD under 2-D and 3-D conditions (scale bar = 5 um), with quantification of fluorescence density per nuclei from n>10 fields per condition and n=3 experiments. (H) Chart of the Gene Ontology (GO) categories enriched in the BrU-RNA sequencing (BrU-Seq) of VEGF/HGF-stimulated endothelial cells cultured in 3-D ECM alone or in the presence of BB-94 (n=2, pooled replicates) with a 2-fold change cutoff. Pink columns represent the GO categories enriched in the 162 down-regulated transcripts. Green columns represent the GO categories enriched in the 39 upregulated genes.

Fig. 4-3.

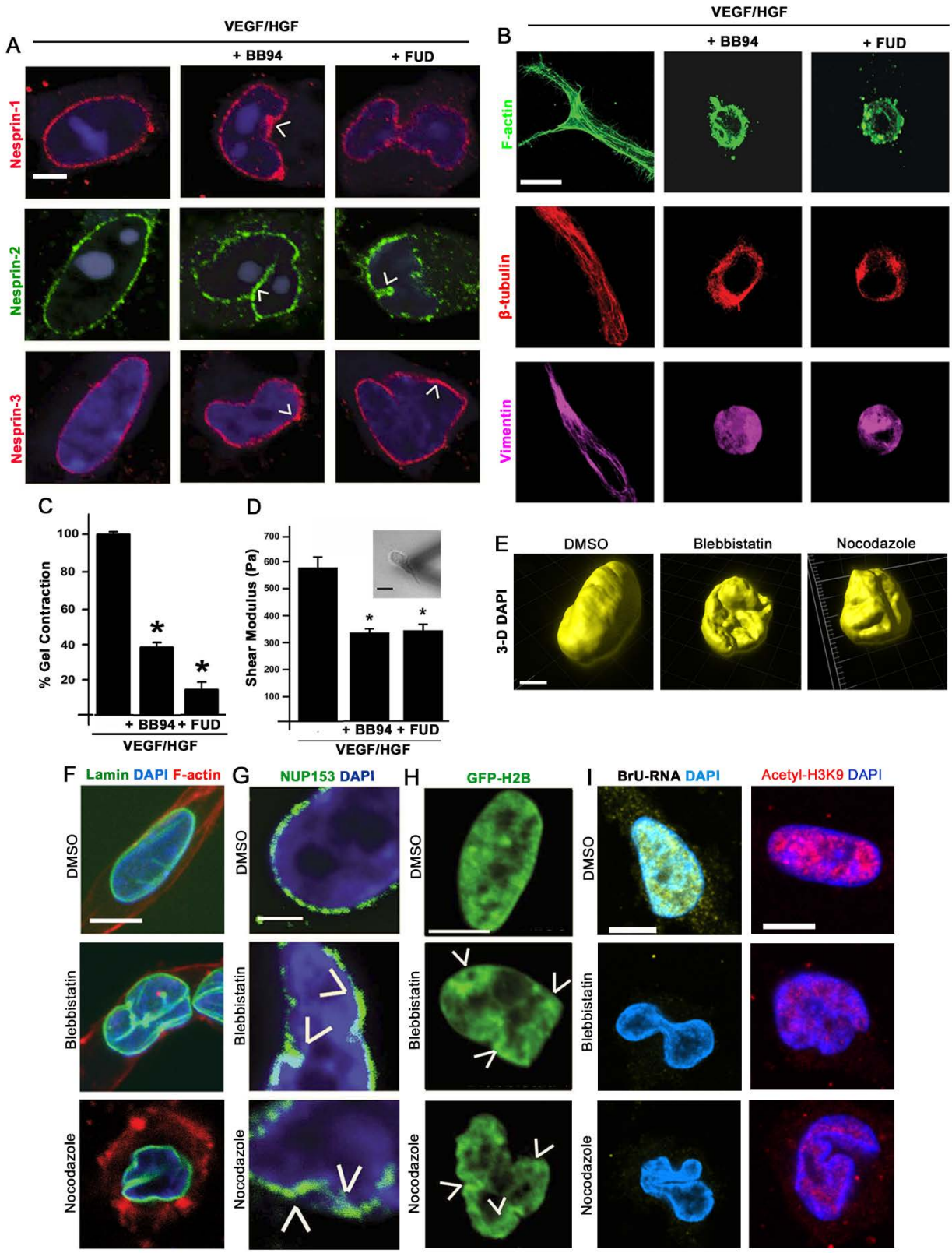
A
VEGF/HGF
+ BB94
+ FUD
Nesprin-1
Nesprin-2
Nesprin-3
B
VEGF/HGF
+ BB94
+ FUD
F-actin
β-tubulin
Vimentin
C
% Gel Contraction
100
80
60
40
20
+ BB94 + FUD
VEGF/HGF
D
Shear Modulus (Pa)
700
600
500
400
300
200
100
+ BB94 + FUD
VEGF/HGF
E
DMSO
Blebbistatin
Nocodazole
3-D DAPI
F Lamin DAPI F-actin
G NUP153 DAPI
H GFP-H2B
I BrU-RNA DAPI
Acetyl-H3K9 DAPI
DMSO
Blebbistatin
Nocodazole

Fig. 4-3. Regulation of nuclear architecture and transcriptional activity by the cytoskeleton in 3-D.

(A) Immunofluorescence for nesprin-1 (top row), nesprin-2 (middle row), and nesprin-3 (bottom row) in VEGF/HGF-stimulated endothelial cells cultured within 3-D fibrin gels for 48 h in the presence or absence of BB-94 or FUD with DAPI nuclear staining (scale bar = 5 μm). (B) Fluorescence of F-actin (top row), β-tubulin (middle row) and vimentin (bottom row) in VEGF/HGF-stimulated endothelial cells cultured in the presence or absence of BB-94 or FUD in 3-D ECM (scale bar = 20 μm). (C) Endothelial cells were cultured in 3-D ECM hydrogels with VEGF/HGF alone or with BB-94 or FUD for 48 h, the hydrogels were released from the culture wells, and the percentage of gel contraction was quantified (*$p < 0.05$). (D) Pericellular ECM rigidity in 3-D cultures of endothelial cells stimulated with VEGF/HGF alone or with BB-94 or FUD was quantified by atomic force microscopy micro-indentation, and the shear modulus of the pericellular ECM environment was determined. The inset shows a representative image of a 3-D-embedded endothelial cell interfacing with the atomic force microscopy probe (scale bar = 40 μm). (E) 3-D reconstructions of the DAPI signal from serial Z-sections through endothelial cells cultured in the presence of DMSO (vehicle), blebbistatin (25 μM) or nocodazole (5 μm) for 48 h (scale bar = 5μm). (F) Endothelial cells expressing GFP-lamin A and cultured in 3-D ECM in the presence of DMSO, blebbistatin or nocodazole for 48 h with DAPI and F-actin staining (scale bar = 15 μm). (G) Immunofluorescence for NUP153 in endothelial cells cultured with VEGF/HGF in the presence of DMSO, blebbistatin or nocodazole. Nuclei were counter-stained with DAPI (scale bar = 2 μm). Arrowheads indicate nuclear pore complex aggregates at nuclear membrane invaginations. (H) Endothelial cells expressing GFP-H2B chromatin and embedded in 3-D ECM for culture in the presence of DMSO, blebbistatin or nocodazole. Arrowheads indicate peripheral chromatin aggregations (scale bar = 10 μm). (I) Immunofluorescence for BrU-RNA or Acetyl-H3K9 in VEGF/HGF-stimulated endothelial cells cultured in 3-D ECM in the presence of DMSO, blebbistatin or nocodazole (scale = 5 μm). All images are representative of n=3 experiments.

Fig. 4-4.

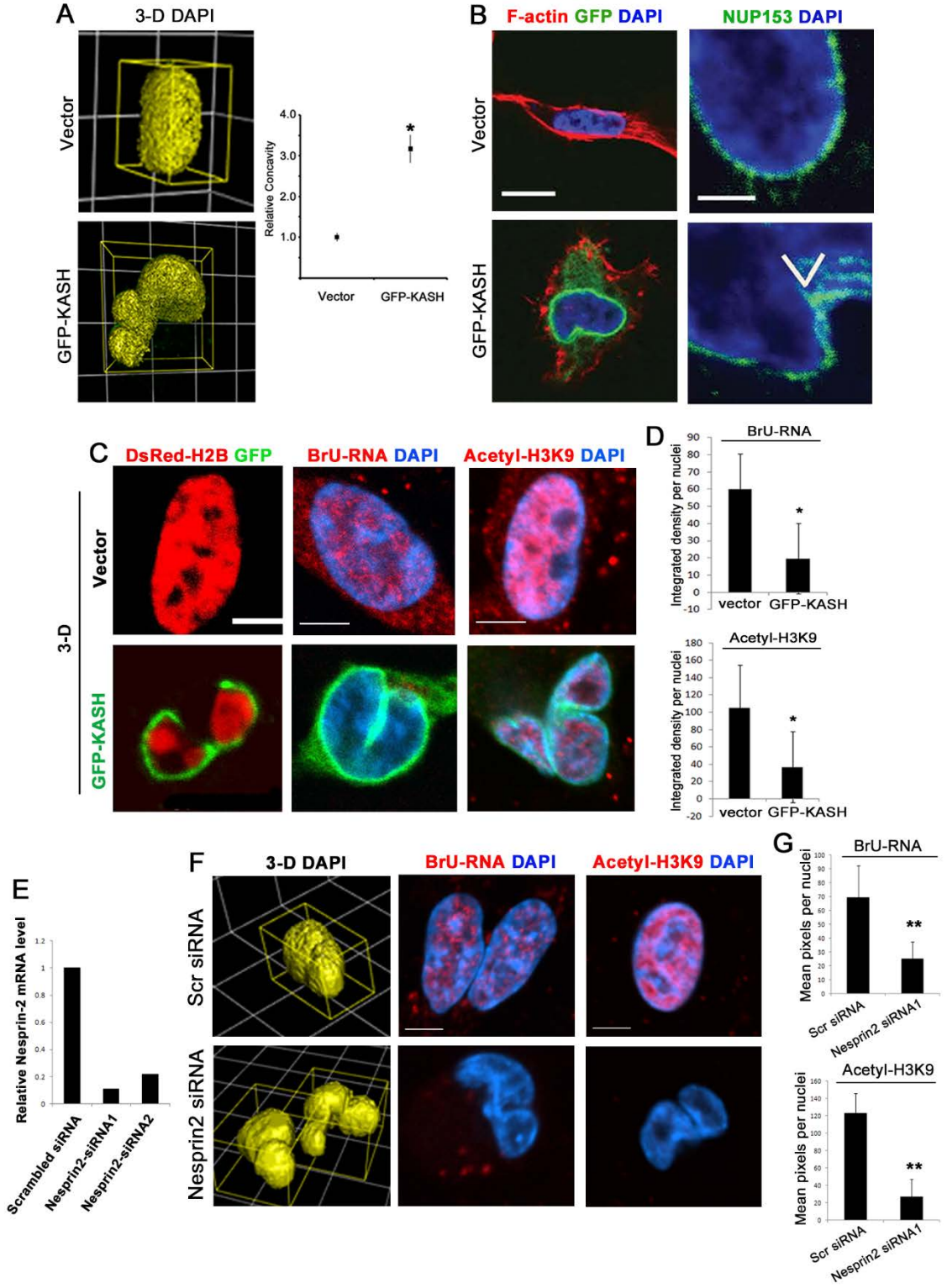
A
3-D DAPI
Vector
GFP-KASH
Relative Concavity
4.0
3.0
2.0
1.0
Vector
GFP-KASH
B
F-actin GFP DAPI
NUP153 DAPI
Vector
GFP-KASH
C
DsRed-H2B GFP
BrU-RNA DAPI
Acetyl-H3K9 DAPI
3-D
Vector
GFP-KASH
D
BrU-RNA
Integrated density per nuclei
vector
GFP-KASH
Acetyl-H3K9
Integrated density per nuclei
vector
GFP-KASH
E
Relative Nesprin-2 mRNA level
Scrambled siRNA
Nesprin2-siRNA1
Nesprin2-siRNA2
F
3-D DAPI
BrU-RNA DAPI
Acetyl-H3K9 DAPI
Scr siRNA
Nesprin2 siRNA
G
BrU-RNA
Mean pixels per nuclei
Scr siRNA
Nesprin2 siRNA1
Acetyl-H3K9
Mean pixels per nuclei
Scr siRNA
Nesprin2 siRNA1

Fig. 4-4. Perturbations of the LINC complex recapitulate ECM remodeling-dependent changes in nuclear shape and nascent transcript production.
Endothelial cells were transduced with an empty (vector) retrovirus or a retrovirus expressing GFP-KASH (green) and embedded within 3-D fibrin for 48 h. (A) Morphology of control and GFP-KASH nuclei in 3-D ECM, as visualized from 3-D reconstructions of DAPI staining (1 unit = 21.3 μm). Nuclear concavity was quantified in endothelial cells by morphometric analysis of confocal Z-sections (*$p<0.05$). (B) Nuclear envelope and F-actin organization in GFP-KASH cells relative to control with DAPI counter-staining (scale bar = 15 μm). Immunofluorescence for NUP153 with DAPI counter-staining. Arrowhead indicates a nuclear pore aggregate at a nuclear membrane invagination site (scale bar = 2 μm). (C) Chromatin organization in vector- and GFP-KASH-transduced endothelial cells in 3-D, as visualized by DsRed-labeled histone H2B (scale bar = 5 μm). Immunofluorescence for BrU-RNA and Acetyl-H3K9 with DAPI counter-staining (scale bar = 5 μm). (D) Quantifications of the integrated density of BrU-RNA and Acetyl-H3K9 per nuclei in vector and GFP-KASH-transduced endothelial cells cultured in 3-D ECM with VEGF/HGF ($n>10$ fields per condition, *$p<0.001$, $n=3$ experiments). (E) qPCR for Nesprin-2 in endothelial cells transfected with scrambled siRNA or Nesprin-2 siRNA as normalized to Gapdh and expressed as mean values ($n=2$ experiments). (F) 3-D reconstructions of nuclei within endothelial cells transfected with scrambled siRNA or Nesprin-2 siRNA and embedded within 3-D fibrin for 48 h-culture with VEGF/HGF. Immunofluorescence for BrU-RNA and Acetyl-H3K9 in 3-D-cultured endothelial cells expressing scrambled siRNA or Nesprin-2 siRNA with DAPI counter-staining. (G) Quantifications of the mean fluorescence density per nuclei for BrU-RNA (top) and Acetyl-H3K9 (bottom) in Nesprin-2 -targeted endothelial cells cultured within 3-D ECM ($n>10$ fields per condition, **$p<0.001$).

Fig. 4-5.

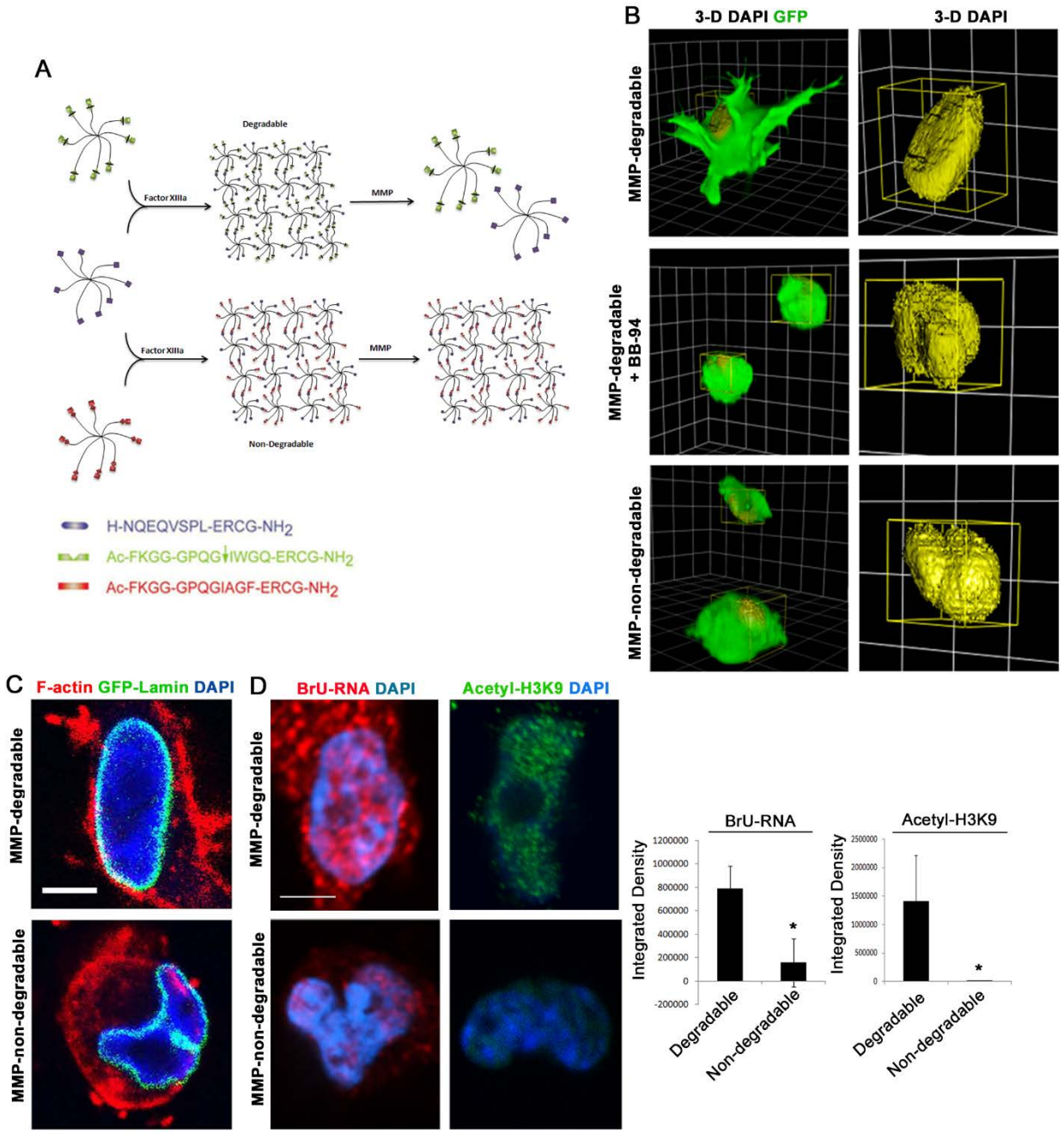

Fig. 4-5. Direct modulation of 3-D cell shape using synthetic PEG-hydrogels controls nuclear architecture and function.

(A) Schematic of PEG-hydrogel structure. Factor XIIIa was used to crosslink two multi-arm PEG-peptide conjugates bearing complementary transglutaminase peptide substrates (NQEQVSPL) derived from the N-terminus of α2-plasmin inhibitor and the synthetic lysine donor peptide Ac-FKGG at a final concentration of 2.0%. To render the gels susceptible to degradation by MMPs,

the lysine donor peptide was designed to contain the MMP substrate GPQG↓IWGQ, derived from the native sequence GPQG↓IAGQ found in α1(I) collagen chain (↓ indicates the cleavage site). The sequence GDQGIAGF was chosen as a MMP-insensitive control linker. To provide cell adhesion sites, the integrin-binding peptide H-NQEQVSPL*RGDSPG*-NH2 was grafted to both gel types at constant concentration. (B) Cell shape of VEGF/HGF-stimulated (GFP-labeled) endothelial cells cultured for 48 h within 3-D PEG hydrogels with MMP-degradable cross-links alone or in the presence of BB-94, or within MMP-nondegradable hydrogels, as visualized with 3-D reconstructions of GFP signal. Morphologies of the corresponding nuclei, as indicated by 3-D reconstructions of the DAPI signal (1 unit = 21.3 μm). (C) Endothelial cells expressing GFP-lamin were embedded in MMP-degradable or MMP-nondegradable hydrogels and stained for F-actin and DAPI following 48 h culture with VEGF/HGF. (D) Immunofluorescence for BrU-RNA or Acetyl-H3K9 in VEGF/HGF-stimulated endothelial cells cultured within 3-D MMP-degradable and MMP-nondegradable hydrogels. Nuclei were counter-stained with DAPI (scale = 5 μm). Quantification of the integrated density of BrU-RNA fluorescence (left) and Acetyl-H3K9 fluorescence (right) per nuclei from n>10 fields and n=3 experiments. *$p<0.01$.

Fig. 4-6.

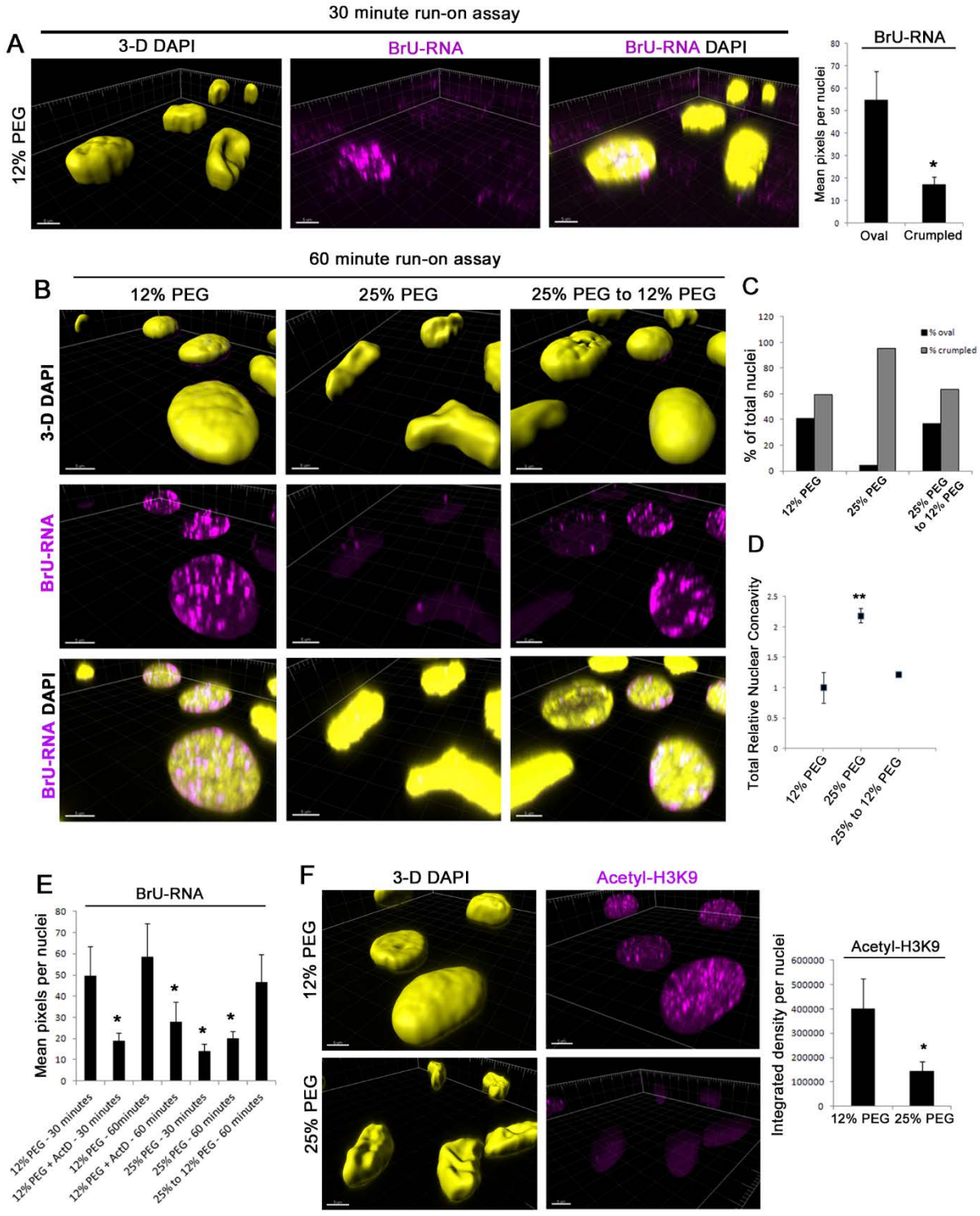
30 minute run-on assay
A
3-D DAPI
BrU-RNA
BrU-RNA DAPI
12% PEG
BrU-RNA
Mean pixels per nuclei
Oval
Crumpled
60 minute run-on assay
B
12% PEG
25% PEG
25% PEG to 12% PEG
3-D DAPI
BrU-RNA
BrU-RNA DAPI
C
% of total nuclei
% oval
% crumpled
12% PEG
25% PEG
25% PEG to 12% PEG
D
Total Relative Nuclear Concavity
12% PEG
25% PEG
25% to 12% PEG
E
BrU-RNA
Mean pixels per nuclei
12% PEG - 30 minutes
12% PEG + ActD - 30 minutes
12% PEG - 60minutes
12% PEG + ActD - 60 minutes
25% PEG - 30 minutes
25% PEG - 60 minutes
25% to 12% PEG - 60 minutes
F
3-D DAPI
Acetyl-H3K9
12% PEG
25% PEG
Acetyl-H3K9
Integrated density per nuclei
12% PEG
25% PEG

Fig. 4-6. Nuclear shape directly regulates chromatin structure and transcriptional activity. (A) 3-D reconstructions of isolated nuclei incubated with 12% w/v PEG solution for 30 min at room temperature followed by a 30-min nuclear run-on transcription assay with Br-UTP. Immunofluorescence for BrU-RNA with DAPI counter-staining and quantification of the mean fluorescence intensity within oval and crumpled nuclei from n=3 experiments. (B) Immunofluorescence for BrU-RNA with DAPI nuclear counter-staining and 3-D reconstructions of the DAPI signal after a 30-min nuclear run-on assay for the following conditions: (i) a 1 hour pre-incubation in 12% w/v PEG, (ii) a 1 hour pre-incubation in 25% w/v PEG, or (iii) a 30 min pre-incubation in 25% w/v PEG followed by a 30 min pre-incubation in 12% w/v PEG. Nuclear run-on assays were performed in the final % w/v PEG. (C) Percentage of oval or crumpled nuclei following 1 hour incubation in 12% or 25% w/v PEG, or a 30 min incubation in 25% w/v PEG followed by a 30 min incubation in 12% w/v PEG. (D) Relative nuclear concavity values of the isolated nuclei from n>10 fields, as normalized to the sum of the nuclear concavities present under the 12% PEG condition (n=3 experiments). (E) Quantification of mean fluorescence intensity for BrU-RNA in the isolated nuclei (F) Immunofluorescence for Acetyl-H3K9 with DAPI counter-staining in isolated nuclei. Following pre-treatment of cells with 50 ng/ml trichostatin A (TSA), intact endothelial cell nuclei were isolated *in situ*, incubated in either 12% or 25% w/v PEG solution and subjected to a 30-min nuclear run-on transcription assay with Br-UTP. The intensity of the Acetyl-H3K9 fluorescence signal per nuclei was quantified from n>10 fields (n=2 experiments).

Fig. 4-7.

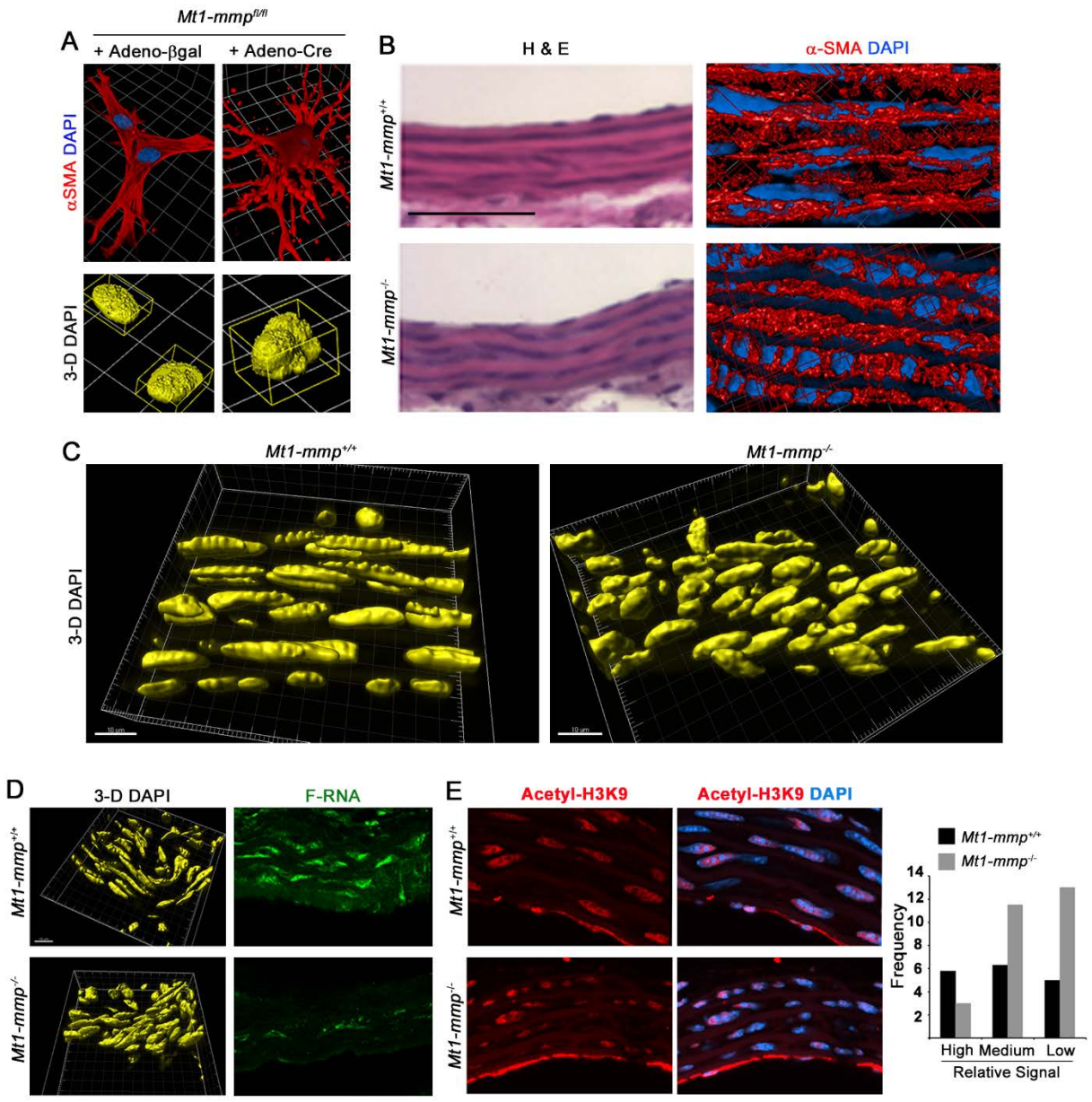

Fig. 4-7. Regulation of 3-D VSMC morphology, nuclear shape and transcriptional activity by MT1-MMP *in vivo*.

(A) Mouse vascular smooth muscle cells (VSMCs) harvested from *Mt1-mmp*$^{fl/fl}$ mice, treated with either adenovirus encoding β-galactosidase (Adeno-βgal) or Cre recombinase (Adeno-Cre), and embedded within 3-D type I collagen for 48 h-culture. 3-D projections of VSMC morphology and corresponding nuclear architecture as assessed from 3-D reconstructions of α-smooth muscle actin (αSMA) and DAPI counter-staining. (1 unit = 21.3 μm). (B) H&E staining of aorta isolated from wildtype (*Mt1-mmp*$^{+/+}$) and global knockout (*Mt1-mmp*$^{-/-}$) mice (left) (scale bar = 100 μm).

Immunofluorescence for αSMA in frozen sections of aorta from the same *Mt1-mmp*$^{+/+}$ *and Mt1-mmp*$^{-/-}$ mice with DAPI counter-staining (right). (C) 3-D reconstructions of DAPI staining in cross-sections of *Mt1-mmp*$^{+/+}$ and *Mt1-mmp*$^{-/-}$ aorta (1 unit = 21.3 μm). (D) Aorta were harvested from *Mt1-mmp*$^{+/+}$ *and Mt1-mmp*$^{-/-}$ mice injected with vehicle or 5'fluorouracil (5'FU). Immunofluorescence for 5'FU-labeled transcripts (F-RNA) was used as a read-out of transcriptional activity. Images are representative of n>150 nuclei per genotype from n=4 replicates. (E) Immunofluorescence for Acetyl-H3K9 in cross-sections of *Mt1-mmp*$^{+/+}$ *and Mt1-mmp*$^{-/-}$ aorta with DAPI counter-staining (scale = 20 μm). VSMC nuclei were classified as having 'high', 'medium', or 'low' signal intensity based on integrated density of the Acetyl-H3K9 fluorescence signal. The mean frequency of nuclei with each signal is presented.

Fig. 4-S1.

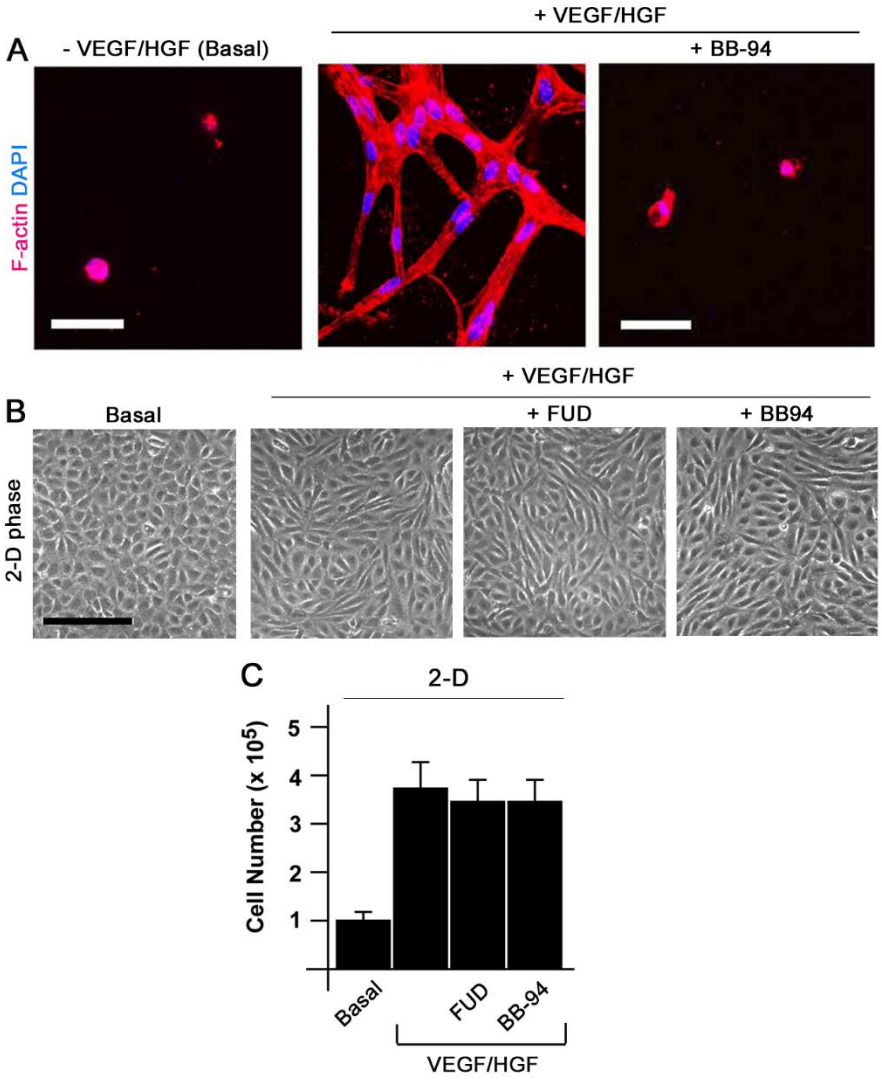

Fig. 4-S1. ECM remodeling-dependent regulation of endothelial cell proliferation under 3-D, and not 2-D, conditions.

(A) F-actin staining of endothelial cells cultured in 3-D fibrin for 6 d in the presence of serum alone (basal), or together with 100ng/ml VEGF and 50ng/ml HGF (VEGF/HGF), or with VEGF/HGF and BB-94 (5 μm). Nuclei were counter-stained with DAPI (n=3 experiments) (scale bar = 50 μm). (B) Phase contrast imaging of endothelial cells cultured atop 2-D fibrin under basal or VEGF/HGF conditions, or with VEGF/HGF and either BB-94 or 250 nM of the FUD for 72 h (scale bar = 200 μm). (B) Quantification of endothelial cell number ($X10^5$) following culture atop 2-D fibrin under basal or VEGF/HGF conditions, or with VEGF/HGF and either BB-94 inhibitor or FUD for 72 h.

Fig. 4-S2.

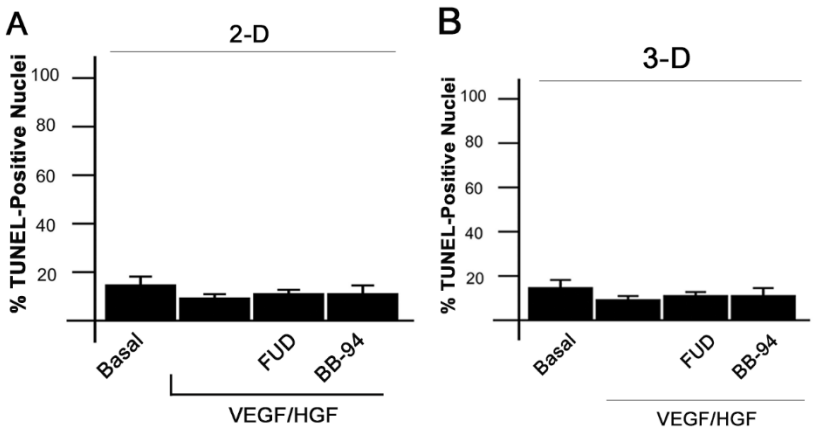

Fig. 4-S2. Pericellular ECM remodeling-inhibition does not induce apoptosis under either 2-D or 3-D conditions.
Endothelial cells were either cultured atop 2-D fibrin or embedded in 3-D ECM under basal or VEGF/HGF conditions, or with VEGF/HGF and either BB-94 inhibitor or FUD for 48 h. Apoptosis was assessed by TUNEL assay. (A) Quantification of TUNEL-positive nuclei following 2-D culture. (B) Quantification of TUNEL-positive nuclei following 3-D culture. Endothelial cells were embedded within 3-D fibrin under the indicated conditions.

Fig. 4-S3.

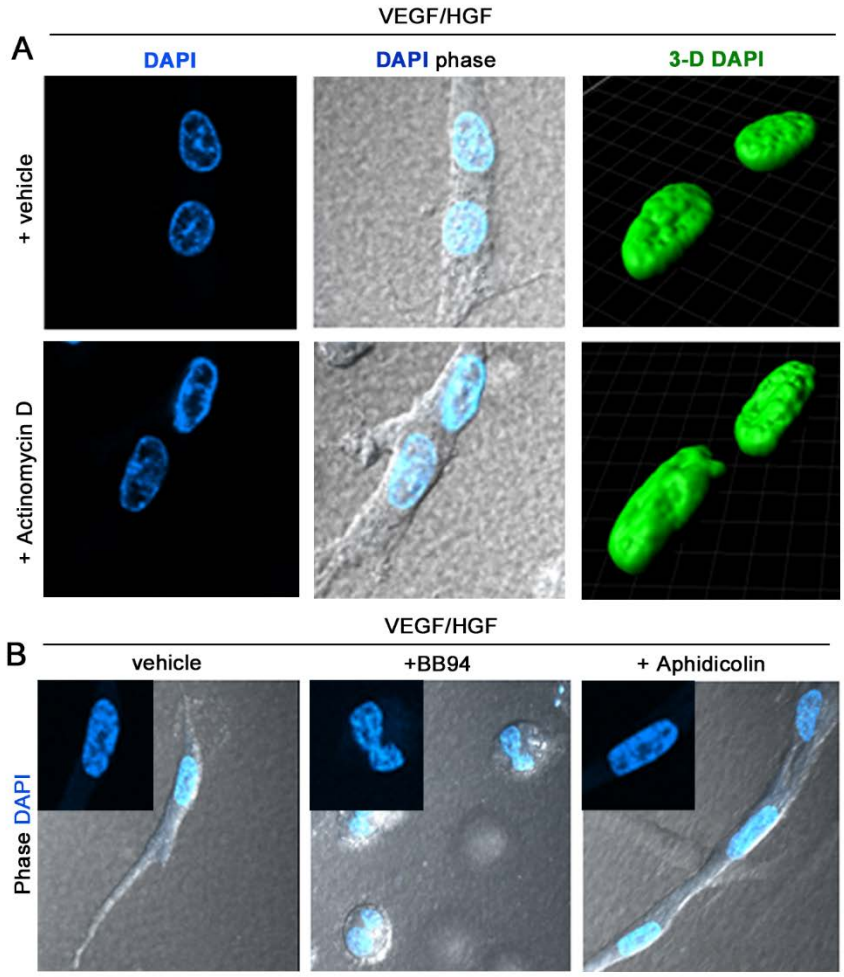

Fig. 4-S3. Blockade of transcriptional activity or S-phase progression do not induce changes in nuclear shape in 3-D ECM.
(A) Phase imaging and DAPI nuclear staining of endothelial cells cultured within 3-D ECM with VEGF/HGF for 42 h, followed by 3 h culture with either vehicle control or Actinomycin D (5 µg/ml). 3-D reconstructions of DAPI staining (right) (1 unit = 21.3 µm). (B) Phase imaging and DAPI nuclear staining of endothelial cells cultured within 3-D ECM with VEGF/HGF alone or together with BB-94 (5 µm) or Aphidicolin (10 µM) inhibitors for 48 h. Insets show close-up of representative DAPI staining without Phase overlay.

Fig. 4-S4.

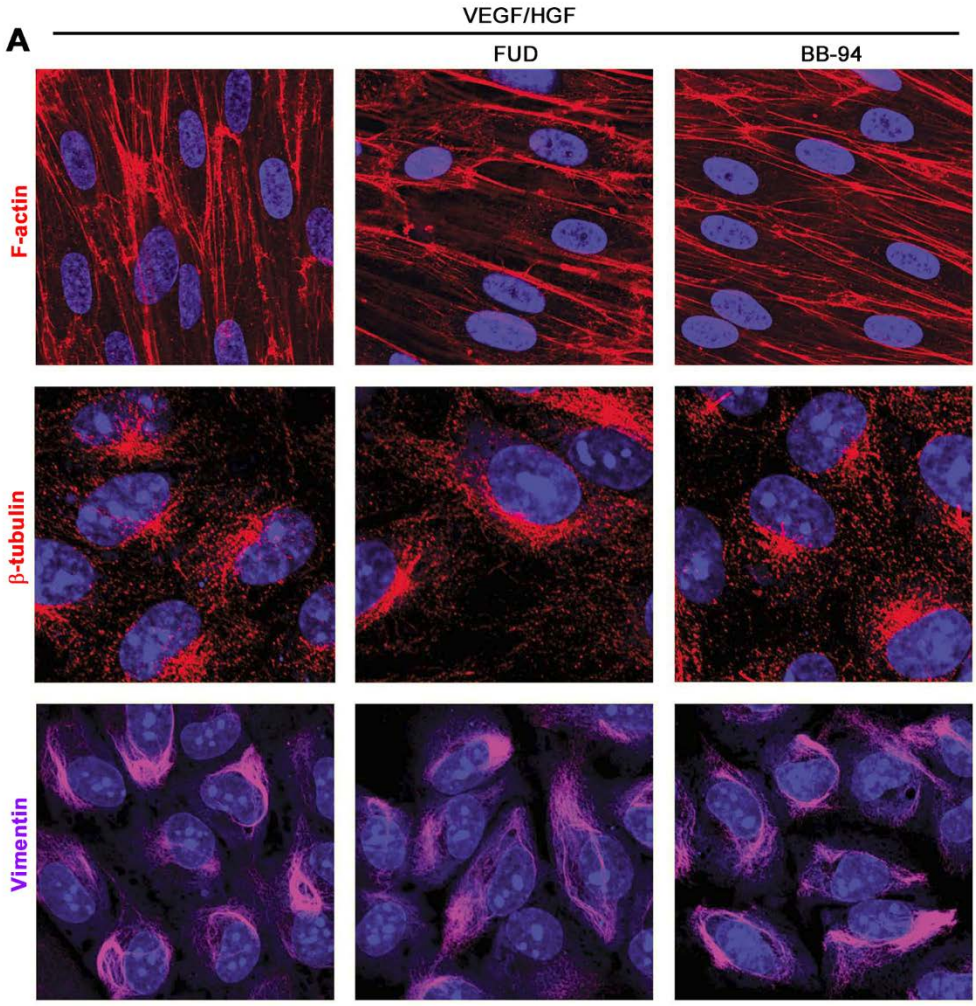

Fig. 4-S4. 2-D cytoskeletal organization is modulated independently of ECM Remodeling Pathways.
(A) Immunofluorescence for F-actin (labeled with phalloidin) (top row), β-tubulin (middle row), or vimentin (bottom row) in endothelial cells cultured with VEGF/HGF alone or in the presence of BB-94 or FUD peptide atop a substratum of fibrin for 48 h. Nuclei were counter-stained with DAPI.

Fig. 4-S5.

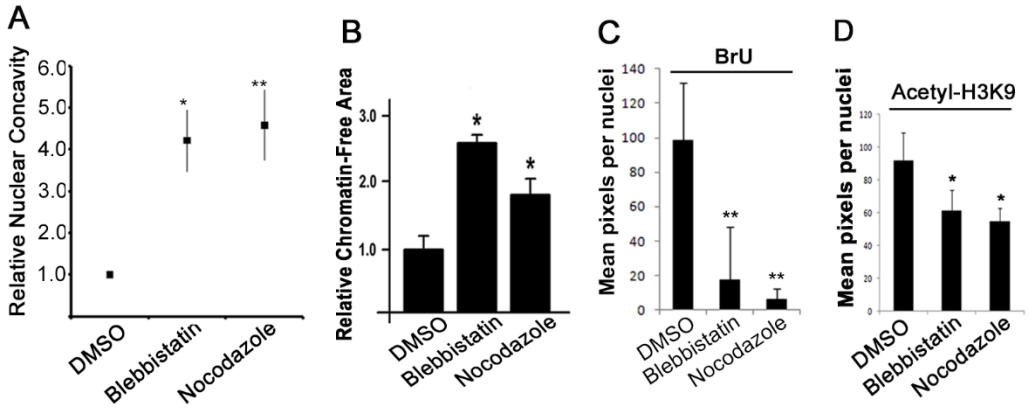

Fig. 4-S5. Regulation of nuclear architecture and transcriptional activity by the cytoskeleton in 3-D.

(A) Relative nuclear concavity of nuclei from VEGF/HGF-stimulated endothelial cells cultured in 3-D fibrin in the presence or absence of DMSO (vehicle), blebbistatin (25 μM) or nocodazole (5 μM) for 48 h. (*$p<0.0001$; **$p=0.0003$). (B) Relative chromatin distribution in nuclei of VEGF/HGF-stimulated endothelial cells expressing the GFP-H2B construct and cultured in 3-D fibrin in the presence of DMSO, blebbistatin or nocodazole. (**$p<0.05$). (C) The mean density of the BrU-RNA fluorescence signal per individual nuclei in endothelial cells cultured in 3-D fibrin in the presence of DMSO, blebbistatin or nocodazole ($n>10$ fields per condition, **$p<0.0001$, $n=3$ experiments). (D) The mean density of Acetyl-H3K9 fluorescence within nuclei of VEGF/HGF-stimulated endothelial cells cultured in 3-D fibrin in the presence of DMSO, blebbistatin or nocodazole ($n>10$ fields per condition, *$p<0.001$, $n=3$ experiments).

Fig. 4-S6.

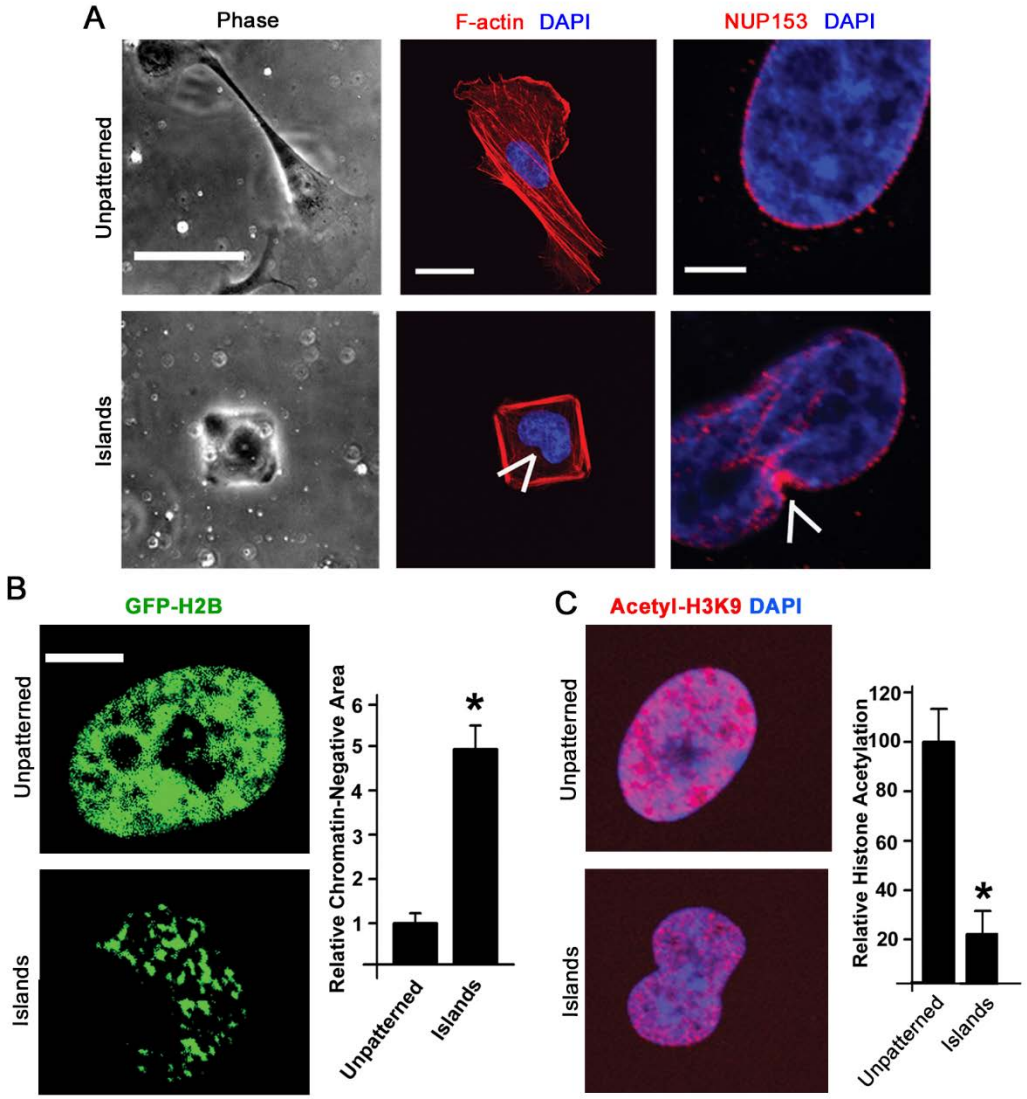

Fig. 4-S6. Nuclear shape and chromatin structure atop micropatterned substrata.
(A) Phase contrast imaging of endothelial cells cultured atop uniformly-coated fibronectin substrata or 35x35 μm fibronectin 'islands' and cell morphology (left panels, scale = 50 μm). F-actin and DAPI staining of respective cells (middle panels, scale = 30 μm). Arrowhead indicates a nuclear membrane infolding. Immunofluorescence of NUP153 with DAPI nuclei counter-staining with arrowhead indicating nuclear member indentation (right panels, scale = 4 μm). (B) Chromatin distribution in endothelial cells expressing GFP-H2B atop unpatterned substrata or fibronectin islands with quantification of the relative chromatin-free area (scale = 5 μm; *$p<0.05$). (C) Immunofluorescence for Acetyl-H3K9 in endothelial cells atop unpatterned substrata or islands with DAPI counter-staining. Relative histone acetylation signal was quantified by morphometric analysis (scale = 30 μm; *$p<0.05$).

Fig. 4-S7.

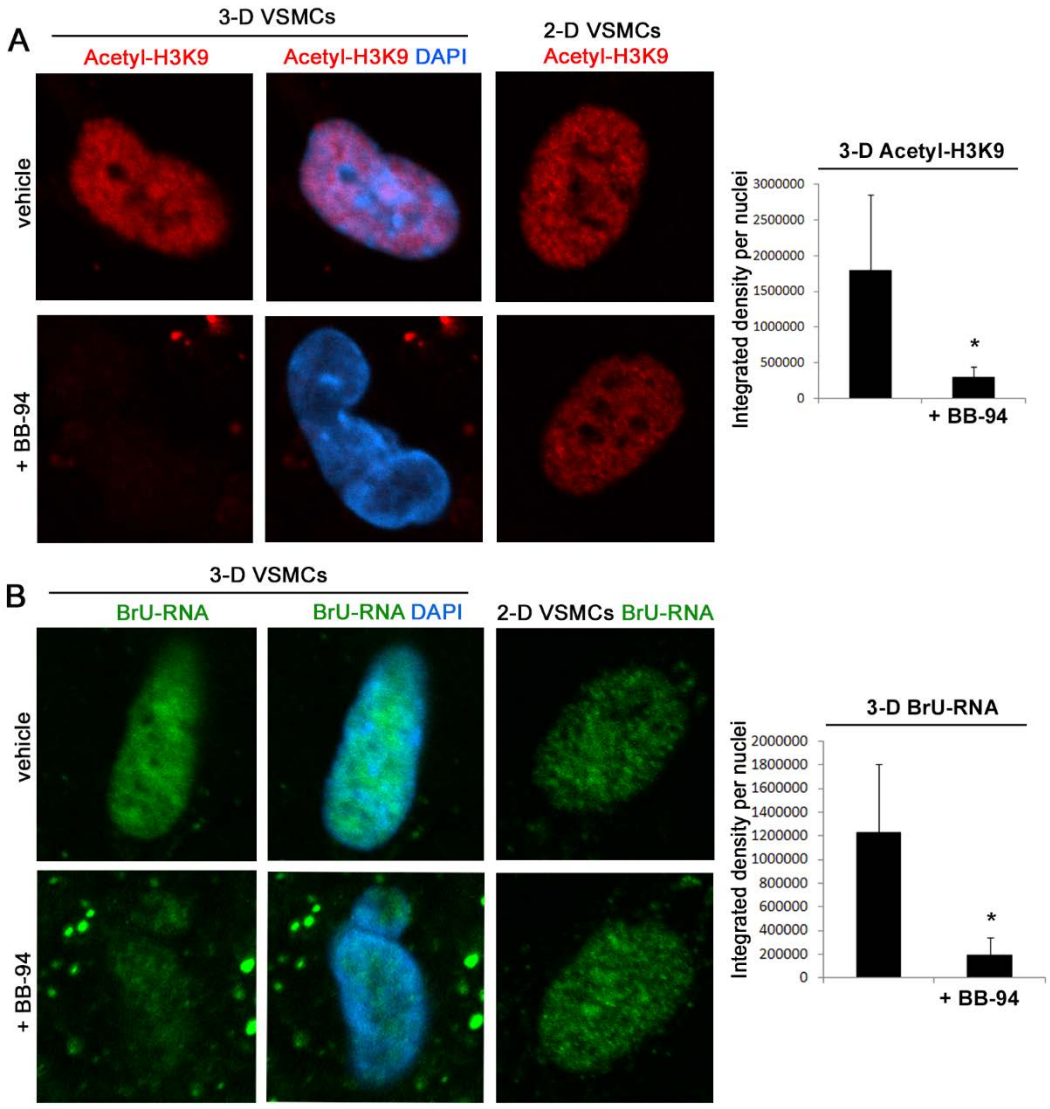

Fig. 4-S7. Pericellular ECM remodeling-dependent regulation of nuclear shape and transcriptional activity in vascular smooth muscle cells.
(A) Immunofluorescence for Acetyl-H3K9 in vascular smooth muscle cells embedded in 3-D type I collagen for 48 h in the presence of PDGF-BB and FGF-2 (10 ng/ml each) (PDGF-BB/FGF-2) with vehicle control or BB-94 inhibitor. Nuclei were counter-stained with DAPI. Quantification of the integrated density of Acetyl-H3K9 immunofluorescence from n>10 fields per condition and n=3 experiments. *p<0.01. (B) Immunofluorescence for BrU-RNA and DAPI staining in vascular smooth muscle cells embedded in 3-D type I collagen for 48 h in the presence of PDGF-BB/ FGF-2 with vehicle control or BB-94 inhibitor. Quantification of the integrated density of BrU immunofluorescence from n>10 fields per condition and n=3 experiments. *p<0.01.

Note.

* This chapter is in preparation for submission as a manuscript, entitled: “MT1-MMP-Mediated Pericellular Proteolysis controls the KASH·SUN-Dependent Regulation of Vascular Cell Nuclear Architecture and Function,” by Tamar Y. Feinberg*, R. Grant Rowe*, Martin Ehrbar, Matthias P. Lutolf, Stephen I. Lentz, Colette J. Shen, Christopher S. Chen, Heidi N. Fridolfsson, Daniel A. Starr, Fei Liu, Daniel Tschumperlin, Deane F. Mosher and Stephen J. Weiss. (* denotes equal contribution).

CHAPTER 5: Discussion

Herein, we document central roles for MT-MMPs and pericellular ECM remodeling in governing the cell motility, proliferation, transcription, and differentiation programs required for postnatal branching morphogenesis. *In vivo,* a subtending and contiguous BM barrier separates mammary epithelial tubules as well as vascular endothelial cells from their surrounding interstitial matrix environment (Williams and Daniel, 1983). However, while normal mammary epithelial cells never establish direct contact with the type I collagen-rich stromal matrix, endothelial cells uniquely respond to angiogenic signals by traversing the BM and directly interfacing with the interstitial ECM (Carmeliet and Jain, 2011). In mature postnatal tissue environments, we find that mammary stromal cell populations rely on MT-MMP-directed proteolytic activity to coordinate morphogenesis. While the roles of MT-MMPs in angiogenic responses *in vivo* remain to be determined, endothelial cells cultured *in vitro* likewise depend on MT-MMP-derived proteolytic activity to alter cell shape and proliferate in 3-D hydrogels of type I collagen or fibrin. In the specific case of endothelial cells, pericellular proteolysis of the 3-D interstitial matrix governs cell function as well as cell behavior by modulating nuclear architecture, and subsequently gauging transcriptional activity to meet the signaling needs required morphogenic responses. Ongoing work will address the *in vivo* role of pericellular ECM remodeling during angiogenic responses as well as its role in controlling nuclear architecture and function of mammary stromal cell populations, including fibroblast-like cells and adipocyte precursors.

Despite accumulating *in vitro* evidence implicating MMP family members in mammary epithelial branching (Alcaraz et al., 2011; Bonnans et al., 2014; Brownfield et al., 2013; Mori et al., 2009; Rebustini et al., 2009; Weaver et al., 2014), embryonic and early postnatal mammary gland branching programs proceed in an unabated fashion following the *in vivo* targeting of the dominant MMPs reported to regulate epithelial morphogenesis, including MT1-MMP and MT2-MMP. Importantly, deletion of epithelial cell-derived *Mt1-mmp* alone, *Mt2-mmp* alone, or both *Mt-mmps* together, failed to impede later stages of postnatal morphogenesis, countering current, largely *in vitro* – based paradigms, where epithelial-derived proteases orchestrate branching organ development when the cells establish direct – albeit artefactual – contact with type I collagen. Alternatively, our study of early postnatal mammary gland development unexpectedly revealed key regulatory roles for both MT1-MMP and MT2-MMP in the mammary stromal fat pad. While global knockout of *Mt1-mmp* down-regulates adipogenesis, *Mt2-mmp* deletion enhances the formation of beige/ brown adipocytes. Beige and brown adipocytes have been reported in wild-type mammary tissue before the onset of puberty, yet disappear by ~ 9 weeks after birth (Gouon-Evans and Pollard, 2002). To evaluate the persistence of this thermogenic gene signature under *Mt2-mmp-null* conditions, mammary fat pad tissue was isolated from 4-to-5 month-old mice. Interestingly, both male and female *Mt2-mmp*$^{-/-}$ mice retain elevated levels of UCP1 protein, as well as increased expression of *Prdm16* and *Pgc1α* (n=3) - two central regulators of brown/beige adipogenesis (Cohen et al., 2014; Wu et al., 2013). As both paracrine and systemic signals from the sympathetic nervous system has been shown to regulate thermogenesis (Whittle et al., 2012), stromal vascular cells will be harvested in subsequent experiments for culture under 2-D versus 3-D conditions to evaluate their preferential differentiation into white versus brown lineages (Chun et al., 2006; McDonald et al., 2015; Tang et al., 2013). Further studies will also evaluate whether

the smaller adipocytes present in stromal cell-targeted *Dermo1Cre*$^{+/-}$*Mmp14*$^{fl/fl}$ mice or adipocyte-targeted *AdipoqCre*$^{+/-}$*Mmp14*$^{fl/fl}$ mice stem from attenuated adipogenesis and lipid metabolism or from changes in lineage commitment and cell fate.

Given the expression of MT1-MMP in the mammary stroma and its evident functional roles during early mammary gland development, we sought to evaluate the consequences of targeting stromal cell-derived *Mt1-mmp* on postnatal mammary gland development. Contrary to current dogma, postnatal mammary gland branching through mature ECM relies on MT1-MMP expression from the stroma, rather than from the epithelium, to orchestrate the remodeling of the interstitial ECM. The abrogated postnatal mammary gland branching in mice with stromal cell-targeted *Mt1-mmp* coincides with a block in interstitial ECM remodeling and a concomitant increase in ECM. While mice with MT1-MMP-resistant type I collagen largely recapitulate the branching defect observed in the stromal cell-targeted model, further studies are needed to determine the mechanisms by which increased type I collagen levels ablate morphogenetic responses. In the simplest scenario, the dense network of type I collagen "simply" presents itself as a physical barrier to tubule elongation. More likely, however, the increased rigidity of the surrounding matrix alters epithelial cell gene expression. We hope to gain better insight into epithelial cell-collagen interactions by culturing wild-type mammary tubule fragments in increasingly dense collagen hydrogels *in vitro* and interrogating changes in gene expression.

Although mammary glands isolated from *AdipoqCre*$^{+/-}$*Mt1-mmp*$^{fl/fl}$ mice show uninterrupted postnatal mammary gland branching, ruling out a critical role for MT1-MMP-expressing adipocytes, preliminary data points to a critical role for the mammary periductal fibroblasts, the dominant cells known to express the interstitial ECM components that surround the mammary epithelium (Keely et al., 1995). Preliminary data show that the tamoxifen-inducible

transgenic mouse model, *Col1a2-CreER*, wherein the *Col1a2* promoter drives Cre recombinase expression, displays more specific expression in the mammary periductal fibroblasts. Further, preliminary data suggests that *Col1a2-CreER*$^{+/-}$*Mt1-mmp*$^{fl/fl}$ mice display a similar block in postnatal mammary gland branching relative to that present in *Dermo1Cre*$^{+/-}$*Mt1-mmp*$^{fl/fl}$ mice. As gene changes from intact tissue lysates would reflect the transcriptional profile of the entire mammary gland, future experiments will use the RiboTag mouse model (Sanz et al., 2009) to specifically isolate and profile the mammary fibroblasts. In the RiboTag model, the presence of Cre recombinase fuses an HA-tag to the ribosomal protein subunit, RPL22, generating RPL22-HA, that can be used to selectively immune-precipitate polyribosomes from cells expressing the *Col1a2*-Cre and evaluate the transcripts that are actively being translated into protein.

Targeting of stromal cell-derived MT1-MMP with *Dermo1-Cre* also results in a marked decrease in terminal end bud (TEB) size and proliferative activity. Since TEBs are thought to drive mammary gland branching (Hinck and Silberstein, 2005; Jackson-Fisher et al., 2004; Kurley et al., 2012), further studies will address whether the postnatal mammary ducts fail to elongate, in part, due to a defect in the TEBs, themselves. A TEB defect might arise from any number of factors, including an insufficiency in paracrine signals from the mammary mesenchyme (Jackson-Fisher et al., 2004; Kurley et al., 2012; Visbal et al., 2011). While the gene expression profile did not reveal sufficient changes in the stromal cell-derived growth factors and signaling receptors to explain the halt in postnatal branching, stromal cell-derived MT1-MMP might still regulate the growth factor/cytokine repertoire at a post-transcriptional level, especially given the proposed roles for MT1-MMP in activating a suite of cell surface- and ECM-bound growth factors with critical roles in tissue morphogenesis (Barbolina and Stack, 2008; Itoh, 2015; Rowe and Weiss, 2009). As intact *Mt1-mmp*$^{-/-}$ mammary epithelial ducts from TEB-deficient glands mount a normal

branching program through wild-type mammary stroma, any defect in TEB function is likely reversible.

Nevertheless, the functional roles of MT1-MMP and MT2-MMP in the epithelial cell compartment *in vivo* remain to be defined – either during virgin branching morphogenesis or during postnatal stages of adult mammary gland remodeling, including pregnancy, lactation and involution. With regard to epithelial cell-derived MT1-MMP, mammary epithelial compartments have been harvested from 4-week *MMTV-Cre*$^{+/-}$*Mt1-mmp*$^{fl/fl}$ and *Mt1-mmp*$^{fl/fl}$ littermates and evaluated by Affymetrix gene expression profiling (n=2 per genotype). However, only 21 genes were differentially expressed in conditional knockout mammary epithelial cells relative to littermate controls using a 2-fold enrichment cutoff. Upon closer inspection, the most down-regulated genes appear tightly related to mammary epithelial cell differentiation, and include *Glycam-1* (41-fold) and Casein genes *Csn1s1* (7-fold), *Csn2* (5-fold) and *Csn1s2b* (2-fold) (Dowbenko et al., 1993; Hou et al., 2000; Yamaji et al., 2013). As *MMTV-Cre*-expressing (line A) mice have reported defects in mammary epithelial cell differentiation (Robinson and Hennighausen, 2011; Yuan et al., 2011), mammary epithelial cells were also harvested from *MMTV-Cre*$^{+/-}$ and wild-type littermates on the same FVB mouse background (n=2 per genotype) and the gene expression profile was evaluated. However, the transcriptome profiling failed to uncover significant changes in these genes, supporting a potential positive role for MT1-MMP in promoting mammary epithelial cell differentiation. Parallel studies will also be performed for epithelial cells harvested from *MMTV-Cre*$^{+/-}$*Mt2-mmp*$^{fl/fl}$ mice. More importantly, future studies will examine the roles of MT1-MMP and MT2-MMP in pregnancy, lactation and involution. Indeed, preliminary studies indicate the MT1-MMP is most highly expressed in involuting mammary glands, a developmental program wherein the ECM undergoes its most striking

remodeling. While the reported defects in lactation in *MMTV-Cre* (line A) mice preclude the use of this model for such studies, future studies to uncover roles for MT1-MMP in pregnancy, lactation and involution will employ a combination of transplant approaches and conditional targeting with transgenic mice expressing Cre recombinase from the *Beta-lactoglobulin* (*Blg*) promoter, which allow efficient targeting of floxed alleles during all stages of pregnancy, lactation, and involution (Naylor et al., 2005). Mice bearing transplanted epithelial ducts from *Mt1-mmp*$^{-/-}$ mice can also be bred to evaluate the roles of epithelial cell-derived MT1-MMP during pregnancy (Miyoshi et al., 2001; Zhang et al., 2011).

Interestingly the unaltered viability of *Mt2-mmp*$^{-/-}$ mice, efforts to mate *Mt2-mmp*$^{-/-}$ mice and address the roles of *Mt2-mmp* in the mammary gland during pregnancy, lactation and involution failed to generate offspring (n>10 females). Further, while *Mt2-mmp*$^{-/-}$ mammary glands showed unaltered branching programs at 4 weeks, whole mount assessments at 8 weeks revealed a delay in duct elongation (n=3 replicates). Since ovaries are key regulators of mammary gland morphogenesis and reproduction, the ovaries of *Mt2-mmp*$^{lacZ/+}$, *Mt2-mmp*$^{-/-}$ and wild-type littermates were assessed. LacZ staining of ovaries harvested from 4 week-old mice reveal marked staining of *Mt2-mmp,* in the secondary follicles (composed of an inner-lying oocyte and several layers of circumscribing granulosa cells) as well as in the surrounding stromal (thecal) cells. Unexpectedly, while adult wild-type mice harbor ovaries with numerous secondary follicles at 8 weeks, serial sections through *Mt2-mmp*$^{-/-}$ ovaries revealed degenerated structures that lacked distinct follicles even at earlier time-points (postnatal day 10). As ovarian follicles are surrounded by a patent basement membrane that undergoes pericellular remodeling during ovulation, this system offers an alternate model to investigate roles for MT-MMP-dependent pericellular ECM remodeling in tissue morphogenesis. Importantly, as the observed defect in ovarian development

precludes assessments of *Mt2-mmp*$^{-/-}$ mammary glands during pregnancy, lactation, and involution, similar conditional targeting and transplant approaches will be employed.

Finally, while deletion of *Mt1-mmp* and *Mt2-mmp* in the mammary epithelial cells with *MMTV-Cre* fails to block postnatal branching morphogenesis, MT1-MMP and MT2-MMP may still modulate mammary gland development from different cellular compartments (i.e., stromal and epithelial, or vice versa). Consistent with the notion that MT1-MMP and MT2-MMP collaborate in the developing embryo to orchestrate tissue morphogenesis, *Mt1-mmp*$^{-/-}$*Mt2-mmp*$^{-/-}$ mice die in utero ~ E10.5 (unpublished observation) (Szabova et al., 2010). Szabova et al argue that this lethality results from defects in placental development and the establishment of the extraembryonic tissues required for nutrient exchange with the maternal blood supply (Szabova et al., 2005). However, preliminary attempts to generate conditional knockout mice with the *Meox2-Cre* knock-in line, which drives Cre expression exclusively in the embryo proper (epiblast) by E7.5 while sparing extraembryonic tissues (Tallquist and Soriano, 2000), have failed to generate dual-targeted *Meox2-Cre*$^{+/-}$*Mt1-mmp*$^{fl/fl}$*Mt2-mmp*$^{fl/fl}$ offspring (P0/ birth, n=4 litters). Further work will explore the stage and cause of this lethality, as it would provide the first example of an MMP requirement during embryonic development in either vertebrate or invertebrate model systems.

To date, most of our efforts to determine the *in vivo* role of MT-MMPs in branching morphogenesis have focused on the mammary gland. Nevertheless, both *Mt1-mmp* and *Mt2-mmp* are expressed in the developing vasculature. However, preliminary studies indicate the *in vivo* targeting of endothelial cell *Mt1-mmp* alone, or *Mt1-mmp* and *Mt2-mmp* in combination with Tie2-Cre (Landskroner-Eiger et al., 2015) fails to abrogate blood vessel development or the angiogenesis that coincides with postnatal mammary gland branching. Importantly, as in the case of embryonic and early postnatal mammary gland development, the vascular bed is assembled

early in embryogenesis and has already formed a highly ramified network of blood vessels by birth (Carmeliet and Jain, 2011). As such, the initial sprouting angiogenesis that contributes to organ growth during early postnatal development occurs through an environment with low interstitial ECM (Carver et al., 1993; Mays et al., 1988). Given the marked angiogenesis that take place during pregnancy in both the postnatal mammary gland and the developing extraembryonic tissue (Betterman et al., 2012; Chaiworapongsa et al., 2014; Chen and Zheng, 2014), ongoing studies will assess conditionally targeted mice as these stages. Further, it remains unclear whether similar rules apply in the vasculature as in the developing mammary gland, i.e., whether endothelial cells are working alone or together with the surrounding mural cells for branching morphogenesis. As such, *Mt1-mmp* and *Mt2-mmp* will be targeted in endothelial cells alone, in mural cells alone, or in both populations in combination.

In sum, we have identified new and important roles for MT1-MMP and MT2-MMP in the distinct morphogenetic programs that apply to both mammary gland development and angiogenesis. In the mammary gland, MT1-MMP-dependent periductal remodeling of type I collagen networks, presumably by stromal fibroblasts, regulates postnatal branching, while both MT1-MMP and MT2-MMP control adipocyte differentiation programs and function. In our analyses of vascular branching morphogenesis programs, we again identify a key role for MT1-MMP in pericellular matrix remodeling, but in this case, we focused our attention on a new axis that links ECM proteolysis to the control of nuclear architecture and function. Together, these studies should encourage efforts to characterize the impact of mammary gland remodeling on LINC complex-dependent transcriptional activity and conversely, the role of endothelial versus mural cell MT-MMPs on angiogenic responses *in vivo.*

BIBLIOGRAPHY

Abraham, R., Schafer, J., Rothe, M., Bange, J., Knyazev, P. and Ullrich, A. (2005). Identification of MMP-15 as an anti-apoptotic factor in cancer cells. *J Biol Chem* **280**, 34123-34132.

Abrahamson, D. R. and Perry, E. W. (1986). Evidence for splicing new basement membrane into old during glomerular development in newborn rat kidneys. *J Cell Biol* **103**, 2489-2498.

Adam, S. A., Sterne-Marr, R. and Gerace, L. (1992). Nuclear protein import using digitonin-permeabilized cells. *Methods Enzymol* **219**, 97-110.

Adams, R. H. and Alitalo, K. (2007). Molecular regulation of angiogenesis and lymphangiogenesis. *Nature reviews* **8**, 464-478.

Affolter, M. and Caussinus, E. (2008). Tracheal branching morphogenesis in Drosophila: new insights into cell behaviour and organ architecture. *Development* **135**, 2055-2064.

Affolter, M., Zeller, R. and Caussinus, E. (2009). Tissue remodelling through branching morphogenesis. *Nat Rev Mol Cell Biol* **10**, 831-842.

Ager, E. I., Kozin, S. V., Kirkpatrick, N. D., Seano, G., Kodack, D. P., Askoxylakis, V., Huang, Y., Goel, S., Snuderl, M., Muzikansky, A., et al. (2015). Blockade of MMP14 activity in murine breast carcinomas: implications for macrophages, vessels, and radiotherapy. *J Natl Cancer Inst* **107**.

Ahmad, M., Attoub, S., Singh, M. N., Martin, F. L. and El-Agnaf, O. M. (2007). Gamma-synuclein and the progression of cancer. *FASEB J* **21**, 3419-3430.

Albrengues, J., Bourget, I., Pons, C., Butet, V., Hofman, P., Tartare-Deckert, S., Feral, C. C., Meneguzzi, G. and Gaggioli, C. (2014). LIF mediates proinvasive activation of stromal fibroblasts in cancer. *Cell Rep* **7**, 1664-1678.

Alcaraz, J., Mori, H., Ghajar, C. M., Brownfield, D., Galgoczy, R. and Bissell, M. J. (2011). Collective epithelial cell invasion overcomes mechanical barriers of collagenous extracellular matrix by a narrow tube-like geometry and MMP14-dependent local softening. *Integr Biol (Camb)* **3**, 1153-1166.

Andrew, D. J. and Ewald, A. J. (2010). Morphogenesis of epithelial tubes: Insights into tube formation, elongation, and elaboration. *Dev Biol* **341**, 34-55.

Arimoto, K., Burkart, C., Yan, M., Ran, D., Weng, S. and Zhang, D. E. (2014). Plakophilin-2 promotes tumor development by enhancing ligand-dependent and -independent epidermal growth factor receptor dimerization and activation. *Mol Cell Biol* **34**, 3843-3854.

Arpino, V., Brock, M. and Gill, S. E. (2015). The role of TIMPs in regulation of extracellular matrix proteolysis. *Matrix Biol* **44-46**, 247-254.

Atkinson, J. J., Holmbeck, K., Yamada, S., Birkedal-Hansen, H., Parks, W. C. and Senior, R. M. (2005). Membrane-type 1 matrix metalloproteinase is required for normal alveolar development. *Dev Dyn* **232**, 1079-1090.

Baker, B. M. and Chen, C. S. (2012). Deconstructing the third dimension: how 3D culture microenvironments alter cellular cues. *Journal of cell science* **125**, 3015-3024.

Baker, M., Robinson, S. D., Lechertier, T., Barber, P. R., Tavora, B., D'Amico, G., Jones, D. T., Vojnovic, B. and Hodivala-Dilke, K. (2012). Use of the mouse aortic ring assay to study angiogenesis. *Nat Protoc* **7**, 89-104.

Barbolina, M. V. and Stack, M. S. (2008). Membrane type 1-matrix metalloproteinase: substrate diversity in pericellular proteolysis. *Semin Cell Dev Biol* **19**, 24-33.

Bateman, J. F., Boot-Handford, R. P. and Lamande, S. R. (2009). Genetic diseases of connective tissues: cellular and extracellular effects of ECM mutations. *Nature reviews* **10**, 173-183.

Ben-Ze'ev, A., Farmer, S. R. and Penman, S. (1980). Protein synthesis requires cell-surface contact while nuclear events respond to cell shape in anchorage-dependent fibroblasts. *Cell* **21**, 365-372.

Betterman, K. L., Paquet-Fifield, S., Asselin-Labat, M. L., Visvader, J. E., Butler, L. M., Stacker, S. A., Achen, M. G. and Harvey, N. L. (2012). Remodeling of the lymphatic vasculature during mouse mammary gland morphogenesis is mediated via epithelial-derived lymphangiogenic stimuli. *Am J Pathol* **181**, 2225-2238.

Black, R. A., Rauch, C. T., Kozlosky, C. J., Peschon, J. J., Slack, J. L., Wolfson, M. F., Castner, B. J., Stocking, K. L., Reddy, P., Srinivasan, S., et al. (1997). A metalloproteinase disintegrin that releases tumour-necrosis factor-alpha from cells. *Nature* **385**, 729-733.

Bond, N. D., Nelliot, A., Bernardo, M. K., Ayerh, M. A., Gorski, K. A., Hoshizaki, D. K. and Woodard, C. T. (2011). ssFTZ-F1 and Matrix metalloproteinase 2 are required for fat-body remodeling in Drosophila. *Dev Biol* **360**, 286-296.

Bonnans, C., Chou, J. and Werb, Z. (2014). Remodelling the extracellular matrix in development and disease. *Nat Rev Mol Cell Biol* **15**, 786-801.

Brisken, C. and O'Malley, B. (2010). Hormone action in the mammary gland. *Cold Spring Harb Perspect Biol* **2**, a003178.

Brosig, M., Ferralli, J., Gelman, L., Chiquet, M. and Chiquet-Ehrismann, R. (2010). Interfering with the connection between the nucleus and the cytoskeleton affects nuclear rotation, mechanotransduction and myogenesis. *Int J Biochem Cell Biol* **42**, 1717-1728.

Brownfield, D. G., Venugopalan, G., Lo, A., Mori, H., Tanner, K., Fletcher, D. A. and Bissell, M. J. (2013). Patterned collagen fibers orient branching mammary epithelium through distinct signaling modules. *Curr Biol* **23**, 703-709.

Burke, B. and Stewart, C. L. (2006). The laminopathies: the functional architecture of the nucleus and its contribution to disease. *Annu Rev Genomics Hum Genet* **7**, 369-405.

Carmeliet, P. and Jain, R. K. (2011). Molecular mechanisms and clinical applications of angiogenesis. *Nature* **473**, 298-307.

Carver, W., Terracio, L. and Borg, T. K. (1993). Expression and accumulation of interstitial collagen in the neonatal rat heart. *Anat Rec* **236**, 511-520.

Chaiworapongsa, T., Chaemsaithong, P., Yeo, L. and Romero, R. (2014). Pre-eclampsia part 1: current understanding of its pathophysiology. *Nat Rev Nephrol* **10**, 466-480.

Chang, W., Worman, H. J. and Gundersen, G. G. (2015). Accessorizing and anchoring the LINC complex for multifunctionality. *J Cell Biol* **208**, 11-22.

Chen, C. S., Mrksich, M., Huang, S., Whitesides, G. M. and Ingber, D. E. (1997). Geometric control of cell life and death. *Science (New York, N.Y* **276**, 1425-1428.

Chen, D. B. and Zheng, J. (2014). Regulation of placental angiogenesis. *Microcirculation* **21**, 15-25.

Chun, T. H., Hotary, K. B., Sabeh, F., Saltiel, A. R., Allen, E. D. and Weiss, S. J. (2006). A pericellular collagenase directs the 3-dimensional development of white adipose tissue. *Cell* **125**, 577-591.

Chun, T. H., Sabeh, F., Ota, I., Murphy, H., McDonagh, K. T., Holmbeck, K., Birkedal-Hansen, H., Allen, E. D. and Weiss, S. J. (2004). MT1-MMP-dependent neovessel

formation within the confines of the three-dimensional extracellular matrix. *J Cell Biol* **167**, 757-767.

Cohen, P., Levy, J. D., Zhang, Y., Frontini, A., Kolodin, D. P., Svensson, K. J., Lo, J. C., Zeng, X., Ye, L., Khandekar, M. J., et al. (2014). Ablation of PRDM16 and beige adipose causes metabolic dysfunction and a subcutaneous to visceral fat switch. *Cell* **156**, 304-316.

Cohen, T. V., Kosti, O. and Stewart, C. L. (2007). The nuclear envelope protein MAN1 regulates TGFbeta signaling and vasculogenesis in the embryonic yolk sac. *Development* **134**, 1385-1395.

Columbaro, M., Capanni, C., Mattioli, E., Novelli, G., Parnaik, V. K., Squarzoni, S., Maraldi, N. M. and Lattanzi, G. (2005). Rescue of heterochromatin organization in Hutchinson-Gilford progeria by drug treatment. *Cell Mol Life Sci* **62**, 2669-2678.

Correia, A. L., Mori, H., Chen, E. I., Schmitt, F. C. and Bissell, M. J. (2013). The hemopexin domain of MMP3 is responsible for mammary epithelial invasion and morphogenesis through extracellular interaction with HSP90beta. *Genes Dev* **27**, 805-817.

Crisp, M. and Burke, B. (2008). The nuclear envelope as an integrator of nuclear and cytoplasmic architecture. *FEBS letters* **582**, 2023-2032.

Crisp, M., Liu, Q., Roux, K., Rattner, J. B., Shanahan, C., Burke, B., Stahl, P. D. and Hodzic, D. (2006). Coupling of the nucleus and cytoplasm: role of the LINC complex. *J Cell Biol* **172**, 41-53.

Csoka, A. B., English, S. B., Simkevich, C. P., Ginzinger, D. G., Butte, A. J., Schatten, G. P., Rothman, F. G. and Sedivy, J. M. (2004). Genome-scale expression profiling of Hutchinson-Gilford progeria syndrome reveals widespread transcriptional misregulation leading to mesodermal/mesenchymal defects and accelerated atherosclerosis. *Aging cell* **3**, 235-243.

Dahl, K. N., Ribeiro, A. J. and Lammerding, J. (2008). Nuclear shape, mechanics, and mechanotransduction. *Circulation research* **102**, 1307-1318.

Davidson, P. M. and Lammerding, J. (2014). Broken nuclei--lamins, nuclear mechanics, and disease. *Trends Cell Biol* **24**, 247-256.

Dechat, T., Pfleghaar, K., Sengupta, K., Shimi, T., Shumaker, D. K., Solimando, L. and Goldman, R. D. (2008). Nuclear lamins: major factors in the structural organization and function of the nucleus and chromatin. *Genes Dev* **22**, 832-853.

Deng, L., Zhou, J. F., Sellers, R. S., Li, J. F., Nguyen, A. V., Wang, Y., Orlofsky, A., Liu, Q., Hume, D. A., Pollard, J. W., et al. (2010). A novel mouse model of inflammatory bowel disease links mammalian target of rapamycin-dependent hyperproliferation of colonic epithelium to inflammation-associated tumorigenesis. *Am J Pathol* **176**, 952-967.

Discher, D. E., Janmey, P. and Wang, Y. L. (2005). Tissue cells feel and respond to the stiffness of their substrate. *Science (New York, N.Y* **310**, 1139-1143.

Dowbenko, D., Kikuta, A., Fennie, C., Gillett, N. and Lasky, L. A. (1993). Glycosylation-dependent cell adhesion molecule 1 (GlyCAM 1) mucin is expressed by lactating mammary gland epithelial cells and is present in milk. *J Clin Invest* **92**, 952-960.

Durnberger, H. and Kratochwil, K. (1980). Specificity of tissue interaction and origin of mesenchymal cells in the androgen response of the embryonic mammary gland. *Cell* **19**, 465-471.

Edgar, R., Domrachev, M. and Lash, A. E. (2002). Gene Expression Omnibus: NCBI gene expression and hybridization array data repository. *Nucleic Acids Res* **30**, 207-210.

Ehrbar, M., Rizzi, S. C., Schoenmakers, R. G., Miguel, B. S., Hubbell, J. A., Weber, F. E. and Lutolf, M. P. (2007). Biomolecular hydrogels formed and degraded via site-specific enzymatic reactions. *Biomacromolecules* **8**, 3000-3007.

Engler, A. J., Sen, S., Sweeney, H. L. and Discher, D. E. (2006). Matrix elasticity directs stem cell lineage specification. *Cell* **126**, 677-689.

Eshkar-Oren, I., Viukov, S. V., Salameh, S., Krief, S., Oh, C. D., Akiyama, H., Gerber, H. P., Ferrara, N. and Zelzer, E. (2009). The forming limb skeleton serves as a signaling center for limb vasculature patterning via regulation of Vegf. *Development* **136**, 1263-1272.

Ewald, A. J., Brenot, A., Duong, M., Chan, B. S. and Werb, Z. (2008). Collective epithelial migration and cell rearrangements drive mammary branching morphogenesis. *Developmental cell* **14**, 570-581.

Ewald, A. J., Huebner, R. J., Palsdottir, H., Lee, J. K., Perez, M. J., Jorgens, D. M., Tauscher, A. N., Cheung, K. J., Werb, Z. and Auer, M. (2012). Mammary collective cell migration involves transient loss of epithelial features and individual cell migration within the epithelium. *Journal of cell science* **125**, 2638-2654.

Fahlman, R. P., Chen, W. and Overall, C. M. (2014). Absolute proteomic quantification of the activity state of proteases and proteolytic cleavages using proteolytic signature peptides and isobaric tags. *J Proteomics* **100**, 79-91.

Fata, J. E., Chaudhary, V. and Khokha, R. (2001). Cellular turnover in the mammary gland is correlated with systemic levels of progesterone and not 17beta-estradiol during the estrous cycle. *Biol Reprod* **65**, 680-688.

Fata, J. E., Mori, H., Ewald, A. J., Zhang, H., Yao, E., Werb, Z. and Bissell, M. J. (2007). The MAPK(ERK-1,2) pathway integrates distinct and antagonistic signals from TGFalpha and FGF7 in morphogenesis of mouse mammary epithelium. *Dev Biol* **306**, 193-207.

Filippov, S., Koenig, G. C., Chun, T. H., Hotary, K. B., Ota, I., Bugge, T. H., Roberts, J. D., Fay, W. P., Birkedal-Hansen, H., Holmbeck, K., et al. (2005). MT1-matrix metalloproteinase directs arterial wall invasion and neointima formation by vascular smooth muscle cells. *J Exp Med* **202**, 663-671.

Finlan, L. E., Sproul, D., Thomson, I., Boyle, S., Kerr, E., Perry, P., Ylstra, B., Chubb, J. R. and Bickmore, W. A. (2008). Recruitment to the nuclear periphery can alter expression of genes in human cells. *PLoS genetics* **4**, e1000039.

Fu, H. L., Sohail, A., Valiathan, R. R., Wasinski, B. D., Kumarasiri, M., Mahasenan, K. V., Bernardo, M. M., Tokmina-Roszyk, D., Fields, G. B., Mobashery, S., et al. (2013). Shedding of discoidin domain receptor 1 by membrane-type matrix metalloproteinases. *J Biol Chem* **288**, 12114-12129.

Fulton, A. B. (1982). How crowded is the cytoplasm? *Cell* **30**, 345-347.

Gaggioli, C., Hooper, S., Hidalgo-Carcedo, C., Grosse, R., Marshall, J. F., Harrington, K. and Sahai, E. (2007). Fibroblast-led collective invasion of carcinoma cells with differing roles for RhoGTPases in leading and following cells. *Nat Cell Biol* **9**, 1392-1400.

George, E. L., Georges-Labouesse, E. N., Patel-King, R. S., Rayburn, H. and Hynes, R. O. (1993). Defects in mesoderm, neural tube and vascular development in mouse embryos lacking fibronectin. *Development* **119**, 1079-1091.

Glasheen, B. M., Robbins, R. M., Piette, C., Beitel, G. J. and Page-McCaw, A. (2010). A matrix metalloproteinase mediates airway remodeling in Drosophila. *Dev Biol* **344**, 772-783.

Glynn, M. W. and Glover, T. W. (2005). Incomplete processing of mutant lamin A in Hutchinson-Gilford progeria leads to nuclear abnormalities, which are reversed by farnesyltransferase inhibition. *Human molecular genetics* **14**, 2959-2969.

Goldman, R. D., Shumaker, D. K., Erdos, M. R., Eriksson, M., Goldman, A. E., Gordon, L. B., Gruenbaum, Y., Khuon, S., Mendez, M., Varga, R., et al. (2004). Accumulation of mutant lamin A causes progressive changes in nuclear architecture in Hutchinson-Gilford progeria syndrome. *Proceedings of the National Academy of Sciences of the United States of America* **101**, 8963-8968.

Gouon-Evans, V. and Pollard, J. W. (2002). Unexpected deposition of brown fat in mammary gland during postnatal development. *Mol Endocrinol* **16**, 2618-2627.

Gross, J. and Lapiere, C. M. (1962). Collagenolytic activity in amphibian tissues: a tissue culture assay. *Proceedings of the National Academy of Sciences of the United States of America* **48**, 1014-1022.

Gruenbaum, Y. and Foisner, R. (2015). Lamins: nuclear intermediate filament proteins with fundamental functions in nuclear mechanics and genome regulation. *Annu Rev Biochem* **84**, 131-164.

Guha, A., Lin, L. and Kornberg, T. B. (2009). Regulation of Drosophila matrix metalloprotease Mmp2 is essential for wing imaginal disc:trachea association and air sac tubulogenesis. *Dev Biol* **335**, 317-326.

Guo, C. L., Ouyang, M., Yu, J. Y., Maslov, J., Price, A. and Shen, C. Y. (2012). Long-range mechanical force enables self-assembly of epithelial tubular patterns. *Proc Natl Acad Sci U S A* **109**, 5576-5582.

Gupta, R. K., Mepani, R. J., Kleiner, S., Lo, J. C., Khandekar, M. J., Cohen, P., Frontini, A., Bhowmick, D. C., Ye, L., Cinti, S., et al. (2012). Zfp423 expression identifies committed preadipocytes and localizes to adipose endothelial and perivascular cells. *Cell Metab* **15**, 230-239.

Gutierrez-Fernandez, A., Soria-Valles, C., Osorio, F. G., Gutierrez-Abril, J., Garabaya, C., Aguirre, A., Fueyo, A., Fernandez-Garcia, M. S., Puente, X. S. and Lopez-Otin, C. (2015). Loss of MT1-MMP causes cell senescence and nuclear defects which can be reversed by retinoic acid. *EMBO J* **34**, 1875-1888.

Haberland, M., Montgomery, R. L. and Olson, E. N. (2009). The many roles of histone deacetylases in development and physiology: implications for disease and therapy. *Nature reviews* **10**, 32-42.

Hancock, R. (2004a). Internal organisation of the nucleus: assembly of compartments by macromolecular crowding and the nuclear matrix model. *Biol Cell* **96**, 595-601.

Hancock, R. (2004b). A role for macromolecular crowding effects in the assembly and function of compartments in the nucleus. *J Struct Biol* **146**, 281-290.

Hancock, R. and Hadj-Sahraoui, Y. (2009). Isolation of cell nuclei using inert macromolecules to mimic the crowded cytoplasm. *PLoS One* **4**, e7560.

Harunaga, J. S., Doyle, A. D. and Yamada, K. M. (2014). Local and global dynamics of the basement membrane during branching morphogenesis require protease activity and actomyosin contractility. *Dev Biol* **394**, 197-205.

Haslam, S. Z., Drolet, A., Smith, K., Tan, M. and Aupperlee, M. (2008). Progestin-regulated luminal cell and myoepithelial cell-specific responses in mammary organoid culture. *Endocrinology* **149**, 2098-2107.

Hawryluk-Gara, L. A., Shibuya, E. K. and Wozniak, R. W. (2005). Vertebrate Nup53 interacts with the nuclear lamina and is required for the assembly of a Nup93-containing complex. *Molecular biology of the cell* **16**, 2382-2394.

Hendrix, M. J., Seftor, E. A., Hess, A. R. and Seftor, R. E. (2003). Vasculogenic mimicry and tumour-cell plasticity: lessons from melanoma. *Nat Rev Cancer* **3**, 411-421.

Hennighausen, L. and Robinson, G. W. (2001). Signaling pathways in mammary gland development. *Developmental cell* **1**, 467-475.

Hens, J., Dann, P., Hiremath, M., Pan, T. C., Chodosh, L. and Wysolmerski, J. (2009). Analysis of gene expression in PTHrP-/- mammary buds supports a role for BMP signaling and MMP2 in the initiation of ductal morphogenesis. *Dev Dyn* **238**, 2713-2724.

Hinck, L. and Silberstein, G. B. (2005). Key stages in mammary gland development: the mammary end bud as a motile organ. *Breast Cancer Res* **7**, 245-251.

Hiraoka, N., Allen, E., Apel, I. J., Gyetko, M. R. and Weiss, S. J. (1998). Matrix metalloproteinases regulate neovascularization by acting as pericellular fibrinolysins. *Cell* **95**, 365-377.

Hogg, N. A., Harrison, C. J. and Tickle, C. (1983). Lumen formation in the developing mouse mammary gland. *J Embryol Exp Morphol* **73**, 39-57.

Holaska, J. M. (2008). Emerin and the nuclear lamina in muscle and cardiac disease. *Circulation research* **103**, 16-23.

Holmbeck, K., Bianco, P., Caterina, J., Yamada, S., Kromer, M., Kuznetsov, S. A., Mankani, M., Robey, P. G., Poole, A. R., Pidoux, I., et al. (1999). MT1-MMP-deficient mice develop dwarfism, osteopenia, arthritis, and connective tissue disease due to inadequate collagen turnover. *Cell* **99**, 81-92.

Hotary, K., Allen, E., Punturieri, A., Yana, I. and Weiss, S. J. (2000). Regulation of cell invasion and morphogenesis in a three-dimensional type I collagen matrix by membrane-type matrix metalloproteinases 1, 2, and 3. *J Cell Biol* **149**, 1309-1323.

Hotary, K., Li, X. Y., Allen, E., Stevens, S. L. and Weiss, S. J. (2006). A cancer cell metalloprotease triad regulates the basement membrane transmigration program. *Genes Dev* **20**, 2673-2686.

Hotary, K. B., Allen, E. D., Brooks, P. C., Datta, N. S., Long, M. W. and Weiss, S. J. (2003). Membrane type I matrix metalloproteinase usurps tumor growth control imposed by the three-dimensional extracellular matrix. *Cell* **114**, 33-45.

Hou, Z., Bailey, J. P., Vomachka, A. J., Matsuda, M., Lockefeer, J. A. and Horseman, N. D. (2000). Glycosylation-dependent cell adhesion molecule 1 (GlyCAM 1) is induced by prolactin and suppressed by progesterone in mammary epithelium. *Endocrinology* **141**, 4278-4283.

Hovey, R. C. and Aimo, L. (2010). Diverse and active roles for adipocytes during mammary gland growth and function. *J Mammary Gland Biol Neoplasia* **15**, 279-290.

Howard, B. A. and Lu, P. (2014). Stromal regulation of embryonic and postnatal mammary epithelial development and differentiation. *Semin Cell Dev Biol* **25-26**, 43-51.

Hu, X., Juneja, S. C., Maihle, N. J. and Cleary, M. P. (2002). Leptin--a growth factor in normal and malignant breast cells and for normal mammary gland development. *J Natl Cancer Inst* **94**, 1704-1711.

Huang, S., Chen, C. S. and Ingber, D. E. (1998). Control of cyclin D1, p27(Kip1), and cell cycle progression in human capillary endothelial cells by cell shape and cytoskeletal tension. *Molecular biology of the cell* **9**, 3179-3193.

Huebner, R. J. and Ewald, A. J. (2014). Cellular foundations of mammary tubulogenesis. *Semin Cell Dev Biol* **31**, 124-131.

Inman, J. L., Robertson, C., Mott, J. D. and Bissell, M. J. (2015). Mammary gland development: cell fate specification, stem cells and the microenvironment. *Development* **142**, 1028-1042.

Irizarry, R. A., Hobbs, B., Collin, F., Beazer-Barclay, Y. D., Antonellis, K. J., Scherf, U. and Speed, T. P. (2003). Exploration, normalization, and summaries of high density oligonucleotide array probe level data. *Biostatistics* **4**, 249-264.

Itoh, T., Ikeda, T., Gomi, H., Nakao, S., Suzuki, T. and Itohara, S. (1997). Unaltered secretion of beta-amyloid precursor protein in gelatinase A (matrix metalloproteinase 2)-deficient mice. *J Biol Chem* **272**, 22389-22392.

Itoh, Y. (2015). Membrane-type matrix metalloproteinases: Their functions and regulation. *Matrix Biol* **44-46**, 207-223.

Jackson-Fisher, A. J., Bellinger, G., Ramabhadran, R., Morris, J. K., Lee, K. F. and Stern, D. F. (2004). ErbB2 is required for ductal morphogenesis of the mammary gland. *Proceedings of the National Academy of Sciences of the United States of America* **101**, 17138-17143.

Jia, Q., Liu, Y., Liu, H. and Li, S. (2014). Mmp1 and Mmp2 cooperatively induce Drosophila fat body cell dissociation with distinct roles. *Sci Rep* **4**, 7535.

Kajita, M., Itoh, Y., Chiba, T., Mori, H., Okada, A., Kinoh, H. and Seiki, M. (2001). Membrane-type 1 matrix metalloproteinase cleaves CD44 and promotes cell migration. *J Cell Biol* **153**, 893-904.

Keely, P. J., Wu, J. E. and Santoro, S. A. (1995). The spatial and temporal expression of the alpha 2 beta 1 integrin and its ligands, collagen I, collagen IV, and laminin, suggest important roles in mouse mammary morphogenesis. *Differentiation* **59**, 1-13.

Kelleher, C. M., McLean, S. E. and Mecham, R. P. (2004). Vascular extracellular matrix and aortic development. *Curr Top Dev Biol* **62**, 153-188.

Kessenbrock, K., Dijkgraaf, G. J., Lawson, D. A., Littlepage, L. E., Shahi, P., Pieper, U. and Werb, Z. (2013). A role for matrix metalloproteinases in regulating mammary stem cell function via the Wnt signaling pathway. *Cell Stem Cell* **13**, 300-313.

Khabibullin, D., Medvetz, D. A., Pinilla, M., Hariharan, V., Li, C., Hergrueter, A., Laucho Contreras, M., Zhang, E., Parkhitko, A., Yu, J. J., et al. (2014). Folliculin regulates cell-cell adhesion, AMPK, and mTORC1 in a cell-type-specific manner in lung-derived cells. *Physiol Rep* **2**, e12107.

Khokha, R. and Werb, Z. (2011). Mammary gland reprogramming: metalloproteinases couple form with function. *Cold Spring Harb Perspect Biol* **3**.

Knauper, V., Will, H., Lopez-Otin, C., Smith, B., Atkinson, S. J., Stanton, H., Hembry, R. M. and Murphy, G. (1996). Cellular mechanisms for human procollagenase-3 (MMP-13) activation. Evidence that MT1-MMP (MMP-14) and gelatinase a (MMP-2) are able to generate active enzyme. *The Journal of biological chemistry* **271**, 17124-17131.

Koshikawa, N., Giannelli, G., Cirulli, V., Miyazaki, K. and Quaranta, V. (2000). Role of cell surface metalloprotease MT1-MMP in epithelial cell migration over laminin-5. *J Cell Biol* **148**, 615-624.

Koziol, A., Gonzalo, P., Mota, A., Pollan, A., Lorenzo, C., Colome, N., Montaner, D., Dopazo, J., Arribas, J., Canals, F., et al. (2012). The protease MT1-MMP drives a combinatorial proteolytic program in activated endothelial cells. *FASEB J* **26**, 4481-4494.

Kurley, S. J., Bierie, B., Carnahan, R. H., Lobdell, N. A., Davis, M. A., Hofmann, I., Moses, H. L., Muller, W. J. and Reynolds, A. B. (2012). p120-catenin is essential for terminal end bud function and mammary morphogenesis. *Development* **139**, 1754-1764.

Landskroner-Eiger, S., Qiu, C., Perrotta, P., Siragusa, M., Lee, M. Y., Ulrich, V., Luciano, A. K., Zhuang, Z. W., Corti, F., Simons, M., et al. (2015). Endothelial miR-17 approximately 92 cluster negatively regulates arteriogenesis via miRNA-19 repression of WNT signaling. *Proceedings of the National Academy of Sciences of the United States of America* **112**, 12812-12817.

Lebreton, G. and Casanova, J. (2014). Specification of leading and trailing cell features during collective migration in the Drosophila trachea. *Journal of cell science* **127**, 465-474.

Li, X. Y., Ota, I., Yana, I., Sabeh, F. and Weiss, S. J. (2008). Molecular dissection of the structural machinery underlying the tissue-invasive activity of membrane type-1 matrix metalloproteinase. *Molecular biology of the cell* **19**, 3221-3233.

Li, Y., Foss, C. A., Summerfield, D. D., Doyle, J. J., Torok, C. M., Dietz, H. C., Pomper, M. G. and Yu, S. M. (2012). Targeting collagen strands by photo-triggered triple-helix hybridization. *Proc Natl Acad Sci U S A* **109**, 14767-14772.

Liu, F. and Tschumperlin, D. J. (2011). Micro-mechanical characterization of lung tissue using atomic force microscopy. *J Vis Exp*.

Liu, X., Wu, H., Byrne, M., Jeffrey, J., Krane, S. and Jaenisch, R. (1995). A targeted mutation at the known collagenase cleavage site in mouse type I collagen impairs tissue remodeling. *J Cell Biol* **130**, 227-237.

Lo, A. T., Mori, H., Mott, J. and Bissell, M. J. (2012). Constructing three-dimensional models to study mammary gland branching morphogenesis and functional differentiation. *J Mammary Gland Biol Neoplasia* **17**, 103-110.

Lochter, A., Galosy, S., Muschler, J., Freedman, N., Werb, Z. and Bissell, M. J. (1997). Matrix metalloproteinase stromelysin-1 triggers a cascade of molecular alterations that leads to stable epithelial-to-mesenchymal conversion and a premalignant phenotype in mammary epithelial cells. *J Cell Biol* **139**, 1861-1872.

Lohler, J., Timpl, R. and Jaenisch, R. (1984). Embryonic lethal mutation in mouse collagen I gene causes rupture of blood vessels and is associated with erythropoietic and mesenchymal cell death. *Cell* **38**, 597-607.

Londhe, V. A., Maisonet, T. M., Lopez, B., Shin, B. C., Huynh, J. and Devaskar, S. U. (2013). Retinoic acid rescues alveolar hypoplasia in the calorie-restricted developing rat lung. *Am J Respir Cell Mol Biol* **48**, 179-187.

Loo, C. S., Chen, C. W., Wang, P. J., Chen, P. Y., Lin, S. Y., Khoo, K. H., Fenton, R. A., Knepper, M. A. and Yu, M. J. (2013). Quantitative apical membrane proteomics reveals vasopressin-induced actin dynamics in collecting duct cells. *Proc Natl Acad Sci U S A* **110**, 17119-17124.

Lu, P., Ewald, A. J., Martin, G. R. and Werb, Z. (2008). Genetic mosaic analysis reveals FGF receptor 2 function in terminal end buds during mammary gland branching morphogenesis. *Dev Biol* **321**, 77-87.

Malhas, A., Lee, C. F., Sanders, R., Saunders, N. J. and Vaux, D. J. (2007). Defects in lamin B1 expression or processing affect interphase chromosome position and gene expression. *J Cell Biol* **176**, 593-603.

Marsili, A., Aguayo-Mazzucato, C., Chen, T., Kumar, A., Chung, M., Lunsford, E. P., Harney, J. W., Van-Tran, T., Gianetti, E., Ramadan, W., et al. (2011). Mice with a

targeted deletion of the type 2 deiodinase are insulin resistant and susceptible to diet induced obesity. *PLoS One* **6**, e20832.

Master, S. R., Hartman, J. L., D'Cruz, C. M., Moody, S. E., Keiper, E. A., Ha, S. I., Cox, J. D., Belka, G. K. and Chodosh, L. A. (2002). Functional microarray analysis of mammary organogenesis reveals a developmental role in adaptive thermogenesis. *Mol Endocrinol* **16**, 1185-1203.

Mays, P. K., Bishop, J. E. and Laurent, G. J. (1988). Age-related changes in the proportion of types I and III collagen. *Mech Ageing Dev* **45**, 203-212.

McBeath, R., Pirone, D. M., Nelson, C. M., Bhadriraju, K. and Chen, C. S. (2004). Cell shape, cytoskeletal tension, and RhoA regulate stem cell lineage commitment. *Developmental cell* **6**, 483-495.

McDonald, M. E., Li, C., Bian, H., Smith, B. D., Layne, M. D. and Farmer, S. R. (2015). Myocardin-related transcription factor A regulates conversion of progenitors to beige adipocytes. *Cell* **160**, 105-118.

Meaburn, K. J., Cabuy, E., Bonne, G., Levy, N., Morris, G. E., Novelli, G., Kill, I. R. and Bridger, J. M. (2007). Primary laminopathy fibroblasts display altered genome organization and apoptosis. *Aging cell* **6**, 139-153.

Minton, A. P. (2001). The influence of macromolecular crowding and macromolecular confinement on biochemical reactions in physiological media. *The Journal of biological chemistry* **276**, 10577-10580.

Miyoshi, K., Shillingford, J. M., Smith, G. H., Grimm, S. L., Wagner, K. U., Oka, T., Rosen, J. M., Robinson, G. W. and Hennighausen, L. (2001). Signal transducer and activator of transcription (Stat) 5 controls the proliferation and differentiation of mammary alveolar epithelium. *J Cell Biol* **155**, 531-542.

Mori, H., Gjorevski, N., Inman, J. L., Bissell, M. J. and Nelson, C. M. (2009). Self-organization of engineered epithelial tubules by differential cellular motility. *Proc Natl Acad Sci U S A* **106**, 14890-14895.

Mori, H., Lo, A. T., Inman, J. L., Alcaraz, J., Ghajar, C. M., Mott, J. D., Nelson, C. M., Chen, C. S., Zhang, H., Bascom, J. L., et al. (2013). Transmembrane/cytoplasmic, rather than catalytic, domains of Mmp14 signal to MAPK activation and mammary branching morphogenesis via binding to integrin beta1. *Development* **140**, 343-352.

Mounkes, L. C., Kozlov, S., Hernandez, L., Sullivan, T. and Stewart, C. L. (2003). A progeroid syndrome in mice is caused by defects in A-type lamins. *Nature* **423**, 298-301.

Mulholland, N. M., Soeth, E. and Smith, C. L. (2003). Inhibition of MMTV transcription by HDAC inhibitors occurs independent of changes in chromatin remodeling and increased histone acetylation. *Oncogene* **22**, 4807-4818.

Naylor, M. J., Li, N., Cheung, J., Lowe, E. T., Lambert, E., Marlow, R., Wang, P., Schatzmann, F., Wintermantel, T., Schuetz, G., et al. (2005). Ablation of beta1 integrin in mammary epithelium reveals a key role for integrin in glandular morphogenesis and differentiation. *J Cell Biol* **171**, 717-728.

Nelson, D. A. and Larsen, M. (2015). Heterotypic control of basement membrane dynamics during branching morphogenesis. *Dev Biol* **401**, 103-109.

Nguyen-Ngoc, K. V., Cheung, K. J., Brenot, A., Shamir, E. R., Gray, R. S., Hines, W. C., Yaswen, P., Werb, Z. and Ewald, A. J. (2012). ECM microenvironment regulates collective migration and local dissemination in normal and malignant mammary epithelium. *Proc Natl Acad Sci U S A* **109**, E2595-2604.

Niederreither, K., D'Souza, R., Metsaranta, M., Eberspaecher, H., Toman, P. D., Vuorio, E. and De Crombrugghe, B. (1995). Coordinate patterns of expression of type I and III collagens during mouse development. *Matrix Biol* **14**, 705-713.

Nielsen, B. S., Egeblad, M., Rank, F., Askautrud, H. A., Pennington, C. J., Pedersen, T. X., Christensen, I. J., Edwards, D. R., Werb, Z. and Lund, L. R. (2008). Matrix metalloproteinase 13 is induced in fibroblasts in polyomavirus middle T antigen-driven mammary carcinoma without influencing tumor progression. *PLoS One* **3**, e2959.

Oblander, S. A., Zhou, Z., Galvez, B. G., Starcher, B., Shannon, J. M., Durbeej, M., Arroyo, A. G., Tryggvason, K. and Apte, S. S. (2005). Distinctive functions of membrane type 1 matrix-metalloprotease (MT1-MMP or MMP-14) in lung and submandibular gland development are independent of its role in pro-MMP-2 activation. *Dev Biol* **277**, 255-269.

Ochoa-Espinosa, A. and Affolter, M. (2012). Branching morphogenesis: from cells to organs and back. *Cold Spring Harb Perspect Biol* **4**.

Oh, J., Takahashi, R., Adachi, E., Kondo, S., Kuratomi, S., Noma, A., Alexander, D. B., Motoda, H., Okada, A., Seiki, M., et al. (2004). Mutations in two matrix metalloproteinase genes, MMP-2 and MT1-MMP, are synthetic lethal in mice. *Oncogene* **23**, 5041-5048.

Ohtake, Y., Tojo, H. and Seiki, M. (2006). Multifunctional roles of MT1-MMP in myofiber formation and morphostatic maintenance of skeletal muscle. *Journal of cell science* **119**, 3822-3832.

Ota, I., Li, X. Y., Hu, Y. and Weiss, S. J. (2009). Induction of a MT1-MMP and MT2-MMP-dependent basement membrane transmigration program in cancer cells by Snail1. *Proc Natl Acad Sci U S A* **106**, 20318-20323.

Page-McCaw, A. (2008). Remodeling the model organism: matrix metalloproteinase functions in invertebrates. *Semin Cell Dev Biol* **19**, 14-23.

Page-McCaw, A., Ewald, A. J. and Werb, Z. (2007). Matrix metalloproteinases and the regulation of tissue remodelling. *Nature reviews* **8**, 221-233.

Page-McCaw, A., Serano, J., Sante, J. M. and Rubin, G. M. (2003). Drosophila matrix metalloproteinases are required for tissue remodeling, but not embryonic development. *Developmental cell* **4**, 95-106.

Paszek, M. J., Zahir, N., Johnson, K. R., Lakins, J. N., Rozenberg, G. I., Gefen, A., Reinhart-King, C. A., Margulies, S. S., Dembo, M., Boettiger, D., et al. (2005). Tensional homeostasis and the malignant phenotype. *Cancer cell* **8**, 241-254.

Paulsen, M. T., Veloso, A., Prasad, J., Bedi, K., Ljungman, E. A., Magnuson, B., Wilson, T. E. and Ljungman, M. (2014). Use of Bru-Seq and BruChase-Seq for genome-wide assessment of the synthesis and stability of RNA. *Methods* **67**, 45-54.

Paulsen, M. T., Veloso, A., Prasad, J., Bedi, K., Ljungman, E. A., Tsan, Y. C., Chang, C. W., Tarrier, B., Washburn, J. G., Lyons, R., et al. (2013). Coordinated regulation of synthesis and stability of RNA during the acute TNF-induced proinflammatory response. *Proceedings of the National Academy of Sciences of the United States of America* **110**, 2240-2245.

Pei, D. and Weiss, S. J. (1995). Furin-dependent intracellular activation of the human stromelysin-3 zymogen. *Nature* **375**, 244-247.

Pei, D. and Weiss, S. J. (1996). Transmembrane-deletion mutants of the membrane-type matrix metalloproteinase-1 process progelatinase A and express intrinsic matrix-degrading activity. *The Journal of biological chemistry* **271**, 9135-9140.

Pellizzoni, L., Charroux, B., Rappsilber, J., Mann, M. and Dreyfuss, G. (2001). A functional interaction between the survival motor neuron complex and RNA polymerase II. *J Cell Biol* **152**, 75-85.

Peschon, J. J., Slack, J. L., Reddy, P., Stocking, K. L., Sunnarborg, S. W., Lee, D. C., Russell, W. E., Castner, B. J., Johnson, R. S., Fitzner, J. N., et al. (1998). An essential role for ectodomain shedding in mammalian development. *Science (New York, N.Y* **282**, 1281-1284.

Pierreux, C. E., Cordi, S., Hick, A. C., Achouri, Y., Ruiz de Almodovar, C., Prevot, P. P., Courtoy, P. J., Carmeliet, P. and Lemaigre, F. P. (2010). Epithelial: Endothelial cross-talk regulates exocrine differentiation in developing pancreas. *Dev Biol* **347**, 216-227.

Pivot-Pajot, C., Caron, C., Govin, J., Vion, A., Rousseaux, S. and Khochbin, S. (2003). Acetylation-dependent chromatin reorganization by BRDT, a testis-specific bromodomain-containing protein. *Mol Cell Biol* **23**, 5354-5365.

Raeber, G. P., Lutolf, M. P. and Hubbell, J. A. (2007). Mechanisms of 3-D migration and matrix remodeling of fibroblasts within artificial ECMs. *Acta biomaterialia* **3**, 615-629.

Ramasamy, S. K., Kusumbe, A. P. and Adams, R. H. (2015). Regulation of tissue morphogenesis by endothelial cell-derived signals. *Trends Cell Biol* **25**, 148-157.

Rebustini, I. T. and Hoffman, M. P. (2009). ECM and FGF-dependent assay of embryonic SMG epithelial morphogenesis: investigating growth factor/matrix regulation of gene expression during submandibular gland development. *Methods Mol Biol* **522**, 319-330.

Rebustini, I. T., Myers, C., Lassiter, K. S., Surmak, A., Szabova, L., Holmbeck, K., Pedchenko, V., Hudson, B. G. and Hoffman, M. P. (2009). MT2-MMP-dependent release of collagen IV NC1 domains regulates submandibular gland branching morphogenesis. *Dev Cell* **17**, 482-493.

Riching, K. M., Cox, B. L., Salick, M. R., Pehlke, C., Riching, A. S., Ponik, S. M., Bass, B. R., Crone, W. C., Jiang, Y., Weaver, A. M., et al. (2014). 3D collagen alignment limits protrusions to enhance breast cancer cell persistence. *Biophys J* **107**, 2546-2558.

Riggins, K. S., Mernaugh, G., Su, Y., Quaranta, V., Koshikawa, N., Seiki, M., Pozzi, A. and Zent, R. (2010). MT1-MMP-mediated basement membrane remodeling modulates renal development. *Exp Cell Res* **316**, 2993-3005.

Robinson, G. W. (2007). Cooperation of signalling pathways in embryonic mammary gland development. *Nature reviews* **8**, 963-972.

Robinson, G. W., Accili, D. and Henninghausen, L. (2000). Rescue of Mammary Epithelium of Early Lethal Phenotypes by Embryonic Mammary Gland Transplantation as Exemplified with Insulin Receptor Null Mice. In *Methods in Mammary Gland Biology and Breast Cancer Research* (ed. M. M. Ip & B. B. Asch), pp. 307-316. New York, NY: Kluwer Academic/Plenum Publishers.

Robinson, G. W. and Hennighausen, L. (2011). MMTV-Cre transgenes can adversely affect lactation: considerations for conditional gene deletion in mammary tissue. *Anal Biochem* **412**, 92-95.

Rosania, G. R. and Swanson, J. A. (1995). Effects of macromolecular crowding on nuclear size. *Exp Cell Res* **218**, 114-122.

Rowe, R. G. and Weiss, S. J. (2008). Breaching the basement membrane: who, when and how? *Trends Cell Biol* **18**, 560-574.

Rowe, R. G. and Weiss, S. J. (2009). Navigating ECM barriers at the invasive front: the cancer cell-stroma interface. *Annu Rev Cell Dev Biol* **25**, 567-595.

Sabeh, F., Shimizu-Hirota, R. and Weiss, S. J. (2009). Protease-dependent versus -independent cancer cell invasion programs: three-dimensional amoeboid movement revisited. *J Cell Biol* **185**, 11-19.

Sakamoto, T., Weng, J. S., Hara, T., Yoshino, S., Kozuka-Hata, H., Oyama, M. and Seiki, M. (2014). Hypoxia-inducible factor 1 regulation through cross talk between mTOR and MT1-MMP. *Mol Cell Biol* **34**, 30-42.

Salpingidou, G., Smertenko, A., Hausmanowa-Petrucewicz, I., Hussey, P. J. and Hutchison, C. J. (2007). A novel role for the nuclear membrane protein emerin in association of the centrosome to the outer nuclear membrane. *J Cell Biol* **178**, 897-904.

Sanz, E., Yang, L., Su, T., Morris, D. R., McKnight, G. S. and Amieux, P. S. (2009). Cell-type-specific isolation of ribosome-associated mRNA from complex tissues. *Proceedings of the National Academy of Sciences of the United States of America* **106**, 13939-13944.

Sato, H., Takino, T., Okada, Y., Cao, J., Shinagawa, A., Yamamoto, E. and Seiki, M. (1994). A matrix metalloproteinase expressed on the surface of invasive tumour cells. *Nature* **370**, 61-65.

Saunders, W. B., Bohnsack, B. L., Faske, J. B., Anthis, N. J., Bayless, K. J., Hirschi, K. K. and Davis, G. E. (2006). Coregulation of vascular tube stabilization by endothelial cell TIMP-2 and pericyte TIMP-3. *J Cell Biol* **175**, 179-191.

Scarpa, E. and Mayor, R. (2016). Collective cell migration in development. *J Cell Biol* **212**, 143-155.

Seals, D. F. and Courtneidge, S. A. (2003). The ADAMs family of metalloproteases: multidomain proteins with multiple functions. *Genes Dev* **17**, 7-30.

Shimi, T., Pfleghaar, K., Kojima, S., Pack, C. G., Solovei, I., Goldman, A. E., Adam, S. A., Shumaker, D. K., Kinjo, M., Cremer, T., et al. (2008). The A- and B-type nuclear lamin networks: microdomains involved in chromatin organization and transcription. *Genes Dev* **22**, 3409-3421.

Shimizu-Hirota, R., Xiong, W., Baxter, B. T., Kunkel, S. L., Maillard, I., Chen, X. W., Sabeh, F., Liu, R., Li, X. Y. and Weiss, S. J. (2012). MT1-MMP regulates the PI3Kdelta.Mi-2/NuRD-dependent control of macrophage immune function. *Genes Dev* **26**, 395-413.

Shumaker, D. K., Dechat, T., Kohlmaier, A., Adam, S. A., Bozovsky, M. R., Erdos, M. R., Eriksson, M., Goldman, A. E., Khuon, S., Collins, F. S., et al. (2006). Mutant nuclear lamin A leads to progressive alterations of epigenetic control in premature aging. *Proceedings of the National Academy of Sciences of the United States of America* **103**, 8703-8708.

Simian, M., Hirai, Y., Navre, M., Werb, Z., Lochter, A. and Bissell, M. J. (2001). The interplay of matrix metalloproteinases, morphogens and growth factors is necessary for branching of mammary epithelial cells. *Development* **128**, 3117-3131.

Soriano, P. (1999). Generalized lacZ expression with the ROSA26 Cre reporter strain. *Nat Genet* **21**, 70-71.

Spencer, V. A., Costes, S., Inman, J. L., Xu, R., Chen, J., Hendzel, M. J. and Bissell, M. J. (2011). Depletion of nuclear actin is a key mediator of quiescence in epithelial cells. *Journal of cell science* **124**, 123-132.

Srivastava, A., Pastor-Pareja, J. C., Igaki, T., Pagliarini, R. and Xu, T. (2007). Basement membrane remodeling is essential for Drosophila disc eversion and tumor invasion. *Proceedings of the National Academy of Sciences of the United States of America* **104**, 2721-2726.

Starr, D. A. (2009). A nuclear-envelope bridge positions nuclei and moves chromosomes. *Journal of cell science* **122**, 577-586.

Sternlicht, M. D. (2006). Key stages in mammary gland development: the cues that regulate ductal branching morphogenesis. *Breast Cancer Res* **8**, 201.

Sternlicht, M. D., Sunnarborg, S. W., Kouros-Mehr, H., Yu, Y., Lee, D. C. and Werb, Z. (2005). Mammary ductal morphogenesis requires paracrine activation of stromal EGFR via ADAM17-dependent shedding of epithelial amphiregulin. *Development* **132**, 3923-3933.

Stewart, C. L., Roux, K. J. and Burke, B. (2007). Blurring the boundary: the nuclear envelope extends its reach. *Science (New York, N.Y* **318**, 1408-1412.

Stresing, V., Baltziskueta, E., Rubio, N., Blanco, J., Arriba, M. C., Valls, J., Janier, M., Clezardin, P., Sanz-Pamplona, R., Nieva, C., et al. (2013). Peroxiredoxin 2 specifically regulates the oxidative and metabolic stress response of human metastatic breast cancer cells in lungs. *Oncogene* **32**, 724-735.

Sullivan, T., Escalante-Alcalde, D., Bhatt, H., Anver, M., Bhat, N., Nagashima, K., Stewart, C. L. and Burke, B. (1999). Loss of A-type lamin expression compromises nuclear envelope integrity leading to muscular dystrophy. *J Cell Biol* **147**, 913-920.

Sutherland, D., Samakovlis, C. and Krasnow, M. A. (1996). branchless encodes a Drosophila FGF homolog that controls tracheal cell migration and the pattern of branching. *Cell* **87**, 1091-1101.

Swift, J., Ivanovska, I. L., Buxboim, A., Harada, T., Dingal, P. C., Pinter, J., Pajerowski, J. D., Spinler, K. R., Shin, J. W., Tewari, M., et al. (2013). Nuclear lamin-A scales with tissue stiffness and enhances matrix-directed differentiation. *Science (New York, N.Y* **341**, 1240104.

Szabova, L., Son, M. Y., Shi, J., Sramko, M., Yamada, S. S., Swaim, W. D., Zerfas, P., Kahan, S. and Holmbeck, K. (2010). Membrane-type MMPs are indispensable for placental labyrinth formation and development. *Blood* **116**, 5752-5761.

Szabova, L., Yamada, S. S., Birkedal-Hansen, H. and Holmbeck, K. (2005). Expression pattern of four membrane-type matrix metalloproteinases in the normal and diseased mouse mammary gland. *J Cell Physiol* **205**, 123-132.

Tallquist, M. D. and Soriano, P. (2000). Epiblast-restricted Cre expression in MORE mice: a tool to distinguish embryonic vs. extra-embryonic gene function. *Genesis* **26**, 113-115.

Tanaka, M., Sato, H., Takino, T., Iwata, K., Inoue, M. and Seiki, M. (1997). Isolation of a mouse MT2-MMP gene from a lung cDNA library and identification of its product. *FEBS Lett* **402**, 219-222.

Tang, C. W., Maya-Mendoza, A., Martin, C., Zeng, K., Chen, S., Feret, D., Wilson, S. A. and Jackson, D. A. (2008). The integrity of a lamin-B1-dependent nucleoskeleton is a fundamental determinant of RNA synthesis in human cells. *Journal of cell science* **121**, 1014-1024.

Tang, Y., Rowe, R. G., Botvinick, E. L., Kurup, A., Putnam, A. J., Seiki, M., Weaver, V. M., Keller, E. T., Goldstein, S., Dai, J., et al. (2013). MT1-MMP-dependent control of skeletal stem cell commitment via a beta1-integrin/YAP/TAZ signaling axis. *Dev Cell* **25**, 402-416.

Taylor, S. H., Yeung, C. Y., Kalson, N. S., Lu, Y., Zigrino, P., Starborg, T., Warwood, S., Holmes, D. F., Canty-Laird, E. G., Mauch, C., et al. (2015). Matrix metalloproteinase 14 is required for fibrous tissue expansion. *Elife* **4**, e09345.

Tran, K. V., Gealekman, O., Frontini, A., Zingaretti, M. C., Morroni, M., Giordano, A., Smorlesi, A., Perugini, J., De Matteis, R., Sbarbati, A., et al. (2012). The vascular endothelium of the adipose tissue gives rise to both white and brown fat cells. *Cell Metab* **15**, 222-229.

Tung, J. J., Tattersall, I. W. and Kitajewski, J. (2012). Tips, stalks, tubes: notch-mediated cell fate determination and mechanisms of tubulogenesis during angiogenesis. *Cold Spring Harb Perspect Med* **2**, a006601.

Van Exan, R. J. and Hardy, M. H. (1984). The differentiation of the dermis in the laboratory mouse. *Am J Anat* **169**, 149-164.

Vandekeere, S., Dewerchin, M. and Carmeliet, P. (2015). Angiogenesis Revisited: An Overlooked Role of Endothelial Cell Metabolism in Vessel Sprouting. *Microcirculation* **22**, 509-517.

Varner, V. D. and Nelson, C. M. (2014). Cellular and physical mechanisms of branching morphogenesis. *Development* **141**, 2750-2759.

Veltmaat, J. M., Mailleux, A. A., Thiery, J. P. and Bellusci, S. (2003). Mouse embryonic mammogenesis as a model for the molecular regulation of pattern formation. *Differentiation* **71**, 1-17.

Vergnes, L., Chin, R., Young, S. G. and Reue, K. (2011). Heart-type fatty acid-binding protein is essential for efficient brown adipose tissue fatty acid oxidation and cold tolerance. *J Biol Chem* **286**, 380-390.

Visbal, A. P., LaMarca, H. L., Villanueva, H., Toneff, M. J., Li, Y., Rosen, J. M. and Lewis, M. T. (2011). Altered differentiation and paracrine stimulation of mammary epithelial cell proliferation by conditionally activated Smoothened. *Dev Biol* **352**, 116-127.

Wagner, K. U., McAllister, K., Ward, T., Davis, B., Wiseman, R. and Hennighausen, L. (2001). Spatial and temporal expression of the Cre gene under the control of the MMTV-LTR in different lines of transgenic mice. *Transgenic Res* **10**, 545-553.

Wang, F., Mullican, S. E., DiSpirito, J. R., Peed, L. C. and Lazar, M. A. (2013). Lipoatrophy and severe metabolic disturbance in mice with fat-specific deletion of PPARgamma. *Proc Natl Acad Sci U S A* **110**, 18656-18661.

Wang, N., Tytell, J. D. and Ingber, D. E. (2009). Mechanotransduction at a distance: mechanically coupling the extracellular matrix with the nucleus. *Nature reviews* **10**, 75-82.

Wang, Q., Uhlirova, M. and Bohmann, D. (2010). Spatial restriction of FGF signaling by a matrix metalloprotease controls branching morphogenesis. *Developmental cell* **18**, 157-164.

Wang, Q. A., Tao, C., Jiang, L., Shao, M., Ye, R., Zhu, Y., Gordillo, R., Ali, A., Lian, Y., Holland, W. L., et al. (2015). Distinct regulatory mechanisms governing embryonic versus adult adipocyte maturation. *Nat Cell Biol* **17**, 1099-1111.

Watson, C. J. and Khaled, W. T. (2008). Mammary development in the embryo and adult: a journey of morphogenesis and commitment. *Development* **135**, 995-1003.

Weaver, S. A., Wolters, B., Ito, N., Woskowicz, A. M., Kaneko, K., Shitomi, Y., Seiki, M. and Itoh, Y. (2014). Basal localization of MT1-MMP is essential for epithelial cell morphogenesis in 3D collagen matrix. *J Cell Sci* **127**, 1203-1213.

Weavers, H. and Skaer, H. (2014). Tip cells: master regulators of tubulogenesis? *Semin Cell Dev Biol* **31**, 91-99.

Whittle, A. J., Carobbio, S., Martins, L., Slawik, M., Hondares, E., Vazquez, M. J., Morgan, D., Csikasz, R. I., Gallego, R., Rodriguez-Cuenca, S., et al. (2012). BMP8B increases

brown adipose tissue thermogenesis through both central and peripheral actions. *Cell* **149**, 871-885.

Wilhelmsen, K., Ketema, M., Truong, H. and Sonnenberg, A. (2006). KASH-domain proteins in nuclear migration, anchorage and other processes. *Journal of cell science* **119**, 5021-5029.

Williams, J. M. and Daniel, C. W. (1983). Mammary ductal elongation: differentiation of myoepithelium and basal lamina during branching morphogenesis. *Dev Biol* **97**, 274-290.

Wiseman, B. S., Sternlicht, M. D., Lund, L. R., Alexander, C. M., Mott, J., Bissell, M. J., Soloway, P., Itohara, S. and Werb, Z. (2003). Site-specific inductive and inhibitory activities of MMP-2 and MMP-3 orchestrate mammary gland branching morphogenesis. *J Cell Biol* **162**, 1123-1133.

Witty, J. P., Wright, J. H. and Matrisian, L. M. (1995). Matrix metalloproteinases are expressed during ductal and alveolar mammary morphogenesis, and misregulation of stromelysin-1 in transgenic mice induces unscheduled alveolar development. *Mol Biol Cell* **6**, 1287-1303.

Wozniak, M. A. and Chen, C. S. (2009). Mechanotransduction in development: a growing role for contractility. *Nature reviews* **10**, 34-43.

Wu, J., Cohen, P. and Spiegelman, B. M. (2013). Adaptive thermogenesis in adipocytes: is beige the new brown? *Genes Dev* **27**, 234-250.

Wu, Y. I., Munshi, H. G., Snipas, S. J., Salvesen, G. S., Fridman, R. and Stack, M. S. (2007). Activation-coupled membrane-type 1 matrix metalloproteinase membrane trafficking. *Biochem J* **407**, 171-177.

Yamada, K. M. and Cukierman, E. (2007). Modeling tissue morphogenesis and cancer in 3D. *Cell* **130**, 601-610.

Yamaji, D., Kang, K., Robinson, G. W. and Hennighausen, L. (2013). Sequential activation of genetic programs in mouse mammary epithelium during pregnancy depends on STAT5A/B concentration. *Nucleic Acids Res* **41**, 1622-1636.

Yana, I., Sagara, H., Takaki, S., Takatsu, K., Nakamura, K., Nakao, K., Katsuki, M., Taniguchi, S., Aoki, T., Sato, H., et al. (2007). Crosstalk between neovessels and mural cells directs the site-specific expression of MT1-MMP to endothelial tip cells. *J Cell Sci* **120**, 1607-1614.

Yana, I. and Weiss, S. J. (2000). Regulation of membrane type-1 matrix metalloproteinase activation by proprotein convertases. *Molecular biology of the cell* **11**, 2387-2401.

Yuan, T., Wang, Y., Pao, L., Anderson, S. M. and Gu, H. (2011). Lactation defect in a widely used MMTV-Cre transgenic line of mice. *PLoS One* **6**, e19233.

Zajac, A. L. and Discher, D. E. (2008). Cell differentiation through tissue elasticity-coupled, myosin-driven remodeling. *Current opinion in cell biology* **20**, 609-615.

Zhang, L., Reidy, S. P., Bogachev, O., Hall, B. K., Majdalawieh, A. and Ro, H. S. (2011). Lactation defect with impaired secretory activation in AEBP1-null mice. *PLoS One* **6**, e27795.

Zhang, Q., Bethmann, C., Worth, N. F., Davies, J. D., Wasner, C., Feuer, A., Ragnauth, C. D., Yi, Q., Mellad, J. A., Warren, D. T., et al. (2007). Nesprin-1 and -2 are involved in the pathogenesis of Emery Dreifuss muscular dystrophy and are critical for nuclear envelope integrity. *Human molecular genetics* **16**, 2816-2833.

Zhou, X., Rowe, R. G., Hiraoka, N., George, J. P., Wirtz, D., Mosher, D. F., Virtanen, I., Chernousov, M. A. and Weiss, S. J. (2008). Fibronectin fibrillogenesis regulates three-dimensional neovessel formation. *Genes Dev* **22**, 1231-1243.

Zhou, Z., Apte, S. S., Soininen, R., Cao, R., Baaklini, G. Y., Rauser, R. W., Wang, J., Cao, Y. and Tryggvason, K. (2000). Impaired endochondral ossification and angiogenesis in mice deficient in membrane-type matrix metalloproteinase I. *Proc Natl Acad Sci U S A* **97**, 4052-4057.

Zimmerman, S. B. and Minton, A. P. (1993). Macromolecular crowding: biochemical, biophysical, and physiological consequences. *Annu Rev Biophys Biomol Struct* **22**, 27-65.